



**HAL**  
open science

# Understanding and targeting USP8 function in endocytosis and Cushing's disease

Thierry Waltrich Augusto

► **To cite this version:**

Thierry Waltrich Augusto. Understanding and targeting USP8 function in endocytosis and Cushing's disease. Cellular Biology. Université Grenoble Alpes [2020-..], 2021. English. NNT : 2021GRALV018 . tel-04213490

**HAL Id: tel-04213490**

**<https://theses.hal.science/tel-04213490v1>**

Submitted on 21 Sep 2023

**HAL** is a multi-disciplinary open access archive for the deposit and dissemination of scientific research documents, whether they are published or not. The documents may come from teaching and research institutions in France or abroad, or from public or private research centers.

L'archive ouverte pluridisciplinaire **HAL**, est destinée au dépôt et à la diffusion de documents scientifiques de niveau recherche, publiés ou non, émanant des établissements d'enseignement et de recherche français ou étrangers, des laboratoires publics ou privés.

## THÈSE

Pour obtenir le grade de

**DOCTEUR DE L'UNIVERSITE GRENOBLE ALPES**

Spécialité : Biologie Cellulaire

Arrêté ministériel : 25 mai 2016

Présentée par

**Thierry WALTRICH AUGUSTO**

Thèse dirigée par **Marie-Odile FAUVARQUE**

préparée au sein du **Laboratoire Biologie a Grande Echelle**  
dans l'**École Doctorale Chimie et Sciences du Vivant**

**Comprendre et cibler la fonction de la  
protéase USP8 dans l'endocytose et la  
maladie de Cushing**

**Understanding and targeting USP8  
function in endocytosis and Cushing's  
disease**

Thèse soutenue à huis clos le 13 avril 2021,  
devant le jury composé de :

**Madame MARIE-ODILE FAUVARQUE**

INGENIEUR HDR, CEA GRENOBLE, Directrice de thèse

**Monsieur GWENAEL RABUT**

CHARGE DE RECHERCHE, INSERM DELEGATION GRAND OUEST,  
Rapporteur

**Monsieur LAURENT PREZEAU**

DIRECTEUR DE RECHERCHE, CNRS DELEGATION OCCITANIE EST,  
Rapporteur

**Monsieur OLIVIER CHABRE**

PROFESSEUR DES UNIVERSITES - PRATICIEN HOSPITALIER,  
UNIVERSITE GRENOBLE ALPES, Président





## Acknowledgements

The present work was carried out at the CEA Grenoble in the BGE Laboratory at the IRIG Institute with funding for my PhD from the CEA, to which I am grateful. I thank also the University of Grenoble Alpes and the CSV Doctoral School for the opportunity of doing my thesis in this great academic environment.

I would like to thank the members of the jury, Dr. Gwenaël Rabut, Dr Laurent Prézeau and Pr. Olivier Chabre for devoting their time to the evaluation of my work presented here and during the defense of my thesis.

Thank you, Marie-Odile. You saw the potential in me and chose to mentor me for this project. Thank you for being patient, for accepting my shortcomings, for accepting my free-spirit and wild curiosity, for sharing the good and the bad moments. For making sure I always had everything I needed to succeed in the project. Thank you for the scientific support as well as the personal support, for the phone calls, for making my integration easier, for making sure I was always fine. You made these years special.

Thank you, Cathy, for all the moments we shared doing science together, for all the help with the project, your contribution was essential. But just as essential was the time we spent laughing and sharing. You made hard moments feel less hard, joyous moments feel even better. I was lucky to have you.

Thank you, Agnès for the scientific counselling and the personal and career mentoring. It was nice being just beside someone as wise and professional and always ready to have a nice discussion about no matter which subject was troubling me.

Thank you, Laurence for your interest in my experiments and the interesting discussions and suggestions. Thank you, Caroline and Magda, for our scientific collaboration. Thank you, Emmanuel for the help with the qPCR technique.

Thanks to all the members of the Gen&Chem team with whom I have shared this time. Emmanuelle, Gilles, Sophie, Alexandre, Giulia, Julie and Isabelle, you all contributed to this work.

Thank you for the members of the thesis committee, Pr. Remy Sadoul and Dr Maxim Balakirev for your assistance during the thesis and for your scientific advising.

I would like to thank my friends, from home and from France, some which I miss so much, for making life easier during this period.

Thank you Florian for being by my side, for being so patient with me, especially during the redaction period, for giving me strength to go on, listening to me, helping me organize

myself and stay focused. But also for taking our breaks to plan the next great adventure around the world.

Thanks to my family, specially you, mom and dad, for all the support. If I am here today it's thanks to you, you know that. The distance doesn't make it any easier, but it's as you say, I'm just a boy chasing his dreams, far far away. I love you.

# PREAMBLE

The discovery of the ubiquitin proteasome system by Irwin A. Rose, Avram Hershko, and Aaron Ciechanover in the early 1980s (Ciechanover et al., 1980; Hershko et al., 1980) (Nobel prize year 2004), has been a true revolution to understand protein turnover and degradation within cells. Many studies further demonstrated the role of the reversible ubiquitin linkage on target protein in most if not all cellular processes. The linkage of various kinds of ubiquitin moieties indeed, not only triggers proteasome degradation but, depending on the kind of ubiquitin moieties linked to the substrates, also act as scaffolding entities triggering protein complex assembly or modifying protein conformation and activation. Consequently, deregulation of actors of the ubiquitin proteasome system is a source of cell dysfunction and of various kinds of pathologies. Here, I will focus on the ubiquitin specific protease USP8 that regulates plasma membrane receptor endocytosis and stability. USP8 may contribute to Cushing's disease, a rare disease caused by a pituitary microadenoma producing an excessive amount of adrenocorticotrophic hormone (ACTH), itself inducing the production of high levels of the hormone cortisol by adrenal glands and causing many pathological outcomes defined as the Cushing's syndrome. Constitutively active variants of USP8 are indeed expressed in tumors from 30 to 60% of patients with Cushing's disease and may cause enhanced *POMC* (proopiomelanocortin) gene expression, encoding the precursor of ACTH, through the stabilization of the EGF receptor. The aim of my thesis was to identify a chemical inhibitor of USP8 catalytic activity and to better understand USP8 function in endocytosis. In my introduction, I describe the cortisol axis and Cushing's disease pathological outcome in a first chapter, the ubiquitin system in a second chapter and the USP8 role in endocytosis in a third chapter.

## Table of contents

INTRODUCTION .....	1
1 1 <sup>ST</sup> CHAPTER – Cushing’s disease and the cortisol axis.....	2
1.1 Cortisol, the stress hormone .....	2
1.2 ACTH and the control of cortisol release .....	5
1.3 Dysfunction of the adrenal cortices .....	7
1.4 Main features of the Cushing’s disease .....	9
2 2 <sup>ND</sup> CHAPTER – The ubiquitin proteasome system (UPS) .....	13
2.1 Ubiquitin properties and its linkage to proteins.....	13
2.2 The ubiquitin code: types of chain and ubiquitin-like proteins .....	17
2.3 The many roles of ubiquitin linkage.....	19
2.3.1 The ubiquitin-dependent proteasomal degradation of protein .....	19
2.3.2 The ubiquitin-dependent degradation of proteins and other substrate by autophagy .....	20
2.3.3 The ubiquitin-dependent endocytosis and lysosomal degradation of plasma membrane receptors.....	22
2.4 Examples of other ubiquitin-dependent cellular processes .....	22
2.4.1 Cell cycle.....	22
2.4.2 NFk-B signaling .....	22
2.4.3 P53 tumor suppressor regulation.....	23
2.5 Reversibility of the ubiquitin-linkage: the role of the deubiquitinases family .....	23
3 3 <sup>RD</sup> CHAPTER – The roles of USP8 and of its substrate CHMP1B in EGFR endocytosis and sorting .....	28
3.1 Remodelling cellular membranes : the ESCRT machinery .....	31
3.1.1 ESCRT 0 .....	32
3.1.2 ESCRT I.....	33
3.1.3 ESCRT II.....	33
3.1.4 ESCRT-III and the Vta1:Vps4 complex .....	33
3.1.5 The cases of CHMP1B and IST1 .....	37
3.2 To degrade or not.....	40
3.3 The EGF receptor as an example for endocytic recycling controlled by ubiquitination.....	40
3.4 The deubiquitinating enzyme USP8 .....	43
3.5 USP8 and the regulation of ESCRT-0.....	45
3.6 USP8 and the regulation of ESCRT-III: CHMP1B.....	45
3.7 USP8 and EGFR endocytosis – the big picture .....	46
3.8 Objectives of the thesis .....	47
RESULTS .....	49
1 1 <sup>ST</sup> CHAPTER – Halogenated salicylanilides inhibit the catalytic activity of USP8 in vitro and ACTH secretion in pituitary cells .....	50
1.1 Introduction .....	50
1.2 Results and discussion .....	52

1.2.1	Selection of USP8 inhibitors .....	52
1.2.2	Hit validation and selectivity assay .....	53
1.2.3	Reversibility assay .....	53
1.2.4	Elimination of irrelevant hits and cytotoxicity assays .....	55
1.2.5	Selection of compounds lowering ACTH secretion in pituitary cells...55	
1.2.6	Closantel and analog compounds efficacy/versus cytotoxicity .....	56
1.2.7	Monitoring of POMC encoding gene expression.....	59
1.2.8	Confirming the in vitro USP8 inhibition by closantel and niclosamide60	
1.2.9	Identification of inactive analogs .....	61
1.3	Conclusion .....	61
1.4	Materials and methods .....	62
1.4.1	Chemicals .....	62
1.4.2	Primary screen.....	62
1.4.3	USP8 inhibition assay .....	63
1.4.4	UHL-3 inhibition assay .....	63
1.4.5	Ub-Rhodamine 110 catalysis assays .....	63
1.4.6	USP8 inhibition reversibility assay .....	63
1.4.7	Papain inhibition .....	63
1.4.8	Cell culture .....	63
1.4.9	ACTH inhibition .....	64
1.4.10	Cell viability.....	64
1.4.11	POMC expression .....	64
1.4.12	FTrees Similarity search .....	64
1.4.13	Molecular docking .....	64
1.4.14	Statistical analysis .....	65
2	2 <sup>ND</sup> CHAPTER – CHMP1B interacts with, and is regulated by, the ubiquitin specific protease Otubain 1 .....	66
2.1	Introduction .....	66
2.2	Results and discussion .....	67
2.2.1	Polymers of CHMP1B are revealed by cross-linking.....	67
2.2.2	Mass spectrometry analysis of CHMP1B containing complexes identify 97 potential partners.....	68
2.2.3	Network analysis reveal a cluster of known proteins of the endosomal pathway .....	69
2.2.4	OTUB1 is a new partner of CHMP1B that also interacts with USP8...70	
2.2.5	OTUB1 and CHMP1B co-purified by affinity purification from HEK293T cell extracts.....	70
2.2.6	OTUB1 silencing results in the accumulation of poly-ubiquitinated forms of CHMP1B .....	72
2.2.7	OTUB1 stabilizes CHMP1B .....	74
2.2.8	OTUB1 promotes EGFR stabilization .....	75
2.3	Conclusion .....	77
2.4	Materials and Methods .....	77
2.4.1	Cell culture .....	77



2.4.2	Plasmids .....	78
2.4.3	siRNAs .....	79
2.4.4	Transfection.....	79
2.4.5	Cross-linking .....	80
2.4.6	Strep-Tactin XT purification for MS experiments.....	80
2.4.7	Strep-Tactin XT purification for CHMP1B:OTUB1 interaction confirmation .....	80
2.4.9	Myc purification for CHMP1B:OTUB1 interaction confirmation .....	80
2.4.10	FLAG purification for ubiquitination analysis.....	81
2.4.11	M/S analysis .....	81
2.4.12	Primary antibodies .....	82
2.4.13	Blot normalization.....	82
2.5	Supplementary Data .....	83
2.5.1	Supplemental Table 1.....	83
2.5.2	Supplemental Figure 1 .....	85
2.5.3	Supplemental Table 2.....	86
2.5.4	Supplemental Figure 2 .....	87
DISCUSSION AND PERSPECTIVES .....		88
1	Clinical potential of salicylanilide compounds.....	89
3	Seeking for new partners of CHMP1B and USP8: methodological difficulties and experimental choices.....	94
4	Interaction between CHMP1B and OTUB1: perspectives .....	97
4.1	Mapping the residues involved in OTUB1/CHMP1B interaction by XL-MS .....	97
4.2	Confirmation and investigation of the role of OTUB1:CHMP1B complex in endocytosis .....	97
4.3	Investigating the putative role of GRAIL in CHMP1B regulation .....	98
5	General conclusion.....	100
BIBLIOGRAPHICAL REFERENCES .....		101

## List of figures and tables

### Introduction

Figure I-01. Synthetic pathways for adrenal steroids .....	3
Figure I-02. Schematic overview of the structures of steroid-secreting cells .....	5
Figure I-03. Proopiomelanocortin processing .....	6
Figure I-04. Physiological cortisol circadian rhythm .....	6
Figure I-05. HPA axis and feedback loops controlling the release of cortisol .....	7
Figure I-06. Classification of the various causes of Cushing's syndrome.....	8
Figure I-07. Management of the patient with suspected Cushing's syndrome.....	10
Figure I-08. The ubiquitin moiety.....	13
Figure I-09. Schematic illustration of CRL1 .....	15
Figure I-10. Signaling pathways regulated by HECT E3s.....	15
Figure I-11. Overview of the different types of E3 ligases.....	16
Figure I-12. Overview of the three steps of ubiquitination.....	17
Figure I-13. Overview of the combination of different ubiquitination types .....	18
Figure I-14. Overview of the mainly described cellular function of ubiquitination.....	19
Figure I-15. Degradation of ubiquitinated proteins by 26S proteasome.....	20
Figure I-16. Overview of the three processes of autophagy leading to access to the degradative lysosome.....	21
Figure I-17. Organization of the deubiquitinases into distinct families.....	24
Figure I-18. Phylogenetic conservation of DUBs.....	24
Figure I-19. Evaluation of the localization of 66 GFP-tagged DUBs expressed in human HeLa cells .....	26
Figure I-20. Mechanisms of DUB regulation .....	27
Figure I-21. Overview of the major steps of clathrin-mediated endocytosis.....	29
Figure I-22. The endosomal network.....	30
Figure I-23. Overview of biological functions of the ESCRT machinery .....	31
Figure I-24. Organization of the ESCRT complexes at the membrane in the yeast.....	34
Figure I-25. Autoinhibitory model for ESCRT-III polymers .....	34
Figure I-26. Visualization of ESCRT-III polymers .....	36
Figure I-27. Helical and dome models for ESCRT-III-mediated membrane remodeling and vesicle scission.....	37
Figure I-28. Stepwise ESCRT machinery assembly and disassembly .....	38
Figure I-29. Helical polymers of CHMP1B and IST1 .....	39
Figure I-30. CHMP1B operates differently to other ESCRT-III members .....	39
Figure I-31. Overview of the major signaling pathways effectors of EGFR activation .....	41
Figure I-32. Endocytic routes for EGFR/ErbB2 heterodimer and the EGFR homodimer .....	42
Figure I-33. USP8 isoform I .....	44
Figure I-34. De-regulated EGFR processing by mutated USP8.....	46
Table I-01. Composition of CRL complexes.....	14
Table I-02. Yeast and mammalian analogs of the ESCRT machinery members.....	32

### Results ó Chapter 1

Figure R1-01: Hit selection process for efficient USP8 catalytic inhibitors .....	53
Figure R1-02: Monitoring the inhibition of 4 druggable confirmed hits on USP8-CD and UCHL3.....	55
Figure R1-03: Closantel inhibits ACTH secretion and is predicted to bind to USP8-CD in-silico.....	56
Figure R1-04. Testing of closantel-related molecules for ACTH-release inhibition.....	57
Figure R1-05. Enzyme immunoassay analysis for closantel and niclosamide.....	58
Figure R1-06. Viability assay .....	59
Figure R1-07. POMC expression assay in two independent experiment (biological replicates) .....	60
Figure R1-08. Confirmation of USP8 catalytic activity inhibition.....	60
Table R1-01. Hit characterization on USP8, UCHL3 and calpain catalytic activity in vitro. .	54
Table R1-02. Compounds presenting similar backbone as closantel but presenting no inhibition of USP8-FL catalytic activity.....	60

## Results ó Chapter 2

Figure R2-01. Cross-linking experiment with SDAD .....	68
Figure R2-02. Comparison of the samples from section 2.2.1 .....	69
Figure R2-03. CHMP1B:USP8 interaction networks.....	70
Figure R2-04. Strep-Tactin XT purification. ....	71
Figure R2-05. Myc purification. ....	72
Figure R2-06. OTUB1 silencing.....	73
Figure R2-07. OTUB1 overexpression. ....	74
Figure R2-08. EGFR immunoblotting .....	75
Figure R2-09. Effects of OTUB1 on EGFR levels. ....	76

## Discussion and Perspectives

Figure C-01. Number of niclosamide publications per year in Pubmed.....	89
Figure C-02. Overview of the chemistries of DSP and SDAD.....	95
Figure C-03. Trimolecular complex. ....	98

## Supplementary Data

Supplemental Figure 1 .....	85
Supplemental Figure 2 .....	87
Supplemental Table 1 .....	83
Supplemental Table 2 .....	86

# INTRODUCTION

# 1 1ST CHAPTER ó E w u j k p i ø u "thekortisol axis " c p f

## 1.1 Cortisol, the stress hormone

The cortisol is a stress hormone produced by the two adrenal (or suprarenal) glands that lie above the kidneys. These glands are composed of two distinguished zones: the medulla and the cortex. The medulla is part of the sympathetic nervous system; it secretes catecholamines (epinephrine and norepinephrine, also known as adrenaline and noradrenaline, respectively) as response to sympathetic stimulation. The cortex secretes two other types of major hormones: mineralocorticoids (which get their name from the effects on salt and potassium on the extracellular fluids) and glucocorticoids (named on their turn because of their effect on blood glucose concentration). The glucocorticoids have equally important effects on fat and protein metabolism, which become quite evident on diseases related to adrenocortical hyperfunction. Cortisol, or hydrocortisone (this last nomenclature is usually reserved for pharmaceutical preparations of the former), is the principal glucocorticoid, although it is important to note that cortisol conserves some mineralocorticoid activity. In addition to these hormones, minor androgenic hormones like dehydroepiandrosterone (DHEA) are also released by the adrenal cortex.

All the adrenocortical hormones are synthesized from cholesterol, with a first common step of conversion of cholesterol to pregnenolone (Fig I-01). Individual steps in each individual synthesis pathway occur either in the mitochondria or on the endoplasmic reticulum. Enzymes of the Cytochrome P450 (CYP, a large family of oxidative enzymes) are highly involved in adrenocortical hormones synthesis. Inherited genetic defects have been described for some of these enzymes, and their relative or absolute deficiencies can impair or shift the type of hormone produced, leading to a disease state.

Steroid hormones produced by the adrenal cortex are not stored to any extent in the producing cells but are rather synthesized and released continuously. Cortisol is highly bound to plasma proteins, which contribute to its half-life of 66 minutes (Weitzman et al., 1971). This might be responsible for a reservoir effect for cortisol, which may dampen rapid fluctuations. In addition, the adrenal cortex is highly vascularized allowing newly synthesized hormone to have a fast access to the systemic circulation.

Adrenal steroid hormones are metabolized mainly in the liver. This degradation ceases their hormone activity and increases their solubility for excretion in the urine. Structural modifications that lead to conjugation to glucuronic acid for excretion in the urine are the most common route of elimination for these hormones. This means that liver diseases may markedly reduce the rate of inactivation for these hormones, and renal disease may reduce the rate of excretion of the inactive conjugates.

Glucocorticoids influence physiologic processes slowly, taking hours to days to produce their full effects. Non-protein bound glucocorticoids in the blood diffuse through the plasma membranes of target cells (most cells in the body) to bind tightly to receptor proteins in the cytoplasm, producing an activated glucocorticoid–receptor complex, which translocates into the nucleus. These complexes then bind to glucocorticoid response elements (GREs) regions in the DNA to either stimulate or inhibit transcription of target genes (Oakley and Cidlowski, 2013).

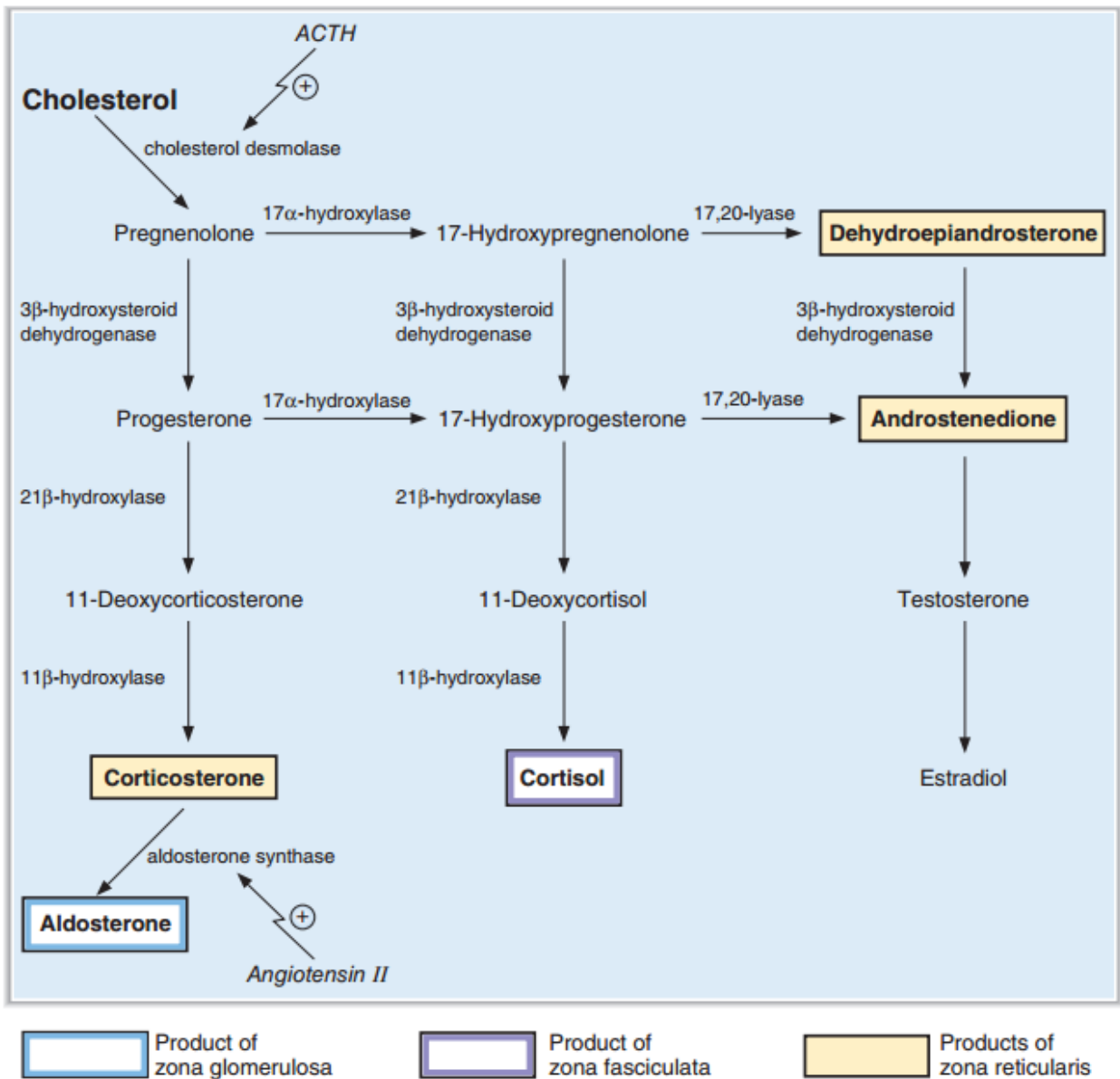


Figure I-01. Synthetic pathways for adrenal steroids. From (Costanzo, 2019)

As mentioned before, glucocorticoids get their name from their effects on glucose metabolism. These hormones can greatly increase gluconeogenesis, i.e., the formation of glucose from protein and lipid sources, and metabolites such as pyruvate and lactate. They are responsible for many of the physiological adaptations seen in fasting, some of these changes only being fully active after days to weeks of fasting. This is accomplished mainly from the direct effect of cortisol on the liver and by antagonizing the actions of insulin on target organs. In the liver, cortisol increases the transcription of proteins needed for gluconeogenesis such as transaminases, pyruvate carboxylase and phosphoenolpyruvate carboxykinase. Extra-hepatically, cortisol leads to the mobilization and use of stored fat, by increasing the production of enzymes needed for lipolysis, such as adipose triglyceride lipase (ATGL) and hormone-

sensitive lipase (HSL). The fatty acids released in the process are used directly for ATP synthesis to spare glucose consumption while the glycerol is routed to gluconeogenesis pathway. When cortisol is present in excessive amounts, all these metabolic changes can be activated outside a fasting state and lead to a disease state (Khani and Tayek, 2001). Of importance is the decreased translocation of the glucose transporters GLUT4 to the cell membrane, especially in skeletal muscle cells, leading on the long term to insulin resistance. This increase in blood glucose concentration can occasionally reach pathological levels, a condition that is referred to as adrenal diabetes.

As for the metabolism of proteins, cortisol causes the reduction of protein stores in virtually all target cells except in the liver resulting in a shift of protein sources into the gluconeogenesis pathway. Reduction of protein levels can also be brought by reduced protein synthesis, increased protein catabolism of the intracellular protein pool, and reduced transport of free amino acids into extrahepatic cells. On the other hand, hepatic protein content is increased, as is plasma proteins concentration (which are produced by the liver). In the presence of excess of cortisol, the skeletal muscles are notably affected by this loss of proteins, resulting in great weakness of the patient (Barrett et al., 2019; Gore et al., 1993).

Cortisol also brings about physiological changes that are important in regulating stress and reducing inflammation (Fukuda and Morimoto, 2001; Hannibal and Bishop, 2014; Lee et al., 2015; Singer et al., 2017; Thau and Sharma, 2020). Types of stressors that have been identified as causing an increase in cortisol include: chronic diseases, surgery, trauma, intense heat or cold, infection, exercise, hypoglycemia and hypotension, as well as emotional stress. One hypothesis is that by increasing degradation of less-essential proteins, the corresponding increase in free amino acids caused by cortisol would allow the synthesis of proteins essential to counteract the stress suffered.

As for inflammation, cortisol inhibits the inflammatory response to injury, which explains its usage and that of its synthetic derivatives as anti-inflammatory agents in acute settings as well as chronic inflammatory conditions such as arthritis (Guerrero, 2017; Straub and Cutolo, 2016). Its effects are pleiotropic. Via the production of a family of proteins called lipocortins, cortisol inhibits phospholipase A2, an enzyme responsible for the production of the pro-inflammatory signalers prostaglandins and leukotrienes. It stabilizes the lysosomal membranes of damaged cells preventing the release of proteolytic enzymes needed for amplification of the inflammatory response. This inhibition of the production of inducers of the inflammatory response has as a secondary effect consisting in the decrease in capillary permeation, leading to reduced swelling and decreased migration of inflammatory cells into the injured area. The immune system is inhibited by T lymphocyte suppression, which in its turn leads to reduced pro-inflammatory antibodies in the area. Fever is attenuated by reduced release of interleukin-1 from leukocytes, one of the principal excitatory inputs of the hypothalamic temperature control system. Even though inflammation is suppressed, the rate of tissue healing is increased, probably by the same hypothesized mechanisms described above that allow the recovery from stress when cortisol is released.

## 1.2 ACTH and the control of cortisol release

Cortisol release is induced by binding of the adrenocorticotrophic hormone (ACTH, or corticotropin) on the melanocortin-2 receptor (also known as the ACTH receptor) on the adrenal cortex. The melanocortin-2 receptor is a G protein-coupled receptor located on the plasma membrane, it exerts its actions via activation of adenylyl cyclase followed by increased intracellular cAMP, and increased phosphorylation of key proteins on the steroidogenesis pathway (Figure I-02).

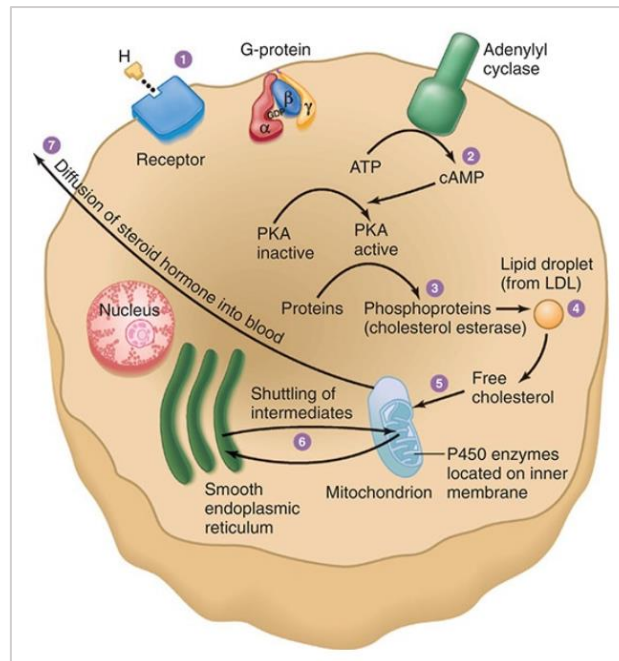


**Figure I-02. Schematic overview of the structures of steroid-secreting cells and the intracellular pathway of steroid synthesis.** LDL, low-density lipoprotein; PKA, protein kinase A. Reproduced from (Barrett et al., 2019)

ACTH is a polypeptide consisting of 39 amino-acids residues, derived from the proteolysis of a larger precursor polypeptide of 241 residues, the proopiomelanocortin (POMC). POMC is expressed by corticotrophic cells of the anterior pituitary and melanotrope cells of the intermediate lobe of the pituitary, as well as in the arcuate nucleus of the hypothalamus, skin and placenta (Cawley et al., 2016). This precursor of ACTH can also give rise to other hormones according to the processing enzymes concomitantly expressed in the tissues where it is expressed. Some examples of hormones derived from POMC include ACTH, melanocyte stimulating hormone (MSH),  $\beta$ -lipotropin and  $\beta$ -endorphin (Figure I-03).



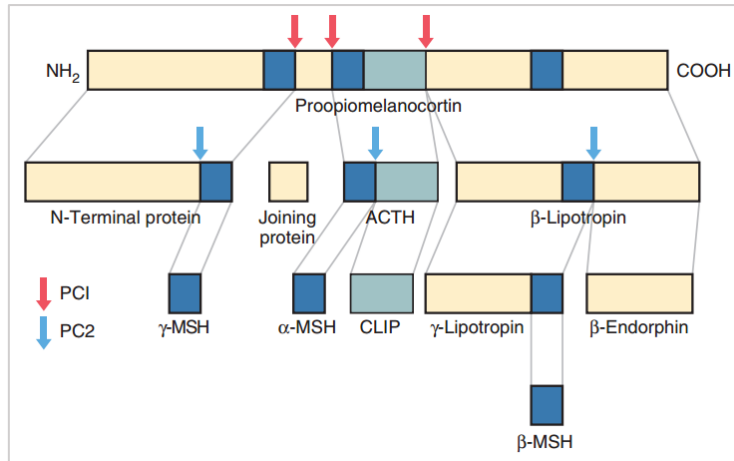


**Figure I-03. Proopiomelanocortin processing** by prohormone convertase 1 (PC1, red arrows) and PC2 (blue arrows). ACTH, adrenocorticotrophic hormone; CLIP, corticotropin-like intermediate peptide; MSH, melanocyte stimulating hormone. Reproduced from (Ph.D, 2015)

ACTH is released by the anterior pituitary gland under the stimulation of the 41 amino acid peptide corticotropin-releasing factor (CRF) in a pulsatile manner. CRF is itself produced in the paraventricular nucleus of the hypothalamus and carried to the pituitary gland via the hypophysial portal system (Le Tissier et al., 2018). This region of the hypothalamus receives many inputs from the limbic system and lower brain stem that are important zones for the relay of stress signals. Cortisol release follows a circadian rhythm marked by intra-period oscillation, with a surge about one hour after waking, and minimal levels at midnight (Figure I-04).

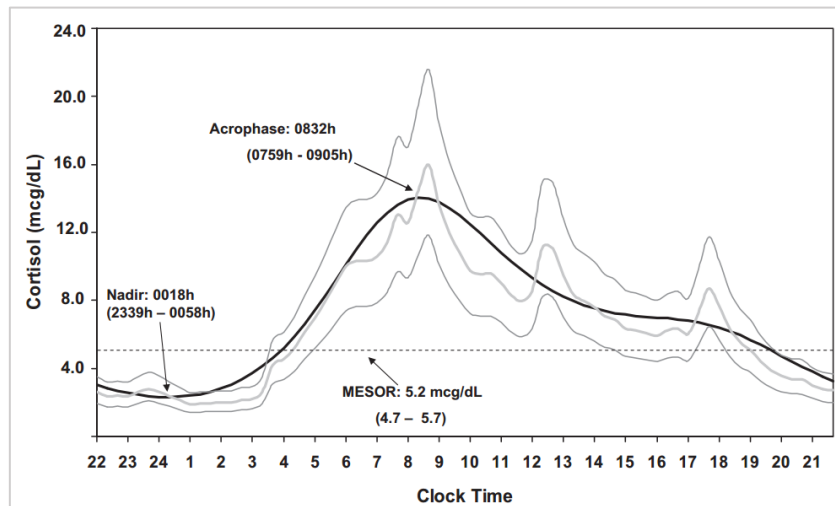


**Figure I-04. Physiological cortisol circadian rhythm.** The figure shows the geometrical mean  $\pm$  2 SD values of serum cortisol concentration calculated from 20 min sampling over a 24-h period in 33 healthy subjects. Cortisol has a distinct circadian rhythm with a peak of 15.5  $\mu$ g/dl (95% reference range 11.7–20.6) occurring at 0832 h and a nadir less than 2.0  $\mu$ g/dl (95% reference range 1.5–2.5) at 0018 h. The mean and 95% CI are shown for the mesor (average levels for the cycle), acrophase (peak of the cycle), and nadir (lowest point of the cycle). mcg,  $\mu$ g. Reproduced from (Debono et al., 2009)

In addition, cortisol regulates its own secretion via inhibitory feedback loops. Increased concentration of cortisol inhibits CRF secretion from the hypothalamus and POMC expression/ACTH release from the pituitary. This axis of regulated hormone control is called the HPA (Hypothalamus-Pituitary-Adrenal) axis (Clarke, 2015) (Figure I-05).

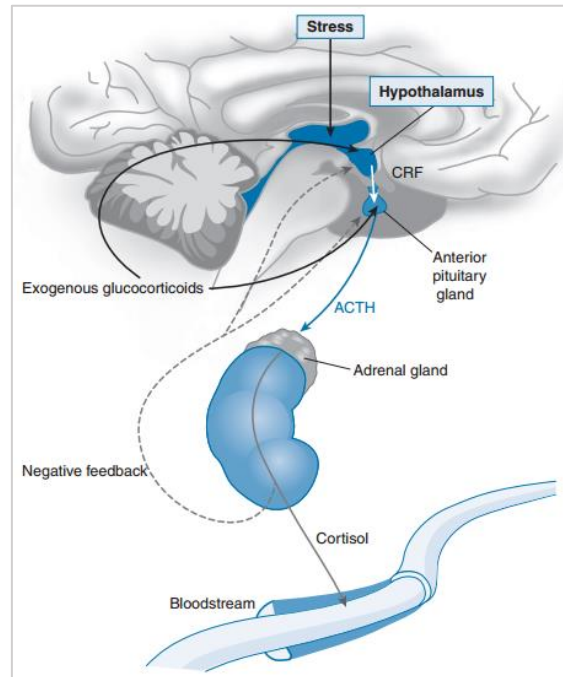


**Figure I-05. HPA axis and feedback loops controlling the release of cortisol.** Reproduced from (Molina, 2013). ACTH, adrenocorticotropic hormone; CRF, corticotropin-releasing factor.

### 1.3 Dysfunction of the adrenal cortices

Adrenal hypofunction can be caused by injury to the adrenal cortices, for example during invasion by an adjacent malignant tumor, or by tuberculous destruction of the adrenal glands (Kasper et al., 2018; Soedarso et al., 2018). In Addison's disease, primary adrenal hypofunction is caused mostly by autoimmunity against the adrenal cortices. In this disease, the lack of aldosterone (the main mineralocorticoid hormone) secretion resulting from hypofunction of the adrenal gland provokes a loss of sodium ions, chloride ions, and loss of water by the kidneys in great profusion. Hyperkalemia, and mild acidosis then develop because of failure of potassium and hydrogen ions to be secreted in exchange for sodium reabsorption. As the plasma volume decreases, cardiac output and blood pressure decrease, and the patient dies in hypovolemic shock, with death usually occurring in the untreated patient. In this disease, cortisol deficiency leads to impaired levels of glucose between meals, and high susceptibility to the negative effects of stressors such as infection. In addition, dark pigmentation of the skin happens because ACTH is overproduced as a measure to counter-balance the lack of cortisol, and ACTH is also the precursor peptide to the melanocyte-stimulating hormone (MSH, melanotropin) (Cawley et al., 2016).

Cushing's syndrome on the other hand is the result of excessive circulating glucocorticoids in the body, which can be caused by the hypersecretion of cortisol from the cortex of the adrenal glands in response to the excessive release of ACTH from either a pituitary microadenoma (defining the Cushing's disease) or from ectopic sites of production (cancerous cell with corticotropic properties). Other causes of cortisol hypersecretion, summarized in Figure I-06, can lead to a similar syndrome (see below).

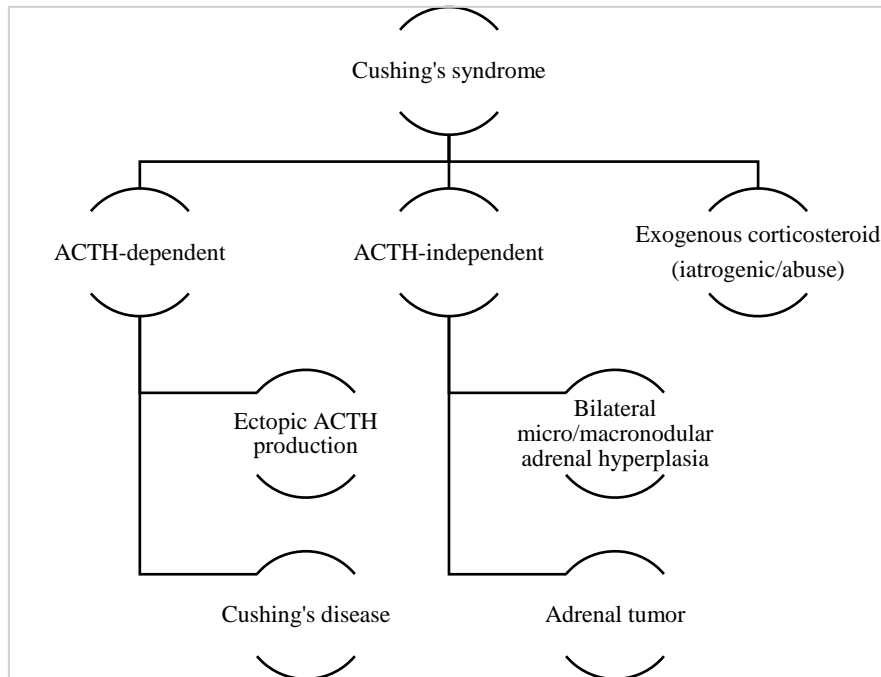


Figure I-06. Classification of v j g " x c t k q w u " e c w u g u." q h " E w u j k p i ø u

The clinical picture characteristic of the Cushing's syndrome include several major features (Barnett, 2016; Ioachimescu, 2018; Liddle, 1977; Shibli-Rahhal et al., 2006). These include loss of muscle volume followed by weakness that are caused by increased protein breakdown, especially on the limbs; deposition of fat that results in a characteristic moon face, buffalo hump and truncal obesity; skin striae caused by abnormal collagen maturation and inhibition of protein synthesis. Wound healing may be delayed in these patients for the same reasons. Hypertension is largely present, probably caused by the mineralocorticoid effects of cortisol (sodium and water retention). Osteoporosis occurs due to impaired osteoblast function and differentiation. Mental symptoms are common, with depression and sometimes psychosis. Diminished glucose tolerance is present, with hyperglycemia and glycosuria (excess glucose in urine) leading to diabetes mellitus in some cases. The androgenic activity of some of the secreted hormones can lead to hirsutism, amenorrhea, acne, reduced fertilization and virilization.

Ectopic ACTH syndrome is due to secretion of ACTH by a non-pituitary tumor. These include occult carcinoid tumors in the lungs, thymus or pancreas. Advanced small-cell lung cancer can cause ectopic ACTH production, although the patients may not develop full-blown clinical features because of the other effects of a rapidly progressing tumor. Due to the hyperstimulation of the adrenals by these tumors, patients present with bilateral diffuse adrenal

hyperplasia, and the glands can weigh up to 20 g each. Rarely, tumors secreting CRF or CRF and ACTH have been found.

A high-dose dexamethasone suppression test can be used to differentiate between ectopic and pituitary tumors ACTH sources: an 8mg dose of dexamethasone is given at 11 pm, and in the early morning of the day after, ACTH and cortisol levels are measured. In ectopic sources of ACTH, the levels of these two markers are not affected. In contrast, pituitary tumors retain some sensitivity to the negative feedback loop driven by dexamethasone, resulting in a decrease of both markers. In the case of which no adrenal tumor is detected, imaging studies of the chest and abdomen are carried out to rule out these ectopic sources of ACTH (which is another cause of Cushing's syndrome, see below).

Primary bilateral adrenal hyperplasia can be present as either micro- or macronodular, they account for less than 2% of the cases of Cushing's syndrome. These nodules are ACTH-independent, and are caused by various somatic or germline mutations, mostly affecting the cAMP/PKA pathway (for review, see (Venanzi et al., 2014)). McCune-Albright syndrome is caused by activating mutations in the stimulatory G protein alpha subunit 1, GNAS-1 (guanine nucleotide-binding protein alpha stimulating activity polypeptide 1), the clinical manifestations of the disorder are variable due to the somatic nature of the mutations and the mosaic distribution of affected tissues, although Cushing's syndrome is one of the observed conditions (Brown et al., 2010).

Adenomas and carcinomas of the adrenals are other causes of Cushing's syndrome, but in these cases, they are classified as ACTH-independent because the rise in cortisol is not caused by direct stimulation of cortisol producing cells by ACTH, but rather by direct dysregulation in the pathways leading to cortisol production. Somatic mutations in the PKA catalytic subunit PRKACA have been identified as cause of disease in 40% of the adenomas. Carcinomas are usually identified in larger lesions. Both these tumors can secrete a large class of hormones, including aldosterone and sex-steroids in addition to cortisol.

Finally, the administration of excessive doses of therapeutic corticosteroids in patients suffering from chronic inflammation might constitute an iatrogenic cause of Cushing's syndrome, especially since these patients might be treated for years with these agents. It is important to note that the cause may also originate from self-diagnosis and auto-medication.

#### 1.4 O c k p " h g c v w t g u " q h " v j g " E w u j k p i ø u " f k u g c u g

When Cushing's syndrome results from an excess secretion of ACTH by the anterior pituitary, this condition is referred to as Cushing's disease (Pivonello et al., 2017a).

Etxabe and Vazquez reported a prevalence of 39.1 per million population and an incidence of 2,4 cases per million population per year (Etxabe and Vazquez, 1994); Lindholm et al. reported an incidence of 1,2-1,7 cases per million population per year over an 11-year follow up period in Denmark (Lindholm et al., 2001). In adults, females are from three to five times more affected than males according to (Lonser et al., 2017). In at least 90% of patients with Cushing's disease, ACTH excess is caused by a corticotropic pituitary microadenoma, often only a few millimeters in diameter while pituitary macroadenomas (i.e., tumors >1 cm in size) are found in only 5–10% of patients (Kasper et al., 2018). Symptoms are essentially the same for those of the other Cushing's syndromes. The small tumors rarely affect surrounding

tissue nor the other functions of the pituitary gland, except in rare cases where tumor growth leads to visual disturbances due to compression of the optic chiasm (Rovit and Duane, 1968)

A diagnosis is established first by excluding exogenous glucocorticoid use, the presence of at least one hallmark symptom, elevated 12pm cortisol, resistance of the cortisol level to fall after an overnight administration of low dose dexamethasone, high plasma ACTH levels, and excluding for an ectopic source of ACTH, in conjunction with further investigation such as MRI imaging of the brain. An updated protocol to diagnosis of different Cushing's syndromes is proposed by (Kasper et al., 2018) and reproduced below.

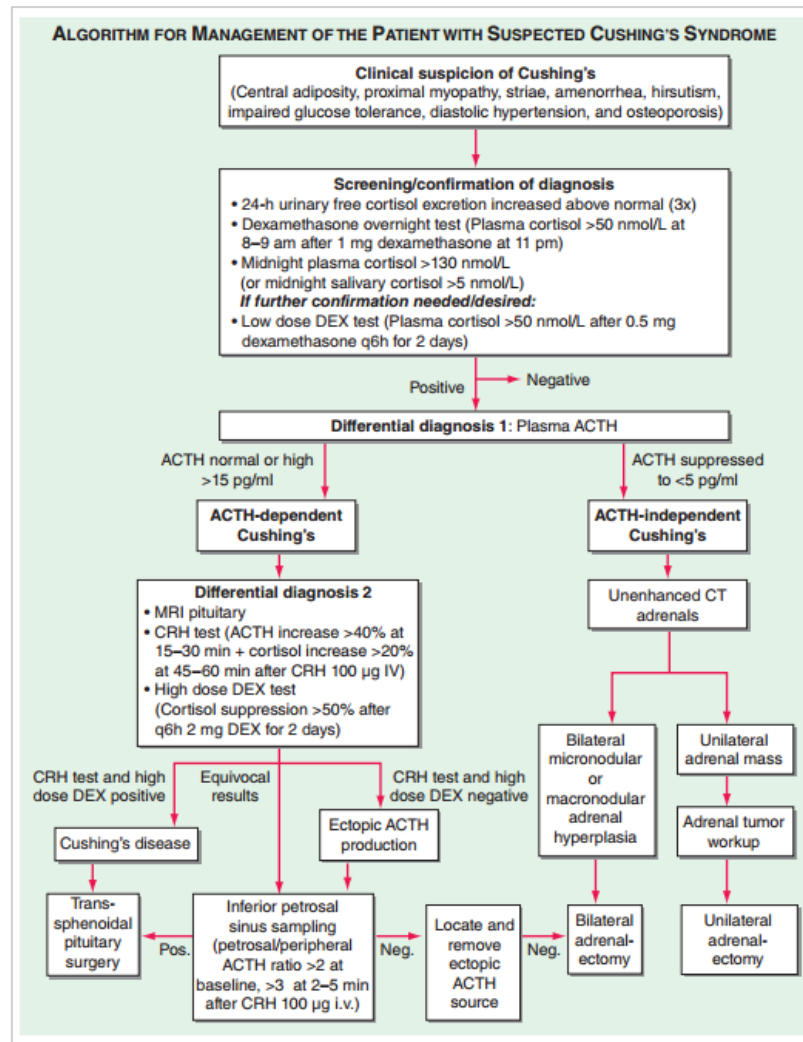


**Figure I-07. Management of the patient with suspected Cushing's syndrome.** ACTH, adrenocorticotropic hormone; CRH, corticotropin-releasing hormone, or corticotropin-releasing factor; CT, computed tomography; DEX, dexamethasone; MRI, magnetic resonance imaging.

Cushing's disease is associated with a high morbidity and mortality. Graversen et al. performed a systematic review of the mortality rates, and found a standardized mortality rate (SMR) of 1,84 for patients after surgical treatment (Graversen et al., 2012). Transsphenoidal surgery is the first-line treatment, with 70-80% success rate (Cristante et al., 2019; Lefournier

et al., 2003), although relapse occurs in a significant number of patients. In this case, there are several options, including second surgery (associated with a significant risk of hypopituitarism), radiotherapy (that may however suffer from a delayed efficacy of typically 2–3 years and significant pituitary deficiency), stereotactic radiosurgery (precisely focused radiation beams), and bilateral adrenalectomy (surgical removal of the two adrenal glands, lifelong mineralocorticoid and glucocorticoid replacement therapy needed).

Oral agents presenting some efficacy against Cushing's disease act at the hypothalamic–pituitary level by decreasing ACTH secretion (neuromodulatory agents), or at the adrenal level by inhibiting cortisol synthesis (steroidogenesis inhibitors), or at the peripheral level by competing with cortisol (glucocorticoid receptor antagonists). Metyrapone inhibits cortisol synthesis at the level of 11 $\beta$ -hydroxylase (Fig I-01), whereas the antimycotic drug ketoconazole inhibits the early steps of steroidogenesis. Both agents are approved in Europe for Cushing's syndrome. Ketoconazole, however, also inhibits androgen synthesis and may cause liver damage. Mitotane, an insecticide derivative, is an adrenolytic agent that is also effective for reducing cortisol. In severe cases of cortisol excess, etomidate, an agent that potently blocks 11 $\beta$ -hydroxylase and aldosterone synthase can be used to lower cortisol. It is administered by continuous IV infusion in low, nonanesthetic doses. Mifepristone, a glucocorticoid receptor antagonist, is approved in the USA for control of hyperglycemia secondary to hypercortisolism in patients with endogenous Cushing's syndrome who have type 2 diabetes or glucose intolerance and have failed, or are not candidates for, surgery, but does not reduce cortisol itself (Buliman et al., 2016; Lonser et al., 2017; Pivonello et al., 2017a).

Many somatic mutations or altered expression of proteins such as several cyclins and tumor suppressors have been described in corticotrope adenomas (Albani et al., 2018a; Hernández-Ramírez and Stratakis, 2018; Sbiera et al., 2019). The ubiquitin specific protease USP8 seems to be of special importance in this disease. Indeed, mutations in the gene encoding for this enzyme have been found in 30 to 60 % depending on the cohort of the cases of Cushing's disease, both in adults (Ma et al., 2015; Reincke et al., 2015) and in the pediatric population of patients (Faucz et al., 2017).

A germline USP8 gain-of-function mutation, causing not only Cushing's disease, but a constellation of other clinical findings, has also been described in a pediatric patient (Cohen et al., 2019) illustrating the pleiotropic functions of this enzyme in many biological processes.

USP8 is a ubiquitin specific protease capable of controlling the ubiquitination status of its substrates (see chapter 2 for a detailed description of the ubiquitin system). The mutations of USP8 found in CD variants cluster close to its 14-3-3 down-regulatory site, leading to a constitutively active enzyme. Tumors presenting this mutation show higher POMC encoding gene expression and increased EGFR (epidermal growth factor receptor) downstream signaling, in a context where EGFR is a known substrate of USP8 (Berlin et al., 2010). Stabilized EGFR would then induce enhanced MAPK signaling and overexpression of POMC. Therefore, EGFR has been proposed as clinical target for treatment of patients.

In patients who underwent transsphenoidal surgery in a single center, Albani et al. reported earlier diagnosis, and earlier and higher recurrence in patients presenting USP8 mutations (Albani et al., 2018b). On the one hand, Ma et al. report that USP8 mutated tumors are smaller in size but produce more ACTH than tumors with wild-type USP8 status (Ma et al., 2015). On the other hand, Losa et al., reported no different hormonal status or tumor

characteristics, but observed a higher remission after surgery in patients with USP8 mutations compared to wild-type USP8 (Losa et al., 2019). Thus, the contribution of USP8 allelic variants to the severity of the disease is still not elucidated.

Recently, Kageyama et al. described that a previously known inhibitor of USP8 is capable of reducing both POMC and ACTH levels in cultured AtT-20 mouse adenocorticotrophic tumor cells model, as well as inhibiting proliferation of these cells and inducing apoptosis (Kageyama et al., 2020). Taken together, the high incidence of USP8 gain-of-function mutations, the putative involvement of USP8 in both ACTH secretion and tumorigenesis, and the preliminary results showing efficient inhibition of ACTH secretion by a small-molecule inhibitor of USP8, render this enzyme an interesting target for treatment of Cushing's disease.

## 2 2<sup>ND</sup> CHAPTER 6 The ubiquitin proteasome system (UPS)

### 2.1 Ubiquitin properties and its linkage to proteins

Ubiquitin is a polypeptide which is ubiquitously expressed in cells of eukaryotic organisms (hence its name), highly conserved in its sequence throughout evolution, found either in its free form or attached to proteins. The sequence representing the human version is composed of 76 amino-acid residues (Figure I-08 A), making up a protein of 8.6 kDa. Composed of a  $\beta$ -sheet with 5 anti-parallel  $\beta$ -strands and a single  $\alpha$ -helix (arranged in a distinctive fashion known as a “ $\beta$ -grasp” or “ubiquitin-like fold”, a fold present in several other proteins with biologically distinct functions); the ubiquitin polypeptide takes a roughly globular form (Figure I-08 B).

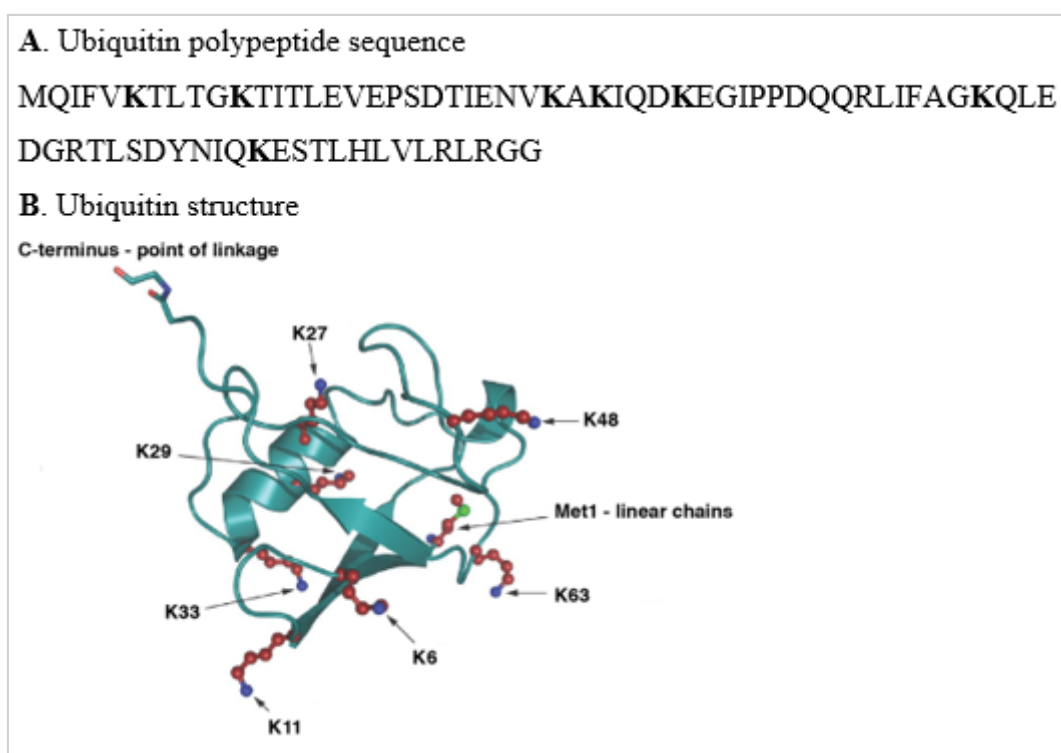


**Figure I-08. The ubiquitin moiety.** A. Amino acid sequence of human ubiquitin. The 7 lysine residues are highlighted. B. Structure of human ubiquitin. C-terminus, lysine residues and initial methionine are highlighted. (Turakhiya, 2018)

Ubiquitin in humans is expressed by four genes: RPS27A and UBA52, which encode ubiquitin as in-frame fusions to a small and large ribosomal protein, respectively; and UBB and UBC, which encode fusions of three and nine ubiquitin molecules, respectively. The monomeric ubiquitin is generated from these precursors by the activity of specific deubiquitinating enzymes (DUBs), majorly UCHL3, USP9X, USP7, USP5 and Otulin/Gumby/FAM105b (Grou et al., 2015).

All four ubiquitin genes contribute to basal cellular ubiquitin levels; however, UBB and UBC are upregulated in response to cellular stress such as heat shock or oxidative stress and may thus ensure specific cell adaptation to environmental signals (Haakonsen and Rape, 2019).



Ubiquitination (also referred as ubiquitylation or ubiquitynylation) consists in the covalent binding of ubiquitin to a substrate protein. This linkage is mediated by the sequential action of ubiquitin-activating enzymes (E1), ubiquitin-conjugating enzymes (E2) and ubiquitin-ligating enzymes (E3 or E3 ligases). They promote, in serial order, the activation of a free ubiquitin moiety, the conjugation of the ubiquitin to the E2 enzyme, and, by action of the E3-ligase, the final transfer of the ubiquitin to the substrate.

In humans, 13 genes coding for E1 enzymes and 49 genes coding for E2s have been annotated (Wong et al., 2003), while for E3, the number of members is as high as 617 genes (Li et al., 2008). E3 ligases recognize sequences in the substrate protein and are mainly responsible for substrate specificity. The two major groups of E3 are: the RING (really interesting new gene) and the HECT (homologous to the E6AP carboxyl terminus). RING E3s, the largest family, catalyze the direct transfer of ubiquitin from the E2 to substrate. Their catalytic domain can be found as a single active polypeptide, or in reconstituted homo/heterodimers (as for BRCA1, Breast cancer type 1 susceptibility protein), as well as part of a larger multicomponent E3 complex such as the cullin-RING ligases (CRL) subfamily, composed of a cullin associated to a RING protein in the C-terminus and a substrate receptor on the N-terminus (often linked to the cullin scaffold via a specific adaptor) (Nguyen et al., 2017; Petroski and Deshaies, 2005; Willems et al., 2004). They are more than 200 different CRLs that are divided into seven families according to their cullin scaffolding proteins (Dubiel et al., 2018). The composition of each complex is limited, different cullin scaffolds assemble with a limited subset of substrate receptors, adaptors, and RING domains. The composition of each class of the most prevalent cullins is presented in Table I-01.

<b>Cullin</b>	<b>Adaptor</b>	<b>Substrate receptor</b>	<b>RING protein</b>
Cul1	Skp1	F-box proteins	Rbx1
Cul2	EloBC	VHL box protein	Rbx1
Cul3	BTB proteins	BTB proteins	Rbx1
Cul4	DDB1	DCAF proteins	Rbx1
Cul5	EloBC	SOCS box proteins	Rbx2
Cul7	Skp1	Fbw8	Rbx1

**Table I-01. Composition of CRL complexes.** Adapted from (Nguyen et al., 2017)

The prototypical CRL are Cullin1-based E3s, which assemble an SCF complex composed of Skp1 adaptor, Cul1, and an F-box protein substrate receptor. F-box proteins derive their name from cyclin F, in which the F-box domain, required for interaction with Skp1, was first discovered (Bai et al., 1996). CRL1 complexes often target cell cycle regulators such as cyclins and the cell cycle inhibitors p21 and p27 for degradation (Dubiel et al., 2018). The spatial arrangement of CRL1 components is represented in Figure I-09, and is representative of the other CRLs:

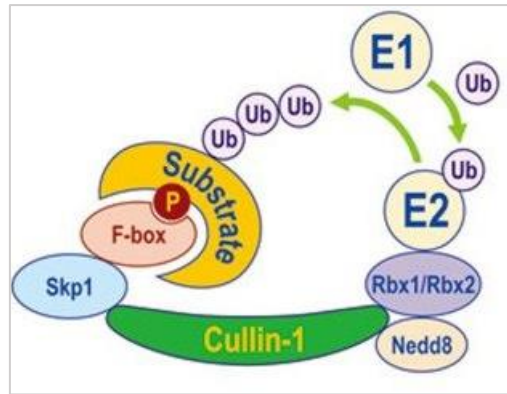


**Figure I-09. Schematic illustration of CRL1.** The C-terminus RING protein acts as a bridge between the E2 and the substrate. It is important to notice that the individual components of the CRL complex can be regulated by post-translational modifications such as neddylation shown in the scheme. The substrate is shown phosphorylated (P). Modifications such as phosphorylation are often required for proper substrate recognition (Sun, 2020). Ub = ubiquitin. Adapted from (Zhou et al., 2013)

In contrast to RING E3s, the HECT E3s contain a catalytic cysteine that first receives ubiquitin from the E2 to form an E3-ubiquitin thioester intermediate and subsequently transfers this ubiquitin to substrate (Scheffner and Kumar, 2014; Weber et al., 2019). An overview of intracellular signaling pathways regulated by HECT E3s is presented in Figure I-10.

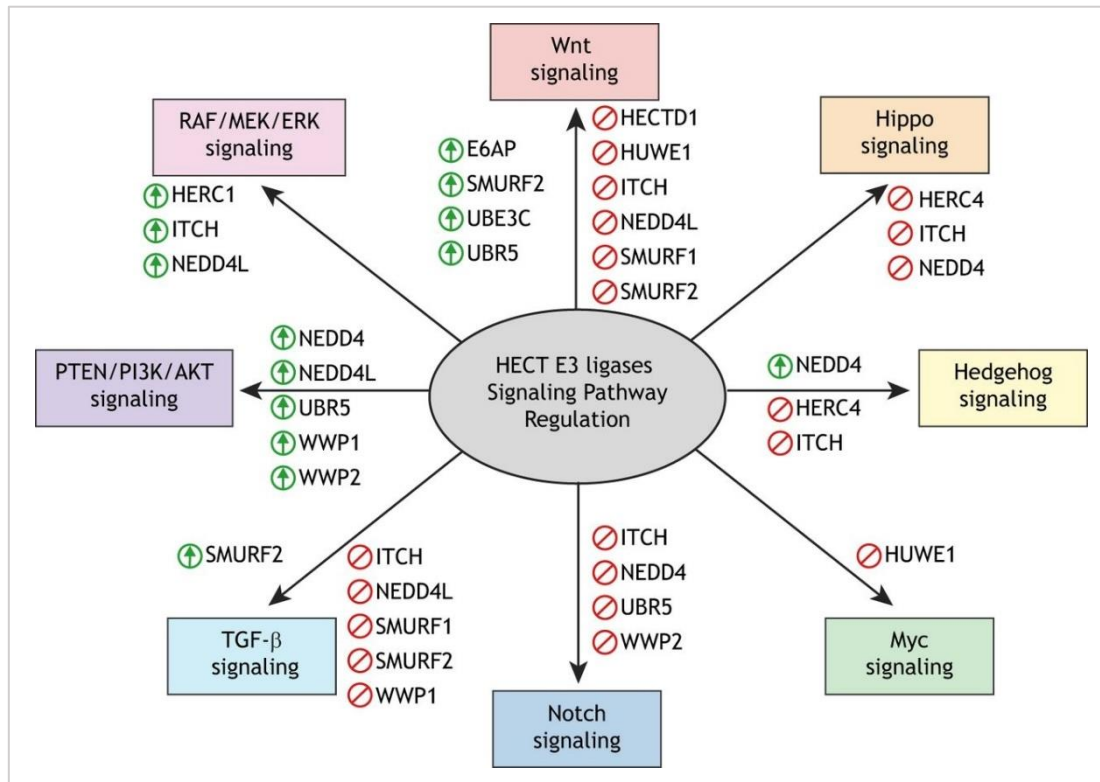


**Figure I-10. Signaling pathways regulated by HECT E3s.** Green means upregulation, red means downregulation. From (Wang et al., 2020).

Recently, a third class of E3-ligases has been identified, the RING-in-between-RING (RBR) E3-ligases, which contain a highly conserved catalytic unit consisting of a RING1, an in-between RING (IBR), and a RING2 domain. As for example, PARKIN, the product of the PARK2 gene whose mutation has been linked to Parkinson's disease, is a RBR E3 ligase. The RBR E3 mechanism is a hybrid of that of RING and HECT E3 ligases, where the RING1 domain recruits E2/ubiquitin and transfers ubiquitin onto the catalytic cysteine of the RING2 domain prior to its conjugation to a substrate (Zheng and Shabek, 2017). See (Buetow and Huang, 2016).

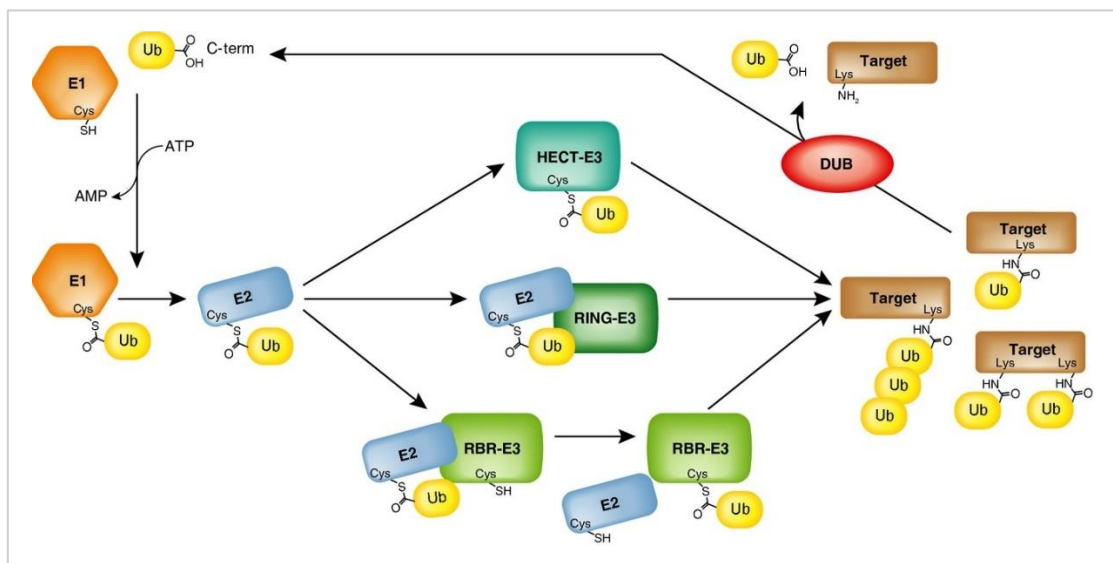


**Figure I-11. Overview of the different types of E3 ligases.** Highlighted is the formation of a thioester intermediate with the ubiquitin (HECT E3-ligases), the direct transfer of the ubiquitin from the E2 onto its target (RING E3-ligases), and RING/HECT-type hybrids (RBR E3-ligases). The removal of the ubiquitin signal by DUBs is also shown. From (Smit and Sixma, 2014)

The linkage of ubiquitin occurs through an isopeptide bond via the side-chain amino group of a lysine residue in the substrate. Other chemical linkages have however been discovered such as a thioester bond on a cysteine residue, an hydroxyester bond on serine and threonine, and a linear peptide bond on the N-terminus of the substrate protein (notably largely described for the first methionine) (McClellan et al., 2019; McDowell and Philpott, 2013).

The attachment of the first ubiquitin moiety to an amino-acid residue occurs via the C-terminus of the ubiquitin moiety, which provides for a monoubiquitination modification of the substrate. Several lysine residues in the same protein can be mono-ubiquitinated potentially resulting in a multi-monoubiquitinated substrate. The lysine residues of ubiquitin can be also themselves ubiquitinated, giving rise to an enormous variety of ubiquitin chain possibilities, triggering different responses in the cell (see above).

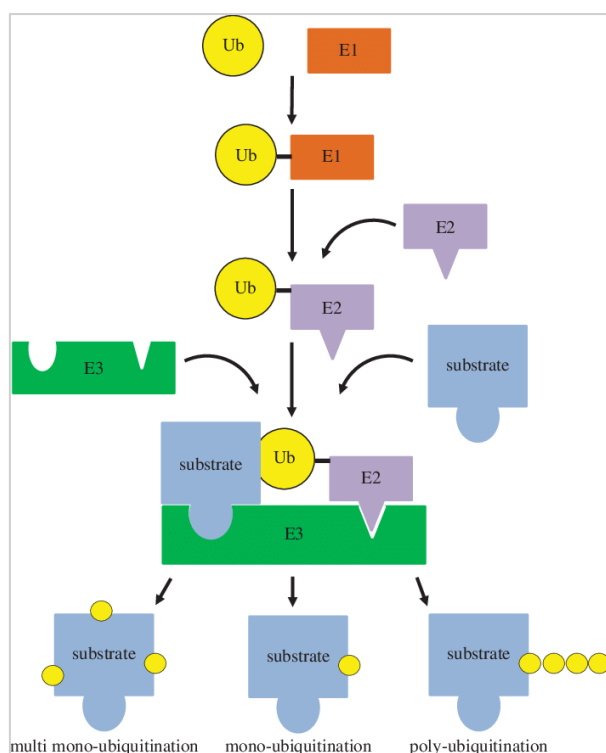


**Figure I-12. Overview of the three steps of ubiquitination:** activation, conjugation, ligation. From (Sharma and Nag, 2014)

## 2.2 The ubiquitin code: types of chain and ubiquitin-like proteins

After the first ubiquitin moiety is bound to a specific residue on the substrate, one methionine (the N-terminus one) and seven lysine residues are available for formation of a di-ubiquitinated residue and further, for the formation of polyubiquitin chains. For ease, these residues are identified in a shortened form according to their position in the sequence of ubiquitin moiety: Met-1 or M1 for the methionine representing the first residue of the sequence, Lys-6 or K6 for the lysine corresponding the 6<sup>th</sup> amino acid residue, and so-on for K11, K27, K29, K33, K48, and K63. Although each new ubiquitin moiety can be added to any of these potential sites, in most cases, as observed so far, the positioning of the first binding is respected, leading to what is called homotypic chains. In this way, M1 chains refer to sequential binding to the first methionine of the previous ubiquitin while K48 and K63 chains refer to sequential binding to K48 or K6 lysine residues, respectively. M1, K48 and K63 polyubiquitin chains are the most frequently described. What is most important is that the kind of the chain can dramatically change the downstream response elicited (see below).

Different outcomes mediated by the various ubiquitin chains can be explained by fully different topologies resulting in a so-called “ubiquitin code”. For example, ubiquitin chains can adopt a compact conformation in which interaction between adjacent moieties are favored (as is the case for K48 chains), or rather an open/linear conformations, without significant interactions between the adjacent ubiquitin moieties (K63 and M1 chains) (Kniss et al., 2018; Liu et al., 2019b; Suryadinata et al., 2014). Chains formed by sequentially different links exist, as well as those containing branches, formed by two different modifications of one moiety in the chain. (Akutsu et al., 2016) reviewed the chains other than K48 and K63 (the “atypical chains”).

In recent years, new modes of ubiquitin chain attachment, other than to the free NH<sub>2</sub> of either first methionine or lysine, have emerged. Covalent modification of non-lysine sites in substrate proteins is theoretically possible according to basic chemical principles underlying the ubiquitination process, and evidence is building that chemical groups such as the hydroxyl group of serine and threonine residues and the thiol groups of cysteine residues can be employed as sites of ubiquitination. McClellan et al recently reviewed the molecular mechanisms and biological importance of non-lysine ubiquitination (McClellan et al., 2019).

Ubiquitin-like proteins (UBL), with similar structure but leading to different outcome than ubiquitin, also exist and can participate in mixed chains with ubiquitin. The two most studied UBLs are SUMO and NEDD8 (reviewed in (Yang et al., 2017) and (Enchev et al., 2015), respectively).

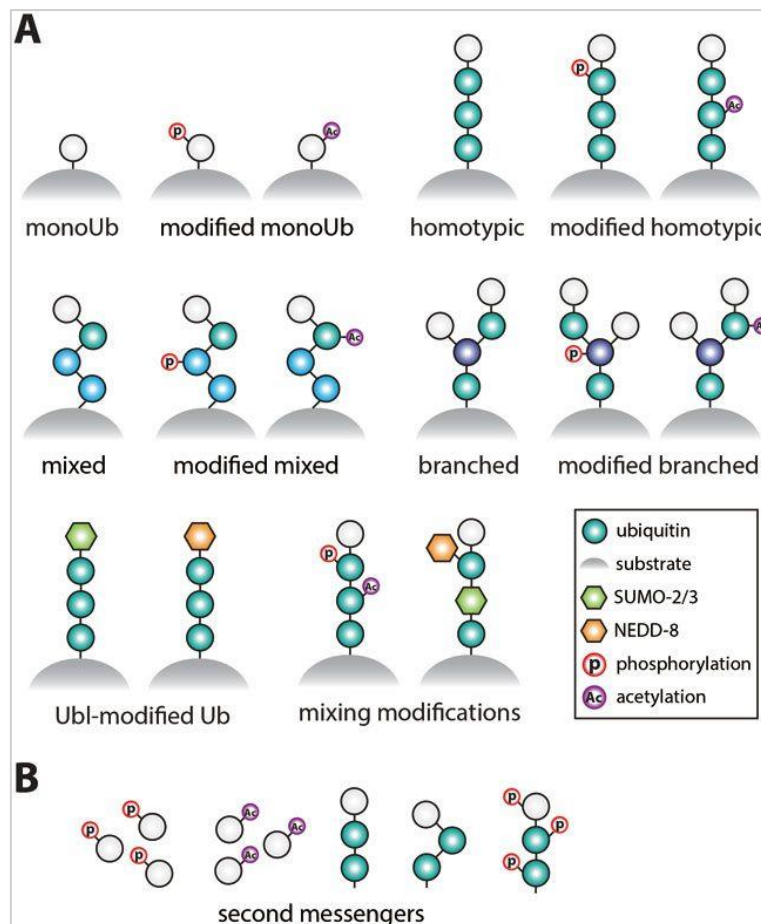


**Figure I-13. Overview of the combination of different ubiquitination types** making up the ubiquitin code. (A) Ubiquitin is also modified by small chemically distinct post-translational modifications such as phosphorylation and acetylation. (B) Unanchored ubiquitin and ubiquitin chains, with or without modifications, can function as second messengers in cells. From (Swatek and Komander, 2016).

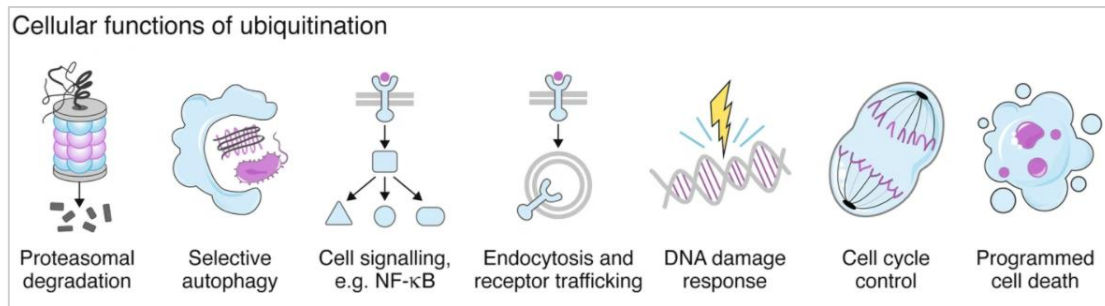


**Figure I-14. Overview of the mainly described cellular function of ubiquitination.** The ubiquitin code dictates the various functions of ubiquitination in cells. From (Damgaard, 2021)

## 2.3 The many roles of ubiquitin linkage

### 2.3.1 The ubiquitin-dependent proteasomal degradation of protein

One of the first identified roles for ubiquitination was the shuttling of proteins to degradation by the 26S proteasome, also known simply as the proteasome, a barrel-shaped proteolytic organelle comprised of a 20S central catalytic complex and two 19S lid complexes (Figure I-15). The 19S complexes play regulatory roles by binding to cargo-loaded shuttling proteins, deubiquitinating the substrates, and channeling them into the six proteolytic sites of the inner core of the 20S central subunit where the target proteins are degraded and recycled (Nam et al., 2017). Specific adaptors (such as RAD23 or ubiquilins) possess ubiquitin-binding domains, that recognize the topology of ubiquitin tagging (the “ubiquitin code”) in regions called “degrons” in the substrates and link them to downstream processes. (Kwon and Ciechanover, 2017). The K48 linkage is the most abundant, representing up to half of all linkages identified by proteomic studies across diverse mammalian cells (Braten et al., 2016; Ciechanover, 2015; Dammer et al., 2011; Kwon and Ciechanover, 2017; Ziv et al., 2011), and serves as a strong signal for proteasomal degradation, (Deng et al., 2017). Monoubiquitination, originally identified as a signal for protein activation and regulation (Sadowski et al., 2012) may be reborn as another degradative signal (Kwon and Ciechanover, 2017). Indeed about 220 mammalian protein are degraded by the proteasome following a forced monoubiquitination accomplished by replacing the polymerizable wild-type ubiquitin by a lysine-less non-polymerizable ubiquitin and thus forcing monoubiquitination (Braten et al., 2016). In addition to K48 and monoubiquitination, K11 chains accumulate when the proteasome is inhibited, indicating that K11 might also contribute to proteasomal degradation of substrates (Komander and Rape, 2012).

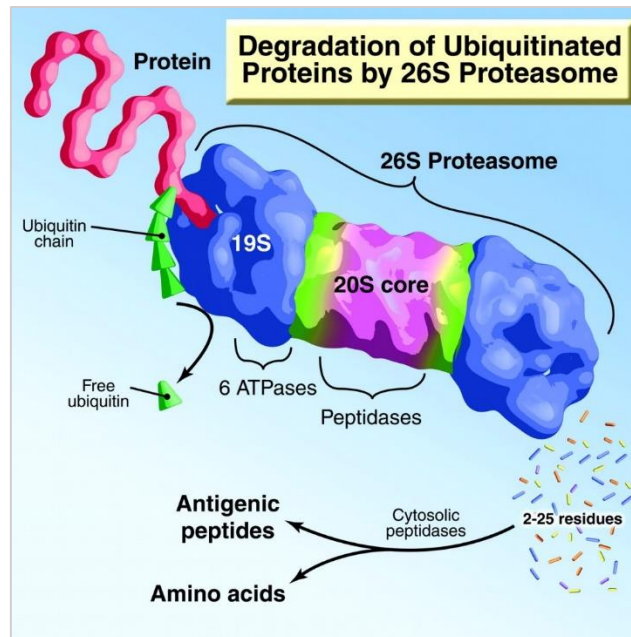


**Figure I-15. Degradation of ubiquitinated proteins by 26S proteasome.** Deubiquitinating enzymes (DUBs) places atop the 19S remove bound ubiquitin from the substrate (not shown). Through the action of ATPases, the 19s caps unfold the protein and translocate it into the 20S core particle for proteolysis into small peptides, which are further degraded into free amino acid residues by cytosolic peptidases. An additional process shown is that of the generation of antigenic peptides, important for the generation of an immunological response to pathogens from their protein content. From (Lecker et al., 2006).

### 2.3.2 The ubiquitin-dependent degradation of proteins and other substrate by autophagy

The main other cellular degradative pathway is the autophagy system which is responsible for bulk degradation of damaged or surplus organelles and protein aggregates by the final action of the lysosome, an acidic compartment (pH  $\approx$ 5.5/5.0) containing acidic hydrolytic enzymes driving degradation of internalized cargo. Autophagy has crucial roles in response to starvation, infection or during development and ageing. Moreover, its activation is also associated with a panel of human diseases, particularly in proteinopathies and neurological diseases (Hansen et al., 2018). Three main autophagic pathways for the delivery of cellular contents have been described (Figure I-16), macroautophagy (often simply referred as “autophagy”), microautophagy and chaperone-mediated autophagy (CMA). In macroautophagy, double membrane vesicles called autophagosomes deliver damaged proteins and organelles to the lysosome for degradation. The conserved metabolic sensor mTORs and longevity determinants AMP-activated kinase (AMPK) are the main regulators of macroautophagy, with mTOR acting as an inhibitor and AMPK acting as an activator. When macroautophagy is induced, cytoplasmic cargo is engulfed by double membranes, starting from the formation of a cup-shaped structure called the phagophore to the sequestration into double-membrane vesicles, called autophagosomes, which then fuse with lysosomes for degradation. Microautophagy also delivers material to the lysosome via vesicles, but in a slightly more direct manner, using vesicles formed from invagination of the lysosomal membrane itself. CMA on the other hand does not use vesicles, but instead uses chaperone proteins to directly target

specific proteins to the lumen of the lysosome. CMA targets very specific proteins for degradation, only those with a conserved penta-peptide motif “KFERQ” in their amino acid sequence.

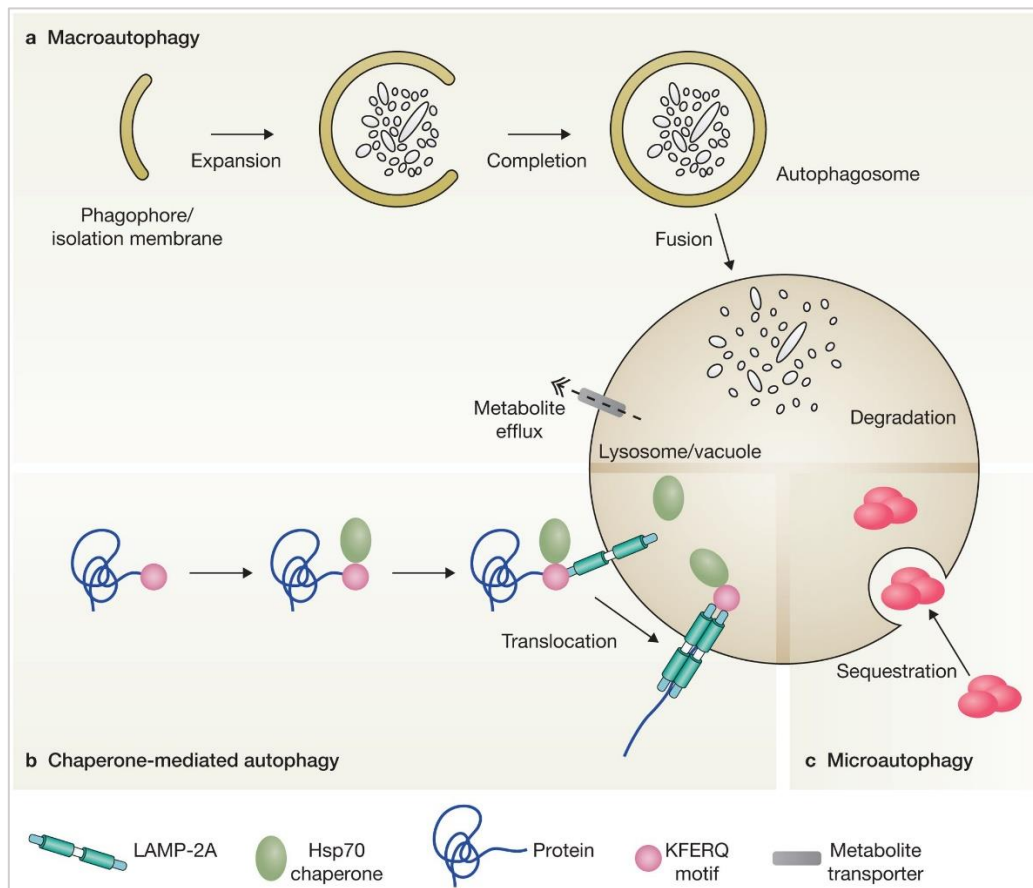


**Figure I-16. Overview of the three processes of autophagy leading to access to the degradative lysosome.** Macroautophagy is based on the formation and maturation of an autophagosome encompassing the contents to be delivered. In microautophagy, cargos to be degraded have access to the lysosome via direct invagination of the latter. In chaperone-mediated autophagy, proteins carrying the KFERQ sequence are recognized by the Hsc70 chaperone, which then associates with the lysosome membrane protein LAMP-2A, triggering its oligomerization and allowing access to the interior of the lysosome through a process that requires Hsc70. Ubiquitination, especially K63 chains, is a major driving signal for this degradation pathway. Note: in plants and yeasts, vacuoles instead of the lysosome play the role of degradative organelle (From (Boya et al., 2013)).

The ubiquitin tag serves not only for directing substrates to the proteasome, but also to the autophagy system, via adaptors containing ubiquitin-binding domains (UBDs) and LIR motif such as p62/SQSTM1, NBR1, NDP52 or optineurin (Boya et al., 2013; Deng et al., 2017). The LIR motif (LC3-interacting region) a 15 to 20 amino acid motif, first discovered in p62, binds to ATG8 family proteins anchored in the membrane at the concave side of the forming autophagosome and drive the entrapment of the cargos (Johansen and Lamark, 2020). K63 linkages serves as the major autophagic signal for protein substrates and for their associated non-proteinaceous materials such as damaged mitochondria (Ji and Kwon, 2017). Although the ubiquitin-proteasome system and autophagy are classically viewed as two



separate cellular mechanisms, ubiquitin is a major effector in both pathways, and the fact that it has been observed that proteasome inhibition affects the autophagy pathway and *vice versa*, has led to the view that both pathways are interconnected. This has been explored in deeper detail in some recent works such as (Nam et al., 2017).

Mitophagy, the degradation of damaged mitochondria via autophagy, is another case in which ubiquitination of substrates activates autophagy via the sequential action of the PINK1 kinase and the E3 ligase Parkin. Here, PINK1 senses damaged mitochondria, and in these conditions is able to activate Parkin, which in its turn is able to poly-ubiquitinate mitochondrial outer membrane proteins to trigger mitophagy (Eiyama and Okamoto, 2015; Oh et al., 2017), which counteracts cytotoxicity by removing damaged or dysfunctional mitochondria.

### 2.3.3 The ubiquitin-dependent endocytosis and lysosomal degradation of plasma membrane receptors

Plasma membrane receptors and proteins, or extracellular material, can be internalized into the cellular cytoplasm through endocytosis, either as a continuous basal mechanism of regulation or in response to external stimuli such as the binding of a ligand to its receptor. By shuttling these internalized cargos through closely localized endosomal compartments, cells can direct the degradation of these material via the lysosome, or recycle them back to the membrane (for membrane receptors), or secrete them back to the extracellular environment as membrane-bound exosomes. In this process, ubiquitination is a major signal driving plasma membrane protein internalization and controlling the sorting of these internalized material in the different endosomal compartments. Ubiquitination is also controlling the fate or functioning of numerous effectors acting in endocytosis (see chapter 3)

## 2.4 **Examples of other ubiquitin-dependent cellular processes**

Ubiquitination has been described in the control of a myriad of cellular events in DNA repair, chromatin state regulation, cell cycle and cell signaling. Here, I briefly present a few examples of these processes.

### 2.4.1 Cell cycle

The CRL family of RING E3 ligases, which includes two structurally similar enzymes, the anaphase-promoting complex/cyclosome (APC/C) and the Skp/cullin/F-box-containing (SCF) complexes drive the ubiquitination and degradation of cyclins and many other cell cycle activators and inhibitors, driving cells through the cellular cycle (Teixeira and Reed, 2013).

### 2.4.2 NFκ-B signaling

The pro-inflammatory pathway driving NF-κB activation following immune challenge (through the recognition of microbial invasion by Toll-like or Nod receptors) or pro-inflammatory cytokines (such as TNF) is one of the main examples of cell signal regulation by the ubiquitin system. Indeed, ubiquitin linkage occurs at each step of the pathway and relies on different type of ubiquitin moieties and ubiquitin-driven degradative or non-degradative

processes. Massive K63 ubiquitination of adaptor proteins associated to the TNF receptor, following TNF stimulation, by example, allows the recruitment of kinases activating complexes, eventually leading to the phosphorylation of the inhibitory molecule I $\kappa$ B, which is itself ubiquitinated by K48 chains triggering its degradation by the proteasome. This allows to free the NF- $\kappa$ B transcription factor that can then translocate into the nucleus where it activates a high number of target genes controlling immune response, and cell survival versus apoptosis. The involvement of the M1 chains has been also discovered in the NF- $\kappa$ B signaling pathway, as evidenced by the capacity of the E3 ligase complex LUBEC to catalyse the formation of M1 chains on the I $\kappa$ B kinase  $\gamma$  (IKK $\gamma$ ) Nemo component of the NF- $\kappa$ B pathway, notably upon bacterial infection (Aalto et al., 2019). See review (Courtois and Fauvarque, 2018).

### 2.4.3 P53 tumor suppressor regulation

The tumor protein 53 (p53), a transcriptional activator continuously expressed at low levels, becomes highly concentrated and upregulated in response to cellular stressors such as DNA damage, osmotic shock and oxidative stress. Considered as the guardian of the genome, it is an important tumor suppressor preventing the formation of cancer. Ubiquitination of p53 driven by MDM2 E3 ligase promotes its degradation and affect its localization (Hammond-Martel et al., 2012; Landré et al., 2017). This MDM2 E3 ligase is itself ubiquitinated and stabilized by the ubiquitin specific proteases USP2 and USP7. Thus, pharmacological approaches aiming at inhibiting USP2 and/or USP7 to prevent MDM2 deubiquitination and subsequent p53 ubiquitination have been undertaken by several pharmaceutical companies (Colland et al., 2009; Schauer et al., 2020).

## 2.5 **Reversibility of the ubiquitin-linkage: the role of the deubiquitinases family**

Ubiquitin linkage is a reversible post-translational modification that can be reversed through the activity of the ubiquitin hydrolases (DUB, for deubiquitinase or deubiquitinating enzymes), a class of enzymes that remove ubiquitin moieties from modified substrates, reversing the modification and at the same time recycling ubiquitin back to its intracellular pool. About one hundred DUBs belonging to six distinct families have been identified. Five of the six families of DUBs (USPs, UCHs, OTUs, MJDs, MINDYs and ZUFSP) are classified as cysteine proteases, while the JAMM (also known as MPN) family consists of zinc-dependent metalloproteinases. An overview of the families of deubiquitinases is presented in Figure I-17, and an analysis of the phylogenetic conservation of the DUBS made in 2019 is recapitulated in figure I-18 (Clague et al., 2019).

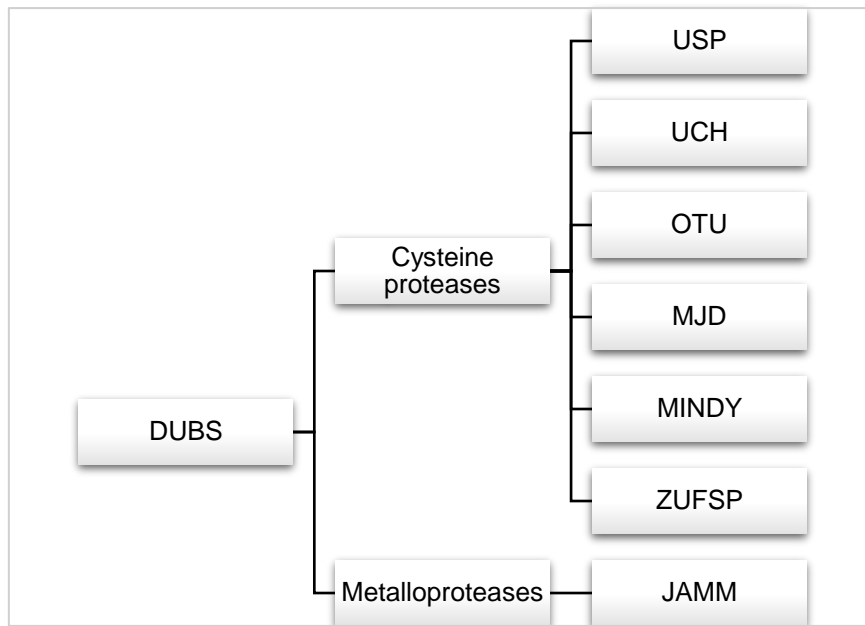


**Figure I-17. Organization of the deubiquitinases into distinct families.**

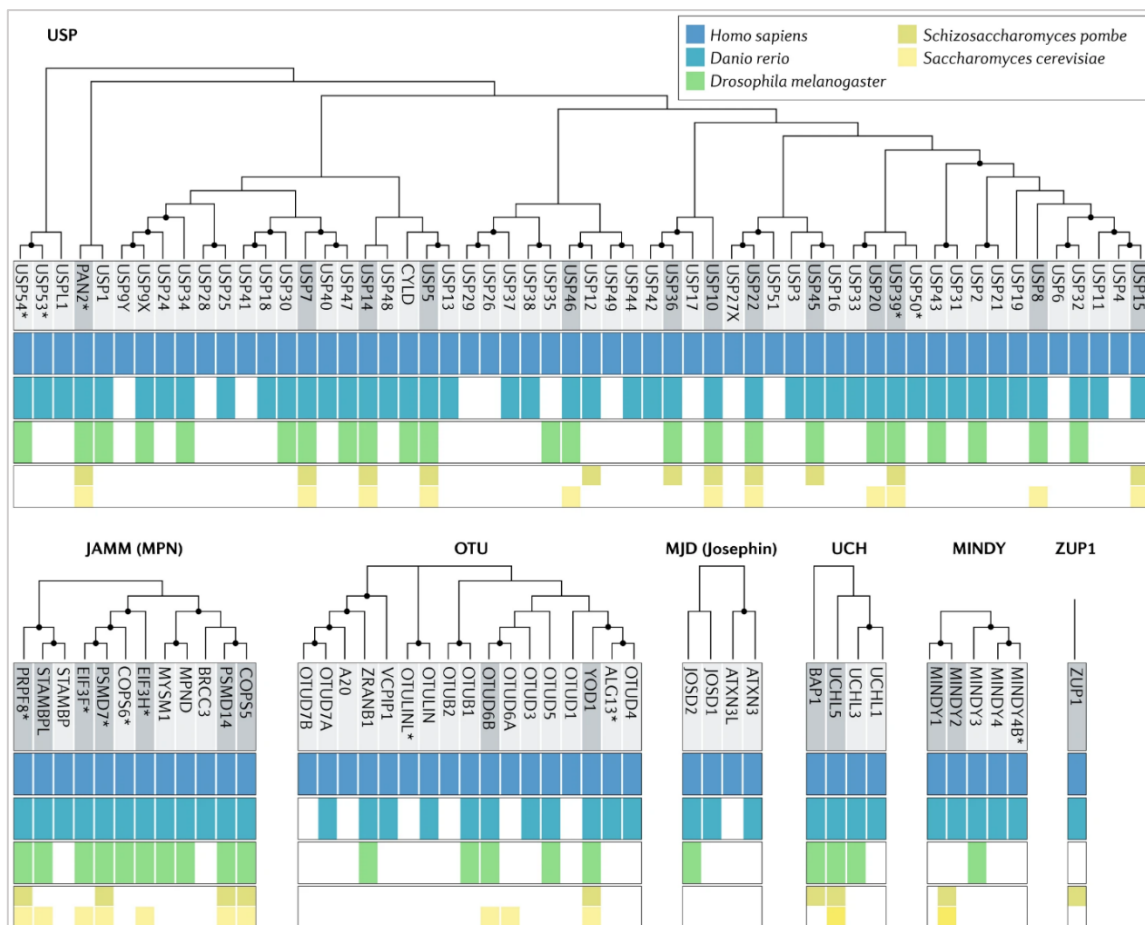


**Figure I-18. Phylogenetic conservation of DUBs.** Deubiquitylating enzymes (DUBs) are arranged according to a bootstrapped neighbor joining phylogenetic analysis of their catalytic domains, with the most reliable nodes indicated by a black dot. \*Predicted to be inactive on the basis of sequence or structural considerations. Figure and text adapted from (Clague et al., 2019)

Different DUBs show different modes of ubiquitin bond hydrolysis: within the chains or down from the distal end, cutting-off an entire ubiquitin chain, cutting only monoubiquitin-modified substrates, etc (Clague et al., 2019). Some DUBs also specifically cleave a particular type chain or a particular length. Nevertheless, most of the members of the largest family, the ubiquitin-specific proteases (USP, comprising 56 members in humans) possess little chain specificity.

Substrate specificity of DUBs is mostly ensured by protein–protein interaction domains outside of, or as insertions within, their catalytic domains. USPs commonly take off the substrate-bound proximal ubiquitin, regenerating an unmodified protein (Mevisen and Komander, 2017).

Multiple CRISPR–Cas9 and RNAi screens of the DUBs family, comprising data from more than 400 cell lines, show consistent effects of several DUBs on cell viability, indicating that the corresponding DUBs are required for cell survival in nearly all cell types. These particular DUBs are USP5, USP39, USP8; and the JAMM family members PRPF8, PSMD14 and PSMD7, COPS5 and COPS6 (Clague et al., 2019).

It can be anticipated that deubiquitinating enzymes are actually required whenever ubiquitination is involved, but particular notorious functions for DUBs include:

- Proteasome-associated DUBs that allow entry into the proteolytic core-particle part of the proteasome (Bard et al., 2018; Budenholzer et al., 2017)
- Histone deubiquitination, leading to chromatin changes regulating transcriptional activation or repression, cell cycle progression, X chromosome inactivation and gene silencing (Atanassov et al., 2011; Chen et al., 2015)
- DNA damage response (Jacq et al., 2013), with implications in tumorigenesis
- Regulation of the NF- $\kappa$ B signaling pathways (Harhaj and Dixit, 2012; Lork et al., 2017; Mulas et al., 2020)
- Regulation of the immune response (Liu et al., 2018; Lopez-Castejon and Edelmann, 2016; Yang and Sun, 2018)
- Tumorigenesis and cancer progression (Bednash and Mallampalli, 2018; Kapadia and Gartenhaus, 2019; Singh and Singh, 2016; Wei et al., 2015)
- Regulation of autophagy and mitophagy (Cornelissen et al., 20141001; Dikic and Bremm, 2014; Fritsch et al., 2019, 2019; Jacomin et al., 2018; M et al., 2017; Stockum et al., 2019)
- Regulating endocytosis (Haglund and Dikic, 2012; Piper et al., 2014).

A systematic approach was undertaken to evaluate the subcellular localization of 66 DUBs by expressing them in fusion with a GFP-tag followed by imaging under fluorescent microscopy (Urbé et al., 2012). This study showed that a significant number of DUBs accumulate in the nucleus (12 exclusively nuclear, 9 predominantly nuclear) (Figure I-19) while others were identified as being cytosolic. In several cases, a clear association with identifiable structures was observed, including endosomes (AMSH/STAMBIP, AMSH-LP/STAMBPL, USP8), mitochondria (USP30), plasma membrane (USP6), and endoplasmic reticulum (USP19) (these results were confirmed by additional colocalization experiments with specific markers of these structures).

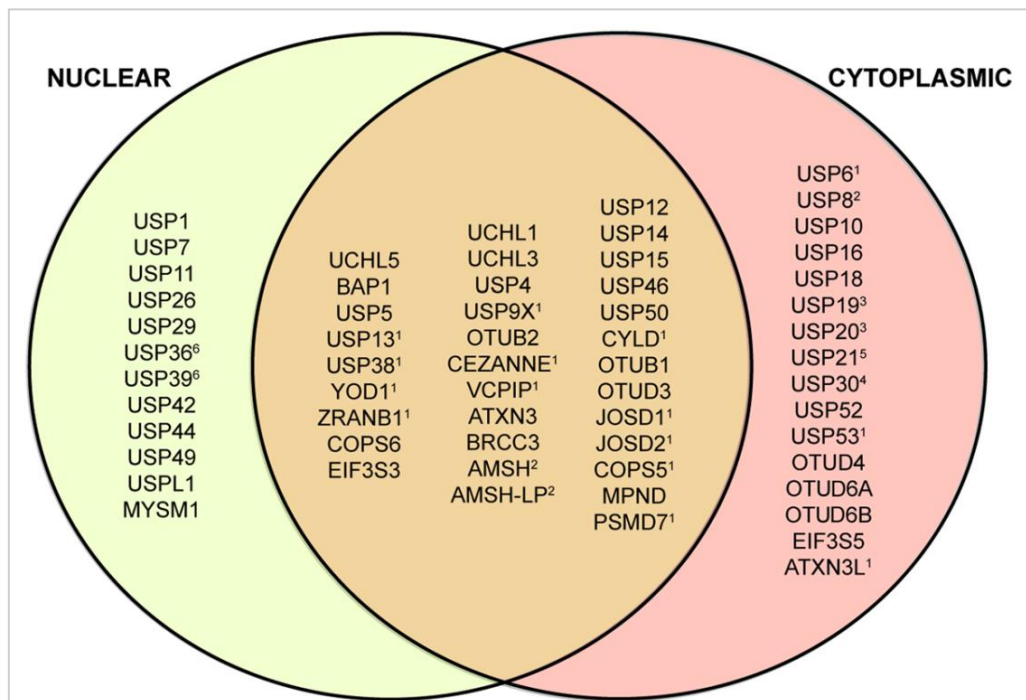


**Figure I-19. Evaluation of the localization of 66 GFP-tagged DUBs expressed in human HeLa cells.** Exclusively nuclear, cytoplasmic or mixed patterns of localization can be observed. From (Urbé et al., 2012)

A systematic of proteomics data was performed in the study “Defining the human deubiquitinating enzyme interaction landscape” that coupled mass-spectrometry analyses, gene Ontology, interactome topology classification, subcellular localization, and functional studies to identify 774 candidate interacting proteins associated with 75 Dubs (Sowa et al., 2009).“ .

The control of DUBs activity is essential to cellular adaptation to changes in their environment, response to external signals and cell survival in different situations. The mechanisms used for regulation of DUB activity can be classified into two main categories: those that control DUB abundance and localization, and those that control their catalytic activity.

One example of control of DUB abundance is that of the zinc finger protein A20, the expression of its cognate gene is induced by NF- $\kappa$ B activation, to which A20 acts as a negative feedback regulator (He and Ting, 2002). Besides the catalytic activity of A20 is regulated via its phosphorylation. Indeed, the I $\kappa$ B kinase  $\beta$  (IKK $\beta$ ), an essential activator of NF- $\kappa$ B, has been shown to phosphorylate A20, increasing its ability to inhibit the NF- $\kappa$ B signaling pathway (Hutti et al., 2007).

Phosphorylation has the potential not only to affect the activity of a DUB, but also its localization: the ubiquitin-specific protease USP4 is a strong inducer of the transforming growth factor- $\beta$  (TGF- $\beta$ ) signaling, acting by deubiquitinating the membrane receptor TGF- $\beta$  type 1. The kinase AKT (protein kinase B), which overexpression is associated with poor prognosis in breast cancer, directly associates with and phosphorylates USP4. AKT-mediated phosphorylation relocates USP4 from the nuclear compartment to the cytoplasm and the plasma membrane and is required for maintaining USP4 stability (Zhang et al., 2012).

DUBs themselves can be ubiquitinated by E3 and are substrates for other DUBs; some can even deubiquitinate themselves: the tumor suppressor BAP1 is a DUB that interacts with chromatin-associated proteins and regulates cell proliferation. UBE2O is a ubiquitin conjugating enzyme that multi-monoubiquitinates BAP1 and induces its cytoplasmic sequestration. This activity is counteracted by BAP1 that can deubiquitinate itself, protecting it from cytoplasmic retention, ensuing tumor suppression (Mashtalir et al., 2014).

The majority of DUBs are cysteine proteases and possess a reactive cysteine residue that is susceptible to oxidation. It has been shown that this oxidation is reversible, and that bursts of reactive oxygen species (ROS) inactivate DUBs via this mechanism. One example is that of USP1, a key regulator of genomic stability, that becomes reversibly inactivated upon oxidative stress (Cotto-Rios et al., 2012).

DUBs activity is also subjected to allosteric modulation by other domains of the enzyme, or to regulation by partners in a macromolecular complex. Moreover, substrate-assisted catalysis is a process in which the ubiquitin moiety of the substrate promotes the rearrangement of the catalytic site and subsequent ubiquitin hydrolysis. The mechanisms of DUB regulation are summarized in figure I-20 (Mevissen and Komander, 2017).

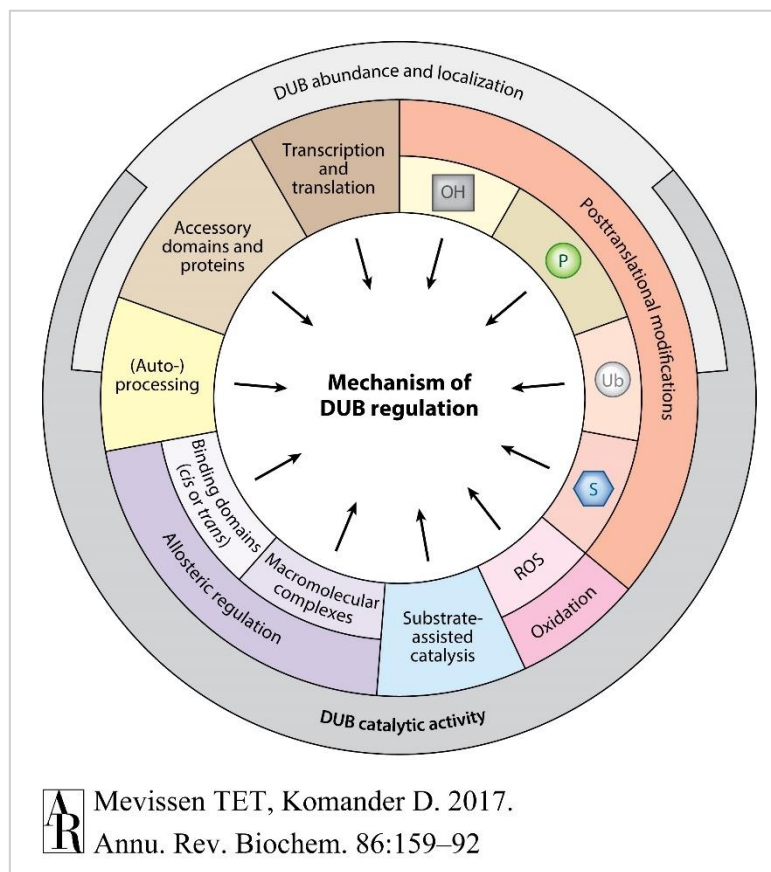


**Figure I-20. Mechanisms of DUB regulation.** Types of posttranslational modifications discussed include hydroxylation (OH), phosphorylation (P), ubiquitination (Ub), and SUMOylation (S). Abbreviation: ROS, reactive oxygen species. Extracted from (Mevissen and Komander, 2017).

### **3 3<sup>RD</sup> CHAPTER 6 The roles of USP8 and of its substrate CHMP1B in EGFR endocytosis and sorting**

The cell membrane is complex, including a large number of proteins that ensures adhesion and communication with its environment, and is under constant re-shaping and renewal. Portions of it are constantly internalized in tubular or vesicular forms under different mechanisms that, grouped together, are named endocytosis. Endocytosis not only allows to reshape portions of the plasma membrane, but also serves to recycle materials embedded into it (and in some cases this serves as regulation of the communication with the extracellular environment), and to capture external materials. The uptake of extracellular fluid in particular, is referred as pinocytosis while the internalization of large solid particles is referred as phagocytosis.

Plasma membrane receptor-mediated endocytosis refers to the process whereby the binding of a ligand to its cognate receptor in the plasma membrane induces the internalization of the ligand-receptor complex. Examples of internalized ligands include transferrin, low density lipoprotein, growth factors and immunoglobulins (Goldstein et al., 1979) and various kinds of cytokines (see below).

Clathrin-mediated endocytosis, which involve the formation of clathrin-coated pits around cargo receptors, is a major endocytic process ensuring the internalization of such receptor-ligand complexes into clathrin-coated vesicles formed from pinching-off of the membrane. Clathrin is a three-legged protein composed of three heavy chains and three light chains that together adopt a triskelion shape. The interaction of multiple clathrin allows the formation of a roughly spherical polyhedral lattice that surrounds and curves the membrane (the clathrin pit). Final scission of the membrane occurs via the action of dynamin, a large GTPase, leading to the clathrin-coated vesicle. Adaptor/accessory-protein complexes allow simultaneous binding to clathrin, membrane lipids, and cargo proteins, and direct the nucleation of the curved lattices and formation of the vesicle around the cargo protein. Disassembly of the coat rapidly occurs via the functioning of the chaperone Hsc70 and auxilin, which bind each vertex point of the clathrin basket, and lead to clathrin-free vesicles (Kaksonen and Roux, 2018).

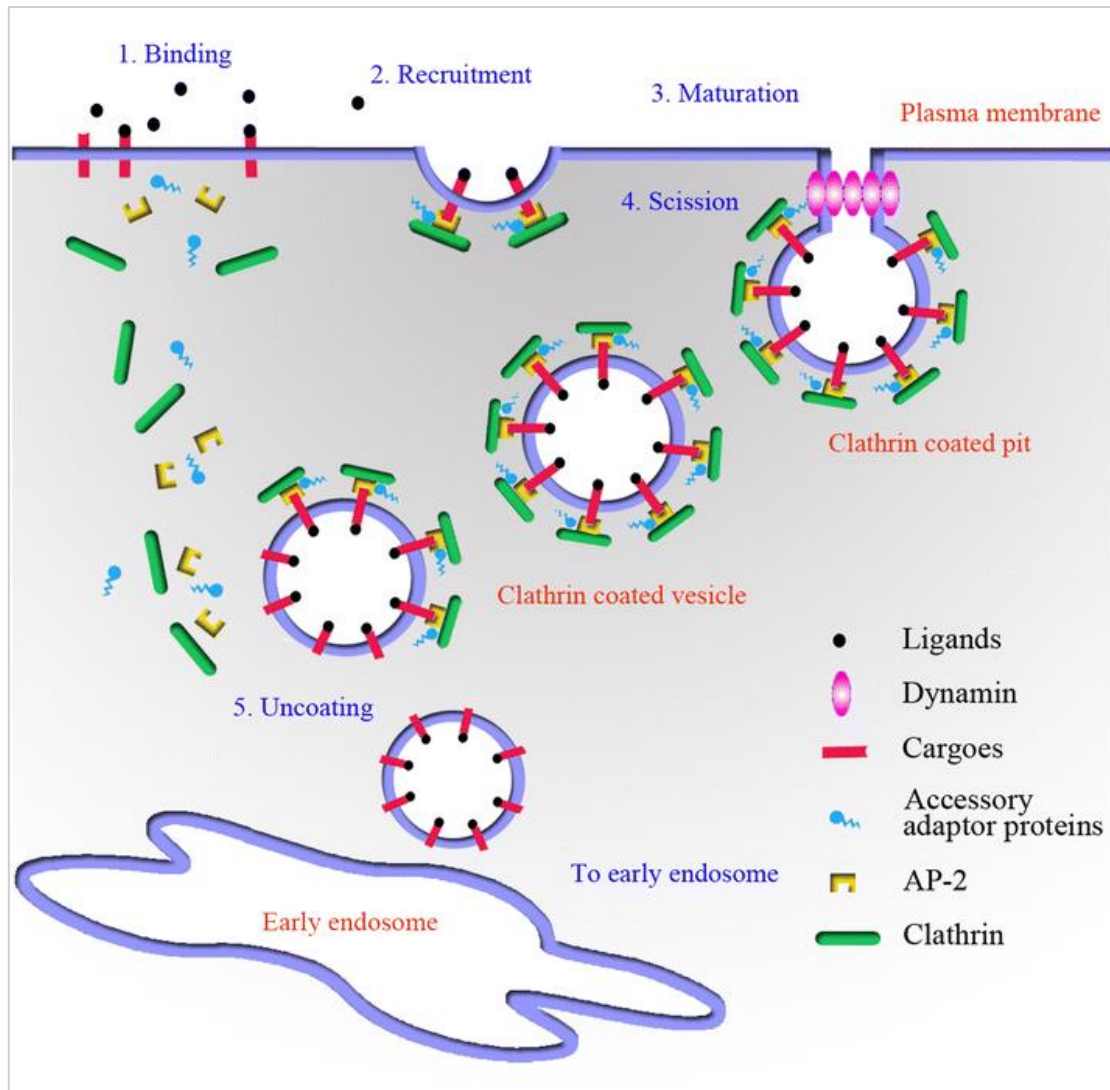


**Figure I-21. Overview of the major steps of clathrin-mediated endocytosis.** From (Zeng et al., 2017)

Other mechanisms of endocytosis exist most often referred to as clathrin-independent endocytosis (Doherty and McMahon, 2009) that will not be detailed in this manuscript.

In the case of clathrin-mediated endocytosis, once internalized, the cargo-protein and ligand-containing vesicles are then available for fusion with an early endosome (Bennett et al., 2001). From there, an access back to the membrane is possible through recycling endosomes (either via a premature, fast recycling, or via a later, slow recycling pathway). Alternatively, the internalized cargo may be sent to the trans-Golgi network by retrograde transport, or to the late endosome compartment and further to the lysosomal compartment ensuring its degradation. In this last case, invaginations of the endosomal membrane drive the formation of intraluminal vesicles (ILVs). The resulting MVB (multivesicular body) compartment containing multiple ILVs further matures and eventually fuses with the lysosomes for degradation but can also be routed toward other destinations – e.g., ILVs can be released extracellularly as exosomes.



Importantly, while the onset of downstream signaling pathways is induced from the activated receptor at the plasma membrane, signaling can continue in the early steps of receptor routing through the endosomes (Miaczynska and Bar-Sagi, 2010). In subsequent steps of receptors trafficking, acidification that starts at the early endosome and increases further on the way to the late endosome helps in receptor-ligand uncoupling and signaling arrest.

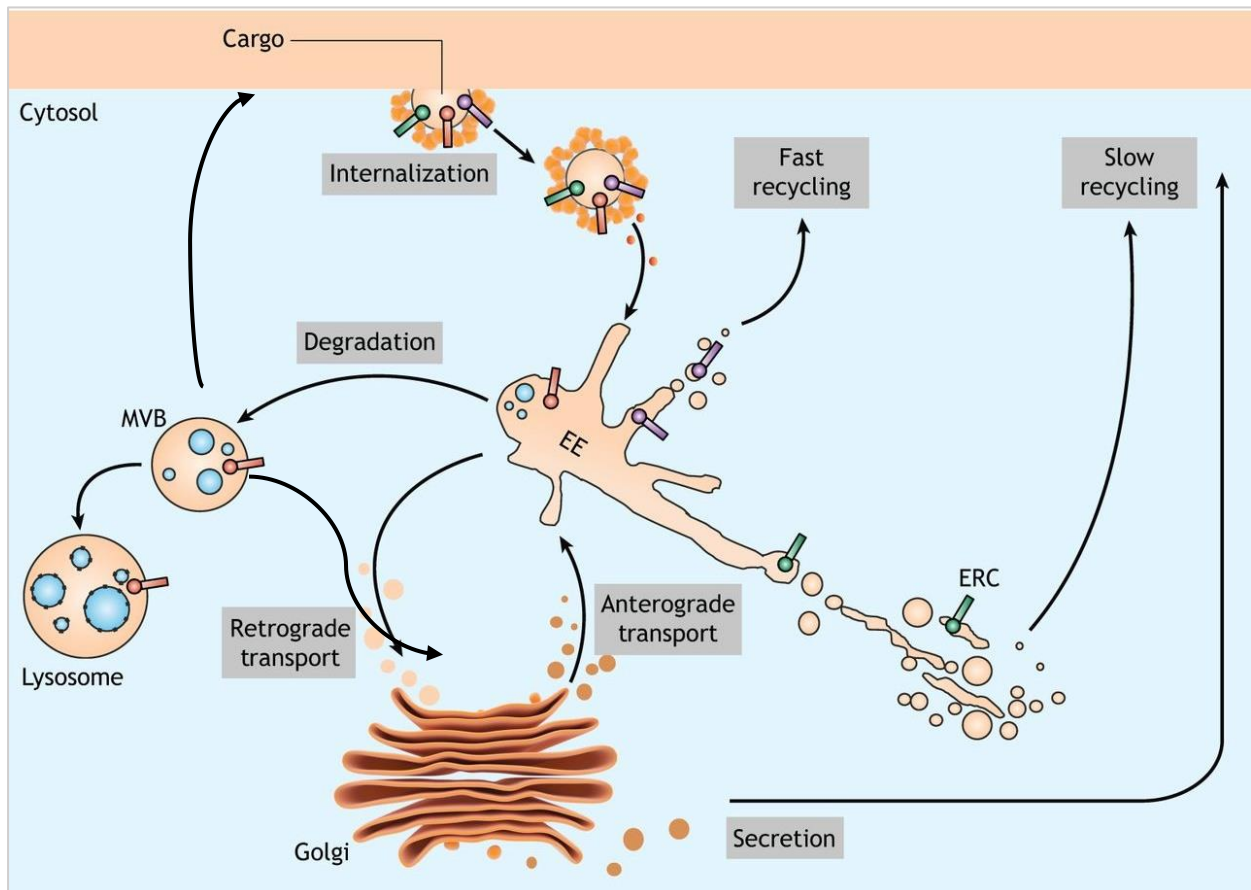


**Figure I-22. The endosomal network.** It is important to note that nomenclature varies, and as the MVB matures it is commonly known as the late endosome. Also, escape of cargo from the early stages or the MVB is not ruled out. MVB = multivesicular body. EE = early endosome. ERC = endocytic recycling compartment. Adapted from (Naslavsky and Caplan, 2018).

### 3.1 Remodelling cellular membranes : the ESCRT machinery

The endosomal sorting complexes required for transport (ESCRT) machinery include five different complexes with different activity in the endocytic process allowing to eventually perform the membrane bending and scission required for vesicle formation in the MVB biogenesis. This machinery also triggers similar membrane remodelling processes as diverse as viral budding, cell abscission and other processes summarized in Figure I-23.

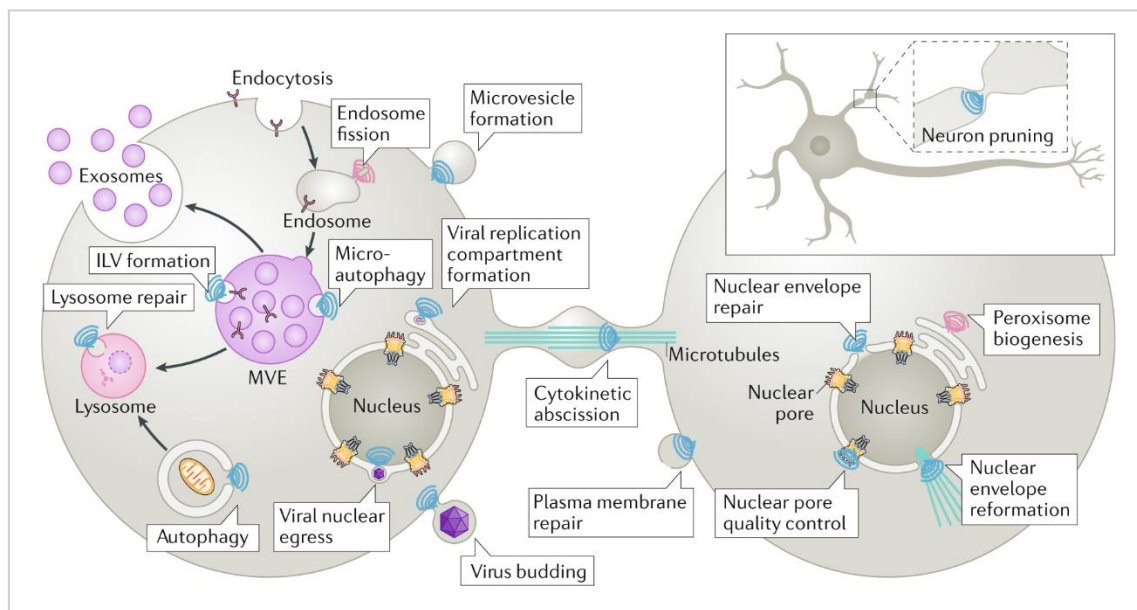


**Figure I-23. Overview of biological functions of the ESCRT machinery.**

(Vietri et al., 2020)

Recognition of the ubiquitinated cargo at the endosomal membrane and membrane constriction and abscission is accomplished by the successive assembly of ESCRT-0, -I, II complexes and of the ESCRT-III complex that ultimately form a polymeric filament that forms a “neck” and brings the membrane together allowing for membrane remodelling and scission to form the ILVs. Each complex performs a specific task that can be roughly defined as: recognition of the ubiquitinated cargo, targeting it to the endosomal compartment, promoting the assembly, nucleation and polymerization of the ESCRT-III complexes that eventually triggers membrane remodelling and scission, and disassembly of the ESCRT filament by a closely associated ATPase complex : Vps4:Vta1.

The ESCRT proteins were first described as a ubiquitin-dependent protein-sorting pathway in yeast, and their analogues are named differently in yeast and in mammals. The reader is referred to Table I-02 for an equivalence chart of the nomenclature for ESCRT members.

Complex	Yeast	Mammalian
ESCRT-0	VPS27	HRS (HGS)
	HSE1	STAM1,2
ESCRT-I	VPS23 (STP22)	TSG101
	VPS28	VPS28
	VPS37 (SRN2)	VPS37A,B,C,D
	MVB12	MVB12a (MVBB, UBAP1)
ESCRT-II	VPS22 (SNF8)	VPS22 (EAP30)
	VPS25	VPS25 (EAP20)
	VPS36	VPS36 (EAP45)
ESCRT-III	VPS2 (DID4, CHM2)	CHMP2A,B
	VPS20 (CHM6)	CHMP6
	VPS24	CHMP3
	SNF7 (VPS32)	CHMP4A,B,C
	VPS60 (CHM5)	CHMP5
	DID2 (CHM1, VPS46)	CHMP7, CHMP1A,B
	IST1	IST1
Vps4-Vta1	VPS4	VPS4A,B (SKD1)
	VTA1	VTA1 (LIP5)

**Table I-02. Yeast and mammalian analoges of the ESCRT machinery members.** Synonyms are in parenthesis.

### 3.1.1 ESCRT 0

The ESCRT-0 complex initiates the MVB pathway by at the same time localizing to endosomes via an interaction with an endosome-enriched phospholipid, phosphatidylinositol-3-phosphate (PI3P) (Burd and Emr, 1998; Gaullier et al., 1998) and binding to ubiquitin moieties that are attached to membrane proteins destined for degradation (also referred as cargo). ESCRT-0 thus executes the first sorting step toward the MVB pathway. ESCRT-0 is a 1:1 heterodimer of HRS (hepatocyte growth factor-regulated tyrosine kinase substrate) and STAM1/2 (signal transducing adaptor molecule 1/2) (Asao et al., 1997; Prag et al., 2007). A single ESCRT-0 complex can bind up to five different ubiquitinated membrane proteins or multiple ubiquitin moieties of poly-ubiquitinated cargo. Here weak interaction with ubiquitin is reinforced by multiple sites of binding to multiple ubiquitin moieties.

### 3.1.2 ESCRT I

ESCRT-I is a heteromeric complex consisting of Tsg101 (tumor susceptibility gene 101), Vps28, Vps37 and Mvb12 (multivesicular body 12) (Chu et al., 2006; Curtiss et al., 2006; Katzmann et al., 2001). The ESCRT-I complex is structured in an elongated rod, capable of interacting with ESCRT-0 from one side via Tsg101 (Katzmann et al., 2001; Kostelansky et al., 2006) and ESCRT-II via Vps28 at the other end, where it is capable of binding to the GLUE domain of the ESCRT-II protein (Gill et al., 2007; Teo et al., 2006).

### 3.1.3 ESCRT II

ESCRT-II is a Y-shaped complex consisting of one subunit each of Vps22 (ELL-associated protein of 30 kDa, or EAP30 or Snf8), and Vps36 (synonym EAP45) (the base of the Y), and two subunits of Vps25 (synonym EAP20) (the arms of the Y) (Babst et al., 2002; Hierro et al., 2004; Langelier et al., 2006; Teo et al., 2004).

The GLUE domain of Vps36/Eap45 connects to Vps28 of ESCRT-I and can bind simultaneously to PI3P and ubiquitin (Slagsvold et al., 2005).

### 3.1.4 ESCRT-III and the Vta1:Vps4 complex

In the last step of membrane remodeling and scission, soluble ESCRT-III monomeric subunits are recruited from the cytosol to their site of action on the endosomal membrane, where they undergo an activating conformational change, recruit various effector proteins and catalyze membrane deformation and scission. In contrast to the early ESCRT complexes, which form stable protein complexes in the cytoplasm, the ESCRT-III complex only transiently assembles on endosomes. The ESCRT-III complex consists of four core subunits, Vps20/CHMP6, Snf7/CHMP4(A-C), Vps24/CHMP3 and Vps2/CHMP2(A,B) (Babst et al., 2002), and three accessory components, Did2/CHMP1(A,B), Vps60/CHMP5 and Ist1 (CHMP stands for charged multivesicular body protein, Ist stands for increased sodium tolerance). The core ESCRT-III monomers are relatively small proteins of about 220-240 amino acids. They include an amino-terminal region consisting of two helices ( $\alpha 1$ ,  $\alpha 2$ ) that form a hairpin structure which is crucial for membrane binding and homo- or hetero-dimerization, and a negatively charged carboxy-terminal region ( $\alpha 5$  and  $\alpha 6$ ) that folds back on the positively charged amino-terminal hairpin. This confers an autoinhibitory mechanism that stabilizes the inactive monomers in the cytoplasm (Bajorek et al., 2009; Muzioł et al., 2006) (Figure I-25).

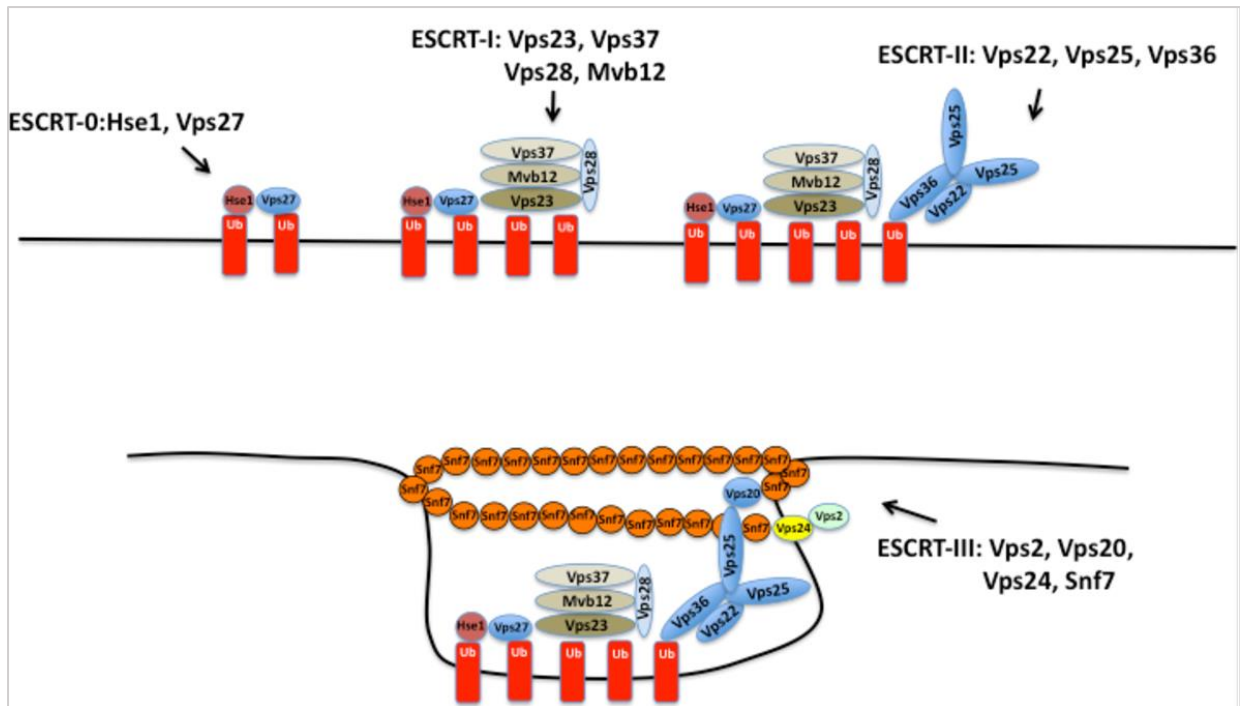


**Figure I-24. Organisation of the ESCRT complexes at the membrane in the yeast.** From (Banh et al., 2017)

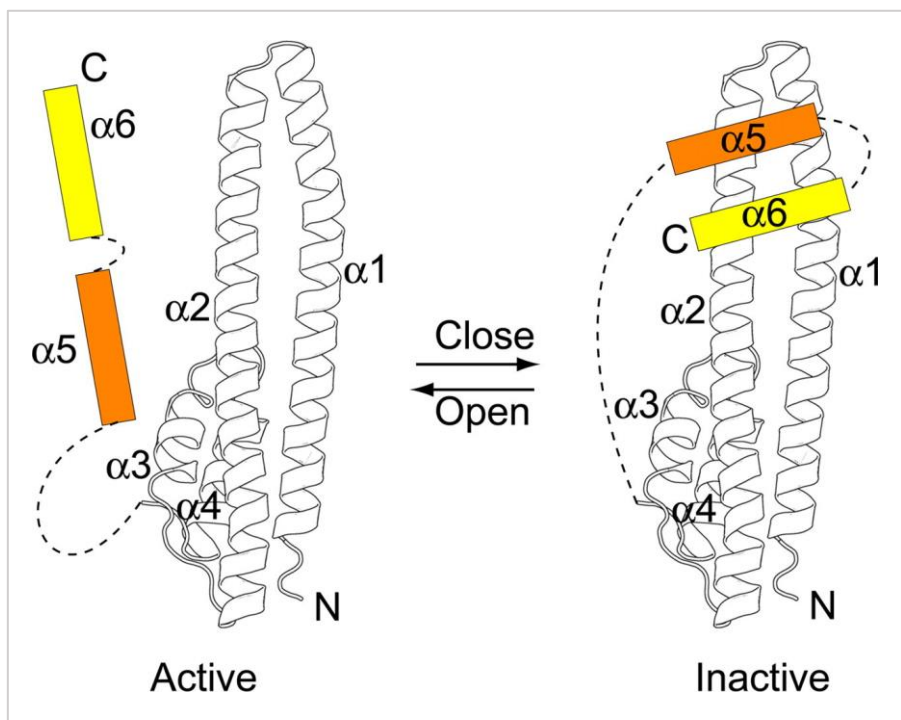


**Figure I-25. Autoinhibitory model for ESCRT-III polymers.** Left: the open, active conformation of the ESCRT-III proteins. Helices  $\alpha 1$ – $\alpha 4$  are adapted from the structure of human CHMP3. Helix  $\alpha 5$  and the C-terminal helix  $\alpha 6$  are shown as arbitrarily placed cartoons and the linkers as dash lines. Right: the closed, cytoplasmic, inactive conformation of the ESCRT-III proteins. From (Xiao et al., 2009)

The ESCRT-III proteins also harbor at their carboxyl terminus, the so-called MIT (microtubule-interacting and transport)-interacting motifs (MIMs) mediating the interaction with effector proteins possessing a MIT domain. Activation of ESCRT-III occurs when the ESCRT-II subunit Vps25 binds to CHMP6, initiating ESCRT-III recruitment to the endosome and subunit polymerization. CHMP6 then recruits CHMP4, which oligomerizes and appears to be the major components of the complex. This oligomerization is capped by the binding of CHMP3 to CHMP4. CHMP3 then recruits CHMP2, completing the ESCRT-III complex assembly (Henne et al., 2011). Although the order of assembly has been elucidated (at least in some situations), the exact stoichiometry of the different members of the ESCRT-III polymers remains to be characterized. Moreover, it may change depending on the type of event (cytokinesis, viral budding, MVB, etc). The complete assembly of the ESCRT-III complex requires a series of conformational changes that reverse autoinhibition, stabilize membrane binding, enable interaction with other ESCRT-III molecules and expose the MIM domain. The MIM domain then recruits deubiquitinases, which mediate cargo deubiquitination. These include AMSH (associated molecule with the SH3 domain of STAM) and USP8/UBPY (ubiquitin-specific protease 8). Once the cargos are entrapped in filament-constricted vesicles, it is thought that deubiquitination can safely happen to promote cargo entry to MVB. In contrast, early deubiquitination of the cargo would rather save it from degradation and triggers its stabilization at the membrane and/or favor its early recycling.

Once assembled, the ESCRT-III complex requires energy to dissociate from the membrane. This energy is provided by the class I AAA (ATPase associated with various cellular activities) Vps4 subunits that are recruited to ESCRT-III complexes via binding to their N-terminal MIT domain (Babst et al., 1997, 1998; Scott et al., 2005). Vta1 forms a heteromeric complex with Vps4, and the presence of MIT domains on both Vta1 and on each Vps4 subunits means that the Vps4-Vta1 supercomplex contains up to 24 MIT domains, allowing it to interact with multiple ESCRT-III subunits simultaneously (Babst et al., 1997; Scott et al., 2005; Yu et al., 2008).

High-resolution imaging allows the visualization of the stepwise ESCRT-III assembly. By overexpressing CHMP4 truncations that lacked the autoinhibitory carboxy-terminal region, using quick freeze deep-etch EM (DEEM) microscopy, Hanson et al. demonstrated that SNF7/CHMP4 assembled into circular arrays on the inner leaflet of the plasma membrane of COS-7 cells (Hanson et al., 2008) (Figure I-26). These arrays were composed of loosely coiled filaments of 4 nm in diameter that extended across the membrane surface. Strikingly, co-expressing CHMP4 with an ATP-hydrolysis defective mutant Vps4 caused the arrays to compact into tightly packed circular lattices. These conditions also generate membrane buds that protruded outward from the plasma membrane in a direction topologically consistent with MVB morphogenesis. Because Vps4 recruitment would follow the assembly of Snf7 polymers, this Vps4-dependent membrane deformation appears consistent with the ordered assembly model for ESCRT-III.

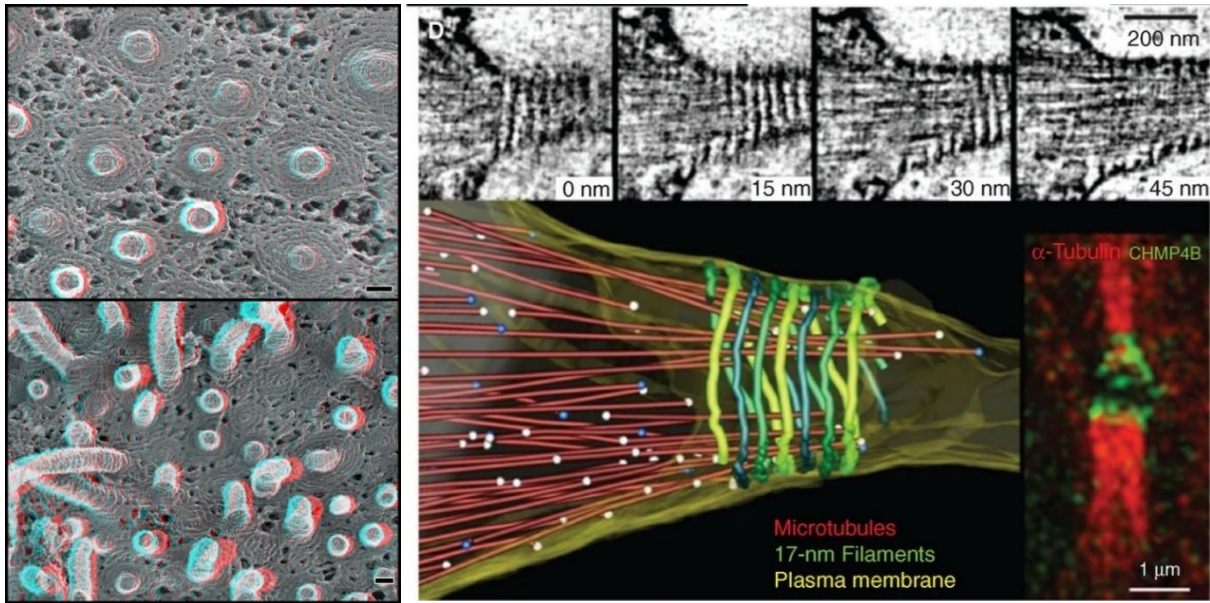


**Figure I-26. Visualization of ESCRT-III polymers.** **Left:** Electron micrograph of circular array protein scaffolds, budlike and tubules of varying lengths on membrane in COS-7 cells expressing CHMP4A and VPS4B(E235Q)-GFP. Bars, 100 nm. (Hanson et al., 2008). **Right:** Electron tomography of high-pressure frozen cells, which show 17-nm filaments spiraling along the constriction zone. Adapted imaged from (Henne et al., 2013), from the original work of (Guizetti et al., 2011).

Visual details for the role of CHMP3 and CHMP2 came from in-vitro studies using these two purified proteins. Using a similar strategy, (Lata et al., 2008) used negative stain electron microscopy to show that truncated CHMP3 and CHMP2 co-assemble into helical cylinders in vitro. The outsides of these cylinders adhered to liposomes, suggesting a membrane-binding interface that was topologically consistent with MVB budding. Notably, these cylinders terminated with domelike caps. These observations have given rise to the “dome model” of ESCRT-III catalyzed membrane scission (Figure I-27) (Fabrikant et al., 2009). In this model, a CHMP3/CHMP2 dome lines the interior of a membrane bud. The protein dome naturally tapers the lipid bilayers into close proximity at the dome base, promoting spontaneous fission. This tapering alone may be sufficient for the fission and Vps4 would function after membrane scission to trigger ESCRT-III complex disassembly. The energy of ATP hydrolysis would be invested to reset the autoinhibition of ESCRT-III subunits. The autoinhibited ESCRT-III proteins could store this energy in the cytoplasm and release it upon membrane binding and incorporation into filaments. The released energy could be transformed into a mechanical force to remodel and scission membranes. In this model, Vps4 would act similar to the AAA-ATPase NSF that disassembles (and reloads) SNARE complexes after vesicle fusion (Adell and Teis, 2011).

(Henne et al., 2013) provides a model that takes into account how CHMP2, CHMP3 and CHMP4 polymerize together into helical polymers that drive vesicle budding by a spring like mechanism. In their “helical model”, CHMP2 and CHMP3 might incorporate into a growing CHMP4 polymer or bind to a preassembled one and modulating its architecture, generate the mechanical force necessary for vesicle budding. (Figure I-27).

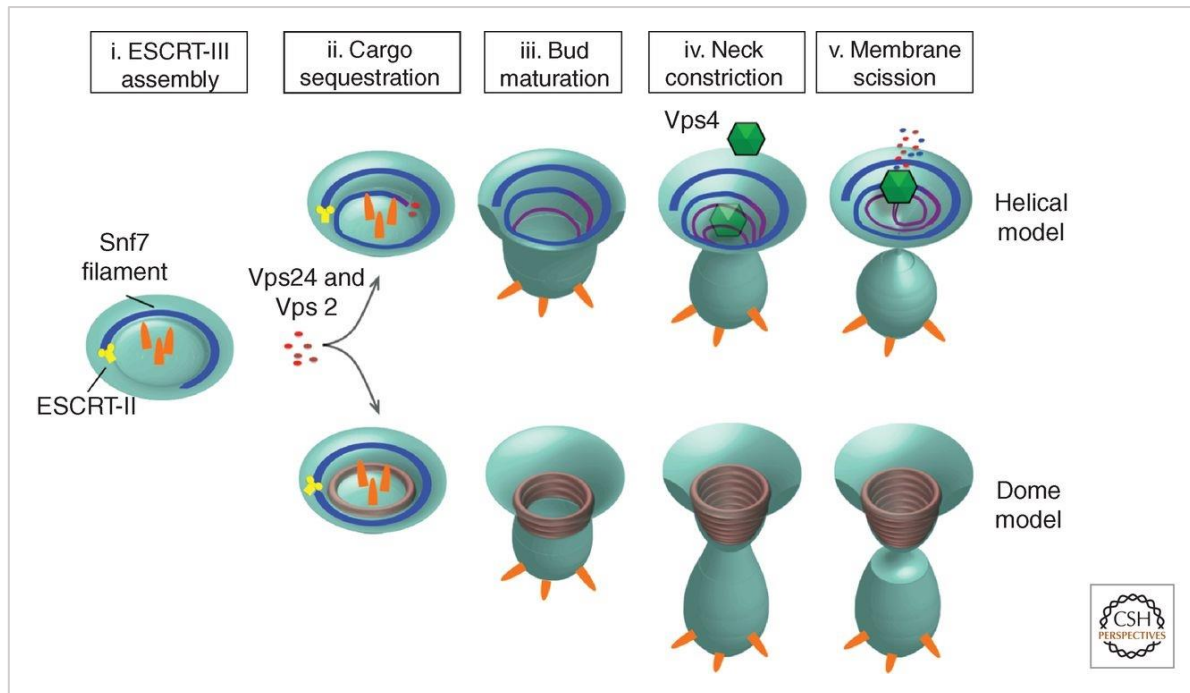


**Figure I-27. Helical and dome models for ESCRT-III-mediated membrane remodeling and vesicle scission.** From (Henne et al., 2013)

Other models have been put forward for how the ESCRT-III polymers contribute to the membrane remodeling and vesicle scission, a fascinating process for which many molecular events stay to be determined (Adell and Teis, 2011)(McCullough et al., 2013) and (Franquelin and Schwille, 2017).

### 3.1.5 The cases of CHMP1B and IST1

Two “accessory” ESCRT-III proteins, CHMP5 and CHMP1, join later during ESCRT assembly, as does the ESCRT-III-like Ist1 (increased salt tolerance 1).

Fundamental interest came from studies performed in yeast by (Rue et al., 2008). In this study, they provided evidence that Ist1 is a new component of the MVB-sorting pathway. Using three different approaches, they have shown that Ist1-CHMP1 and Vta1-CHMP5 form two complexes that are recruited and function at key steps late in the MVB-sorting pathway. By using a synthetic genetic analysis, they demonstrated that Ist1-CHMP1 and Vta1-CHMP5 form separate functional units: simultaneous deletion of one member of each functional complex causes a severe synthetic cargo-sorting phenotype and the formation of a class E compartment visible by EM (the class E compartment is an exaggerated prevacuolar endosome-like compartment that occurs in yeast due to ESCRT dysfunction). Second, their fluorescence microscopy analysis of the localization of GFP fusions of Ist1, CHMP1, and Vta1 in mutants lacking each of the other three members of this group of proteins revealed that CHMP1 specifically recruits its functional partner Ist1 to endosomes. Third, the results of pulldown assays using purified bacterially expressed proteins indicate that Ist1-CHMP1 and Vta1-CHMP5 form two distinct protein complexes.

They were not able to detect the interaction between Ist1 and CHMP1 in cell lysates, though, citing that the interaction is difficult to detect in vivo because this protein complex is



very unstable and transient in cells, owing to the fact that Ist1 and CHMP1 are constantly cycling on and off on endosomes. However, their fluorescence microscopy data indicate that CHMP1 recruits Ist1 to endosomes, which, coupled with the fact that Ist1 directly binds CHMP1 *in vitro*, strongly suggest that the Ist1-CHMP1 complex exists within yeast cells.

Both members of the Ist1-CHMP1 functional complex bind to Vps4 (Lottridge et al., 2006; Nickerson et al., 2006; Obita et al., 2007). According to the findings of (Rue et al., 2008), the Ist1-CHMP1 and Vta1-CHMP5 complexes clearly function late in MVB sorting, and given that at least three of these four components bind to Vps4 (CHMP5-Vps4 binding remains to be tested), it is very probable that these two complexes modulate Vps4 in conjunction with the Vps2-Vps24 subcomplex of ESCRT-III. In light of their new findings, (Rue et al., 2008) proposed an updated model for the stepwise assembly and later disassembly of the ESCRT machinery, summarized in figure I-28.

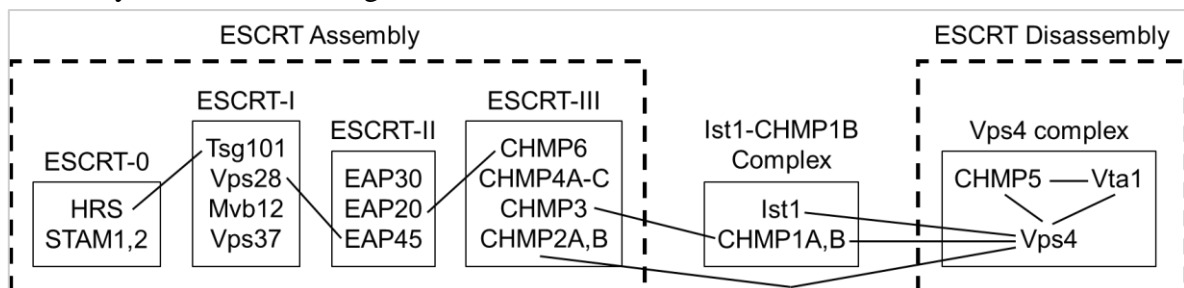


**Figure I-28. Stepwise ESCRT machinery assembly and disassembly.**  
Lines represent inter-complex interactions. Adapted from (Rue et al., 2008).

Xiao et al. later published the crystal structure of the N-terminal of the yeast equivalent of IST1 and examined its interaction with Did2/CHMP1B. Ist1NTD contains a fold similar to the ESCRT-III subunit CHMP3 despite a low level of sequence identity, indicating that Ist1 is a divergent member of the ESCRT-III subunit family. Ist1NTD specifically interacted with the MIM1 element within CHMP1B via a novel MIM1-binding site. Disruption of Ist1-CHMP1B interaction through mutagenesis led to a synthetic MVB-sorting defect in *x v c y 3* yeast (of note, deletion of IST1 by itself without deletion of vta1 or vps60 display no obvious phenotype in the yeast (Dimaano et al., 2007)). In mammalian cells, disruption of the Ist1-CHMP1B interaction produces a defect in abscission during mammalian cell division. These results validate the relevance of the Ist1-CHMP1B interaction observed. This characterization of the specific interaction between two ESCRT-III subunits, CHMP1B and Ist1, illustrated for the first time a potential mechanism by which ordered assembly of ESCRT-III is achieved via intermolecular association. Moreover, this complex also suggested a conformation of an ESCRT-III subunit in which intramolecular interaction led to an autoinhibited state (Xiao et al., 2009).

McCullough et al. further explored this complex between CHMP1B and IST by cryogenic electron microscopy. They showed that the CHMP1B conformation *in vitro* is sensitive to ionic strength, adopting the closed state at high ionic strength, and opening as ionic strength lowers, becoming available for the formation of conical tubes with closed-conformation IST monomers. This results in a one-start, double-stranded helical copolymer with a remarkable cationic interior, composed of an inner strand of “open” CHMP1B subunits

that interlock in an elaborate domain-swapped architecture and is encircled by an outer strand of “closed” IST1 subunits, as illustrated in Figure I-29 (McCullough et al., 2015).

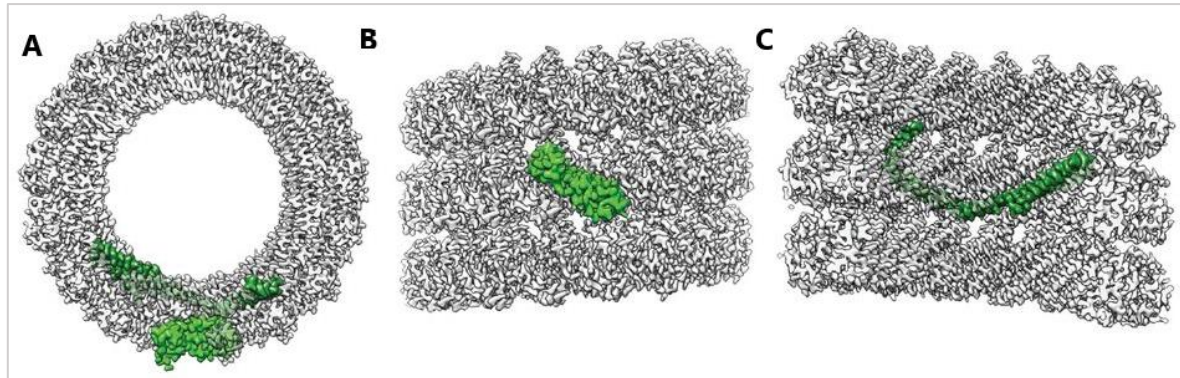


**Figure I-29. Helical polymers of CHMP1B and IST1.** (A) End-on view of the reconstructed IST1<sub>NTD</sub>-CHMP1B tube highlighting single subunits of IST1<sub>NTD</sub> (light green, outer strand) and CHMP1B (dark green, inner strand). (B) External view of the reconstructed helix with a highlighted IST1<sub>NTD</sub> subunit. (C) Internal cutaway view of the reconstructed helix, with a highlighted CHMP1B subunit. NTD = N-terminal domain. Adapted from (McCullough et al., 2015).

In the polymeric reactions that had been described so far, the ESCRT machinery assembles on the interior of a negatively curved, cytoplasm-filled membrane, and pulls the membrane toward itself to the fission point, “away” from the cytoplasm. In the in-vivo work with liposomes described by (McCullough et al., 2015), CHMP1B and CHMP1B/IST1 formed an external coat on positively-curved membranes. Figure I-30.

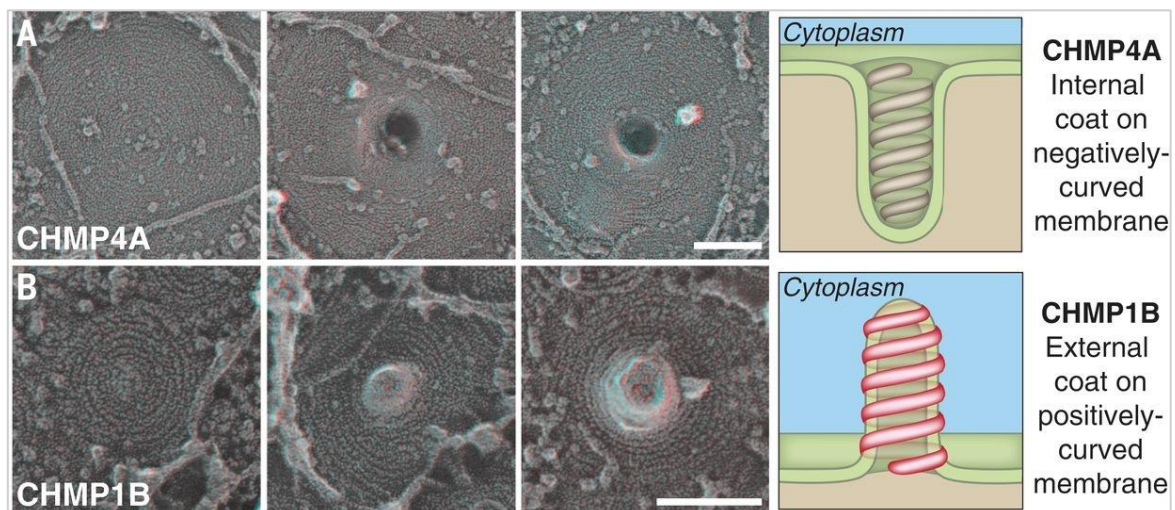


**Figure I-30. CHMP1B operates differently to other ESCRT-III members** (A) Series of filament spirals on the plasma membrane of COS-7 cells expressing CHMP4A1-164 show development of the outwardly directed protrusions previously associated with ESCRT-III filaments. Drawing highlights relationship between a CHMP4A conical spiral and a negatively curved plasma membrane tubule. (B) Series of filament spirals on the plasma membrane of COS-7 cells expressing FLAG-CHMP1B show development of invaginations directed into the cell. Drawing highlights relationship between a CHMP1B conical spiral and a positively curved plasma membrane tubule. Scale bars, 100 nm. From (McCullough et al., 2015)

### **3.2 To degrade or not**

The traditional ESCRT assembly model – that of an internal coat on a negatively curved membrane – nicely accounts for the intraluminal vesicle (ILV) formation that occurs inside the MVB: that which leads to further maturation of the MVB and degradation of its contents. The type of vesicle shown to be made by CHMP1B in the previous section is rather compatible with that of a recycling vesicle: one which forms in a direction away from the endosome, being able to escape it and explaining how cargo could avoid degradation and move back to membrane. Such a model would probably be dependent on regulation of CHMP1B itself and/or on specific association with different ESCRT-III partners.

### **3.3 The EGF receptor as an example for endocytic recycling controlled by ubiquitination**

The EGFR receptor is part of the four-membered family of the structure-related tyrosine kinase receptors ErbB/HER, composed of ErbB-1/HER1 (EGFR itself), ErbB-2/HER2, ErbB-3/HER3 and ErbB-4/HER4. These receptors are activated by polypeptidic growth factors ligands. Binding of their ligands induces the formation of homodimers, heterodimers and possibly higher-ordered oligomers of EGFR. EGF (endothelial growth factor), a 6 kDa polyprotein is the canonical binder of ErbB-1, which can additionally be activated in a similar fashion by the closely related transforming growth factor alpha (TGF- $\alpha$ ), amphiregulin, and other additional ligands capable also of activating other receptors of the family. ErbB-2/HER2 is the preferred dimerization partner of EGFR, further, the EGFR/ErbB2 heterodimer binds EGF with a 7-fold higher affinity than the EGFR homodimer (Li et al., 2012). The oligomerization that follows the binding of the ligands allow the establishment of the activation loop of the tyrosine kinase domains and activation of downstream signaling pathways which ultimately leads to cell proliferation and differentiation. This downstream signaling is mediated via a variety of well-established signaling pathways, such as Ras-Raf-MAPK, PI3-K/AKT, and JAK-STAT. The association with receptor activation and increased cell proliferation leads to the involvement of deregulated/excessive EGFR signaling in oncogenesis, especially in lung and breast cancer, which together form a majority of the incidence of new cancers worldwide.

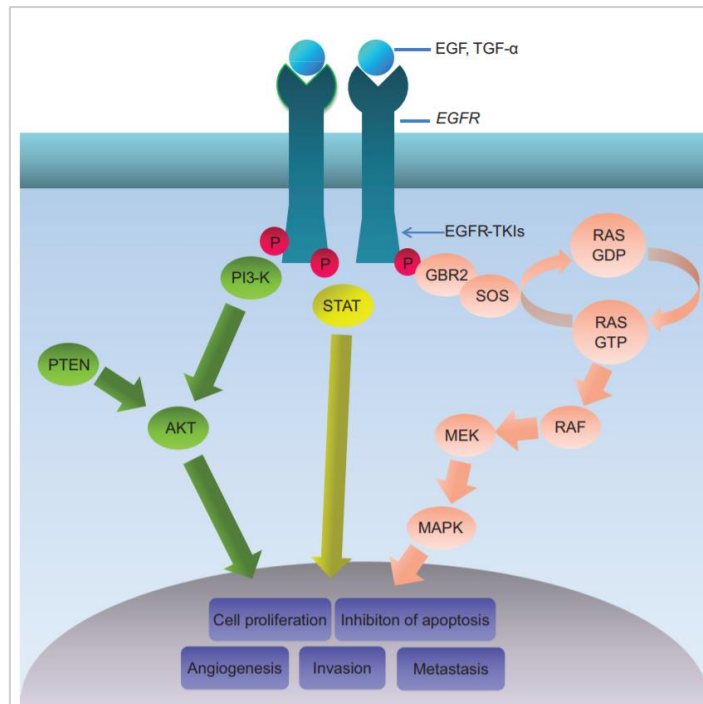


**Figure I-31. Overview of the major signaling pathways effectors of EGFR activation.** Shown also is the site of action tyrosine kinase inhibitors (EGFR-TKIs), one of the major therapeutic strategies for cancers related to EGFR signaling deregulation. From (Fang and Wang, 2014)

The EGF receptor is a transmembrane receptor, found embedded in the plasma membrane with an extracellular ligand-binding region, a transmembrane domain, and an intracellular region containing the kinase domain, the tyrosine residues to be phosphorylated upon ligand binding, and acceptor lysine residues critical to receptor ubiquitination. The Cbl E3-ligase associates with EGFR and promotes its ubiquitination that leads to its endocytosis (Melker et al., 2001; Visser Smit et al., 2009). Quantitative mass spectrometry demonstrated that more than 50% of all EGFR bound ubiquitin was in the form of polyubiquitin chains, primarily of the K63 type (Huang et al., 2006). At basal state, the recycling of EGFR is slow, but binding of EGF to EGFR results in acceleration of receptor internalization, with several lines of experimental evidences supporting the view that this acceleration is due to endocytosis of EGF-receptor complexes through clathrin-coated pits (Sorkin and Goh, 2008). Clathrin-independent endocytosis mechanisms also operate on EGFR, but this seems to be activated at much higher concentrations (near-saturation) of EGF (Boucrot et al., 2015). The internalization routes for the EGFR/ErbB2 heterodimer and the EGFR homodimer are summarized in Figure I-32.

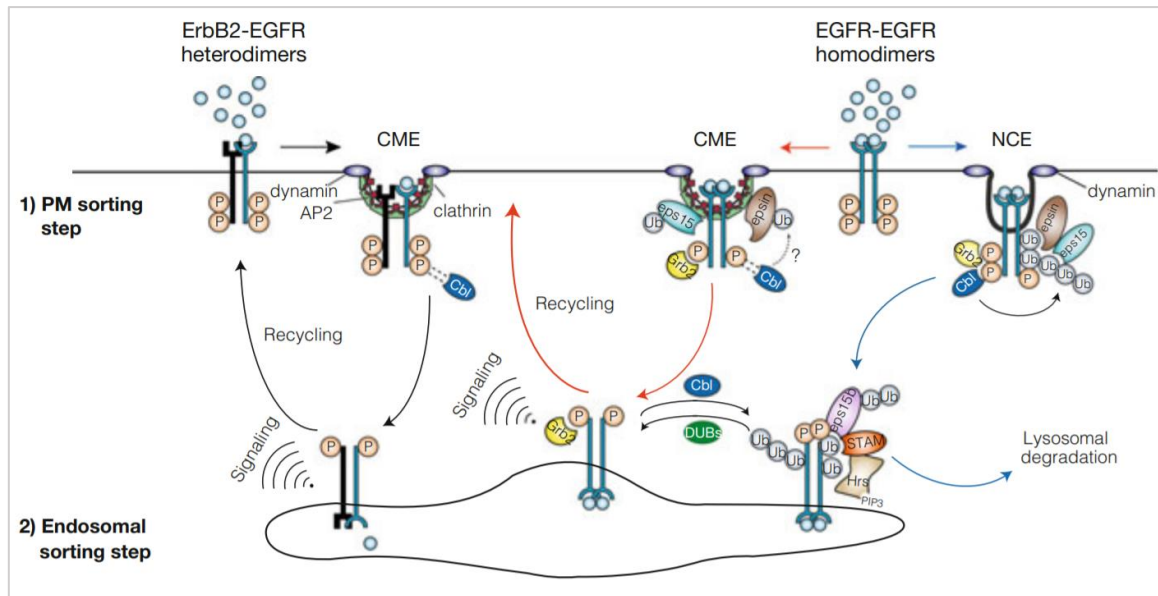


**Figure I-32. Endocytic routes for EGFR/ErbB2 heterodimer and the EGFR homodimer.** Activated, phosphorylated EGFR–ErbB2 heterodimers (left) are internalized via clathrin-mediated endocytosis (CME) but are poorly ubiquitinated due to the inefficient recruitment of Cbl. Once at the endosomal station, ligand dissociates from the receptor due to the more acidic pH of the endosomes, and the heterodimers are almost exclusively recycled back to the PM, thus sustaining signaling. On the other hand, at high dose of ligand, EGFR homodimers (right) can be internalized via both CME and non-clathrin endocytosis (NCE). EGFRs entering via CME (red lines) recruit endocytic adaptors (e.g., eps15 and epsin), AP2, and signaling proteins (e.g., Grb2) and are mainly recycled back to the PM. CME is required to sustain signaling from endosomes and/or through cycles of receptor recycling. Receptor ubiquitination by Cbl is not required for CME. In parallel, a fraction of EGFR, which is extensively ubiquitinated by Cbl, in complex with Grb2, at the PM, enter the cell via NCE and is primarily targeted to the lysosome for degradation. Receptors coming from both CME and NCE reach the endosomal station, where they are subjected to further regulation by ubiquitination/deubiquitination reactions. At the level of the early endosomes, ubiquitinated EGFRs are recognized by the ESCRT-0 complex (Hrs, STAM and apator protein EPS15b), which drives the receptor to degradation, as explained below. From (Caldieri et al., 2018).

Once internalized, recycling appears to be the default pathway of internalized EGFRs, and escape from this fate is achieved through efficient receptor ubiquitination. Once EGFR-Ub reaches the limiting membrane of the MVB, it is recognized by the ESCRT-0 complex (as explained previously). Retention of EGFR-Ub triggers a series of events leading to the sequential recruitment of ESCRT-I, ESCRT-II, and ESCRT-III complexes to the MVB membrane and packaging into ILVs. ILVs are then released from MVB into the lumen of the lysosome, the main hydrolytic compartment of the cell. During this process, E3 ligases and DUBs finely coordinate the fate of EGFR into the endocytic pathway. The E3 ligase Cbl, recruited at the plasma membrane, as explained before, remains associated with the EGFR all along the endocytic route (Melker et al., 2001; Umebayashi et al., 2008). This probably ensures maintenance of EGFR ubiquitination at later stages of trafficking.

Several DUBs are also involved in EGFR trafficking and sorting. Short interfering RNA knockdown of AMSH for example enhances the degradation rate of EGFR following acute stimulation, and ubiquitinated EGFR is a substrate for AMSH *in vitro*, indicating that AMSH would act at the endosomal level to protect EGFR from degradation and favoring its recycling (McCullough et al., 2004)

Cezanne-1, another DUB, also prevents receptor degradation and enhances EGFR signaling. These functions require the catalytic- and ubiquitin-binding domains of Cezanne-1, and involve physical interactions and transphosphorylation of Cezanne-1 by EGFR. This enzyme is overexpressed in breast cancer, and high transcript levels predict an aggressive disease course (Pareja et al., 2012). Similarly, USP2a localizes to early endosomes and associates with EGFR, stabilizing the receptor, and USP2a and EGFR proteins are coordinately overexpressed in non-small cell lung cancers (Liu et al., 2013; Zhu and Gao, 2017)

USP8 appears to be a major DUB protecting EGFR from degradation. Its role will be further explored in the next section.

### 3.4 The deubiquitinating enzyme USP8

The ubiquitin-specific protease USP8 has originally been identified as a growth-related DUB (Naviglio et al., 1998) that accumulated upon growth stimulation of starved human fibroblasts, and had its levels decreased in response to growth arrest induced by cell-cell contact. USP8 knockout mice present embryonic lethality; its conditional inactivation in adult mice causes fatal liver failure accompanied by a strong reduction or absence of several growth factor receptor tyrosine kinases (RTKs), like epidermal growth factor receptor, hepatocyte growth factor receptor (c-met), and ERBB3 (Niendorf et al., 2007). Its cognate gene localizes to the chromosome 15 in humans, two isoforms produced by alternative splicing have been identified. The canonical isoform 1 (Figure I-33 A) corresponds to a protein of 1118 amino-acid residues and ~127kDa. Isoform 2 differs from isoform I by the deletion of residues 35-111 and 601-629. Besides de C-terminus catalytic domain, USP8 possess a N-terminus microtubule interacting and trafficking (MIT) domain, a rhodanese domain and two STAM SH3 interaction domains (Figure I-33 B).

A					
	10	20	30	40	50
MPAVASVPKE	LYLSSSLKDL	NKKTEVKPEK	ISTKSYVHSA	LKIFKTAEEC	
60	70	80	90	100	
RLDRDEERAY	VLYMKYVTVY	NLIKKRPDFK	QQQDYFHSIL	GPGNIKKAVE	
110	120	130	140	150	
EAERLSESLK	LRYEAEVRK	KLEEKDRQEE	AQRLQQRQE	TGREDGGTLA	
160	170	180	190	200	
KGSLENVLDS	KDKTQKSNGE	KNEKCETKEK	GAITAKELYT	MMTDKNISLI	
210	220	230	240	250	
IMDARRMQDY	QDSCILHSLS	VPEEAISPGV	TASWIEAHLF	DDSKDTWKKR	
260	270	280	290	300	
GNVEYVLLD	WFSSAKDLQI	GTTLRSLKDA	LFKWESKTVL	RNEPLVLEGG	
310	320	330	340	350	
YENWLLCYPQ	YTTNAKVTPP	PRRQNEEVS	SLDFTYPSLE	ESIPSKPAAQ	
360	370	380	390	400	
TPPASIEVDE	NIELISGQNE	RMGPLNISTP	VEPVAASKSD	VSPIIQPVPS	

410	420	430	440	450		
IKNVPQIDRT	KKPAVKLPEE	HRIKSESTNH	EQQSPQSGKV	IPDRSTKPVV		
460	470	480	490	500		
FSPTLMLTDE	EKARIHAETA	LLMEKNKQEK	ELRERQQEEQ	KEKLRKEEQE		
510	520	530	540	550		
QKAKKKQEAE	ENEITEKQKQ	AKEEMEKKES	EQAKKEDKET	SAKRGKEITG		
560	570	580	590	600		
VKRQSKSEHE	TSDAKKSVED	RGKRCPTPEI	QKKSTGDVPH	TSVTGDSGSG		
610	620	630	640	650		
KPFKIKGQPE	SGILRTGTFR	EDTDDTERNK	AQREPLTRAR	SEEMGRIVPG		
660	670	680	690	700		
LPSGWAKFLD	PITGTFRYYH	SPTNTVHMYP	PEMAPSSAPP	STPPTHKAKP		
710	720	730	740	750		
QIPAERDREP	SKLKRYSYSSP	DITQAIQEEE	KRKPTVTPTV	NRENKPTCYP		
760	770	780	790	800		
KAEISRLSAS	QIRNLNPVFG	GSGPAL	TGLR	NLGNTCYMNS	ILQ	CLCNAPH
810	820	830	840	850		
LADYFNRCY	QDDINRSNLL	GHKGEVAEEF	GIIMKALWTG	QYRYISPKDF		
860	870	880	890	900		
KITIGKINDQ	FAGYSQQDSQ	ELLLFLMDGL	HEDLNKADNR	KRYKEENNDH		
910	920	930	940	950		
LDDFKAAEHA	WQKHKQLNES	IIVALFQGQF	KSTVQCLTCH	KKSRTFEAFM		
960	970	980	990	1000		
YLSLPLASTS	KCTLQDCLRL	FSKEEKLTDN	NRFYCSHCRA	RRDSLKIEI		
1010	1020	1030	1040	1050		
WKLPPVLLVH	LKRFSYDGRW	KQKLQTSVDF	PLENLDSLQY	VIGPKNNLKK		
1060	1070	1080	1090	1100		
YNLFSVSNHY	GGLDGGHYTA	YCKNAARQRW	FKFDDHEVSD	ISVSSVKSSA		
1110						
AYILFYTSLG	PRVTDVAT					

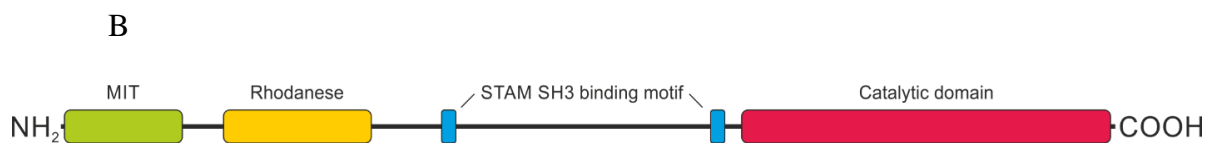


**Figure I-33. USP8 isoform I.** A. Amino acid sequence; cysteine and histidine box, hallmarks of the cysteine protease category of DUBs, are highlighted in yellow. B. Domain organization.

USP8 interacts with the E3 ligase NRDP1 (Wu et al., 2004b), leading to altered effects on cytokine receptor sorting and processing (De Ceuninck et al., 2013). It also regulate a number of cellular processes such as  $\beta$ -cell mitophagy (Pearson et al., 2018). USP8 also suppresses apoptosis by stabilizing FLICE-like inhibitory protein (FLIP) (Jeong et al., 2017) and has additional roles in ciliogenesis, sperm acrosome formation, hedgehog signaling, autophagy and neurological disorders as well as T-cell function as recently reviewed in (Dufner and Knobeloch, 2019).

### **3.5 USP8 and the regulation of ESCRT-0**

Association of E3 ligases and DUBs with the ESCRT complexes is known to mediate endocytic trafficking through reversible ubiquitination of cargo; however, the ESCRT-III complexes themselves are also subjected to regulation by ubiquitin linkage. The ESCRT-0 protein STAM interact with two DUBs, USP8 and AMSH (associated molecule with the SH3 domain of STAM - also known as STAMBIP) via the SH binding motif of these DUBS (Berlin et al., 2010; Kato et al., 2000; Sierra et al., 2010). A first set of experiments (Berlin et al., 2010) have demonstrated that USP8 associates with STAM to mediate direct deubiquitination of activated EGFR, thereby stabilizing the receptor against down-regulation by the lysosome. Further, another study (Niendorf et al., 2007) demonstrated that a conditional mouse knock-out of USP8 is characterized by marked destabilization of Hrs and STAM, with cells exhibiting aberrantly enlarged early endosomes and a strong reduction of EGFR levels. AMSH also regulates the ubiquitination levels of HRS and STAM. Interestingly, cells expressing a catalytically inactive mutant of AMSH show hyperubiquitination but not increased degradation of STAM1 and Hrs suggesting that these two proteins are ubiquitinated by non-degradative chains that are a substrate for AMSH (Sierra et al., 2010). This hypothesis is consistent with the fact that AMSH is a K63-specific DUB. In contrast USP8 hydrolyses both K63 and K48 ubiquitin chains, and this has been proposed by Clague and Urbé as an explanation for differential effects on STAM and HRS (Clague and Urbé, 2006).

### **3.6 USP8 and the regulation of ESCRT-III: CHMP1B**

As mentioned before, ESCRT-III members can recruit deubiquitinase enzymes via their MIM domains for the deubiquitination of sequestered cargo. CHMP1B is able to recruit USP8 to the endosomes by interaction with the MIT domain of USP8, which is dispensable for its catalytic activity but is essential for its localization to endosomes (Row et al., 2007). The MIT-deleted USP8 mutant is unable to reverse the blockade of EGFR degradation imposed by small interfering RNA-mediated depletion of USP8, pointing to the importance of MIT-associated functions to the proper functioning of USP8 in EGFR processing. In the laboratory, a former PhD student, Xenia Crespo-Yañez, mapped the interaction with USP8 to  $\alpha$ -helices 4, 5, and 6 of CHMP1B (Crespo-Yañez et al., 2018). She showed that CHMP1B is ubiquitinated *in vivo* and its data indicated that USP8 deubiquitinates CHMP1B. She further showed that ubiquitination of CHMP1B is dynamically regulated in response to EGF within 5 to 15 minutes following EGF stimulation and that concomitant accumulation of ubiquitinated dimers of CHMP1B is observed at cellular membranes. Furthermore, CHMP1B ubiquitination was required for proper EGFR degradation and CHMP1B function as shown both in human cells and in the *Drosophila* fly models. Hence, USP8 may indirectly contribute to EGFR trafficking through regulation of CHMP1B ubiquitinated status. Her results also suggested that dynamic deubiquitination of CHMP1B at the endosomal membrane by USP8 would favor CHMP1B polymerization into the growing ESCRT-III complex, a model that stays to be further documented.



### 3.7 USP8 and EGFR endocytosis ó the big picture

As seen above, via its multiple actions on the ESCRT machinery, USP8 has the possibility to control the fate of EGFR at the endosomal levels. Corroborating evidence comes from the study of Mizuno and colleagues, who demonstrated *in vitro* the deubiquitination of EGFR by purified USP8 (Mizuno et al., 2005). They also showed a reduced ubiquitination level of EGFR and its delayed degradation in EGF-stimulated cells upon USP8 overexpression and partially localized this interaction to endosomes. Moreover, USP8, which is recruited by Hrs-STAM, directly binds with ubiquitinated EGFR to deubiquitinate it (Komada, 2008).

Clinical interest stems from this regulation of EGFR by USP8. As exposed in chapter one, it might be behind one of the mechanisms leading to Cushing’s disease (at least in patients presenting tumors expressing mutated forms of USP8).

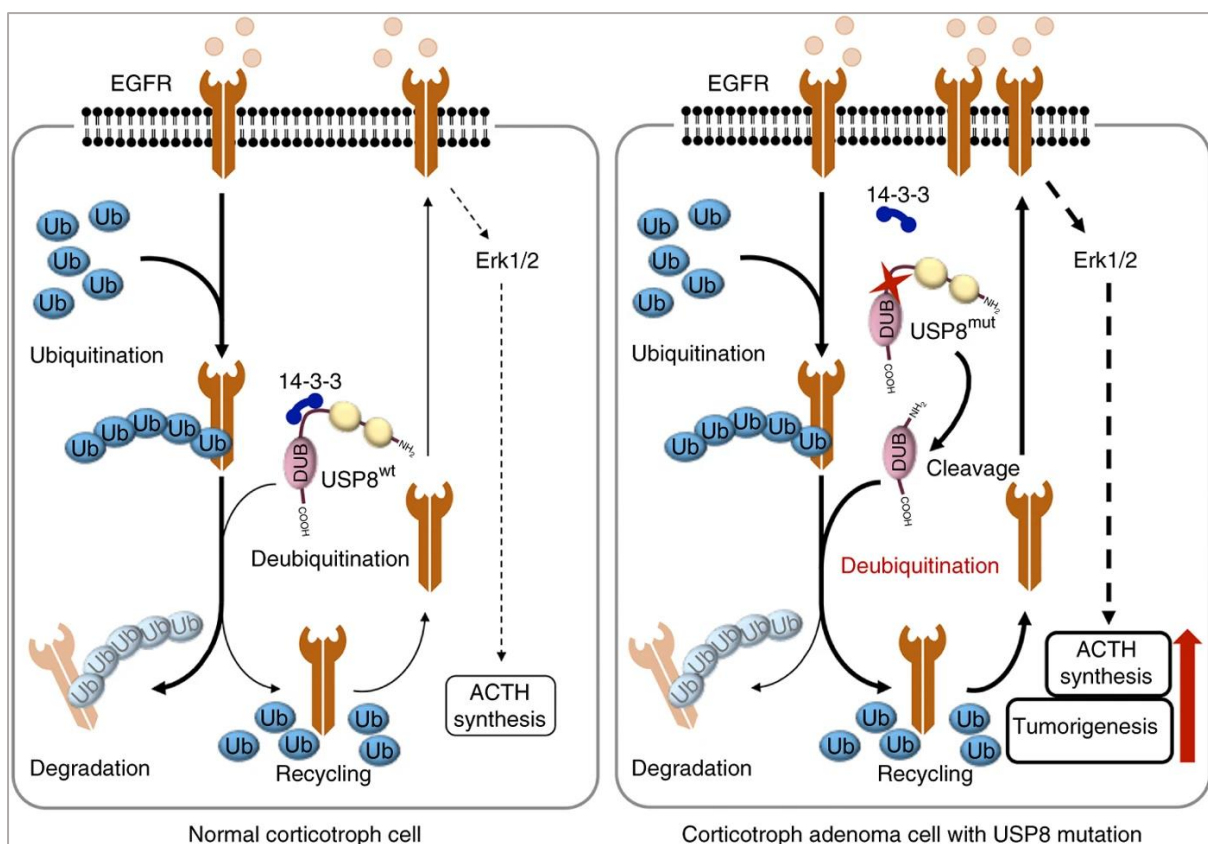


**Figure I-34. De-regulated EGFR processing by mutated USP8:** proposed mechanism of Cushing’s disease. EGFR is able to mediate POMC expression and ACTH synthesis via a Erk1/2 mediated pathway. Ubiquitinated EGFR is continuously internalized into the cell. The DUB USP8 is capable of determining EGFR fate between degradation, by promoting its recycling, by deubiquitinating it, leading to maintained Erk 1/2 signaling. Mutated USP8 strongly diminishes its binding affinity for the down-regulatory 14-3-3 proteins, leading to a constitutively active USP8 due to the generation of a cleaved USP8 C-terminus fragment. This would lead to excessive recycling of internalized EGFR, being responsible for tumorigenesis and sustained ACTH synthesis. From (Reincke et al., 2015).

In addition to Cushing's disease, clinical interest of USP8 inhibition also exists for lung cancer treatment, which remains the leading cause of cancer deaths worldwide (Sung et al., 2021), with non-small cell lung cancer (NSCLC) being the most common form. Presently, EGFR tyrosine kinase inhibitors (EGFR-TKIs) such as gefitinib or erlotinib are used in a subset of NSCLC patients, as it has been reported that somatic mutations in EGFR confer sensitivity to these agents (Lynch et al., 2004; Paez et al., 2004; Pao et al., 2004). However, many patients develop resistance to the drugs after varying periods of time from the acquisition of a secondary mutation (T790M) in the EGFR gene or and/or amplification of the MET encoding gene (Engelman et al., 2007; Kobayashi et al., 2005; Kosaka et al., 2006; Pao et al., 2005). Since USP8 is overexpressed in lung cancers; it may contribute to EGFR or other RTKs stabilization and resistance to chemotherapy. Therefore, USP8 inhibition may constitute an interesting strategy for the development of treatments for cancers resistant to epidermal growth factor receptor tyrosine kinase inhibitors.

In line of this hypothesis, Byun et al demonstrated that knockdown of USP8 selectively kills gefitinib-resistant NSCLCs, (while having little toxicity toward normal cells), that genetic silencing of USP8 led to the downregulation of EGFR as well as several other receptor tyrosine kinases, including ERBB2, ERBB3, and MET. They also performed experiments with a mouse xenograft model using gefitinib-resistant and -sensitive NSCLC cells, where the USP8 inhibitor led to significant reductions in tumor size in both conditions (Byun et al., 2013).

Evidences for reciprocal cross-talk between USP8 and EGFR came from a number of other studies. Ciliogenesis is an example of a developmental process in which EGFR regulates USP8. The primary cilium, is a solitary organelle that emanates from the cell surface of most mammalian cell types during growth arrest. Increasing evidence suggests that primary cilia are key coordinators of signaling pathways during development and in tissue homeostasis and, when defective, are a major cause of human diseases and developmental disorders (now commonly referred to as ciliopathies) (Satir et al., 2010). Ciliogenesis is generally inhibited in dividing cells, and in their search to better understand the factors behind this inhibition, Kasahara and colleagues were able to determine that EGFR activation suppresses ciliogenesis by inducing the phosphorylation of different substrates and the activation of USP8 by phosphorylation, which in turns deubiquitinates effectors of the ciliogenesis pathway (Kasahara et al., 2018).

### **3.8 Objectives of the thesis**

USP8 somatic mutations have been found in corticotroph tumors of patients with Cushing's disease. The underlying mutations in USP8 were shown to promote the generation of an activated catalytic fragment of USP8. USP8 was identified as a regulator of EGFR levels, so one of the current hypotheses is that, due to diminished ubiquitination, up-regulation of the EGFR is behind the pathogenesis of Cushing's disease. Indeed, sustained EGFR signaling was identified as a cause of enhanced promoter activity of the gene encoding proopiomelanocortin (POMC), the precursor of ACTH. A first objective of this thesis was to find new inhibitors of USP8 catalytic activity reducing ACTH secretion, with therapeutical potential in Cushing's disease. This is explored in chapter 1 of the results section.

The recycling of EGFR is a canonical example of endosomal-mediated recycling of membrane receptors. Much evidence has accumulated for the regulation of EGFR by USP8 at the endosomal level. The ESCRT-III protein CHMP1B has been demonstrated to be required for proper EGFR degradation, is itself deubiquitinated by USP8, and is dynamically ubiquitinated in-vivo upon EGF exposure in cultured cells. Furthermore, its additional mode of functioning in close partnerships with Ist1, that may promote the formation of positively-curved vesicles reminiscent of recycling vesicles originating from the MVB, really spark-up interesting putative role of this protein as an effector of the EGFR recycling pathway. A second objective of this thesis was then to stabilize and identify CHMP1B-containing complexes occurring in-vivo in cell cultures of human origin to better understand its function and/or regulation. This is explored in chapter 2 of the results section.

# RESULTS

# 1 1<sup>ST</sup> CHAPTER 6 Halogenated salicylanilides inhibit the catalytic activity of USP8 in vitro and ACTH secretion in pituitary cells

This part of the thesis describes a fully automated screening campaign of 2,240 FDA-approved drugs that led to the identification of new chemical inhibitors of USP8 catalytic activity. This screen was performed at the CMBA screening platform by Dr. C. Barette using an automated enzymatic assay previously setup in the laboratory and the USP8 catalytic domain of the protein previously purified by Dr. C. Aguilar-Gurrieri. The enzymatic inhibitory potential of selected hits on USP8, papain or UCHL3 was analyzed by Mrs. M. Mortier, while I performed the search for analogs, the characterization of hits and analogs activity on ACTH secretion and POMC expression, the preliminary docking studies and the search for known pharmacological information on the selected hits. These results will be submitted for patenting on the one side and academic publication, most probably to the journal “Frontiers in pharmacology” on the other side. They are presented here on an article format

## 1.1 Introduction

Cushing’s disease is a rare and severe disease in which a pituitary tumor (corticotroph adenoma) causes an excess of adrenocorticotrophic hormone (ACTH) resulting in an increased release of cortisol and adrenal androgens by the adrenal gland cortex (Pivonello et al., 2017) (Fig.1). Patients suffer from central obesity, skin atrophy, muscle wasting, cardiovascular disease, diabetes, metabolic syndrome, osteoporosis, disturbed mood and impaired reproductive function (Barnett, 2016; Ioachimescu, 2018; Liddle, 1977; Shibli-Rahhal et al., 2006). These morbidities are related to an excess of corticoid hormones and define the Cushing’s syndrome. This syndrome can also result from extra pituitary tumor cells secreting ACTH or adrenocortical tumor secreting corticoid hormones, or be induced by chronic glucocorticoid treatment.

First-line treatment of Cushing’s disease is trans-sphenoidal surgery allowing a remission rate of 70 to 80% (Cristante et al., 2019; Lefournier et al., 2003; Pivonello et al., 2015; Sarkis et al., 2019). However, other therapeutic strategies are mandatory for the patients who are initially not cured by neurosurgery or who show recurrences after neurosurgery. These strategies include radiotherapy, bilateral adrenalectomy (and lifelong glucocorticoid replacement therapy) or the use of drugs that inhibit either pituitary ACTH release or adrenal cortisol synthesis or block activation of the glucocorticoid receptor. These drugs all suffer from a limited efficacy and produce many side effects, some of which severe. As for examples, metyrapone inhibits cortisol synthesis and the antimycotic drug ketoconazole inhibits the early steps of steroidogenesis. Ketoconazole, however, also inhibits androgen synthesis and may cause liver damage (Lonser et al., 2017; Pivonello et al., 2015; Sarkis et al., 2019).

Three independent human genetic sequencing projects have revealed that the gene encoding the ubiquitin specific protease USP8 is frequently mutated in tumor from Cushing’s disease patients (1-3). USP8 (also known as UBPY) is a cysteine protease that belongs to the

ubiquitin-specific processing protease family. Mutations in USP8, identified in the context of Cushing's disease cluster in a region upstream of the catalytic domain that binds the 14-3-3 adaptor protein (LKRSYS718SP720) (Figure R1-01). The 14-3-3 protein functions as a negative regulator of USP8 activity. The most frequent mutation on USP8 affects the serine residue S718, the phosphorylation of which is necessary for 14-3-3 binding, and/or the close proline P720, that is also a key residue for 14-3-3 binding. These mutations are dominant: they abolish or reduce the ability of USP8 to bind 14-3-3, causing a constitutive deubiquitinating activity and subsequent deregulation of USP8 targets and cell homeostasis. Interestingly, no such USP8 mutations were detected in non-corticotroph pituitary adenomas, indicating a high specificity of ACTH-secreting adenomas.

In pituitary corticotroph cells, the epidermal growth factor receptor (EGFR) activates a mitogen activated protein kinase (MAPK)-dependent pathway that stimulates the expression of the ACTH precursor proopiomelanocortin (POMC) and ACTH secretion (Perez-Rivas and Reincke, 2016). Accordingly, inhibitors of EGFR, such as gefitinib or lapatinib, down-regulate POMC expression and ACTH secretion in cultured pituitary cells and have been proposed as therapeutic drugs for suppressing ACTH in corticotroph adenomas (Asari et al., 2019; Ben-Shlomo and Cooper, 2017; Ma et al., 2015).

Very interestingly, the EGFR is one of the main targets of USP8 which degradation and recycling is tightly controlled by ubiquitination. Gain-of-function mutations of USP8 found in Cushing's disease patients interfere with EGFR trafficking to lysosomes and degradation and favor its recycling back to the plasma membrane (Reincke et al., 2015). Stabilization of EGFR in cells expressing USP8 gain-of-function mutations may therefore be the main cause of enhanced POMC expression and ACTH production.

Noteworthy, USP8 gene silencing in primary USP8-mutated corticotroph adenoma cells efficiently reduced ACTH secretion. USP8 knock-down or chemical inhibition of USP8 also reduce the growth of various kind of cancer cells (Colombo et al., 2010; Fauvarque et al., 2016; Han et al., 2020; Jian et al., 2016). Finally, a previously described USP8 inhibitor (Colombo et al., 2010) induces both down-regulation of EGFR and POMC expression levels and significantly reduces ACTH secretion in AtT-20 mice pituitary cells (Jian et al., 2015). These results indicate that inhibiting USP8 is a relevant strategy to reduce ACTH secretion. This compound was developed by further chemical synthesis and biological evaluation of cyanopyrazines compounds identified in a screening campaign for inhibitors of USP7 from a library of chemically diverse compounds. However this compound does not display enough selectivity among DUBs family (Ritorto et al., 2014).

USP8 is thus a promising target in a therapeutic perspective for Cushing's disease patients. This is particularly the case for patients carrying USP8 gain-of-function mutations in view of personalized treatment, and possibly for patients with other alterations, at least if USP8 inhibition allows efficient decrease in ACTH secretion per se. Presently, published or patented USP8 enzymatic inhibitors do not reach sufficient selectivity among ubiquitin proteases to be considered as therapeutic leads and/or present toxicity requiring further development.

In an effort to find new chemicals inhibiting the enzymatic activity of USP2, a related DUB and a regulator of cell cycle, DNA repair, and tumor cell growth (Bonacci and Emanuele, 2020), we screened a subset of the ChemBioFrance consortium's Chimiotèque Nationale (<https://chembiofrance.cn.cnr.fr/fr/composante/chimiotheque>). This led to the selection of

PCR6236, a heterocyclic naphthoquinone (Fauvarque et al., 2016), that actually displays a much more potent and relatively selective inhibition of USP8 compared to USP2 and other DUBs. This compound however includes a naphthoquinone group that may act as an oxidizing chemical group irreversibly inhibiting USP8 and possibly leading to increased toxicity and hindered drug development (Mortier M. and Fauvarque M.O., personal communication).

To circumvent the lengthy combined processes of drug discovery and drug development involved in delivering new therapeutical tools from completely new molecules, we chose then to proceed with a drug repurposing strategy, and screen for collections of existing drugs that are either approved or in advanced steps of development.

## 1.2 Results and discussion

### 1.2.1 Selection of USP8 inhibitors

In order to screen for new inhibitors of USP8, the Prestwick library including 1,280 FDA-approved drugs or compounds under clinical development was chosen to select hits presenting a high degree of druggability. In addition, we identified and ordered 960 additional FDA-approved drugs from commercial suppliers herein referred as CMBA-FDA library, and thus setup a final library of 2,140 compounds (1280+960).

The screening procedure was based on an enzymatic assay using a ubiquitin-conjugated to fluorescent leaving group substrate (i.e. ubiquitin-acetylmethylcoumarin (Ub-AMC, which has been miniaturized to adapt the 96-well format. We determined the lowest values of substrate for which the initial velocity of the enzyme rises linearly with the increasing substrate concentration. Moreover, the robustness and reliability of the assay had been verified reaching a statistical Z' factor of 0.75 (where  $0.5 < Z' < 1$ ). The bio-inactive control, showing no inhibition of USP8-CD, was the solvent DMSO at 0.5 % (corresponds to 0% inhibition). The bioactive control, mimicking the desired inhibitory activity, was the reaction mix without USP8-CD (corresponds to 100% inhibition). Primary screening was performed in triplicate at a final concentration of 50  $\mu$ M in DMSO 0.5% and USP8-CD catalytic activity was monitored both before adding the substrate (T0) and after 2 hours of incubation at room temperature (TF).

Data analysis was done using the in-house TAMIS software (<http://www.bge-lab.fr/Pages/CMBA/TAMIS.aspx>): raw data from each compound-containing well, were normalized using the mean values of bioactive and bio-inactive controls (100% and 0% inhibiting activity, respectively) to obtain a percentage of inhibition activity for each compound value. The percentage of inhibition was calculated as follows:  $((\text{Sample raw value} - \text{bioinactive controls mean value}) * 100) / (\text{Bioactive controls mean value} - \text{bioinactive controls mean value})$ ). A set of 320 compounds inducing more than 30% inhibition of USP8-CD enzymatic activity were considered as primary hits. Primary hits were tested in triplicate at the same 50 $\mu$ M final concentration allowing for the selection of 36 confirmed hits showing more than 50% of USP8 catalytic activity inhibition. Confirmed hits were then tested in triplicate at 5  $\mu$ M, and 7 hits (2 from Prestwick and 5 from CMBA-FDA) showing more than 85% inhibition at 5  $\mu$ M concentration were kept for further analysis (Fig. R1-01).

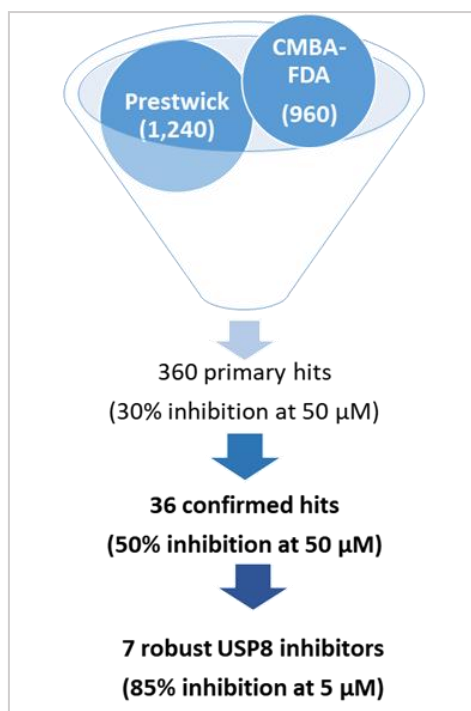


**Figure R1-01: Hit selection process for efficient USP8 catalytic inhibitors**

### 1.2.2 Hit validation and selectivity assay

Hit validation was performed using freshly ordered compounds and a different fluorescent probe as substrate: ubiquitin-rhodamine (Ub-Rho) (Table R1-01, Figure R1-02). Since fluorescence emitted by rhodamine (excitation peak at 546 nm and an emission peak at 568 nm) is different than that emitted by AMC (excitation peak at 341 nm and an emission peak at 441 nm), this renders unlikely an artefact due to direct inhibition of fluorescence emission.

Selectivity towards DUBs was then assessed by testing the inhibitory efficacy of hits over a non-DUB cysteine protease (papain), while selectivity towards USP8 compared to other DUBs was assessed by monitoring the inhibitory potential of each compound towards either USP8 full length (FL) or catalytic domain (CD) versus a more distant DUB, UCHL3 (Table R1-01). All compounds were active in the  $\mu\text{M}$  range against USP8 while they were inactive (except one) against UCHL3.

### 1.2.3 Reversibility assay

DUB activity relies on a conserved catalytic cysteine residue which is particularly sensitive to oxidation by reactive oxygen species (ROS) (Lee et al., 2013). Selected compounds were tested for the reversibility of the USP8 inhibition by a dilution assay (Table R1-01). All but one of the compounds (gallotannin) inhibited USP8 in a reversible manner.



Compound	Formula	Molecular weight	Pharmacology	USP8-CD inhibition		USP8-FL inhibition	UCHL3 inhibition	Papain inhibition	Reversibility of USP8 inhibition	Druggability vs effect
				Ub-AMC	Ub-Rho	Ub-Rho	Ub-Rho			
<b>Closantel</b>	C22H14Cl2I2N2O2	663.08	anthelmintic (Swan, 1999)	2.5	1.2	7.5	>20	>=20	Reversible	Good
<b>Gallotannin</b>	C76H52O46	1701.2	antioxidant, anti-inflammatory, antiviral, and antiproliferative (Kiss and Piwowarski, 2018; Smeriglio et al., 2017)	2	0.25	5.5	>10	>=10	Irreversible	Good
<b>MIF Antagonist</b>	C34H24N6Na4O16S4	992.80	investigative anti-inflammatory (Cvetkovic et al., 2005; Lubetsky et al., 2002)	3.5	0.4	0.4	6	>=50	Reversible	Good
<b>Zafirlukast</b>	C31H33N3O6S	575.69	leukotriene receptor antagonist - asthma medication (Adkins and Brogden, 1998; Kelloway, 1997; Trinh et al., 2019)	7.5	7	4	>20	None	Reversible	Good
<b>Docusate sodium salt</b>	C20H37NaO7S	444.6	laxative (Fakheri and Volpicelli, 2019; Sykes, 1994)	5	3.6	8	>20	None	Reversible	Irrelevant
<b>Evan's blue</b>	C34H24N6Na4O14S4	960.8	diagnostic agent (Béchet et al., 2016; Yao et al., 2018)	1.6	0.25	0.5	9	None	Reversible	Irrelevant
<b>Methylcobalamine</b>	C63H91CoN13O14P	1344.4	vitamin, cofactor in DNA synthesis (Kräutler, 2012)	7	10	N/A	N/A	N/A	N/A	Irrelevant

**Table R1-01. Hit characterization on USP8, UCHL3 and papain catalytic activity in vitro.** Doses are shown in  $\mu\text{M}$ , and correspond to 50% inhibition of the maximal activity observed in control conditions.

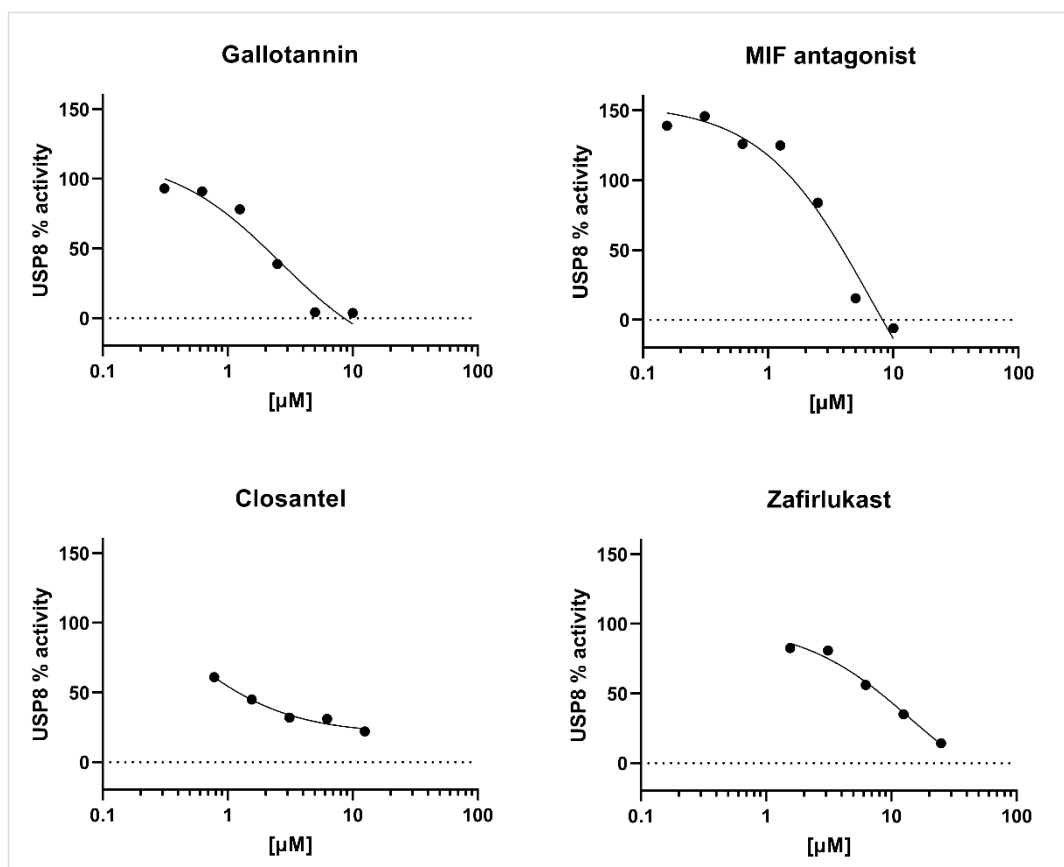


**Figure R1-02: Monitoring the inhibition of 4 druggable confirmed hits on USP8-CD** using the following substrates: Ub-AMC (gallotannin and MIF antagonist) and Ub-Rho (closantel and zafirlukast). Results from one experiment.

#### 1.2.4 Elimination of irrelevant hits and cytotoxicity assays

Two hit compounds issued from the Prestwick library were considered irrelevant as they present poor exploitable pharmacokinetics properties, Docusate sodium salt in particular corresponds to a laxative agent with untoward pharmacodynamics (Table R1-01).

Hits obtained from the FDA approved drugs are predicted to satisfy MedChem properties and we indeed observed no major toxicity of hits on either HEK293T human or AtT-20 mice pituitary cell models as assessed through the monitoring of the cells' reducing capacity mitochondrial ATPase activity (PrestoBlue® assay, Molecular Probes) using a fully automated protocol at the CMBA robotic platform. All compounds showed proper solubility and no cell toxicity and were kept for further analysis.

#### 1.2.5 Selection of compounds lowering ACTH secretion in pituitary cells

The therapeutic aim to select USP8 inhibitors is here to dampen ACTH secretion by pituitary cells. We therefore used the mouse AtT-20 pituitary cell line as a powerful and well-characterized model to monitor ACTH secretion using an enzyme immunoassay (EIA) kit which was adapted to the automated robotic platform in a 96-well format.

Confirmed hits issued from the screening of Prestwick, FDA-CMBA libraries were tested at three doses (2.5, 5 and 10μM) in triplicate on ACTH secretion using an ELISA assay

(data not shown). From this, we selected closantel as the only molecule showing a robust inhibition of ACTH secretion (Fig. R1-03 A). The observed inhibition was as strong as that observed with DUB-IN-2 (as tested at 5  $\mu$ M), a previously described USP8 inhibitor (Kageyama et al., 2020). It therefore represents a lead compound for further optimization aiming at enhancing its efficacy and specificity towards USP8 and ACTH secretion. We also showed that the inhibitor PCR6236, previously selected in our lab, was efficient in lowering ACTH secretion at a low concentration of 0.5  $\mu$ M (Fig. R1-03 A). This is consistent with the fact that PCR6236 inhibits USP8 catalytic activity with an  $IC_{50}$  of 40 nM (Fauvarque et al., 2016).

Preliminary docking studies using the program Autodock Vina (<https://mucle.com/apps/1-click-docking/>) indicate that Closantel may bind the ubiquitin binding domain of USP8-CD and therefore likely prevent substrate recognition by USP8 (Figure R1-03 B).

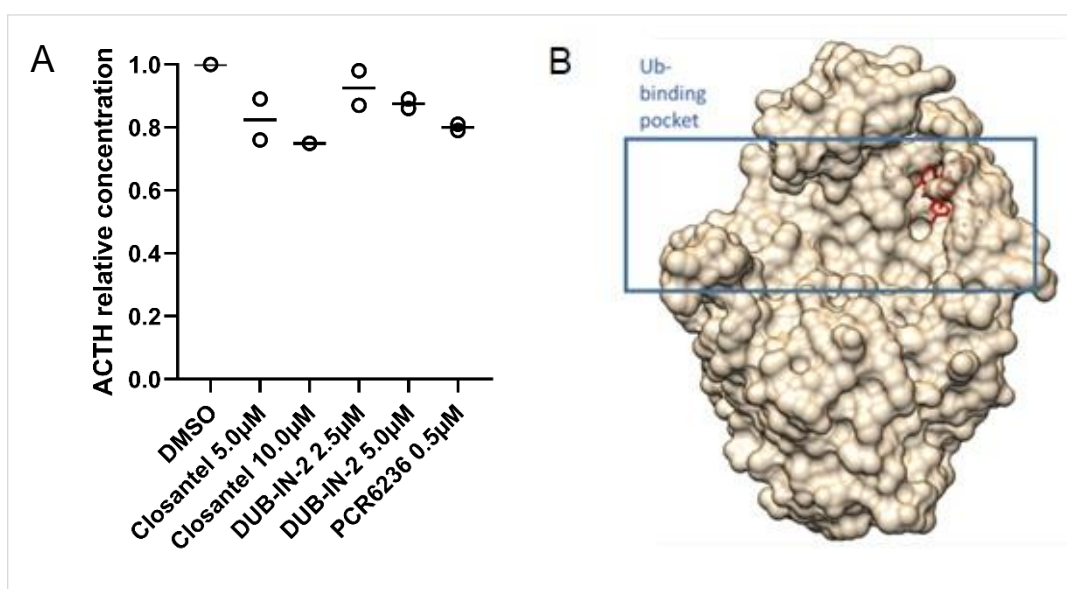


**Figure R1-03: Closantel inhibits ACTH secretion and is predicted to bind to USP8-CD in-silico.** **A.** Secreted ACTH was monitored on AtT-20 cells supernatant after 24 hours incubation with the indicated compounds. Shown are the levels relative to the DMSO control condition. Duplicate analysis. Bar at mean. Results from one experiment done with duplicate conditions. **B** Docking analysis reveals putative binding in the ubiquitin binding domain of USP8-CD. Chemical groups that potentially directly interact with USP8 are highlighted.

### 1.2.6 Closantel and analog compounds efficacy/versus cytotoxicity

Closantel belongs to the family of halogenated salicylanilides that also includes niclosamide, oxiclozanide and rafxanide (Figure R1-04 A), that were all tested on ACTH secretion levels on AtT-20 mice corticotroph cells, as well as the salicylanilide backbone itself (Figure R1-04 B).

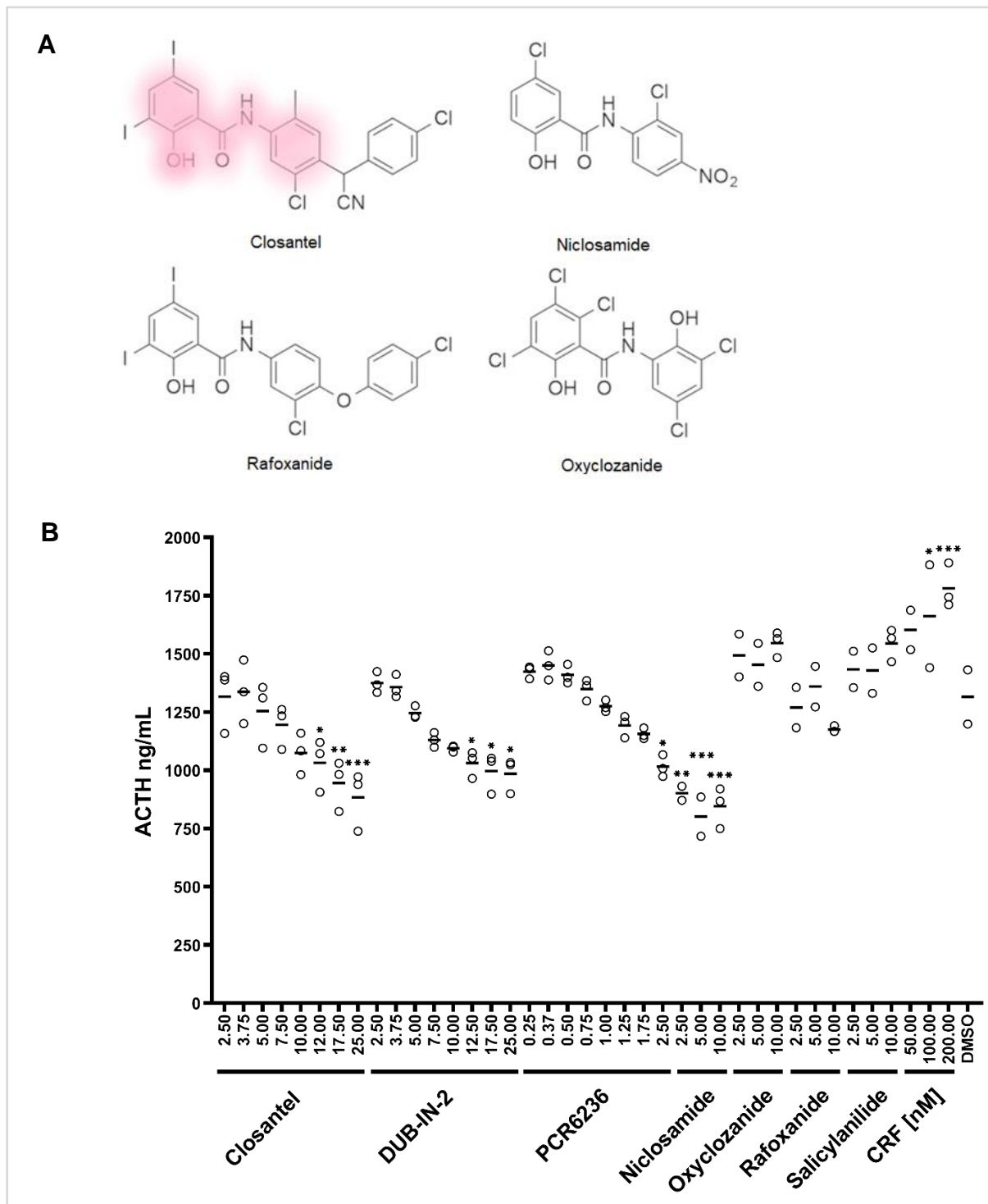


**Figure R1-04. Testing of closantel-related molecules for ACTH-release inhibition.**

**A.** Overview of the chemical structure of the halogenated salicylanilides tested for ACTH release inhibition. The salicylanilide backbone is highlighted in the closantel structure in the upper left.

**B.** ACTH secretion levels monitored in supernatant of AtT-20 cells treated or not with the indicated compound at increasing doses. Doses are indicated in  $\mu\text{M}$  except for CRF (in  $\text{nM}$ ) as indicated. CRF: corticotropin releasing factor at 50, 100 and 200  $\text{nM}$  was used as a control inducing ACTH secretion while DMSO at 0,05% was used a bioinactive control (solvent). Bars at mean levels. Results from one experiment. \* =  $P \leq 0.05$ . \*\* =  $P \leq 0.01$ . \*\*\* =  $P \leq 0.001$ . (one way ANOVA)

Both closantel and niclosamide showed a clear and significant dose-response decrease of ACTH release (Figure R1-04 B). In contrast, oxyclozanide, rafoxanide and the salicylanilide backbone had no significant dose-response decrease on ACTH secretion at the tested concentrations of 2.5 to 10  $\mu\text{M}$  (Figure R1-04 B).

The ACTH secretion level was then further monitored on the supernatant of AtT-20 cells treated or not by increasing doses of either closantel or niclosamide. This assay confirmed efficient inhibition of ACTH secretion by both compounds at several doses (Fig. R1-05).

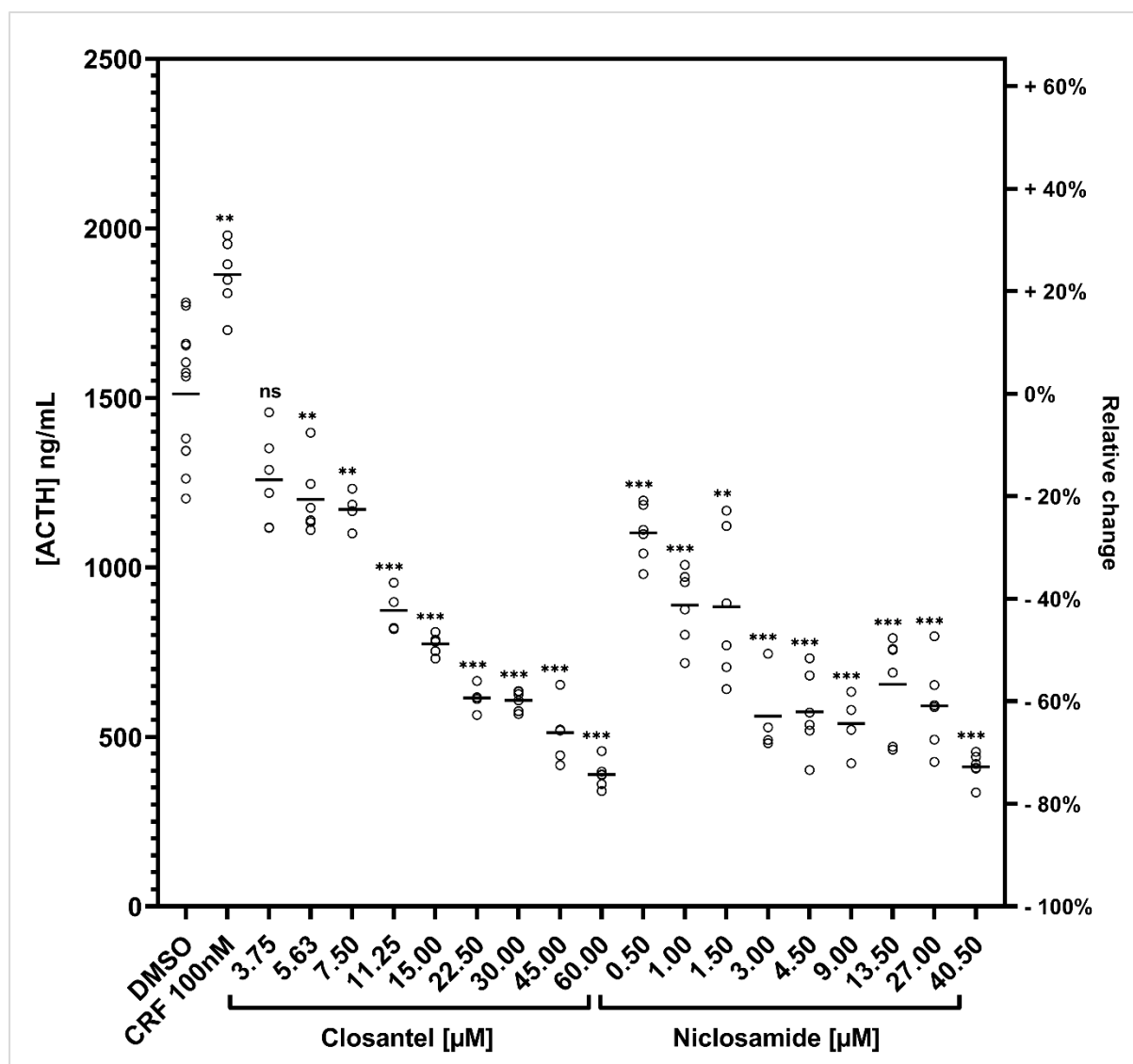


**Figure R1-05. Enzyme immunoassay analysis for closantel and niclosamide.** The ACTH concentration of the cell culture supernatant from At-T20 murine cells after 24-hour compound exposure was measured. Comparisons to DMSO control. CRF = corticotropin releasing factor. ACTH = adrenocorticotrophic hormone. Bars at mean levels. Results from one experiment. ns =  $P > 0.05$ . \* =  $P \leq 0.05$ . \*\* =  $P \leq 0.01$ . \*\*\* =  $P \leq 0.001$ .

Inhibition of ACTH secretion by either closantel or niclosamide was highly significant at non-toxic doses as shown by monitoring cell viability in the same conditions of compounds

treatment (Fig. R1-06). Indeed, at 5,63  $\mu\text{M}$ , closantel treatment induced no toxicity and a 20% reduction in ACTH release and at 30  $\mu\text{M}$  treatment, closantel treatment still induced no major toxicity and an ACTH secretion reduction as important as 60% compared to control conditions. Niclosamide treatment showed higher inhibition of ACTH secretion than closantel, inducing a 27% and 41% reduction of ACTH secretion levels at 0.5  $\mu\text{M}$  and 1.0  $\mu\text{M}$ , respectively with no significant toxicity albeit with considerable effects on viability upon higher doses.

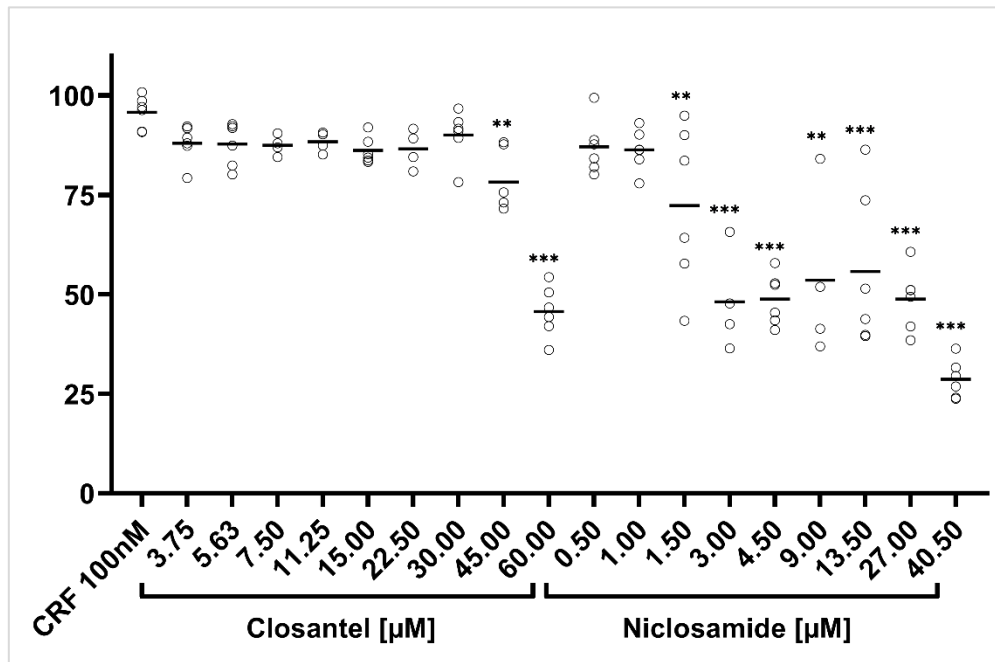
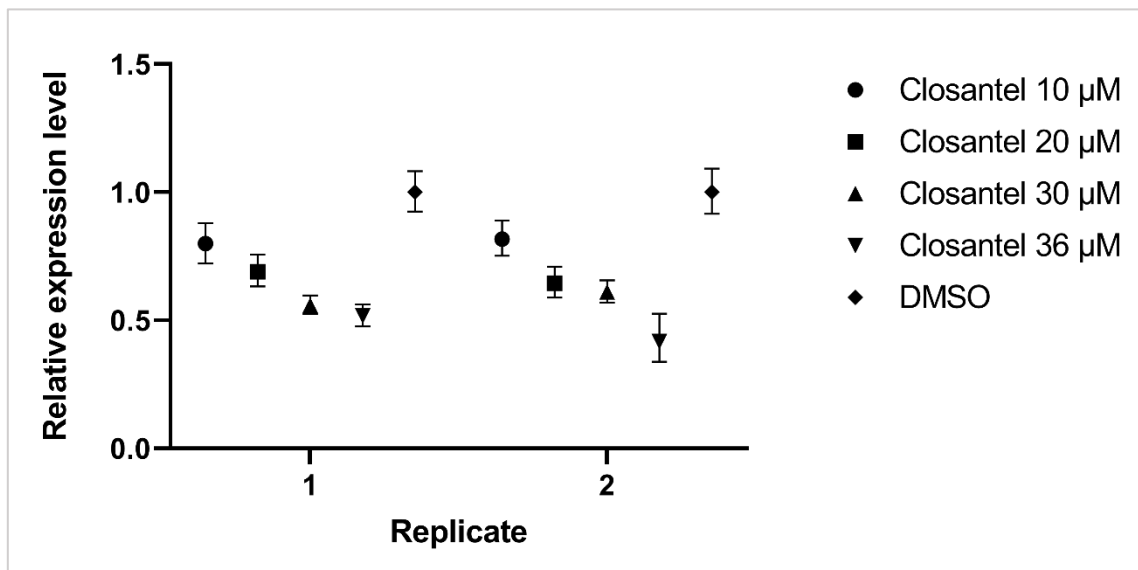


**Figure R1-06. Viability assay** of the AtT20 murine cells after 24-hour compound exposure, reported to DMSO control levels. Bars at mean levels. CRF = corticotropin releasing factor. Results from one experiment. \*\* =  $P \leq 0.01$ . \*\*\* =  $P \leq 0.001$ .

Taken together, our results show that both closantel and niclosamide efficiently inhibits ACTH secretion and that closantel is better tolerated than niclosamide in AtT-20 cells.

### 1.2.7 Monitoring of POMC encoding gene expression

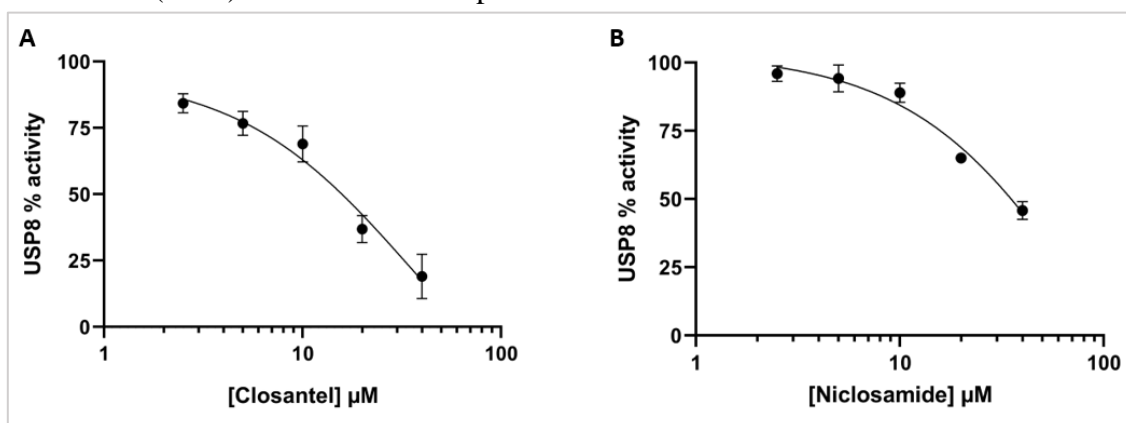
ACTH production depends on the expression of the *proopiomelanocortin (POMC)* gene encoding the ACTH precursor POMC. In order to determine if the ACTH reduction that we observed in AtT-20 cells treated by closantel could be attributable to a reduction of *POMC* gene expression, we monitored *POMC* transcripts by quantitative RT-PCR performed with specific primers on total RNA samples extracted from cells treated or not with increased doses of closantel (Figure R1-07). We actually repeatedly observed a strong decrease of *POMC* mRNA species (Figure R1-07) suggesting that closantel acts by negatively regulating upstream signaling pathways controlling *POMC* encoding gene expression. This is in accordance with the fact that USP8 constitutive catalytic activity stabilizes the EGFR, itself activating a MAP kinase pathway leading to *POMC* gene expression. Hence, inhibition of ACTH expression in cells treated with closantel may result from the inhibition of *POMC* gene expression, itself resulting from EGFR stabilization provoked by USP8 inhibition.



**Figure R1-07. POMC expression assay in two independent experiment (biological replicates).** Each dot represents the POMC expression normalized to the housekeeping gene HPRT and then compared to the DMSO control condition. Mean of technical triplicates with errors bars (SEM).

### 1.2.8 Confirming the in vitro USP8 inhibition by closantel and niclosamide

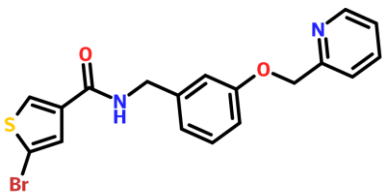
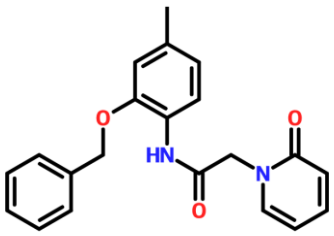
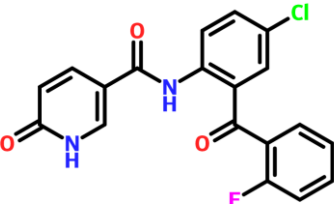
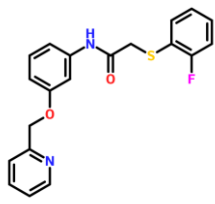
The inhibition of the catalytic activity of USP8-FL by either closantel or niclosamide was further monitored using the ubiquitin-rhodamine substrate (Ub-Rho), reaching 73% (closantel) and 54% inhibition (niclosamide) at the highest concentration of 40 μM (Figure R1-08). A larger dilution scale should allow us to reach a maximal and minimal inhibitory concentration and be able to determine then the pharmacological half maximal inhibitory concentration (IC<sub>50</sub>) for these two compounds.



**Figure R1-08. Confirmation of USP8 catalytic activity inhibition.** USP8-FL catalytic activity inhibition by increasing doses of closantel (A) or niclosamide (B) was monitored through the cleavage of the ubiquitin-rhodamine substrate in *in-vitro* assay. Results from one experiment done with triplicate conditions. Mean ± SEM.

### 1.2.9 Identification of inactive analogs

We used the program F-trees similarities search to identify four additional analogs presenting similar backbone as closantel and niclosamide with the aim to identify active or inactive analogs (Table R1-02). None of these four compounds inhibited USP8 catalytic activity at 40  $\mu$ M (not shown).

Structure	InChIKey	Similarity score
	CZAVGBVZBUNOPK- UHFFFAOYSA-N	0.8955
	GCVUBNTYPNMKAU- UHFFFAOYSA-N	0.8941
	BQMISNHKYUGCOB- UHFFFAOYSA-N	0.8933
	YOOOTZRCDIISJO- UHFFFAOYSA-N	0.8788

**Table R1-02. Compounds presenting similar backbone as closantel but presenting no inhibition of USP8-FL catalytic activity.**

### 1.3 Conclusion

We present here the screening of a library of 2,240 compounds for USP8 catalytic activity inhibition, followed by a characterization of hit selectivity towards another protease and the reversibility of the inhibition. Due to the recent discovery of mutations of USP8 in pituitary tumors of patients of Cushing's disease and its implications for the physiopathology



of the disease, we follow up with monitoring the hit capacity of decreasing ACTH release and POMC expression in a murine pituitary cellular model and the test of analogs of the most promising inhibitory molecule. This procedure led us to the selection of two FDA-approved molecules: closantel and niclosamide, which belong to the class of compounds known as halogenated salicylanilides and are currently used for their anthelmintic activity in livestock. Interestingly, these compounds inhibit USP8 in a reversible manner. Niclosamide is currently the subject of intensive drug repurposing in humans in the field of cancer treatment (Chen et al., 2018; Kadri et al., 2018). In comparison to the previously identified USP8 inhibitors, closantel and niclosamide present no chemical group with major undesirable properties for pharmaceutical development, and the available accumulated pre-clinical and clinical data for these two compounds should allow for a faster development of drugs for clinical use. Our findings also reiterate evidence for the role of USP8 in ACTH production and release, and so as a target in Cushing's disease, and offer renovated hope for the development of treatments for this disease.

## **1.4 Materials and methods**

### **1.4.1 Chemicals**

PCR6236 was kindly provided by our collaborators Pr. P. Vanelle and Dr. V. Remusat from Aix-Marseille University (Fauvarque et al., 2016). The inhibitor DUB-IN-2 (HY-50737A), the closantel (HY-17596), the niclosamide (HY-B0497), the rafoxanide (HY-17598) the oxyclozanide (HY-17594) and the salicylanilide (HY-B1408) were purchased from MedChemExpress. Corticotropin-releasing factor (ref #1151) was purchased from Tocris. Ub-AMC (ref. 60-0116-050) and Ub-Rho (ref. 60-0117-050) were purchased from Ubiquigent. USP-FL (ref. E-520) was purchased from BostonBiochem. Papain (ref. P4762) was purchased from Sigma. Casein (ref.VM874644) was purchased from Merck. USP8-CD was produced in-house using standard procedure.

### **1.4.2 Primary screen**

The primary screen was performed on the Prestwick library including 1,280 FDA-approved drugs or compounds under clinical development and 960 additional FDA-approved drugs from commercial suppliers herein referred as CMBA-FDA library, thus totalizing 2,140 compounds. This collection was screened in triplicate at a 50  $\mu$ M average final concentration. Dilution, distribution and screening of chemicals were carried out in a fully automated manner on 384-well microplates, on the robotic TECAN's Genesis 200 workstation using the TECAN's LiHa 8-channel pipetting head and the TECAN's Infinite M1000 microplate reader. Compounds were added to the reaction mix just before the substrate. The enzymatic reaction kinetics were monitored by measuring fluorescence elicited by the hydrolysis of the peptidyl Ub-AMC over 30 minutes. The negative control was the solvent DMSO at 0.5%. The bioactive control, mimicking the desired inhibitory activity, was the reaction mix without USP8-CD (corresponds to 100% inhibition).

#### 1.4.3 USP8 inhibition assay

The in-house purified catalytic domain of USP8 (USP8-CD) was used at a concentration of 40 nM in the presence of the artificial substrate Ub-AMC at a final concentration of 1  $\mu$ M, in conditions ensuring linearity of enzyme activity throughout the assay incubation time in a specific buffer. Compounds were added to the reaction mix just before the substrate. The enzymatic reaction kinetics were monitored by measuring fluorescence elicited by the hydrolysis of the peptidyl Ub-AMC over 30 minutes.

#### 1.4.4 UCHL3 inhibition assay

UCHL3 was used at a concentration of 3nM in the presence of the Ub-Rhodamine. The validation the hits was performed as described in 1.4.3 for USP8.

#### 1.4.5 Ub-Rhodamine 110 catalysis assays

For hit validation using another ubiquitin substrate, USP8-CD (in-house purified) or USP8-FL were used at a concentration of 40 nM or 75 nM, respectively, in the presence of Ub-Rhodamine 110 (Ub-Rho) at a final concentration of 0.1  $\mu$ M. Enzymatic assays were performed as described by the manufacturer's instructions. Compounds were added to the reaction mix just before the substrate. The enzymatic reaction kinetics were monitored by measuring fluorescence elicited by the hydrolysis of the Ub-Rho bound over 20 or 30 minutes using the same bioactive and bioinactive controls as for Ub-AMC.

#### 1.4.6 USP8 inhibition reversibility assay

Purified USP8-CD (6  $\mu$ M) was incubated for 15 min with the inhibitory compound at efficient inhibitory concentration or with DMSO in buffered conditions. The catalytic activity of each mix was monitored on Ub-AMC substrates (1  $\mu$ M) before and after 20-fold dilution of the reagent mix

#### 1.4.7 Papain inhibition

Papain and casein were dissolved in 40mM Tris-HCl buffers pH6.8 and pH9.5 respectively. Casein at the concentration of 0.5 $\mu$ g/ $\mu$ l was incubated with the inhibitory compounds at efficient inhibitory concentration or with DMSO for 15min and then digested by papain (2.5ng/ $\mu$ l) at RT over 45 min. The digestion samples were collected at time: 5, 15, 30 and 45min. To inactivate the protease Laemmli buffer 2x was added and each sample was heated at 95°C for 5 min then analyzed with SDS-PAGE and stained with Coomassie Blue.

#### 1.4.8 Cell culture

Mouse AtT-20 cells were obtained from the American Type Culture Collection and maintained on DMEM containing 10% fetal bovine serum, 100  $\mu$ g/mL streptomycin and 100 U/mL penicillin at 37°C with 5% CO<sub>2</sub> after recovery from long-term storage on liquid nitrogen-vapor phase.

#### 1.4.9 ACTH inhibition

$1.25 \times 10^4$  AtT20 cells were seeded on polylysine-coated 96-well culture vessels on 150 $\mu$ L of complete medium. After 24 hours, cells were treated with stock compounds to a final DMSO concentration of 0,5%. After 24 hours of treatment, cell culture supernatant was collected, cleared for 10 min at 1000 x g at 4°C, diluted in assay buffer (Phoenix Peptide ACTH EIA EK-001-21) and frozen at -80°C for subsequent processing according to the instructions of the kit's manufacturer.

#### 1.4.10 Cell viability

After the collection of the supernatant sample for the ACTH assay in the previous step, cells were supplemented with the PrestoBlue™ cell viability reagent (Invitrogen™ A13261) at 10% final volume, and re-incubated at 37°C for 30 minutes. Fluorescence was then read with a FLUOstar OPTIMA microplate reader.

#### 1.4.11 POMC expression

$3.75 \times 10^5$  AtT20 cells were seeded on polylysine-coated 6-well culture vessels on 2,4 mL complete medium. After 24 hours, cells were treated with stock compounds to a final DMSO concentration of 0,5%. After 24 hours of treatment, cells were briefly rinsed with 37°C DPBS (no calcium, no magnesium modification), lysed with the LBP reagent from the NucleoSpin® RNA Plus kit (Macherey-Nagel 740984.50) and then frozen at -70°C before continuing with the RNA extraction protocol as per manufacturer's instructions. 1 $\mu$ g RNA was used to synthesize cDNA using the AffinityScript QPCR cDNA Synthesis Kit (Agilent #600559). qPCR reaction was performed using the primers against the mouse POMC gene (5'-CCT CCT GCT TCA GAC CTC CAT AGA T-3' and 5'-GTC TCC AGA GAG GTC GAG TTT). The expression of the HPRT gene was used as a normalizer (primer pair 5'-ATG GAC AGG ACT GAA AGA CTT GCT-3' and 5'-TTG AGC ACA CAG AGG GCC ACA ATG-3'). Primers were synthesized by Eurofins Genomics. Detection was done using the Brilliant II SYBR® Green QPCR Master Mix (Agilent #600828), and readings were done using a Stratagene Mx3005P equipment.

#### 1.4.12 FTrees Similarity search

The search was done using Mcule (<https://mcule.com/>) "1-CLICK SCAFFOLD HOP" tool, with closantel as input molecule and the Mcule "10k diverse subset of Purchasable compounds" proprietary library as the chemical space. The top 4 molecules that were available "in-stock" from suppliers were acquired for further testing.

#### 1.4.13 Molecular docking

Closantel's docking to USP8 was evaluated using Autodock Vina via Mcule's (<https://mcule.com/>) 1-CLICK DOCKING tool. PDB accession number 3N3K ("USB8 catalytic domain bound to UB-variant") was processed with UCSF Chimera (<https://www.cgl.ucsf.edu/chimera/>) to remove the UB-variant and generate the template for

docking. The binding center was target to the middle surface of the ubiquitin binding pocket (coordinates X: -1.685 Y: -31.711 Z: -23.15), and the binding area was set to 100x100x100 Angstrom. Other parameters were unchanged. Only the best pose for each molecule was further considered.

#### 1.4.14 Statistical analysis

Data was processed with the Graphpad Prism 8 software. For both ACTH production and viability assays, data normality was determined by QQ plot inspection. For the ACTH production assay, treatment conditions were compared using a Welch's ANOVA test followed by a Dunnett's T3 multiple comparisons test. Data for the viability assay was treated via a Kruskal-Wallis test followed by a Dunn's multiple comparisons test. For the POMC expression assay, the Ct valued of the technical triplicates were first validated via one-sample t-tests for significance using Prism. Normalization to the reference gene and the relative expression levels were then calculated with the Stratagene MxPro v4.0.

## 2 2<sup>ND</sup> CHAPTER ó CHMP1B interacts with, and is regulated by, the ubiquitin specific protease Otubain 1

This part of the thesis describes my experimental work that led to the identification of a new partner of CHMP1B using M/S strategy combined with in silico analysis of the CHMP1B interacting network. It also describes biochemical experiments that I further performed to confirm the interaction between CHMP1B and OTUB1 using co-immunoprecipitations assays. Finally, a set of first results from my collaborator C. Pillet and I show the role of OTUB1 in the control of the ubiquitination levels of CHMP1B and its stabilization, as well as its potential function in EGFR stabilization. These results are presented here under an article format that will be submitted after additional confirmation of some preliminary results as described in this section.

### 2.1 Introduction

Trafficking of plasma membrane receptors along the endocytic pathway is a major process regulating the activation versus termination of downstream signaling pathways. In the case of the epidermal growth factor (EGF) receptor, EGF binding triggers both the activation of downstream MAPK signaling pathway and the linkage of ubiquitin moieties to the EGFR, which subsequently promotes its internalization to early endosomes (Tomas et al., 2014). From there, some cargos are rapidly recycled back to the plasma membrane for reutilization; others, including downregulated receptors, are transported to late endosomes and lysosomes for degradation (Gruenberg, 2001). Transport to late endosomes is mediated by multivesicular body (MVB). This process is highly dependent on the ESCRT (endosomal sorting complexes required for transport) assembly: a multisubunit cargo-recognition and membrane-sculpting machine that performs the topologically unique membrane bending and scission reactions required for vesicle formation and cargo entrapment inside the MVB (Schmidt and Teis, 2012). ESCRT assembly is a multi-step approach, consisting of five distinctive successive complexes: ESCRT-0, -I, -II, -III and Vps4-Vta1, that result in the deposition of a membrane-constricting polymer of ESCRT-III.

CHMP1B (charged multivesicular body protein 1B) belongs to the ESCRT-III complex and interacts with other ESCRT-III such as IST1 (Bajorek et al., 2009; McCullough et al., 2015; Xiao et al., 2009) as well the ESCRT-III-related ATPases Vps4A/B, (Lottridge et al., 2006; Nickerson et al., 2006; Obita et al., 2007), which catalyzes the disassembly of membrane-associated ESCRT-III polymers therefore ensuring the final step of membrane scission at the MVB. Recognition of the CHMP substrates is mediated by the presence of a MIT (microtubule interacting and trafficking domain in Vps4 interacting with the MIM (MIT-interacting motif) domain of CHMP1B (Obita et al., 2007; Scott et al., 2005; Stuchell-Brereton et al., 2007). The vacuolar protein sorting-associated protein VTA1 acts as a cofactor for VPS4 (Yang and Hurley, 2010).

CHMP1B and other ESCRT-III also control other membrane remodeling processes such as viral budding (Votteler and Sundquist, 2013), nuclear pore reformation (Olmos et al., 2015) and cytokinesis, a process that also depends on a close interaction with the microtubule severing ATPase Spastin (SPAST).

E3 ligases and DUBs tightly regulate the ubiquitination levels of the cargos at different steps of the process, as particularly exemplified in the case of the EGFR: while ubiquitination at the level of the plasma membrane by the E3 CBL promotes EGFR endocytosis and its subsequent degradation by the lysosomal pathway (Melker et al., 2001), its deubiquitination at the membrane or at early steps of the endocytic process may save the EGFR from degradation by preventing either its internalization or promoting its early recycling. In contrast, deubiquitination of the EGFR at later steps of the endocytic process, notably at the level of the MVB, would be required for cargo engagement into the ILVs and subsequent EGFR degradation.

Two main DUBs control plasma membrane receptor fate along the endocytic pathway, ASMH and USP8, that are recruited to the endosomes through their interaction with the ESCRT machinery, and are critical in maintaining receptor ubiquitination levels and down-regulation (McCullough et al., 2006) (Row et al., 2007) (Mizuno et al., 2006). Unlike AMSH that hydrolyses specifically Lys-63 polyUb chains, USP8 deubiquitinates both Lys-63 and Lys-48 polyubiquitin chains (Row et al., 2006). Moreover, the catalytic activity of AMSH is stimulated by its interaction with the ESCRT-0 subunit STAM (McCullough et al., 2006).

In addition to the cargo, several ESCRT proteins are themselves regulated by ubiquitination. USP8 actually controls the ubiquitination levels and stability of the ESCRT-0 protein STAM (Row et al., 2006). USP8 also deubiquitinates the ESCRT-III protein CHMP1B. In this case, a dynamic and transient ubiquitination of CHMP1B within 5 to 15 min after EGF stimulation would promote its recruitment as ubiquitinated dimers to the endosomal membrane where deubiquitination by USP8 would induce its integration into growing ESCRT-III complex (Crespo-Yañez et al., 2018).

Here we used a mass spectrometry strategy coupled to *in silico* analysis to identify new partners of the USP8 target CHMP1B with the aim to better understand its regulation and function. Our results pointed towards specific interaction of CHMP1B with the ubiquitin thioesterase OTUB1 (Otubain 1), an interaction that was further confirmed by co-immunoprecipitation experiments in human cells. We further show that CHMP1B stability is regulated by OTUB1, possibly through deubiquitination of degradative ubiquitin chains.

## **2.2 Results and discussion**

### **2.2.1 Polymers of CHMP1B are revealed by cross-linking**

To find new interactors of CHMP1B, we setup a biotin affinity purification strategy (IBA's Strep-Tactin®XT system) of a two-STREP-tag construct of human CHMP1B expressed under inducible promoter (Promega's Regulated Mammalian Expression System) on HEK-293-T cells. Due to the unsuccessful capture of the bait using common non-denaturing lysis buffers, a purification regimen under denaturing conditions of 6M urea was essayed, which led to a successful capture of the CHMP1B bait. The protocol was then amended with a chemical cross-linking step with the heterobifunctional agent SDAD (NHS-SS-Diazirine) before the lysis step in order to stabilize protein interactions during and throughout the entire downstream processing, and further help the identification of either transient or weak

interactions as they happened in their native environment. Indeed, SDAD is cell-permeant and cross-linking is done in physiological conditions (DPBS pH 7,4).

Western-blot analysis of the whole cell lysate showed that CHMP1B cross-linked complexes displayed a “ladder” pattern, with spacing between each step seemingly corresponding to the addition of a further unit of CHMP1B. This result confirms the already published polymeric nature of this protein.

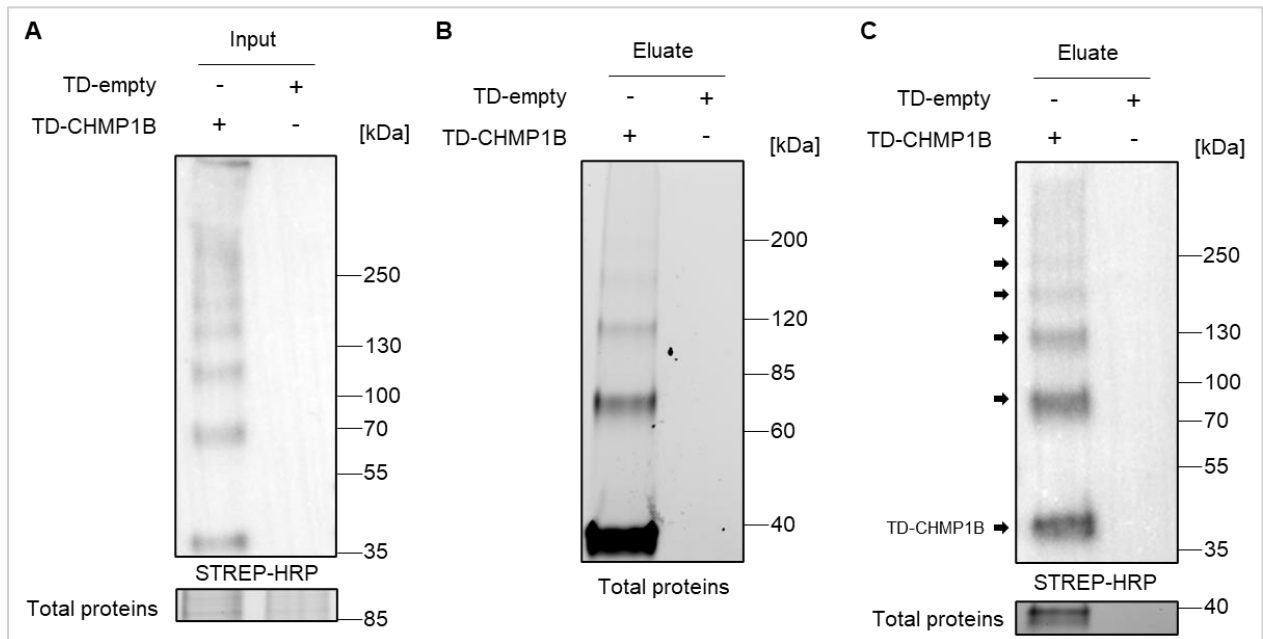


**Figure R2-01. Cross-linking experiment with SDAD.** HEK293-T cells were transfected alone or in combination with constructs expressing either CHMP1B with a double-STREP-FLAG tag (TD-CHMP1B) or double-STREP-FLAG tag empty vector (TD-empty) as indicated. At 48h post-transfection, cells were cross-linked with SDAD at 1mM, and purified over a Strep-Tactin®XT resin under denaturing conditions. The input and eluate fractions were blotted with a Strep-HRP conjugate on (A) and (C). (B) Represents the total protein analysis of the eluate samples.

### 2.2.2 Mass spectrometry analysis of CHMP1B containing complexes identify 97 potential partners

In order to identify CHMP1B partners, purified complexes were reduced by the addition of dithiothreitol (DTT), a reducing agent allowing for the cleavage of the thiol link, and the resulting samples were analyzed by shotgun mass-spectrometry (Figure R2-02). In the M/S analysis, the two individual arms of the cross-linker moiety were entered as modifications to the residues.

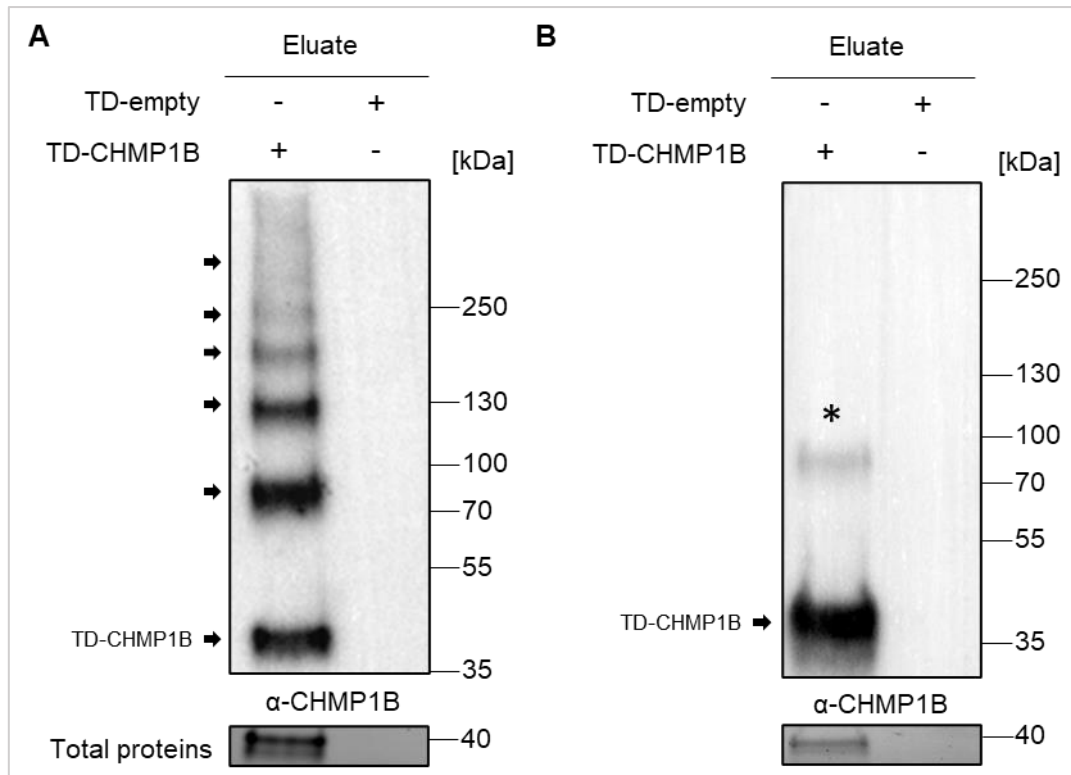


**Figure R2-02. Comparison of the samples from section 2.2.1 before (A) and after (B) reduction with DTT.** We are currently not aware if the band indicated with an asterisk (\*) represents remnants of a CHMP1B doublet or a CHMP1B heterocomplex resistant to reduction, or a non-specific signal.

A list of 97 proteins that respond to MS quality criteria (see methods) were identified as potential partners of CHMP1B (Supplementary table data). The list included both nuclear, such as XPO1 (Azmi et al., 2020), IPO5 (Chao et al., 2012) and CLIC1 (Valenzuela et al., 1997) as well as cytoplasmic proteins, such as ESCRT or ESCRT-associated proteins (see below), EZR (Naba et al., 2008) or ACAT2 (Song et al., 1994). This is in accordance with dual subcellular localization and function of CHMP1B in both compartments.

### 2.2.3 Network analysis reveal a cluster of known proteins of the endosomal pathway

We further generated an interacting map of the 97 candidate CHMP1B partners using the STRING tool and database of known and predicted protein-protein interaction issued from the literature (Szklarczyk et al., 2019).

The resulting interaction map clearly identified a cluster of already known CHMP1B-interacting proteins acting in close association with the ESCRT machinery during endocytosis (VTA1, VPS4A/B), or in other membrane remodeling processes (SPAST) (Figure R2-03 A).

The identification of these proteins that form a network of known CHMP1B partners involved in membrane remodeling and endocytosis fully validate the experimental strategy undertaken.



#### 2.2.4 OTUB1 is a new partner of CHMP1B that also interacts with USP8

We manually included USP8 in the analysis (that was not present in the experimental data) as a major known regulator of CHMP1B playing a major role in the control of CHMP1B ubiquitination status during endocytosis (resulting network figure R2-03 B). Remarkably, we observed that USP8 bridges the network of CHMP1B closely interacting proteins of the ESCRT machinery with OTUB1, one of the newly identified candidate partner of CHMP1B.

OTUB1 is actually a known partner of USP8. As described in the introduction, the two DUBs OTUB1 and USP8 act together to control the ubiquitination status of a common target, the E3 ligase GRAIL. Our results thus suggest that USP8 and OTUB1 may similarly regulate the ubiquitination status of CHMP1B and that another tripartite complex OTUB1:USP8:CHMP1B could exist.

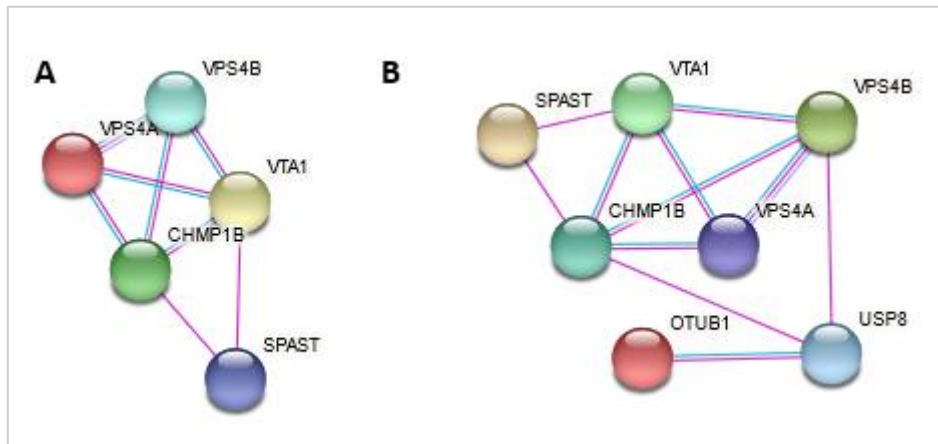


**Figure R2-03. CHMP1B:USP8 interaction networks** obtained from the the experimental procedure in described in section 2.2.1. UBC (ubiquitin precursor) was removed from the input list used to generate this network due to its promiscuity. Only “Databases” (light blue line) and “Experiments” (pink lines) were kept as sources of interactions. **A.** Network of closely-related CHMP1B interactors. **B.** Network obtained after the manual addition of USP to the input list.

#### 2.2.5 OTUB1 and CHMP1B co-purified by affinity purification from HEK293T cell extracts

In order to confirm the interaction between OTUB1 and CHMP1B, both proteins were expressed as recombinant tagged proteins in HEK 293T cells.

In previous experiments, we used SDAD which is a heterofunctional cross-linker; amine-reactive at one end via its NHS moiety, and non-specific via its UV-activable diazirine moiety at the other end, which allows binding to lysine and N-terminal residues from one partner and virtually any other residue from another partner that is placed at the correct distance. This increases exponentially the number of interactions stabilized but also increases the number of putative false interactions. To further confirm the interaction in more specific conditions, we further proceed with the homobifunctional NHS-NHS agent (dithiobis(succinimidyl propionate)), which has a spacer arm of similar length do SDAD and is similarly cleavable by reducing agents, but is less promiscuous due to its limited reactivity.

We set-up a purification strategy similar to the one described earlier, for cells co-expressing STREP-tagged CHMP1B and myc-OTUB1 as compared to control cells expressing a STREP-tag empty-vector and myc-OTUB1, followed by purification under denaturing conditions and stringent salt conditions of 500mM NaCl (Figure R2-04).

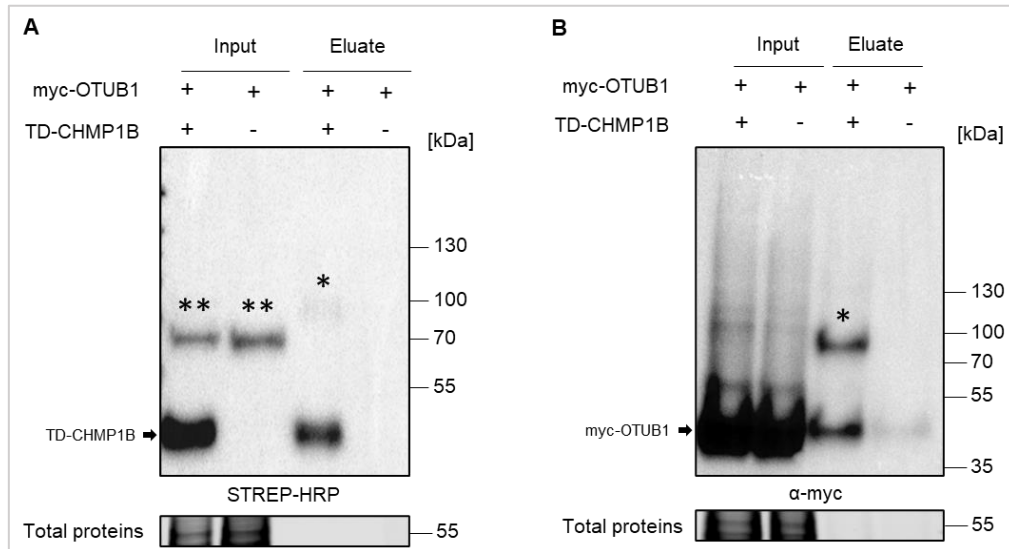


**Figure R2-04. Strep-Tactin XT purification.** HEK-293-T cells were transfected alone or in combination with constructs expressing: CHMP1B with a double-STREP-FLAG tag (TD-CHMP1b) and OTUB1 with a myc tag (myc-OTUB1). At 48h post-transfection, cells were cross-linked with DSP at 1mM, and TD-CHMP1B containing complexes were purified over a Strep-Tactin XT resin under denaturing conditions. The input and eluate fractions were blotted with a Strep-HRP conjugate in (A) and an anti-myc antibody in (B) after reduction of the samples with DTT. The myc-OTUB1 band present in both eluate lanes (indicated by an arrow) in (B) is enriched by a factor of ~10 in the sample transfected with both plasmids. \* represents a higher-order band commonly seen in cross-linking experiments both with OTUB1 and CHMP1B. \*\* represents a probable biotinylated band commonly detected in inputs on immunoblots of HEK-293-T cells revealed with Strep-HRP. Results show one representative experiment out of three experiments showing similar results.

Reciprocally, we then setup a purification strategy using myc-OTUB1 as a bait instead of TD-CHMP1B (Figure R2-05).

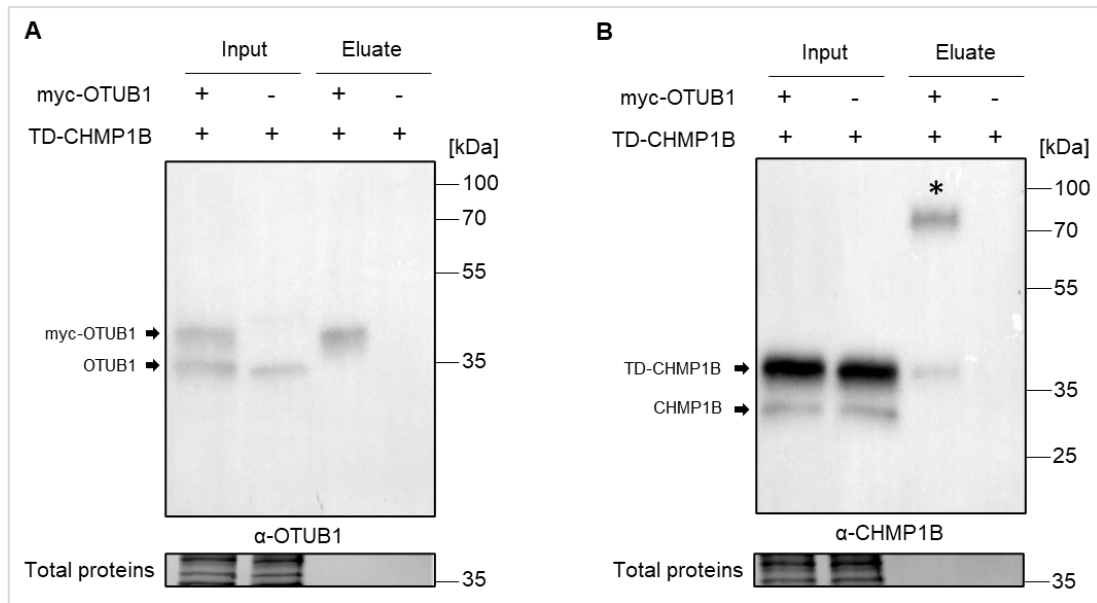


**Figure R2-05. Myc purification.** HEK-293-T cells were transfected alone or in combination with the indicated constructs expressing CHMP1B with a double-STREP-FLAG tag (TD-CHMP1B), OTUB1 with a myc tag (myc-OTUB1). At 48h post-transfection, cells were treated with a cross-linker agent DSP at 1mM, and purified over a myc-Trap agarose resin under high-stringency conditions. The input and eluate fractions were blotted with an anti-OTUB1 antibody on (A) and an anti-CHMP1B antibody on (B) after reduction of the samples with DTT. Results show one representative experiment out of three experiments showing similar results

These two experiments allowed us to purify myc-OTUB1 from TD-CHMP1B containing complexes and TD-CHMP1B from myc-OTUB1 containing complexes formed *in-cellulo* and stabilized by DSP.

### 2.2.6 OTUB1 silencing results in the accumulation of poly-ubiquitinated forms of CHMP1B

In order to determine the role of OTUB1 on CHMP1B ubiquitination status, we performed a FLAG purification of CHMP1B from cells co-transfected with TD-CHMP1B and HA-UB, a construct allowing to express tagged-ubiquitin, in cells treated or not with a siRNA targeting *OTUB1* gene expression. Since ubiquitination is a covalent modification, we decided to perform the initial lysis step under denaturing conditions to selectively purify covalently linked ubiquitin and avoid background signals possibly due to sticky ubiquitin species. We observed that under siOTUB1 extinction, there is an increase of 53% in the ubiquitinated forms of CHMP1B (Figure R2-06).

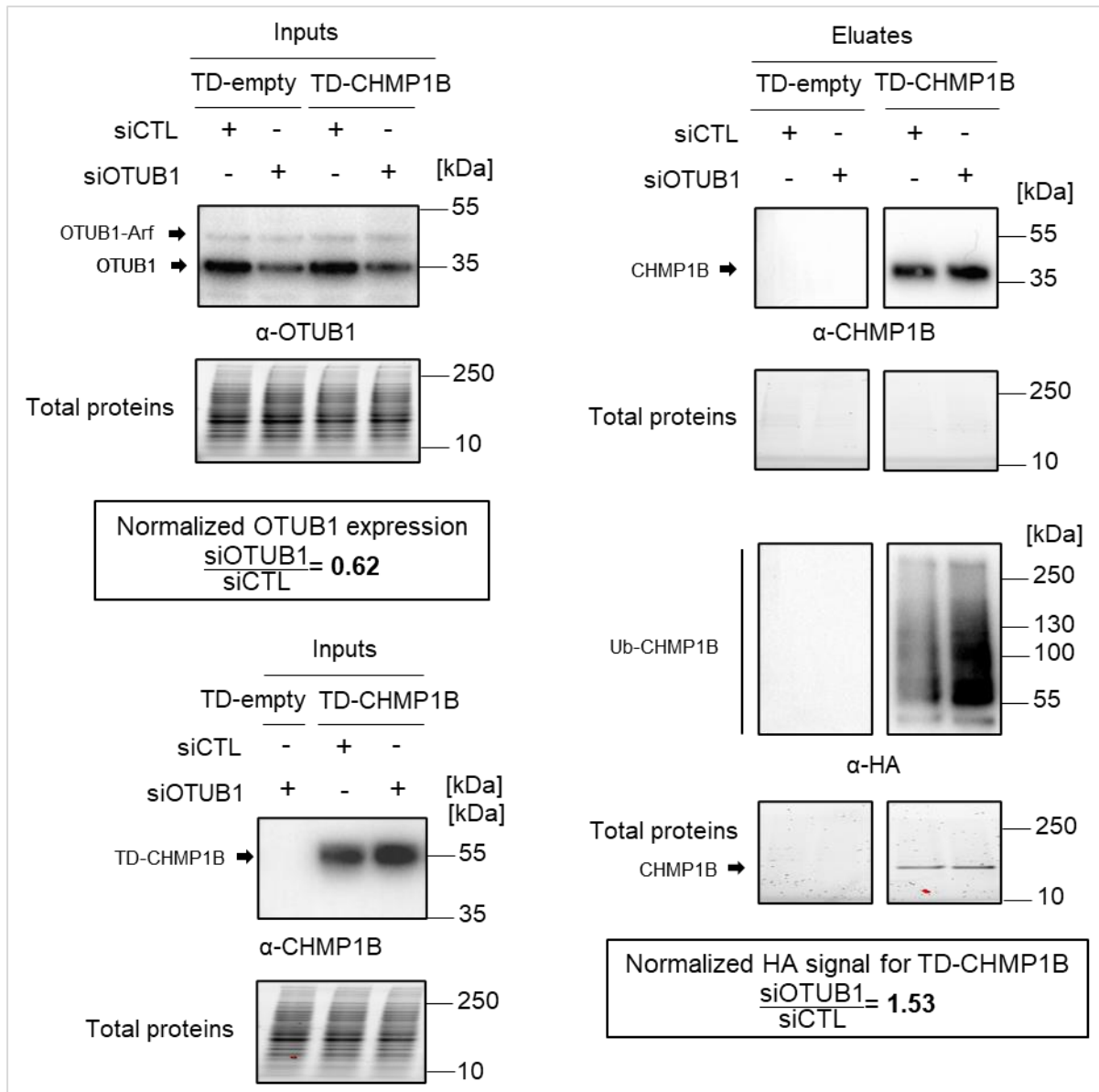


**Figure R2-06. *OTUB1* silencing.** HEK-293-T cells were transfected with siRNA targeting *OTUB1* or with a non-targeting control (siCTL). 24h post siRNA transfection, cells were additionally transfected with a HA-Ub construct encoding HA-tagged ubiquitin and either a construct expressing CHMP1B with a double-STREP-FLAG tag (TD-CHMP1B) or an empty vector expressing the double-STREP-FLAG tag only. At 48h post-siRNA transfection, cells were lysed under denaturing conditions of 6M urea and purified over a FLAG resin under mild (<1M urea) conditions. Inputs and eluates were then immunoblotted.

This results together with the fact that OTUB1 and CHMP1B belong to a same complex (see above), strongly suggest a direct deubiquitinating effect of OTUB1 on CHMP1B. Although we measured a significant change in the accumulated ubiquitinated forms, we were not able in this experiment to differentiate putative mono- from poly-ubiquitinated forms of CHMP1B. The wide smear of ubiquitin strongly signals the existence of poly-ubiquitinated forms of CHMP1B, in addition to the previously described mono-ubiquitinated forms of

CHMP1B that strongly accumulate in OTUB1 knockdown cells. Thus, OTUB1 may hydrolyze CHMP1B-linked polyubiquitin chains.

### 2.2.7 OTUB1 stabilizes CHMP1B

To further analyze if OTUB1 is capable of stabilizing CHMP1B, cells were co-transfected with TD-CHMP1B and either myc-OTUB1 or an empty vector (Figure R2-07). Overexpression of OTUB1 clearly resulted in a strong stabilization of CHMP1B by a 6.7 factor compared to control cells transfected with only TD CHMP1B. This result suggests that OTUB1 hydrolyze CHMP1B-linked degradative poly-ubiquitin chains that may correspond to Lys-48 polyUb chains species acting as a signal for degradation by the proteasome. This hypothesis could be reinforced by testing the effect of a proteasome inhibitor and/or using specific antibodies recognizing Lys-48 polyUb chains.

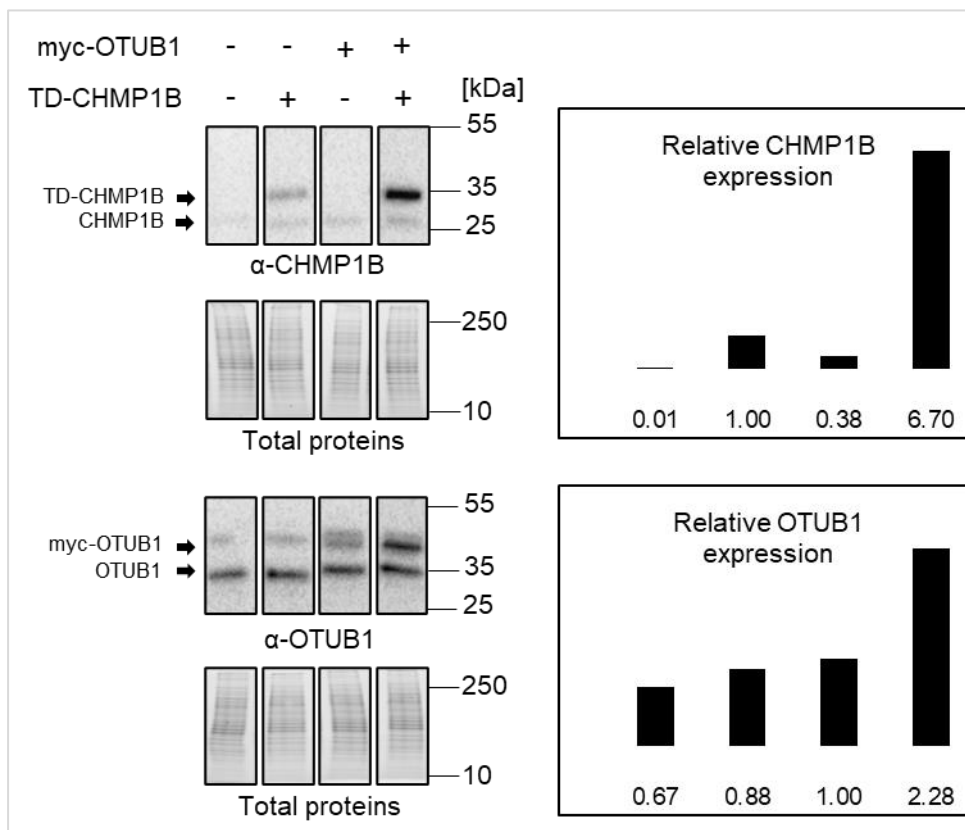


**Figure R2-07. OTUB1 overexpression.** HEK-293-T cells were transfected with high expression constructs expressing either CHMP1B with a double-STREP-FLAG tag (TD-CHMP1B), myc-tagged OTUB1, or both. At 48h post-transfection, cells were lysed under denaturing conditions of 6M urea and the cleared lysates were immunoblotted. Total DNA was the same among all conditions, and was adjusted using backbone vector.

### 2.2.8 OTUB1 promotes EGFR stabilization

Given the function of CHMP1B in EGFR endocytosis and degradation and the role of OTUB1 in stabilizing CHMP1B, we asked whether OTUB1 knockdown in HEK293T cells could also affect EGFR expression levels. Indeed, EGFR immunoblotting revealed a 20% lower EGFR level in cells treated with *siOTUB1* versus control cells suggesting that OTUB1 contributes to EGFR stabilization (Figure R2-08).

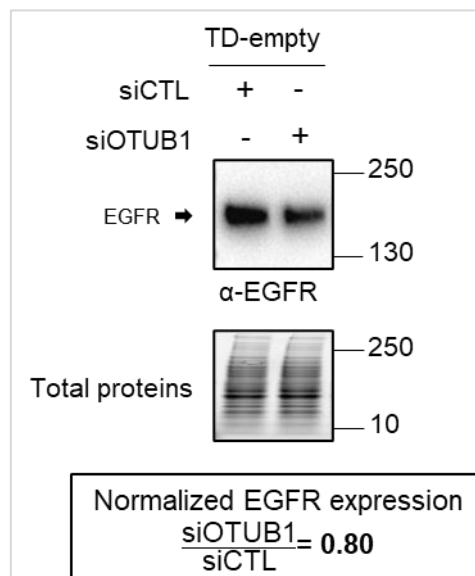


**Figure R2-08. EGFR immunoblotting** of the samples transfected with TD-empty plasmids from the experiments originally shown in figure R2-06. It is important to notice that the samples in this experiment were co-transfected with HA-Ub and consequently the cellular pool of ubiquitin was increased. We currently do not know how this affects EGFR stability.

We then set up a series of experiments to confirm these effects of OTUB1 upon EGFR, first by reproducing a similar siRNA experiment (Figure R2-09 A), and comparing the results obtained with those obtained with a strong overexpression of OTUB1 (Figure R2-09 B).

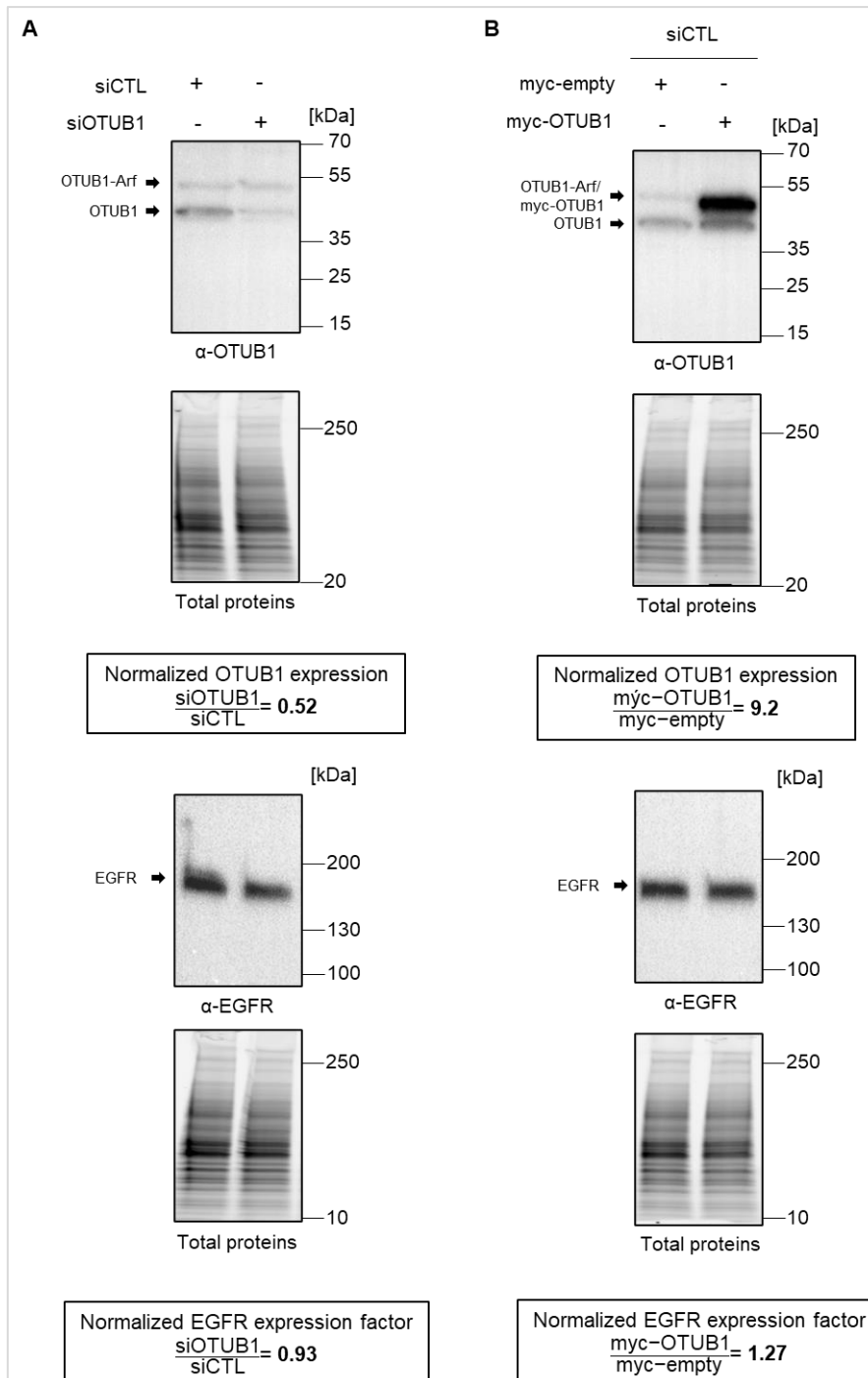


**Figure R2-09. Effects of OTUB1 on EGFR levels.** **A.** HEK-293-T cells were transfected with siRNA targeting *OTUB1* or with a non-targeting control (siCTL). At 48h post-siRNA transfection, cells were lysed under denaturing conditions of 6M urea and whole cell lysates were immunoblotted. **B.** HEK-293-T cells were transfected with high expression constructs expressing either myc-OTUB1 or control plasmid (myc-empty). At 48h post-transfection, cells were lysed under denaturing conditions of 6M urea and the cleared lysates were immunoblotted. Total DNA was the same among all conditions, and was adjusted using control vector.

This second experiment confirmed the reduction in EGFR level upon *OTUB1* gene silencing (Fig. R2-09 A), although to a less extent (-7%) compared to the first experiment (-

20%), a difference which may be due to differential *OTUB1* gene extinction efficacy. In contrast to its silencing, overexpression of *OTUB1* resulted in a significant stabilization of 27% of EGFR levels compared to control conditions (Fig. R2-09 B).

Our results indicate that OTUB1 may contribute to EGFR stabilization though this needs to be reinforced by additional experiments. Moreover, it would be interesting to investigate if this role on EGFR stabilization indirectly depends on the CHMP1B stabilization by OTUB1.

## 2.3 Conclusion

Taken together, our results identify OTUB1 as a new actor of intracellular trafficking regulation acting together with USP8 to differentially regulate CHMP1B ubiquitination status. While this study shows that OTUB1 may catalyze degradative polyubiquitin chains on CHMP1B resulting in its stabilization, previous studies in the laboratory demonstrated that USP8 catalyzes ubiquitin moieties dynamically linked to CHMP1B following EGF stimulation allowing for its integration in the growing ESCRT-III polymers at the endosomal membrane.

Of particular interest, OTUB1 (via its two isoforms, see Supplementary Data) is a known regulator of the E3 ligase GRAIL, a 428-amino acid RING domain-containing protein that catalyzes K-48 and K-63-linked polyubiquitin chains formation, and also interacts with USP8 (Soares et al., 2004). Moreover, GRAIL is critical in the endocytic process: GRAIL localizes to the transferrin-recycling endocytic pathway and further data suggest its contribution to an intact endocytic trafficking critical for cytokine transcriptional regulation (Anandasabapathy et al., 2003).

In a similar way as described for GRAIL, our results suggest that CHMP1B may be a common target of USP8 and OTUB1. Whether or not these two DUBs act in a common complex, as in the case of the E3 ligase GRAIL, to both stabilize CHMP1B and regulate its activity at the endosomal membrane in response to EGF stimulation, stays to be determined. It may be interesting also to determine if OTUB1 and USP8 control the ubiquitination levels of other members of the ESCRT machinery to finely control the stability and activity of membrane remodeling complexes all along the endocytic pathway.

## 2.4 Materials and Methods

### 2.4.1 Cell culture

HEK293T cells were purchased from the American Type Tissue Culture (ATCC) and culture in Dulbecco's Modified Eagle's Medium (DMEM) containing supplemented with 200 mM L-alanyl-L-glutamine, 10% heat-inactivated fetal bovine serum and 1% penicillin/streptomycin mix; and grown in 5% CO<sub>2</sub> at 37°C in a humidified incubator.



## 2.4.2 Plasmids

Except for experiments in Figures R2-07 and R2-09, inserts TD-CHMP1B and TD-empty were custom-synthesized and inserted into the pF12A RM Flexi® Vector supplied by Promega by restriction enzyme cloning into sites HindIII/PmeI. Myc-OTUB1 and myc-empty were obtained similarly. Sequences are:

### TD-CHMP1B

```
AAGCTTGCGGCCATGGACTACAAGGACGACGACAAGGGCAGCGCCGCCAGCTGGTCCACATCCCCA
GTTTCGAGAAAGGTGGAGGCAGCGGCGGCGGAAGTGGCGGAGGCAGCTGGTCCACACCCACAATTTGAAAAAG
CGATCGCCTCTAACATGGAGAAACACCTGTTCAACCTGAAAGTTCGCGGCCAAAGAACTGAGTAGGAGTGCC
AAAAAATGCGATAAGGAGGAAAAGGCCGAAAAGGCCAAAAATTA AAAAGGCCATTTCAGAAGGGCAACATGGA
AGTTGCGAGGATACACGCCGAAAATGCCATCCGCCAGAAGAACCAGGCGGTGAATTTCTTGAGAATGAGTG
CGCGAGTCGATGCAGTGGCTGCCAGGGTCCAGACGGCGGTGACGATGGGCAAGGTGACCAAGTCGATGGCT
GGTGTGTTAAGTCGATGGATGCGACATTGAAGACCATGAATCTGGAGAAGATTTCTGCTTTGATGGACAA
ATTTCGAGCACCAGTTTGAGACTCTGGACGTCCAGACGCAGCAAATGGAAGACACGATGAGCAGCACGACGA
CGCTCACCACTCCCCAGAACCAAGTGGATATGCTGCTCCAGGAAATGGCAGATGAGGCGGGCCTCGACCTC
AACATGGAGCTGCCGAGGGCCAGACCGGCTCCGTGGGCACGAGCGTGGCTTCGGCGGAGCAGGATGAACT
GTCTCAGAGACTGGCCCGCCTTCGGGATCAAGTGTGAGTTTAAAC
```

### MYC-OTUB1

```
AAGCTTGCGATCGCAGGGAGACCCAAGCTATGGAGCAAAAGCTCATCTCAGAGGAAGATCTGGAA
TTAGAGCAAAAGCTCATCTCAGAGGAAGATCTGTTAATTAATACCATGGCGGGGAGGAACCTCAGCAGCA
GAAGCAGGAGCCGCTGGGCAGCGACTCCGAAGGTGTTAACTGTCTGGCCTATGATGAAGCCATCATGGCTC
AGCAGGACCGAATTCAGCAAGAGATTGCTGTGCAGAACCCTCTGGTGTGAGAGCGGCTGGAGCTCTCGGTC
CTATAAAGGAGTATGCTGAAGATGACAACATCTATCAACAGAAGATCAAGGACCTCCACAAAAGTACTC
GTACATCCGCAAGACCAGGCTGACGGCAACTGTTTCTATCGGGCTTTTCGGATTCTCCCACTTGAGGCAC
TGCTGGATGACAGCAAGGAGTTGCAGCGGTTCAAGGCTGTGTCTGCCAAGAGCAAGGAAGACCTGGTGTCC
CAGGGCTTCACTGAATTCACAATTGAGGATTTCCACAACACGTTTCATGGACCTGATTGAGCAGGTGGAGAA
GCAGACCTCTGTGCGCCGACCTGCTGGCCTCCTTCAATGACCAGAGCACCTCCGACTACCTTGTGGTCTACC
TGCGGCTGCTCACCTCGGGCTACCTGCAGCGCGAGAGCAAGTTCTTCGAGCACTTCATCGAGGGTGGACGG
ACTGTCAAGGAGTTCTGCCAGCAGGAGGTGGAGCCCATGTGCAAGGAGAGCGACCACATCCACATCATTGC
GCTGGCCCAGGCCCTCAGCGTGTCCATCCAGGTGGAGTACATGGACCGCGGCGAGGGCGGCACCACCAATC
CGCACATCTTCCCTGAGGGCTCCGAGCCCAAGGTCTACCTTCTTACC GGCCCTGGACACTACGATATCCTC
TACAAATAGTCGACTCTAGAGGGCCCGTTTAAAC
```

### TD-VD

```
AAGCTTGCGGCCATGGACTACAAGGACGACGACAAGGGCAGCGCCGCCAGCTGGTCCACATCCCCA
GTTTCGAGAAAGGTGGAGGCAGCGGCGGCGGAAGTGGCGGAGGCAGCTGGTCCACACCCACAATTTGAAAAAG
CGATCGCCATGGAATAAGTAAGGAATCCACTAATGTTTAAAC
```

### MYC-VD

```
AAGCTTGCGATCGCAGGGAGACCCAAGCTATGGAGCAAAAGCTCATCTCAGAGGAAGATCTGGAA
TTAGAGCAAAAGCTCATCTCAGAGGAAGATCTGTTAATTAATGAGTTTAAAC
```

Myc-OTUB1 and TD-CHMP1B used in experiments in Figures R2-07 and R2-09 were similarly custom-synthesized and inserted into the pcDNA3.1(+) (designed by ThermoFisher and kindly supplied by Dr. Agnès Journet of the CEA Grenoble) by restriction enzyme cloning into sites HindIII/KpnI. Sequences are:

TD-CHMP1B

AAGCTTGC GGCCATGGACTACAAGGACGACGACAAGGGCAGCGCCGCCAGCTGGTCACATCCCCA  
GTTTCGAGAAAGGTGGAGGCAGCGGCGGCGGAAGTGGCGGAGGCAGCTGGTCACACCCACAATTTGAAAAAG  
CGATCGCCTCTAACATGGAGAAACACCTGTTCAACCTGAAGTTCGCGGCCAAAGAACTGAGTAGGAGTGCC  
AAAAAATGCGATAAGGAGGAAAAGGCCGAAAAGGCCAAAAATAAAAAGGCCATTTCAGAAGGGCAACATGGA  
AGTTGCGAGGATACACGCCGAAAATGCCATCCGCCAGAAGAACCAGGCGGTGAATTTCTTGAGAATGAGTG  
CGCGAGTCGATGCAGTGGCTGCCAGGGTCCAGACGGCGGTGACGATGGGCAAGGTGACCAAGTCGATGGCT  
GGTGTGGTTAAGTCGATGGATGCGACATTGAAGACCATGAATCTGGAGAAGATTTCTGCTTTGATGGACAA  
ATTTCGAGCACCAGTTTGAGACTCTGGACGTCCAGACGCAGCAAATGGAAGACACGATGAGCAGCAGCAGCA  
CGCTCACCCTCCCCAGAACCAAGTGGATATGCTGCTCCAGGAAATGGCAGATGAGGCGGGCCTCGACCTC  
AACATGGAGCTGCCGCAGGGCCAGACCGGCTCCGTGGGCACGAGCGTGGCTTCGGCGGAGCAGGATGAACT  
GTCTCAGAGACTGGCCCCGCTTCGGGATCAAGTGTGAGTTTAAACGAATTCGGGCTCGGTACC

MYC-OTUB1

AAGCTTGC GATCGCAGGGGAGACCCAAGCTATGGAGCAAAAAGCTCATCTCAGAGGAAGATCTGGAA  
TTAGAGCAAAAGCTCATCTCAGAGGAAGATCTGTTAATTAATACCATGGCGGCGGAGGAACCTCAGCAGCA  
GAAGCAGGAGCCGCTGGGCAGCGACTCCGAAGGTGTTAACTGTCTGGCCTATGATGAAGCCATCATGGCTC  
AGCAGGACCGAATTCAGCAAGAGATTGCTGTGCAGAACCTCTGGTGTGAGAGCGGCTGGAGCTCTCGGTC  
CTATAACAAGGAGTATGCTGAAGATGACAACATCTATCAACAGAAGATCAAGGACCTCCACAAAAAGTACTC  
GTACATCCGCAAGACCAGGCTGACGGCAACTGTTTCTATCGGGCTTTTCGGATTCTCCCACCTTGAGGCAC  
TGCTGGATGACAGCAAGGAGTTGCAGCGGTTCAAGGCTGTGTCTGCCAAGAGCAAGGAAGACCTGGTGTCC  
CAGGGCTTCACTGAATTCACAATTGAGGATTTCCACAACACGTTTCATGGACCTGATTGAGCAGGTGGAGAA  
GCAGACCTCTGTGCGCCGACCTGCTGGCCTCCTTCAATGACCAGAGCACCTCCGACTACCTTGTGGTCTACC  
TGCGGCTGCTCACCTCGGGCTACCTGCAGCGCGAGAGCAAGTTCTTCGAGCACTTCATCGAGGGTGGACGG  
ACTGTCAAGGAGTTCTGCCAGCAGGAGGTGGAGCCCATGTGCAAGGAGAGCGACCACATCCACATCATTGC  
GCTGGCCCAGGCCCTCAGCGTGTCCATCCAGGTGGAGTACATGGACCGCGGCGAGGGCGGCACCACCAATC  
CGCACATCTTCCCTGAGGGCTCCGAGCCCAAGGTCTACCTTCTCTACCGGCCTGGACACTACGATATCCTC  
TACAAATAGTCGACTCTAGAGGGCCCGTTTAAACGAATTCGGGCTCGGTACC

### 2.4.3 siRNAs

Dharmacon's ON-TARGETplus J-021061-08 with target sequence was used against OTUB1, J-005203-07 with target sequence CCACUAGCAUCCACAAGUA was used against USP8, and D-001810-01 with target sequence UGGUUUCAUGUCGACUAA was used as a non-targeting control.

### 2.4.4 Transfection

Purified DNA was transfected with the Promega Fugene HD transfection reagent at a 1:2 µg DNA:µL Fugene HD ratio. Cells transfected with plasmids of the Promega Regulated Mammalian Expression System were additionally induced 3 hours later with Coumermycin A1 included in the kit. siRNA were transfected at 12.5nM with the Lipofectamine RNAiMAX reagent as per manufacturer's instructions.

#### 2.4.5 Cross-linking

Adherent cells were briefly rinsed with 37°C DPBS (no calcium, no magnesium modification). SDAD (Thermo Scientific #26169) or DSP (Thermo Scientific Pierce #PG82082) were dissolved to 1mM concentration in 10% DMSO in warm DPBS solvent, and added carefully to the cell monolayer at a ratio of 10mL per 175cm<sup>2</sup> cell culture surface. After 30 minutes at room temperature, cross-linking with DSP was quenched by addition of 1M Tris pH 7,5 to 50mM final concentration, for 15 minutes at room temperature. Cross-linking with SDAD was proceeded first with 15 minutes of exposure of the bottom of the cell culture flask to a 365nm UV-transilluminator before quenching as described for DSP. After quenching, the cell monolayer was rinsed with 37°C DPBS, and the flasks were kept at -80°C until further processing.

#### 2.4.6 Strep-Tactin XT purification for MS experiments

Adherent cells were lysed with a buffer containing 6M urea, 1mM EDTA, 150mM NaCl, 100mM Tris pH 8.0, 0,5% NP-40® and Sigma Protease Inhibitor Cocktail P8340 at 5µL/mL for 1 hour at 4°C and centrifuged for 20 min at 16000g 4°C. Cleared lysates were incubated with Strep-Tactin XT resin for 3 hours under rotation at 4°C. The resin was then washed with 20 column volumes of lysis buffer, and eluted with 3,6 column volumes of elution buffer (1mM EDTA, 150mM NaCl, 100mM Tris pH 8,0, 50mM biotin). Eluates were concentrated with a Corning® Spin-X® UF 30K MWCO concentrator, and diluted in Laemmli loading buffer supplement with DTT to 50mM final concentration.

#### 2.4.7 Strep-Tactin XT purification for CHMP1B:OTUB1 interaction confirmation

Adherent cells were lysed with a buffer containing 6M urea, 50mM NaCl, 100mM Tris pH 8.0, 1% NP-40®, Sigma Protease Inhibitor Cocktail P8340 at 5µL/mL and Benzonase® Nuclease at 1.6µL/mL for 1 hour at 4°C. Salt concentration was then adjusted to 500mM NaCl. Lysates were centrifuged for 20 min at 16000g 4°C. Cleared lysates were incubated with Strep-Tactin XT resin for 3 hours under rotation at 4°C. The resin was then washed with 30 column volumes of lysis buffer at 500mM NaCl, and eluted with 3,6 column volumes of elution buffer (1mM EDTA, 500mM NaCl, 100mM Tris pH 8,0, 50mM biotin). Eluates were concentrated with a Corning® Spin-X® UF 30K MWCO concentrator, and diluted in Laemmli loading buffer supplement with DTT to 50mM final concentration.

#### 2.4.8 Myc purification for CHMP1B:OTUB1 interaction confirmation

Adherent cells were lysed with a buffer containing 50mM NaCl, 100mM Tris pH 7.5, 1% NP-40®, Sigma Protease Inhibitor Cocktail P8340 at 5µL/mL and Benzonase® Nuclease at 1.6µL/mL for 1 hour at 4°C. Salt concentration was then adjusted to 500mM NaCl. Lysates were centrifuged for 20 min at 16000g 4°C. Cleared lysates were incubated with myc-Trap agarose resin for 1 hour under rotation at 4°C. The resin was washed with 20 column volumes of lysis buffer at 500mM NaCl, and boiled with Laemmli loading buffer. The eluate was then treated with DTT and boiled again.

#### 2.4.9 FLAG purification for ubiquitination analysis

Adherent cells were lysed with a buffer containing 6M urea, 150mM NaCl, 50mM Tris pH 7.5, 0.5% Triton X-100, Sigma Protease Inhibitor Cocktail P8340 at 5 $\mu$ L/mL and 1mM EDTA for 1 hour at 4°C. Lysates were centrifuged for 20 min at 16000g 4°C. Cleared lysates were diluted with dilution buffer (150mM NaCl, 50mM Tris pH 7.5, 0.5% Triton X-100) to a final urea concentration of 0.75M and incubated with FLAG M2 resin for 3 hours at 4°C. The resin was washed with 12.5 column volumes of stringent buffer (500mM NaCl, 50mM Tris pH 7.5, 1% Triton X-100), 12.5 column volumes re-equilibration buffer (150mM NaCl, 50mM Tris pH 7.5) and eluted with FLAG peptide 300ng/ $\mu$ L in re-equilibration buffer 2x 2.5 column volumes for 30 minutes at 4°C.

#### 2.4.10 M/S analysis

M/S analysis was performed by Edyp platform (<http://www.edyp.fr/web/>). Each protein sample was stacked by a 1 cm-migration on the top of a NuPAGE 4–12% gel, Invitrogen) before Coomassie blue staining (R250, Bio-Rad). Gel bands of concentrated proteins were manually excised and then treated automatically by TECAN Robot EVO150. Pieces being washed by 6 successive incubations of 15 min in 25 mM NH<sub>4</sub>HCO<sub>3</sub> containing 50% (v/v) acetonitrile. Gel pieces were then dehydrated in 100% acetonitrile and incubated at 53 °C with 10 mM DTT in 25 mM NH<sub>4</sub>HCO<sub>3</sub> for 45 min and in the dark with 55 mM iodoacetamide in 25 mM NH<sub>4</sub>HCO<sub>3</sub> for 35 min. Alkylation was stopped by adding 10 mM DTT in 25 mM NH<sub>4</sub>HCO<sub>3</sub> and mixing for 10 min. Gel pieces were then washed again by incubation in 25 mM NH<sub>4</sub>HCO<sub>3</sub> before dehydration with 100% acetonitrile. Modified trypsin (Promega, sequencing grade) in 25 mM NH<sub>4</sub>HCO<sub>3</sub> was added to the dehydrated gel pieces for an overnight incubation at 37 °C. Peptides were then extracted from gel pieces in three 15-min sequential extraction steps in 30  $\mu$ l of 50% acetonitrile, 30  $\mu$ l of 5% formic acid and finally 30  $\mu$ l of 100% acetonitrile. The pooled supernatants were then vacuum-dried. The dried extracted peptides were resuspended in 5% acetonitrile and 0.1% trifluoroacetic acid and analyzed by online nanoLC-MS/MS (NCS, and Q-Ex\_HF, ThermoFischer Scientific). Peptides were sampled on a 300  $\mu$ m  $\times$  5 mm PepMap C18 precolumn and separated on a reprosyl 25 cm 1.9  $\mu$ m (Cluzeau). The nanoLC method used a 140-min gradient ranging from 4% to 40% acetonitrile in 0.1% formic acid (in 123 min) and wash to 90% and equilibration at 4% at a flow rate of 300 nL/min. MS and MS/MS data were acquired using Xcalibur (Thermo Fischer Scientific). Spray voltage and heated capillary were set at 2 kV and 270 °C, respectively. Survey full-scan MS spectra (m/z  $\approx$  400–1600) were acquired in the Orbitrap with a resolution of 60,000. The 20 most intense ions from the preview survey scan delivered by the Orbitrap were fragmented by collision induced dissociation (collision energy 30%) in the LTQ. Next the MS/MS spectra are searched against theoretical spectra from in silico digestion of the the organism-specific protein sequences database. This search allows to determine the sequence of most peptides. Once peptides have been identified, the proteins can also be identified. A validation procedure is applied in order to eliminate as much as possible of false identifications. An additional protocol is performed to get quantification values of every detected peptide and in turn of the proteins. The database search is performed with Mascot (commercial, Matrix Science ) and validation

and quantification are performed with the EdyP-made Proline software (Proline; <http://www.profi-proteomics.fr/proline/>). The two SDAD moieties resulting from crosslinking break with DTT were entered as modifications to the detected residues. The abundance values were used to rank the proteins identified in the database which corresponds to an April 2019 snapshot of Uniprot with commonly identified contaminants flagged.

#### 2.4.11 Primary antibodies

CUSABIO's CSB-PA03595A0Rb against OTUB1, Milipore's ABE1974 against CHMP1B, Sigma's HPA004869 against USP8 (rabbit polyclonals) and Cell Signaling Technology's D38B1 #4267 against EGFR (rabbit monoclonal) were used in this study.

#### 2.4.12 Blot normalization

Whole cell lysates (which includes cleared lysates and "inputs" for purification steps) were normalized in the following way: using the software ImageLab, the merged images obtained after ECL exposure was used to draw same-size volumes around the band from each lane, plus variable sized lanes as background volumes. One lane was defined as the reference volume, and the "Relative Quantity" factors around the value of 1.0 were then exported. These were corrected for loading of the gels by using the Stain-Free images obtained of the corresponding gels before membrane-transfer, which were processed by automatic lane detection (and manual adjustment when needed) and background correction. The "Adjusted Total Lane Volume (Int)" values were then exported, and once again one lane was defined as the reference volume, allowing to obtain correction factors around the value of 1.0. The relative blot factors were divided by the relative Stain-Free factors, allowing the obtention of the normalized correction factors followed by inter-condition comparison. HA-immunoblot eluates were normalized to the single purified CHMP1B band visible in the gel used to produce the blot.

## 2.5 Supplementary Data

### 2.5.1 Supplemental Table 1

Raw MS list of SDAD experiment (first results in the list only, equivalent to green categories on the key below)

Protein se id	Accession	Gene name	Coverage	Mol. Weight	Sequence Specific	TD-CHMP1B	TD-empty				TD-CHMP1B							
						TD-empty	Pep	SC	SSC	WSC	Pep	SC	SSC	WSC				
147631	B2RA72_HUMAN		40.82	21777	41	25.375												
147567	PP1B_HUMAN	PPP1CB	29.66	37187	3	TD-CHMP1B only						10	10	3	6			
147488	AOAO24RB85_HUMAN	PA2G4	29.7	43787	10	11	1	1	1	1		9	11	11	11			
147496	AOAO24R7C7_HUMAN	ILF3	14.43	95338	9	10	1	1	1	1		9	10	10	10			
146984	AOAO87WY55_HUMAN	VTA1	32.86	31102	8	TD-CHMP1B only						8	8	8	8			
146934	DCTP1_HUMAN	DCTPP1	32.94	18681	7	TD-CHMP1B only						7	7	7	7			
147478	STRAP_HUMAN	STRAP	29.43	38438	6	TD-CHMP1B only						6	6	6	6			
147466	A8K4W5_HUMAN		23.68	41379	6	TD-CHMP1B only						6	7	7	7			
147465	B5BUB5_HUMAN	SSB	20.34	46867	8	TD-CHMP1B only						8	8	8	8			
146832	B4DY09_HUMAN	ILF2	23.01	38910	6	TD-CHMP1B only						6	7	7	7			
147076	A8K651_HUMAN		31.56	31380	5	TD-CHMP1B only						5	6	6	6			
147610	AOA384N5Z8_HUMAN		9.62	76149	5	29.16666667	1	1	0	0.24		5	7	7	7			
147459	AOAO24R9O4_HUMAN	CACYBP	37.28	26210	7	TD-CHMP1B only						7	7	7	7			
147403	B2RDX5_HUMAN		10.41	82114	7	TD-CHMP1B only						7	7	7	7			
147408	AOAO24RDYO_HUMAN	RANBP5	8.75	123630	6	TD-CHMP1B only						6	6	6	6			
147400	AOAO24R821_HUMAN	EIF3S9	8.35	92482	5	TD-CHMP1B only						5	5	5	5			
147228	XPO1_HUMAN	XPO1	6.07	123386	6	TD-CHMP1B only						6	6	6	6			
147402	PROF1_HUMAN	PFN1	28.57	15054	5	TD-CHMP1B only						5	5	5	5			
147399	BOQY89_HUMAN	EIF3L	9.23	70902	4	TD-CHMP1B only						4	5	5	5			
146833	AOAO24RBB7_HUMAN	NAP1L1	20.2	45374	4	TD-CHMP1B only						4	5	5	5			
147106	AOAOS2Z3LO_HUMAN	ETFA	22.22	35080	5	TD-CHMP1B only						5	5	5	5			
146729	AOAOS2Z410_HUMAN	HSD17B10	34.1	26923	5	TD-CHMP1B only						5	6	6	6			
147091	AOA2R8Y4I8_HUMAN	SPAST	12.01	63535	5	TD-CHMP1B only						5	5	5	5			
147009	SPI6H_HUMAN	SUPT16H	6.21	119914	5	TD-CHMP1B only						5	6	6	6			
147096	CLIC1_HUMAN	CLIC1	34.02	26923	5	TD-CHMP1B only						5	5	5	5			
147371	ASNS_HUMAN	ASNS	10.34	64370	5	TD-CHMP1B only						5	5	5	5			
147389	I3L397_HUMAN	EIF5A	36.73	16118	4	TD-CHMP1B only						4	7	7	7			
146821	AOAOS2Z2Z6_HUMAN	ANXA6	10.55	75873	5	TD-CHMP1B only						5	5	5	5			
146698	AOA2P9APZ7_HUMAN	BQ8482_34C	3.68	20748	2	TD-CHMP1B only						2	10	10	10			
147618	G3P_HUMAN	GAPDH	52.84	36053	12	5	3	3	3	3		11	15	15	15			
147602	A8K486_HUMAN		49.09	18013	10	6	2	2	2	2		9	12	12	12			
147518	AOA384MEJ3_HUMAN		29.84	49229	7	5.825396825	2	2	1	1.89		10	12	7	11			
147525	PGK1_HUMAN	PGK1	33.09	44615	9	9	1	1	1	1		8	9	9	9			
147632	A8K674_HUMAN		10.51	68448	1	5.494382022	3	4	0	2.67		8	21	2	14.7			
147485	B2R7P8_HUMAN		16.55	64635	8	7	1	1	1	1		7	7	7	7			
147568	AOA14OVJS9_HUMAN		21.99	38631	2	TD-CHMP1B only						9	9	2	4			
147468	AOAOS2Z3G9_HUMAN	ACTN4	9.11	104854	4	8.036144578	1	1	0	0.83		6	7	5	6.67			
147531	PSD11_HUMAN	PSMD11	17.77	47464	6	6	1	1	1	1		6	6	6	6			
147385	IPO7_HUMAN	IPO7	7.8	119517	6	5	1	1	1	1		5	5	5	5			
147391	6PGD_HUMAN	PGD	17.81	53140	6	5	1	1	1	1		5	5	5	5			
147405	B4DPD5_HUMAN	OTUB1	13.96	35181	4	5	1	1	1	1		4	5	5	5			
147519	AOAO24R7T3_HUMAN	HNRPF	18.31	45672	4	TD-CHMP1B only						5	5	4	4.31			
147407	AOA14OVK94_HUMAN	RANBP1	36.82	23310	4	5	1	1	1	1		4	5	5	5			
147387	A8K492_HUMAN		6.11	101144	4	TD-CHMP1B only						4	4	4	4			
147450	B4DDU6_HUMAN		12.72	55421	6	5	1	1	1	1		5	5	5	5			
147394	PSMD2_HUMAN	PSMD2	7.05	100200	4	TD-CHMP1B only						4	4	4	4			
146805	AL9A1_HUMAN	ALDH9A1	10.32	53802	4	TD-CHMP1B only						4	4	4	4			
147208	AOAO24R4Z6_HUMAN	SSRP1	7.33	81075	4	TD-CHMP1B only						4	4	4	4			

147500	B2R858_HUMAN		10.38	53216	4	TD-CHMP1B only				4	4	4	4	
146981	AOAO24R9D3_HUMAN	RPL30	40.87	12784	3	TD-CHMP1B only				3	3	3	3	
147490	AOAO24R3Z2_HUMAN	SUMO1	43.56	11557	4	TD-CHMP1B only				4	4	4	4	
147103	AOAO24R2C5_HUMAN	VPS4B	13.29	49302	4	TD-CHMP1B only				5	5	4	4.57	
147051	B4DRT4_HUMAN		51.61	17326	4	TD-CHMP1B only				4	4	4	4	
147010	AOAO24ROO7_HUMAN	PPP5C	6.61	56879	3	TD-CHMP1B only				3	3	3	3	
147084	B4E2J2_HUMAN		33.82	16129	4	TD-CHMP1B only				4	4	4	4	
146751	ELAV1_HUMAN	ELAVL1	16.26	36092	4	TD-CHMP1B only				4	4	4	4	
146777	AOA384MDR8_HUMAN		11.14	39233	3	TD-CHMP1B only				3	3	3	3	
146823	OOVGA5_HUMAN	SARS	9.39	58407	3	TD-CHMP1B only				3	3	3	3	
146880	AOAOB4J1W3_HUMAN	NAA15	7.75	101201	4	TD-CHMP1B only				4	4	4	4	
147200	SPEE_HUMAN	SRM	14.57	33825	4	TD-CHMP1B only				4	4	4	4	
147203	AOAO24R7B7_HUMAN	CDC37	12.17	44468	3	TD-CHMP1B only				3	3	3	3	
147062	B3KNN7_HUMAN		8.03	57232	3	TD-CHMP1B only				3	3	3	3	
147102	AOAO24R7O5_HUMAN	VPS4A	10.07	48898	3	TD-CHMP1B only				4	4	3	3.43	
146818	AOAO24RCN6_HUMAN	VAR5	3.24	140476	3	TD-CHMP1B only				3	3	3	3	
147012	VDAC3_HUMAN	VDAC3	14.84	30659	3	TD-CHMP1B only				3	3	3	3	
147171	AOAOS2Z4T1_HUMAN	MCM3	4.95	90981	3	TD-CHMP1B only				3	3	3	3	
147027	AOA14OVK27_HUMAN		6.87	69285	3	TD-CHMP1B only				3	3	3	3	
146768	A8QI98_HUMAN		3.44	109058	3	TD-CHMP1B only				3	3	3	3	
147132	AOAO24RB41_HUMAN	NCG_2016482	19.53	23384	3	5	1	1	1	1	3	5	5	5
147061	AOAO24RBX9_HUMAN	PDHA1	9.74	43296	3	TD-CHMP1B only				3	3	3	3	
147168	A8K6D2_HUMAN		14.75	26692	3	TD-CHMP1B only				3	3	3	3	
147178	AOA384MDW7_HUMAN	ECHS1	13.45	31399	2	TD-CHMP1B only				2	3	3	3	
147368	AOAOS2Z4A5_HUMAN	MCM7	6.95	81308	4	TD-CHMP1B only				4	4	4	4	
147436	B4DRS4_HUMAN		4.58	82022	3	TD-CHMP1B only				3	3	3	3	
147221	B4DJB4_HUMAN		11.08	34506	3	TD-CHMP1B only				3	3	3	3	
146800	AOA3B3IT15_HUMAN	COPA	3.74	136020	3	TD-CHMP1B only				3	3	3	3	
146982	HAT1_HUMAN	HAT1	12.89	49513	3	TD-CHMP1B only				3	3	3	3	
147117	SYAC_HUMAN	AARS	3.72	106810	3	TD-CHMP1B only				3	3	3	3	
147440	B4EOS6_HUMAN		4.72	89547	3	TD-CHMP1B only				3	3	3	3	
147014	AOAO24RAMQ_HUMAN	TNPO1	3.56	102355	3	TD-CHMP1B only				3	3	3	3	
146779	B7Z7P8_HUMAN	ETF1	7.8	47476	3	TD-CHMP1B only				3	3	3	3	
146788	AOAO24R1Q8_HUMAN	RPL23	25	14865	2	TD-CHMP1B only				2	3	3	3	
147082	B4DNN4_HUMAN		6.56	86452	3	TD-CHMP1B only				3	3	3	3	
147374	AOAO24R5K8_HUMAN	SERPINH1	9.09	46441	3	TD-CHMP1B only				3	3	3	3	
146980	AOAO24QZZ7_HUMAN	HIST1H2BD	26.19	13936	3	TD-CHMP1B only				3	3	3	3	
147431	AOAO87WVN4_HUMAN	FDPS	15.69	31774	3	TD-CHMP1B only				3	3	3	3	
147001	FEN1_HUMAN	FEN1	12.37	42593	3	TD-CHMP1B only				3	3	3	3	
146978	AOA14OVJY7_HUMAN		26.83	13941	3	TD-CHMP1B only				3	3	3	3	
146766	AOAO9ON7UO_HUMAN	CUL1	6.96	89679	3	TD-CHMP1B only				3	3	3	3	
147022	E9PGT1_HUMAN	TSN	21.08	25572	3	TD-CHMP1B only				3	3	3	3	
147121	MOR21O_HUMAN	RPS16	22.48	14419	3	TD-CHMP1B only				3	3	3	3	
146826	AOAO24R8P8_HUMAN	RPL38	35.71	8218	2	TD-CHMP1B only				2	3	3	3	
147129	AOAO24R2O3_HUMAN	PSME3	10.57	30890	2	TD-CHMP1B only				2	3	3	3	
147150	A4GYY8_HUMAN	KFZp686F17	9.24	50263	3	TD-CHMP1B only				3	3	3	3	
147434	AOAO24RC65_HUMAN	NCG_1991735	2.84	189252	3	TD-CHMP1B only				3	3	3	3	
146719	B4E1K8_HUMAN	EIF3D	4.66	52828	2	TD-CHMP1B only				2	3	3	3	
146692	HEAT3_HUMAN	HEATR3	3.68	74583	3	TD-CHMP1B only				3	3	3	3	

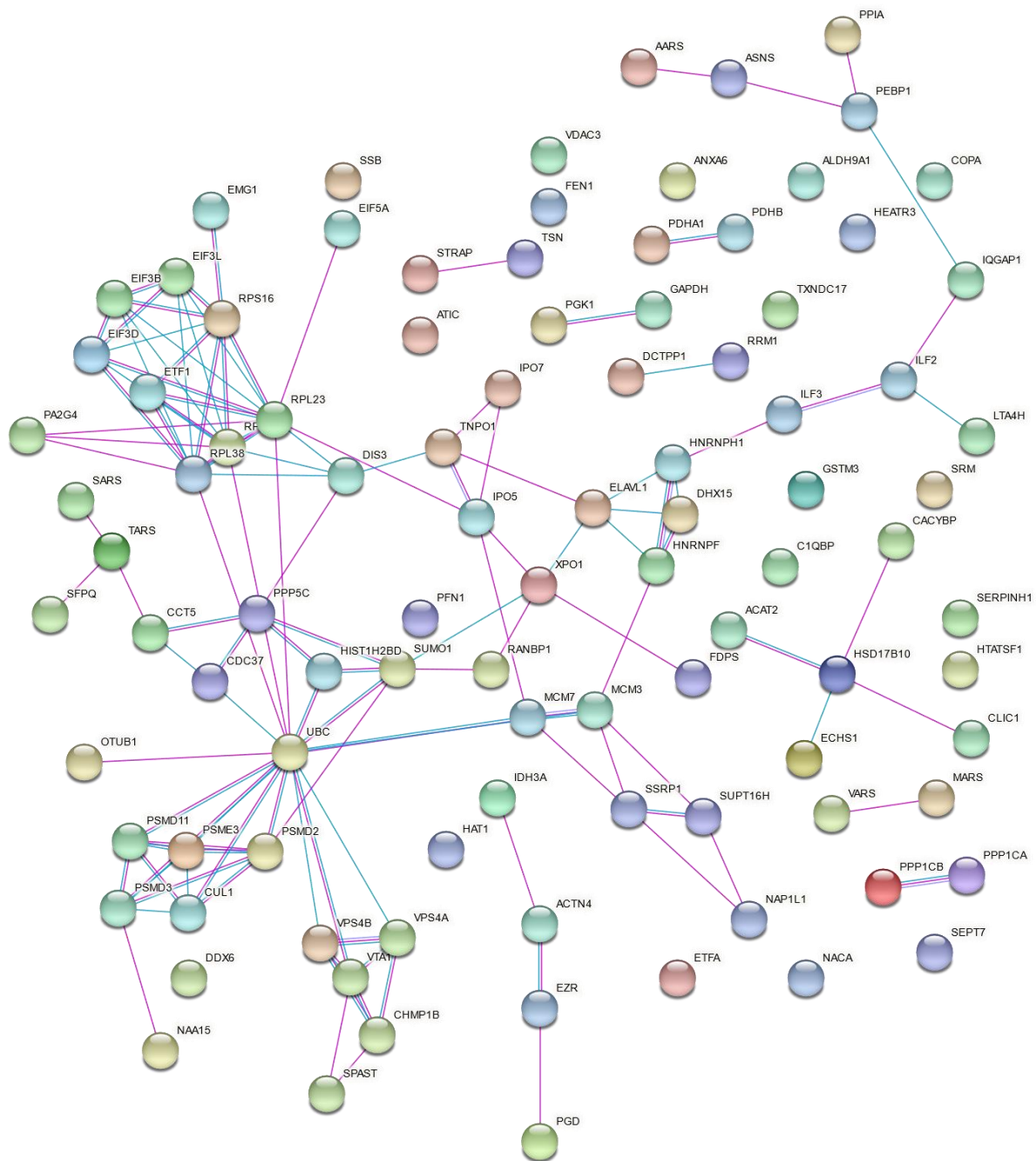
Pep	Number of identified peptides												
SC	Spectral Counts: mass spectra allow the identification of peptides belonging to the protein												
SSC	Specific Spectral Counts: mass spectra allow the identification of peptides belonging specifically to the protein												
WSC	Weighted Spectral Counts: SSC + the weight of unspecific SC (in the case of peptides shared between several proteins)												
	Classical contaminant												
	Identified with 1 peptide but with SC and SSC >= 2												
	Identified with several peptides but with SSC = 1												
	Identified with 1 peptide and SC = 1												
	Protein with SSC = 0												

Key:

	Identified only in TD-CHMP1B sample with WSC >= 5 or enriched at least 10 times in TD-CHMP1B sample compared to other samples
	Identified only in TD-CHMP1B sample with WSC >= 3 or enriched at least 5 times in TD-CHMP1B sample compared to other samples

## 2.5.2 Supplemental Figure 1

String-db.org network of interaction among the 97 hits from the MS list of the SDAD experiment.



### Network Stats

number of nodes: 97  
 number of edges: 128  
 average node degree: 2.64  
 avg. local clustering coefficient: 0.548

expected number of edges: 68  
 PPI enrichment p-value: 6.14e-11  
*your network has significantly more interactions than expected (what does that mean?)*

\* the image was generated with the following criteria = only “Databases” (light blue line) and “Experiments” (pink lines) were kept as sources of interactions. Permanent link = <https://version-11-0b.string-db.org/cgi/network?networkId=b1NM5tKeNO6z>



### 2.5.3 Supplemental Table 2

Gene Ontology (GO) term analysis of the network in Supplemental Figure 1, generated by String-db.org. Results were sorted by strength, and a cutoff value of 1.7 was applied. FDR = false discovery rate. IRES = internal ribosome entry site

#term ID	term description	observed in network	category count	strength	FDR	matching proteins in the network
GO:0061738	late endosomal microautophagy	2	3	2.13	0.0041	VPS4B,VPS4A
GO:0075525	viral translational termination-reinitiation	3	5	2.08	0.00021	EIF3D,EIF3B,EIF3L
GO:0019076	viral release from host cell	3	6	2	0.00027	VPS4B,VPS4A,PPIA
GO:0052192	movement in environment of other organism involved in symbiotic interaction	3	6	2	0.00027	VPS4B,VPS4A,PPIA
GO:1904903	ESCRT III complex disassembly	4	10	1.91	3.03E-05	VPS4B,VPS4A,VT A1,CHMP1B
GO:0090611	ubiquitin-independent protein catabolic process via the multivesicular body sorting pathway	2	5	1.91	0.0076	VPS4B,VPS4A
GO:0006610	ribosomal protein import into nucleus	3	8	1.88	0.00047	IPO5,TNPO1,RPL23
GO:0061732	mitochondrial acetyl-CoA biosynthetic process from pyruvate	2	6	1.83	0.0095	PDHB,PDHA1
GO:0019081	viral translation	4	13	1.79	6.03E-05	EIF3D,EIF3B,SSB,EIF3L
GO:0075522	IRES-dependent viral translational initiation	3	10	1.78	0.00075	EIF3D,EIF3B,SSB
GO:0006449	regulation of translational termination	2	8	1.7	0.0144	EIF5A,ETF1
GO:0042780	tRNA 3'-end processing	2	8	1.7	0.0144	HSD17B10,SSB

## 2.5.4 Supplemental Figure 2

Alignment of OTUB1 (top) and OTUB1-Arf1 (bottom) isoforms amino acid sequences. Highlighted in yellow the immunogen sequence used to produce the antibody CSB-PA03595A0Rb used in this study.

```
1 ----- 0
1 MMKPSWLSRTEFSKRLLCRTLWCQSGWSSRSYTRSMLKMTTSINRRSRTS 50
1 -----MAAEEPQQKQEPLGSDSEG 20
      |.|.....:|.....|
51 TKSTRTSARPGLTATVSIGLSDSPTWRHRCWMTARSCSGEKGHWPAPRVG 100
21 VNCLAYDEAIMAQDRIQQEIAVQNPLVSEERLELSVLYKEYAEDDNIYQQ 70
   |..| ..|: ..|||:..|. ..|:
101 VYLL-----PGRV-----GCVSSRVSPSF-----PGDGL--- 124
71 KIKDLHKKYSYIRKTRPDGNCFYRAFGFHLEALLDDSKEL-----QR 113
      |.....|.....|.|.:.|.:.|. .|
125 -----DSGLARRGSAVSALASGLVEEPMLGPPFHPTPR 157
114 FKAVSAKSKEDLVSQGFTEFTIEDFHNTFMDLIEQVEKQTSVADLLASFN 163
   |||
158 FKAVSAKSKEDLVSQGFTEFTIEDFHNTFMDLIEQVEKQTSVADLLASFN 207
164 DQSTSDYLVVYLRLLTSGYLQRESKFFEHFIEGGRTVKEFCQQEVEPMCK 213
   |||
208 DQSTSDYLVVYLRLLTSGYLQRESKFFEHFIEGGRTVKEFCQQEVEPMCK 257
214 ESDHIHIIALAQALSVS IQVEYMDRGEGGTTNPHIFPEGSEPKVYLLYRP 263
   |||
258 ESDHIHIIALAQALSVS IQVEYMDRGEGGTTNPHIFPEGSEPKVYLLYRP 307
264 GHYDILYK 271
```

# DISCUSSION AND PERSPECTIVES

## 1 Clinical potential of salicylanilide compounds

The first part of my thesis work identified closantel and niclosamide, two members of the salicylanilides family, as potent reversible inhibitors of USP8 catalytic activity in vitro, and of ACTH secretion in AtT-20 pituitary cells. These two compounds are presently used in livestock mainly rather than in humans, although niclosamide is under clinical assays for cancer treatments. The question of their potential development as medicinal drugs for Cushing's disease treatment is therefore an open question that is worth to further investigate.

The primary action of salicylanilides has generally been associated with the uncoupling of oxidative phosphorylation, closantel is used extensively for the control of *Haemonchus spp.* and *Fasciola spp.* infestations in sheep and cattle and *Oestrus ovis* in sheep in many parts of the world. Niclosamide is used extensively for its anticestodal activity in a wide range of animals. Antiparasitic activity of the halogenated salicylanilides has also been demonstrated against a large number of other internal parasites, in particular haematophagous helminths, and external parasites including ticks and mites, in a variety of animal species (Swan, 1999).

The salicylanilide anthelmintic drugs have been the subject of renewed interest and intensive repurposing studies these last 10 years. In Pubmed, search results for the keyword « niclosamide » increased significantly from an average of 11 in the 1950-2009 of 11 per year to reach a peak of 88 new publications in 2018 (Figure C-01).

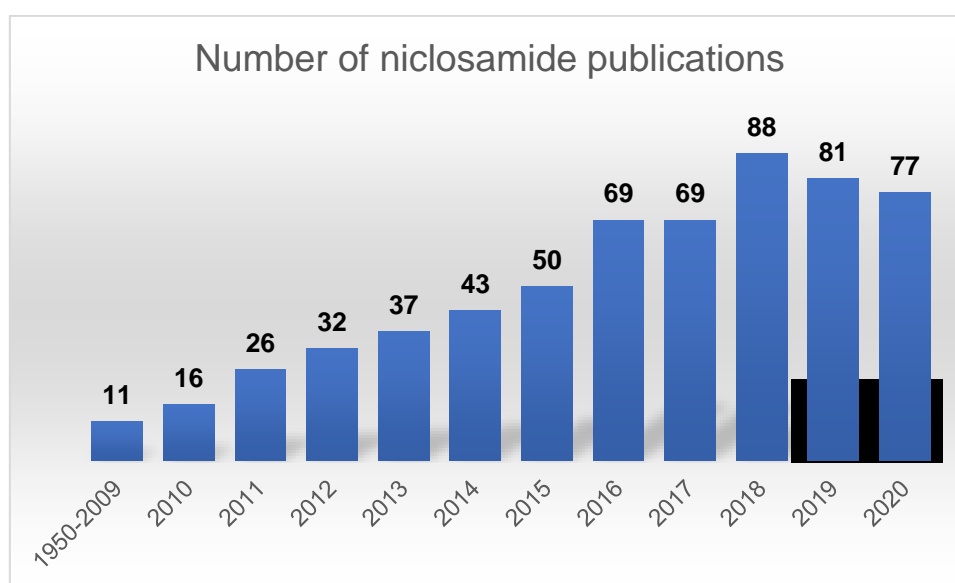


**Figure C-01. Number of niclosamide publications per year in Pubmed** as of February 2021. The value for 1950-2009 represents the average per year for the period.

A great number of these studies deals with niclosamide's potential as an anti-cancer drug (Barbosa et al., 2019; Gyamfi et al., 2019, 2019; Newton, 2019), including one finished phase I (Schweizer et al., 2018) and one phase II (Burock et al., 2018) clinical studies. Other fields where niclosamide has shown interesting therapeutical potential are diabetes and obesity (Guo et al., 2019, 2019; Han et al., 2018; Tao et al., 2014), as an antibacterial agent (including drug resistant *Staphylococcus aureus*) (Imperi et al., 2013; Rajamuthiah et al., 2015; Sun and

Zhang, 1999; Zhu et al., 2009), as a broad-spectrum antiviral agent with potential activity in viral infections by SARS-CoV-2 (COVID-19) (Jeon et al., 2020; Wu et al., 2004a; Xu et al., 2020). As of February 2021, the website ClinicalTrials.gov identifies one further finished clinical trial for rheumatoid arthritis (Al-Gareeb et al., 2018), two recruiting studies in cancerology, one for diabetic nephropathy, and four for COVID-19 infection.

Closantel itself presents a more different research paradigm: the majority of the recent studies are still related to its usage as an anti-parasitic for use in cattle and sheep, and repositioning studies are much more timid. It has been shown to be an inhibitor (via molecular docking) of the V600E mutation of the B-Raf protein (Li et al., 2016), a protein kinase which is mutated in a broad range of human cancers and especially in malignant melanoma (Holderfield et al., 2014). This activity may be direct, or, in light of our results the indirect consequence of USP8 inhibition in a context where USP8 regulate the stability of upstream receptors activating B-Raf such as the EGFR (David H. Ilson, 2019). It has also been shown to suppress angiogenesis in zebrafish and cancer growth in zebrafish xenotransplanted with human lymphoma, cervical cancer, pancreatic cancer, and liver cancer cells (Zhu et al., 2016). Other reported biological activities of closantel include an amplification of the effect of polymyxin B against multidrug-resistant *Acinetobacter baumannii* (Tran et al., 2016), inhibitory effects on canine parvovirus (Zhou et al., 2019) and inhibition of the SPAK and OSR1 kinases (AlAmri et al., 2017) (two kinases able to phosphorylate a series of sodium, potassium, and chloride ion co-transporters, that are new targets in the discovery of new antihypertensive agents). No finished or recruiting clinical trials are registered on the website ClinicalTrials.gov as of February 2021.

There have been a few reports of toxicity in humans with closantel (15 cases), all due to overexposure to the product, with the central nervous system, retina, and optic nerve commonly being affected (Asoklis et al., 2018; Essabar et al., 2014; Koziolk et al., 2015; Kumar et al., 2019; Tabatabaei et al., 2016). Ocular symptoms following closantel overdose range from sudden onset blurring of vision to total blindness. Some of the cases were reversible (Koziolk et al., 2015; Kumar et al., 2019) while in some cases vision alterations were persistent even after 22 years (Asoklis et al., 2018). The doses ranged from unknown to 1500 mg once, 2250 mg closantel once, 600 mg/day for 3 days, 500 mg/day for 8 days.

Our results showed a higher overall cellular toxicity for niclosamide in comparison to closantel, although the reduction in ACTH release with niclosamide was more potent (that is, for a same reduction of ACTH release, lower doses of niclosamide could be used than of closantel, potentially compensating an increased toxicity).

It is important to notice that the assay we used to analyze cellular toxicity here, the Prestoblue viability assay, is a general assay that “monitors changes to the cellular reducing environment or metabolic activity by using resazurin-based reagents and is a reliable indicator of cell viability or death”, thus working as a proxy for toxicity. An anti-cancerous compound that inhibits viability and cellular proliferation by specific mechanisms (as might be the case for niclosamide, see above) would potentially give a very significant “toxic” effect on the Prestoblue viability assay. To better differentiate the effect of inhibition of viability of niclosamide and simple gross toxicity, we propose to test it using more specific assays for toxicity such enzyme leakage assays (commercial kits such as CytoTox-Glo Cytotoxicity Assay; Promega Corporation Catalog No. G9290) and apoptosis detection by caspase marking

(CellEvent™ Caspase-3/7 Green Detection Reagent) or simply by following cell growth and confluence over a five to seven days period. The fact that clinical trials are currently being done with niclosamide are rather enthusiastic nevertheless, and signal for the safety of this compound for clinical use.

As for closantel, we are not currently able to estimate what dose would be necessary for a significant effect in humans and if such dose would be safe. It is currently noted that the drug is largely used in livestock and is considered safe, with toxicity occurring with similar effects in the cases of human exposure in animals exposed to large accidental overdoses (Swan, 1999).

Further MedChem studies are necessary to define which of these two compounds has the best druggability potential. Possibly, structure activity relationships studies coupled with MedChem analysis will help in defining a potent derivate analog with no or poor toxicity, a very important challenge in the context of a chronic disease necessitating long-term treatment.

In the study of the USP8 inhibitor DUB-IN-2 (Kageyama et al., 2020) put forward the fact the importance that DUB-IN-2 inhibits the viability of AtT-20 cells while not inhibiting other commonly used cell lines. In our experience (not published) when using this compound as control with HEK-293-T and HeLa cells, there was a strong cell death induced by DUB-IN-2 treatment, even at the same concentrations of 5µM were a significant effect on ACTH release and POM expression in AtT-20 cells were found. As explained in chapter 1 of the introduction, the tumor of Cushing's disease is not one characterized by overt expansion and tissue invasion, being self-localized and limited in size, with macroadenomas of tumors causing a local compression effect being rare. The primary outcome expected from a chemical treatment then should be first and foremost, a reduction of circulating cortisol brought about by a reduction in ACTH release by the pituitary and not a cell killing effect that would be damaging for the pituitary gland

It is important to notice that niclosamide was included in the initial collection screened in the primary campaign (in the Prestwick library), but it was not selected due to limited inhibition of USP8 (5,5% only, not shown). Inhibition of 50% of the maximal USP8 activity was only achieved at about 40µM niclosamide (Figure R1-08). Moreover, at doses displaying significant inhibition of ACTH release, USP8 inhibition *in vitro* was minimal (doses 0,5 and 1 µM) (Figures R1-05 and R1-08). This leads us to believe that the contribution of USP8 inhibition to niclosamide effects on ACTH release are limited or that niclosamide inhibition of USP8 is more efficient *in cellulo* than *in vitro*, which is highly possible as we cannot determine the effective concentration of each compound within the cells. It might be possible then that better biocompatibility of niclosamide compared to closantel is one of the reasons while the first is more subjected to clinical trials, a hypothesis that need to be further explored. The toxic effects of niclosamide should be carefully taken into consideration, nevertheless at the doses 0,5 and 1 µM, there were significant reductions of ACTH secretion of 27 and 41%, respectively (Figure R1-05), but no significant effects on viability (Figure R1-06).

## 2 Mechanisms of ACTH release inhibition by halogenated salicylanilides

The ACTH precursor POMC expression is known to be mediated, at least partly, by EGF stimulation (Childs et al., 1991) and EGFR activation (Fukuoka et al., 2011; Liu et al., 2019a), which is itself stabilized by USP8 as described in the introduction of this manuscript. Hence, USP8 inhibition may decrease EGFR levels, itself provoking a decrease in POMC expression and ACTH production. Indeed, we have observed a decrease in POMC transcripts in cells treated by closantel. Nevertheless, we have not yet investigated the expression levels of EGFR in cells treated by either closantel or niclosamide and further experiments should be performed to assess if closantel and niclosamide act mainly through USP8 inhibition or through other targets putatively implicated in ACTH production. It would be particularly interesting to test whether or not these two compounds can reverse *in cellulo* the effect of the expression of constitutive variants of USP8 found in Cushing's disease patients on EGFR stabilization, POMC gene expression and ACTH release.

Two possible mechanisms for the activity of niclosamide as an antiviral and more specifically as an agent for SARS-CoV-2 can be suggested. First, it has been shown that niclosamide inhibits infection with human rhinoviruses and influenza virus by blocking the acidification of the endolysosomal compartments (these viruses need a low-pH step for successful entry), although with a mode of action different from classical agents such as the v-ATPase inhibitor Bafilomycin A1, or the lysosomotropic agents ammonium chloride (NH<sub>4</sub>Cl) or chloroquine (Jurgeit et al., 2012). A similar pH-dependent effect has been shown recently for SARS-CoV-2 infection, in which the receptor binding domain (RBD) of SARS-CoV-2 was shown to be internalized via the clathrin and dynamin-independent, pH-dependent CLIC/GEEC endocytic pathway. This kind of internalization process is inhibited by endosomal acidification inhibitors like Bafilomycin A1 and NH<sub>4</sub>Cl, as well as by niclosamide (Prabhakara et al., 2020). It could be possible that the observed effects on ACTH secretion with niclosamide might arise, in addition or as an alternative mechanism to USP8 inhibition, from a similar interference on the endocytic recycling of plasma membrane receptors such as the EGF or CRF receptors, thus affecting the production of ACTH. In fact, internalized EGFR bound to its ligand is still partially active in signaling (Caldieri et al., 2018), the pH shift occurring in endosomes induces the unbinding of the EGF and cessation of the signal. An acidification inhibitor like the niclosamide could ultimately lead to a blockade of the process and subsequent shutdown of the downstream signaling pathways triggering POMC expression. Of note, our tests were done in relatively long timescales (24 hours compound exposure) to better capture such responses that happen with chronic drug treatments.

A second potential mechanism for niclosamide action as an antiviral drug stems from the interference of niclosamide on autophagy. Autophagy (see introduction) is an essential component of host defense against viral infection (Dong and Levine, 2013; Orvedahl et al., 2010), and Beclin1 (BECN1) is one of its key regulators. Gassen et al identified the S-phase kinase-associated protein 2 (SKP2) as an E3 ligase that triggers the K-48- poly-ubiquitination of BECN1, thus promoting its proteasomal degradation. Middle East respiratory syndrome

coronavirus (MERS-CoV) multiplication results in reduced BECN1 levels and blocks the fusion of autophagosomes and lysosomes. They showed that niclosamide is an inhibitor of SKP2 that enhances autophagy and reduces the replication of MERS-CoV up to 1000-fold. (Gassen et al., 2019). The same team later evaluated the effects of SARS-CoV-2 infection on autophagy, and determined that niclosamide inhibited SARS-CoV-2 replication >99% by similar pathways (Gassen et al., 2020).

Interestingly, niclosamide has been described as an inhibitor of STAT3 activation, which motivated its use as an anti-cancer agent (Lee et al., 2020; Li et al., 2013; Ren et al., 2010). The EGFR actually catalyzes the tyrosine phosphorylation of the transcription factor STAT3 in response to EGF, affecting cell growth, apoptosis, and cell cycle arrest. Moreover, STAT3 activation is required for POMC expression, at least in the hypothalamus (Dey et al., 2016; Dubin John H. et al., 2013; Ernst et al., 2009; Münzberg et al., 2003), and also mediates POMC expression and ACTH release in pituitary cells (Bousquet and Melmed, 1999; Bousquet et al., 2000). The reported role of niclosamide on STAT3 activation may be actually indirectly caused by USP8 inhibition and is fully consistent with its inhibitory effect on ACTH release. Alternatively, the niclosamide may interfere with STAT3 activation through a different or additional pathway than EGFR that stays to be determined and may explain its high efficacy on ACTH secretion while its inhibitory effect on USP8 *in vitro* is rather modest.

The lack of clear effects of oxyclozanide leads us to believe that biological effects of niclosamide and closantel do not seem to be fully attributable to the common molecular scaffold of halogenated salicylanilides. Further structure activity relationships studies and docking analysis will be necessary to determine the chemical groups essential for the activity of these two compounds.

As explained in chapter 1 of the introduction, gain-of-function mutations in USP8 have been found in a subset of patients harboring Cushing's disease. The development of a biocompatible non-toxic compound targeting the constitutive activity of USP8 could be of great advantage, on a personalized approach for these patients, in particular.



### **3 Seeking for new partners of CHMP1B and USP8: methodological difficulties and experimental choices**

The experiments for this article were the ones that took the longest time to be accomplished during my thesis. A great part of the first year and second year of thesis was indeed devoted to setting-up the constructs and purification conditions before to get samples ready for M/S analysis. The initial idea was to perform a sequential TAP-tag of either STREP or FLAG tagged USP8 and CHMP1B under physiological, non-denaturing conditions. This was made very difficult by the apparent inability to purify either of these proteins in non-denaturing conditions. Moreover, while USP8 showed slight expression levels, sometimes almost undetectable compared to endogenous levels, CHMP1B showed a rather strong expression levels that could be however efficiently controlled by varying the amount of induction agent of the expression system. Having clearly shown the high levels of expression of CHMP1B in the cell lysates, we still could not purify the protein. The question of accessibility of the tag started being addressed at this moment. The small double-STREP and FLAG tags had been chosen on purpose instead of large tags for the compromise of avoiding steric hindrance and possibly losing complex interactions, at the expense of a smaller accessible surface. It was then that the fusion of these two tags (the “tandem, TD” tag was tried), under the denaturing conditions of 6M urea was tried, and we obtained great recovery levels. This was thought to be due to relaxation of the tertiary structure and exposure of the tag. We then faced the obvious problem of loss of interactions by adding the urea. This was solved by using the chemical cross-linkers agents. These small-molecule reagents have amino-acid reacting moieties at each opposing sites and the capacity to form stable bonds between the two, effectively stabilizing two adjoining interacting residues (from the same protein/peptide, in the case of a intramolecular link, or from an adjacent one)

At first, we ran some trials with paraformaldehyde (PFA) at different concentrations. (Srinivasa et al., 2015; Tayri-Wilk et al., 2020), it is a broad, “zero-length”, non-specific, partially reversible in Laemmli buffer cross-linker, specially used to capture protein-DNA interactions. In our hands, it provided results that were irregular from one experiment to another, always with very extensive cross-linking and a considerable loss of protein after lysate clearing by centrifugation (the pellets were accordingly larger in comparison to same ones treated with other cross-linkers). The reversibility in Laemmli sample buffer was limited. Its zero-length character (meaning it does not add any atoms to the cross-linked species due to the lack of a spacer arm) was also more limiting for finding new interactors and would be perhaps more useful to explore the topography of known interactors.

That’s why we decided to follow-up with two compounds of similar chemistries: DSP (dithiobis succinimidyl propionate) and SDAD (succinimidyl 4,4'-azipentanoate):

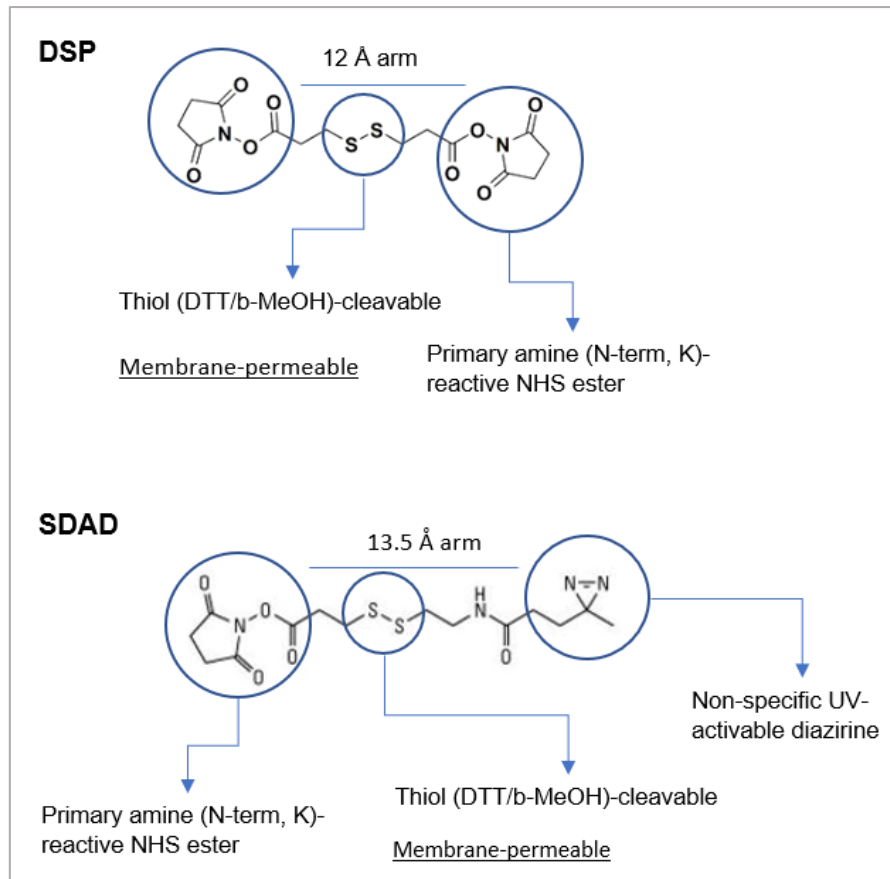


**Figure C-02. Overview of the chemistries of DSP and SDAD.**

- Both of these two agents are based on an NHS-ester chemistry on one side (meaning there are N-terminal and lysine-reactive);
- they provide a medium length spacer-arm (allowing to capture interactions with residues that are farther apart than with a zero-length cross-linker, increasing efficiency but potentially increasing non-specificity);
- they are reversible with thiols;
- they are membrane permeable and functional at physiological buffering conditions (meaning that cross-linking can be done with intact cells).
- DSP is a mirror molecule, containing another NHS-ester moiety at the other side, while SDAD contains a non-specific UV-activable (320-370 nm) diazirine that has the potential to bind to any other chemical bond on any other residue or peptide backbone.

Overall, the change of strategy from physiological TAP-tag STREP-FLAG successive purification of CHMP1B to denaturing tandem-tag cross-linking CHMP1B purification was one that initially served for troubleshooting to permit us to start with the MS analysis. This strategy was eventually very beneficial in the sense that it provided for 1) probable capture of a higher-complex structure we would not be able to capture with a simple immunoprecipitation technique 2) very clean starting material for the MS analysis since the cross-linking allows harsher washing with urea without loss of information.

A first mass-spectrometry experiment with DSP cross-linking provided a list of only 4 proteins: VTA1, PBEF1, CPNE1, PSME2, PCBD1. VTA1 being a known partner of both

CHMP1B and USP8 that was also identified in the second SDAD analysis, which identified 97 putative partners of CHMP1B as presented in the article manuscript of this result's chapter.

The samples used for MS analysis were also used to probe the previously known partners of CHMP1B by immunoblotting using specific antibodies, mainly VTA1, SPAST and VPS4. Strangely, none of these proteins were detected by immunoblotting on purified CHMP1B containing complexes. Although we still ignore the reasons why we failed to detect these partners, it might be possible that after the treatment with DTT, the half arm of SDAD that remains attached to each of the corresponding protein, may hinder antibody-antigen interaction and explain a loss of signal on the blot. We are not aware of examples of this occurring though, and this remains speculative.

Similarly, new candidate partners of specific interest were probed by immunoblotting of purified CHMP1B complexes without success (Cacybp, PSME3, TCP1-y, PSMD11, XPO1, RING1B, Cbl, Cul, RNF126, B-TrCP, USP47, Skp1, HRS, UCHL1) except for OTUB1 which interaction with CHMP1B was further investigated by co-purification experiments (see results).

A preliminary M/S analysis was also done with myc-USP8 being purified with a myc-trap resin. Most of the identified partners were one of the several 14-3-3 proteins. The other hits responding to criteria for inclusion as potential partners of USP8 were GRB2, TPI1, GRWD1, UCHL5, RBM17, SERPINB3, MED13, TIMM8B, NUP62, SF1, TBC1D15 and UBR7 (GRB2 already being a known partner of USP8 (Kato et al., 2000)). The finding of known partners such as 14.3.3 and GRB2 validate the data that needs to be further investigated to identify new relevant USP8 partners among the list obtained by M/S strategy.

We thus conclude that other experiments based on the native interactions native lysates are needed to further confirm protein-protein interaction identified here under chemical stabilizing conditions.

## 4 Interaction between CHMP1B and OTUB1: perspectives

### 4.1 Mapping the residues involved in OTUB1/CHMP1B interaction by XL-MS

The crosslinking step not only provides for stabilization of interactions, but also adds for an entire level of information since, when, by being coupled to the mass-spectrometry identification of the cross-linked peptides between the interacting proteins, if sufficient residues are cross-linked it allows for the “mapping” of the interaction. This is what has been developed in the last years as the exciting technique of “XL-MS” (cross-linking/MS) (Holding, 2015; Yu and Huang, 2018). Obtaining samples for XL-MS analysis with collaborating platforms has been a tempting objective during this thesis to map the residues involved in the interaction between CHMP1B and OTUB1 but has been postponed due to major inherent problems with this technique (Dr: Alexander Leitner, Institute of Molecular Systems Biology ETH Zurich, personal communication): 1) need for a great amount of starting material 2) far greater experience with in-vitro cross-linking or purified proteins than purified complexes originating from intracellular cross-linking (samples too complex).

### 4.2 Confirmation and investigation of the role of OTUB1:CHMP1B complex in endocytosis

As mentioned before, even though we have various evidence for the interaction between CHMP1B and OTUB1, the extent and the role of this interaction on EGFR stabilization need to be further characterized.

Immunofluorescence labelling of cells overexpressing CHMP1B and OTUB1 could allow us to 1) confirm the existence of co-localization hubs for these proteins, strengthening the evidence they interact, 2) localize these proteins to the endocytic machinery (with the help of markers such as the early endosome antigen 1 – EEA1 or one of the several Ras-related protein – Rab). Validation could be obtained from the interaction being lost upon OTUB1 siRNA transfection. siUSP8 extinction could help in determine its role in bridging the interaction if the signal is abrogated, although simple increases or decreases in the fluorescence signal in this condition might be harder to interpret due to USP8 being a DUB acting both on CHMP1B and OTUB1.

Since the OTUB1::CHMP1B complex has been found here in conditions that favor the stabilization of interaction of labile nature due to the stabilization by cross-linking, the information obtained by the proposed immunofluorescence labelling could similarly be obtained by the very sensitive technique of proximity-ligation assay (Alam, 2018) with the native proteins.

Experiments could also be carried in-vitro to reconstitute this complex. We could work with GST pull-down assay using either immobilized GST-tagged CHMP1B or OTUB1 and a HEK-293-T whole-cell lysate to capture the other protein. Interactions are highly favored in this setup, unlike the in-situ cross-linking experiments performed in this study, so the information is complimentary to the one presented here.

Protein-fragment complementation assay (PCA) have recently been adapted for the detection of ubiquitination. Boulch et al. describe a sensitive method for examining mono- or

polyubiquitin signals conjugated to proteins expressed at endogenous levels using PCA derived from the NanoLuc luciferase and designed to probe the ubiquitylation of select proteins and using the budding yeast as a model system (Boulch et al., 2019). This system could be used for the detection of deubiquitination of CHMP1B by OTUB1 and could circumvent the pitfalls of the assay presented here, mainly the need for overexpression of a tagged ubiquitin precursor to increase the intracellular pool of ubiquitin (to permit the detection of ubiquitination by Western blot), which unfortunately might override the endogenous ubiquitin conjugation pathways.

### 4.3 Investigating the putative role of GRAIL in CHMP1B regulation

As described before, USP8, GRAIL (RNF128) and OTUB1 exist in a functional trimolecular complex (Soares et al., 2004) (Whiting et al., 2011) (Figure C-03). GRAIL, a ubiquitin-protein ligase (E3), is an important gatekeeper of T cell unresponsiveness, being most well characterized as a negative regulator of TCR responsiveness and cytokine production.

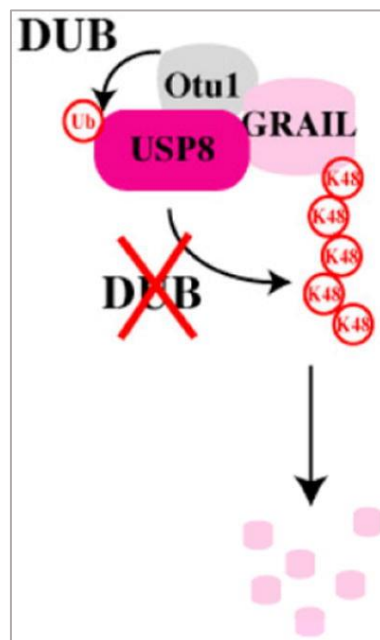


**Figure C-03. Trimolecular complex.** GRAIL is associated with and regulated by two isoforms of OTUB1. OTUB1 binds to Ub-GRAIL but does not deubiquitinate it. USP8, binds to GRAIL and to OTUB1 in a tri-molecular complex. USP8 can function as a DUB for auto-ubiquitinated GRAIL, however USP8's DUB function is blocked by OTUB1, but not catalytic mutants of OTUB1 or its alternatively spliced isoform, OTUB1-ARF1. USP8 must be ubiquitinated to function as a DUB for auto-ubiquitinated GRAIL. OTUB1, (but not catalytic mutants), deubiquitinates USP8, inactivating it and allowing auto-ubiquitinated GRAIL to be degraded by the 26S proteasome.

GRAIL partially colocalizes with the ER marker bip/GRP 78, with Golgi marker syntaxin 5, and with the late endosomal GTPase Rab7, further, GRAIL localization closely associates with the recycling endosomal compartments defined by transferrin receptor recycling (Anandasabapathy et al., 2003). GRAIL is associated with cell proliferation and promotes malignant behaviors in different cancers via EGFR (Bai et al., 2020; Gao et al., 2019)

induced pathways. The trimolecular complex with USP8, GRAIL and OTUB1, the localization of GRAIL to the endocytic pathway and the existence of a function for GRAIL in the EGFR pathways are different remarkable features that all lead us to suggest that it could indeed exist a tripartite GRAIL::OTUB1:CHMP1B complex controlling EGFR stabilization. Although we do not know if GRAIL is expressed in AtT-20 cells or human pituitary gland, the Human Protein Atlas (Uhlen et al., 2017) lists several positive GRAIL RNA-seq samples for human, mouse, and pig pituitary tissue. In light of this, it would be of interest to determine if a GRAIL:CHMP1B or a GRAIL:OTUB1:CHMP1B complex exists, and if GRAIL controls the ubiquitination status of CHMP1B. It would be worth also to further evaluate the impact of GRAIL and OTUB1 on EGFR stabilization, in a manner similar to what has been presented in this thesis.

## 5 General conclusion

The work we performed allowed us to better understand the regulation of CHMP1B, by identifying another deubiquitinase, OTUB1, controlling its ubiquitinated status and stability, and to further suggest that this interaction plays a role on EGFR stabilization. It remains to be investigated how this interaction and the subcellular localization of the complex within the cells may dynamically respond to EGF stimulation, in the continuation of my thesis work.

The field of the regulation by ubiquitination of the ESCRT proteins is vast. We would like to have more time to investigate to which extend other ESCRT proteins are ubiquitinated and regulated by USP8 and how it could impact the pathological state of patients with cancers or Cushing's disease. Similarly, just as important is finding the E3-ligases and DUBs acting on these ESCRT proteins and associated partners involved in cell membrane remodeling such as SPAST. We hope the methods used in our study will be helpful to others in accomplishing this, although we recognize that M/S analysis of affinity purifications might not be sensitive enough to capture transient interactions occurring between an enzyme and a substrate. Despite several assay, we could not identify any E3 as candidate CHMP1B partners, except Cullin 1 for which we were unable to confirm the interaction by independent experimental strategy. Functional studies using siRNA screening of candidate E3 known to act in endocytosis (such as CBL or NRDP1) or of a wider collection of E3 might be a good strategy to identify the E3 mediating CHMP1B (and possibly other ESCRT) ubiquitination.

As for the findings related to the new inhibitors of USP8 catalytic function and ACTH release, we hope they will serve as tools for the research community allowing to dynamically assess and better understand USP8-dependent biological processes, and that they will be further serve as a starting point for the development of new treatments for patients with Cushing's disease or other pathologies associated to USP8 gain-of-function such as cancer.

# BIBLIOGRAPHICAL REFERENCES



- Aalto, A.L., Mohan, A.K., Schwintzer, L., Kupka, S., Kietz, C., Walczak, H., Broemer, M., and Meinander, A. (2019). M1-linked ubiquitination by LUBEL is required for inflammatory responses to oral infection in *Drosophila*. *Cell Death Differ.* *26*, 860–876.
- Adell, M.A.Y., and Teis, D. (2011). Assembly and disassembly of the ESCRT-III membrane scission complex. *FEBS Lett.* *585*, 3191–3196.
- Adkins, J.C., and Brogden, R.N. (1998). Zafirlukast. A review of its pharmacology and therapeutic potential in the management of asthma. *Drugs* *55*, 121–144.
- Akutsu, M., Dikic, I., and Bremm, A. (2016). Ubiquitin chain diversity at a glance. *J. Cell Sci.* *129*, 875–880.
- Alam, M.S. (2018). Proximity Ligation Assay (PLA). *Curr. Protoc. Immunol.* *123*, e58.
- AlAmri, M.A., Kadri, H., Alderwick, L.J., Simpkins, N.S., and Mehellou, Y. (2017). Rafoxanide and Closantel Inhibit SPAK and OSR1 Kinases by Binding to a Highly Conserved Allosteric Site on Their C-terminal Domains. *ChemMedChem* *12*, 639–645.
- Albani, A., Theodoropoulou, M., and Reincke, M. (2018a). Genetics of Cushing's disease. *Clin. Endocrinol. (Oxf.)* *88*, 3–12.
- Albani, A., Pérez-Rivas, L.G., Dimopoulou, C., Zopp, S., Colón-Bolea, P., Roeber, S., Honegger, J., Flitsch, J., Rachinger, W., Buchfelder, M., et al. (2018b). The USP8 mutational status may predict long-term remission in patients with Cushing's disease. *Clin. Endocrinol. (Oxf.)* *89*, 454–458.
- Al-Gareeb, A.I.A., Gorial, F.I., and Mahmood, A.S. (2018). Niclosamide as an adjuvant to etanercept in treatment patients with active rheumatoid arthritis: an 8-week randomized controlled pilot study. *Clin. Rheumatol.* *37*, 2633–2641.
- Anandasabapathy, N., Ford, G.S., Bloom, D., Holness, C., Paragas, V., Seroogy, C., Skrenta, H., Hollenhorst, M., Fathman, C.G., and Soares, L. (2003). GRAIL: an E3 ubiquitin ligase that inhibits cytokine gene transcription is expressed in anergic CD4+ T cells. *Immunity* *18*, 535–547.
- Asao, H., Sasaki, Y., Arita, T., Tanaka, N., Endo, K., Kasai, H., Takeshita, T., Endo, Y., Fujita, T., and Sugamura, K. (1997). Hrs Is Associated with STAM, a Signal-transducing Adaptor Molecule: ITS SUPPRESSIVE EFFECT ON CYTOKINE-INDUCED CELL GROWTH\*. *J. Biol. Chem.* *272*, 32785–32791.
- Asari, Y., Kageyama, K., Sugiyama, A., Kogawa, H., Niioka, K., and Daimon, M. (2019). Lapaninib decreases the ACTH production and proliferation of corticotroph tumor cells. *Endocr. J.* *66*, 515–522.
- Asoklis, R., Cimbalas, A., Augyte, A., Jasinskiene, E., and Strupaite, R. (2018). Late ocular changes after closantel poisoning in five women. *Eye* *32*, 1800–1802.
- Atanassov, B.S., Koutelou, E., and Dent, S.Y. (2011). The Role of Deubiquitinating Enzymes in Chromatin Regulation. *FEBS Lett.* *585*, 2016–2023.
- Azmi, A.S., Uddin, M.H., and Mohammad, R.M. (2020). The nuclear export protein XPO1 — from biology to targeted therapy. *Nat. Rev. Clin. Oncol.* 1–18.
- Babst, M., Sato, T.K., Banta, L.M., and Emr, S.D. (1997). Endosomal transport function in yeast requires a novel AAA-type ATPase, Vps4p. *EMBO J.* *16*, 1820–1831.
- Babst, M., Wendland, B., Estepa, E.J., and Emr, S.D. (1998). The Vps4p AAA ATPase regulates membrane association of a Vps protein complex required for normal endosome function. *EMBO J.* *17*, 2982–2993.
- Babst, M., Katzmann, D.J., Snyder, W.B., Wendland, B., and Emr, S.D. (2002). Endosome-Associated Complex, ESCRT-II, Recruits Transport Machinery for Protein Sorting at the Multivesicular Body. *Dev. Cell* *3*, 283–289.
- Bai, C., Sen, P., Hofmann, K., Ma, L., Goebel, M., Harper, J.W., and Elledge, S.J. (1996). SKP1 connects cell cycle regulators to the ubiquitin proteolysis machinery through a novel motif, the F-box. *Cell* *86*, 263–274.

Bai, X.-S., Zhang, C., Peng, R., Jiang, G.-Q., Jin, S.-J., Wang, Q., Ke, A.-W., and Bai, D.-S. (2020). RNF128 Promotes Malignant Behaviors via EGFR/MEK/ERK Pathway in Hepatocellular Carcinoma. *OncoTargets Ther.* *13*, 10129–10141.

Bajorek, M., Schubert, H.L., McCullough, J., Langelier, C., Eckert, D.M., Stubblefield, W.-M.B., Uter, N.T., Myszka, D.G., Hill, C.P., and Sundquist, W.I. (2009). Structural basis for ESCRT-III protein autoinhibition. *Nat. Struct. Mol. Biol.* *16*, 754–762.

Banh, B.T., McDermott, H., Woodman, S., Gadila, S.K.G., Saimani, U., Short, J.C.W., and Kim, K. (2017). Yeast dynamin interaction with ESCRT proteins at the endosome. *Cell Biol. Int.* *41*, 484–494.

Barbosa, E.J., Löbenberg, R., de Araujo, G.L.B., and Bou-Chacra, N.A. (2019). Niclosamide repositioning for treating cancer: Challenges and nano-based drug delivery opportunities. *Eur. J. Pharm. Biopharm. Off. J. Arbeitsgemeinschaft Pharm. Verfahrenstechnik EV 141*, 58–69.

Bard, J.A.M., Goodall, E.A., Greene, E.R., Jonsson, E., Dong, K.C., and Martin, A. (2018). Structure and Function of the 26S Proteasome. *Annu. Rev. Biochem.* *87*, 697–724.

Barnett, R. (2016). Cushing's syndrome. *The Lancet* *388*, 649.

Barrett, K., Barman, S., Yuan, J., and Brooks, H. (2019). *Ganong's Review of Medical Physiology* (New York, N.Y.: McGraw-Hill Education).

Béchet, S., Hill, F., Gilheaney, Ó., and Walshe, M. (2016). Diagnostic Accuracy of the Modified Evan's Blue Dye Test in Detecting Aspiration in Patients with Tracheostomy: A Systematic Review of the Evidence. *Dysphagia* *31*, 721–729.

Bednash, J.S., and Mallampalli, R.K. (2018). Targeting Deubiquitinases in Cancer. *Methods Mol. Biol. Clifton NJ 1731*, 295–305.

Bennett, E.M., Lin, S.X., Towler, M.C., Maxfield, F.R., and Brodsky, F.M. (2001). Clathrin Hub Expression Affects Early Endosome Distribution with Minimal Impact on Receptor Sorting and Recycling. *Mol. Biol. Cell* *12*, 2790–2799.

Ben-Shlomo, A., and Cooper, O. (2017). Role of tyrosine kinase inhibitors in the treatment of pituitary tumours: from bench to bedside. *Curr. Opin. Endocrinol. Diabetes Obes.* *24*, 301–305.

Berlin, I., Schwartz, H., and Nash, P.D. (2010). Regulation of epidermal growth factor receptor ubiquitination and trafficking by the USP8-STAM complex. *J. Biol. Chem.* *285*, 34909–34921.

Bonacci, T., and Emanuele, M.J. (2020). Dissenting degradation: Deubiquitinases in cell cycle and cancer. *Seminars in Cancer Biology* *67*, 145–158.

Boucrot, E., Ferreira, A.P.A., Almeida-Souza, L., Debard, S., Vallis, Y., Howard, G., Bertot, L., Sauvonnet, N., and McMahon, H.T. (2015). Endophilin marks and controls a clathrin-independent endocytic pathway. *Nature* *517*, 460–465.

Boulch, M.L., Brossard, A., Dez, G.L., and Rabut, G. (2019). Sensitive detection of protein ubiquitylation using a protein-fragment complementation assay. *BioRxiv* 791897.

Bousquet, C., and Melmed, S. (1999). Critical Role for STAT3 in Murine Pituitary Adrenocorticotropin Hormone Leukemia Inhibitory Factor Signaling \*. *J. Biol. Chem.* *274*, 10723–10730.

Bousquet, C., Zatelli, M.C., and Melmed, S. (2000). Direct regulation of pituitary proopiomelanocortin by STAT3 provides a novel mechanism for immuno-neuroendocrine interfacing. *J. Clin. Invest.* *106*, 1417–1425.

Boya, P., Reggiori, F., and Codogno, P. (2013). Emerging regulation and functions of autophagy. *Nat. Cell Biol.* *15*, 713–720.

Braten, O., Livneh, I., Ziv, T., Admon, A., Kehat, I., Caspi, L.H., Gonen, H., Bercovich, B., Godzik, A., Jahandideh, S., et al. (2016). Numerous proteins with unique characteristics are

degraded by the 26S proteasome following monoubiquitination. *Proc. Natl. Acad. Sci. U. S. A.* *113*, E4639-4647.

Brown, R.J., Kelly, M.H., and Collins, M.T. (2010). Cushing Syndrome in the McCune-Albright Syndrome. *J. Clin. Endocrinol. Metab.* *95*, 1508–1515.

Budenholzer, L., Cheng, C.L., Li, Y., and Hochstrasser, M. (2017). Proteasome Structure and Assembly. *J. Mol. Biol.* *429*, 3500–3524.

Buetow, L., and Huang, D.T. (2016). Structural insights into the catalysis and regulation of E3 ubiquitin ligases. *Nat. Rev. Mol. Cell Biol.* *17*, 626–642.

Buliman, A., Tataranu, L., Paun, D., Mirica, A., and Dumitrache, C. (2016). Cushing's disease: a multidisciplinary overview of the clinical features, diagnosis, and treatment. *J. Med. Life* *9*, 12–18.

Burd, C.G., and Emr, S.D. (1998). Phosphatidylinositol(3)-phosphate signaling mediated by specific binding to RING FYVE domains. *Mol. Cell* *2*, 157–162.

Burock, S., Daum, S., Keilholz, U., Neumann, K., Walther, W., and Stein, U. (2018). Phase II trial to investigate the safety and efficacy of orally applied niclosamide in patients with metachronous or synchronous metastases of a colorectal cancer progressing after therapy: the NIKOLO trial. *BMC Cancer* *18*, 297.

Byun, S., Lee, S.-Y., Jeong, C.-H., Lee, J., Lim, S., Reddy, K., Farrand, L., Kim, J.Y., Lee, M.-H., Lee, K.W., et al. (2013). USP8 is a novel target for overcoming gefitinib-resistance in lung cancer. *Clin. Cancer Res. Off. J. Am. Assoc. Cancer Res.* *19*, 3894–3904.

Caldieri, G., Malabarba, M.G., Di Fiore, P.P., and Sigismund, S. (2018). EGFR Trafficking in Physiology and Cancer. In *Endocytosis and Signaling*, C. Lamaze, and I. Prior, eds. (Cham: Springer International Publishing), pp. 235–272.

Cawley, N.X., Li, Z., and Loh, Y.P. (2016). 60 YEARS OF POMC: Biosynthesis, trafficking, and secretion of pro-opiomelanocortin-derived peptides. *J. Mol. Endocrinol.* *56*, T77–T97.

Chao, H.-W., Lai, Y.-T., Lu, Y.-L., Lin, C., Mai, W., and Huang, Y.-S. (2012). NMDAR signaling facilitates the IPO5-mediated nuclear import of CPEB3. *Nucleic Acids Res.* *40*, 8484–8498.

Chen, D., Dai, C., and Jiang, Y. (2015). Histone H2A and H2B Deubiquitinase in Developmental Disease and Cancer. *Cancer Transl. Med.* *1*, 170.

Chen, W., Mook, R.A., Premont, R.T., and Wang, J. (2018). Niclosamide: Beyond an antihelminthic drug. *Cell. Signal.* *41*, 89–96.

Childs, G.V., Patterson, J., Unabia, G., Rougeau, D., and Wu, P. (1991). Epidermal growth factor enhances ACTH secretion and expression of POMC mRNA by corticotropes in mixed and enriched cultures. *Mol. Cell. Neurosci.* *2*, 235–243.

Chu, T., Sun, J., Saksena, S., and Emr, S.D. (2006). New component of ESCRT-I regulates endosomal sorting complex assembly. *J. Cell Biol.* *175*, 815–823.

Ciechanover, A. (2015). The unravelling of the ubiquitin system. *Nat. Rev. Mol. Cell Biol.* *16*, 322–324.

Ciechanover, A., Heller, H., Elias, S., Haas, A.L., and Hershko, A. (1980). ATP-dependent conjugation of reticulocyte proteins with the polypeptide required for protein degradation. *Proc. Natl. Acad. Sci.* *77*, 1365–1368.

Clague, M.J., and Urbé, S. (2006). Endocytosis: the DUB version. *Trends Cell Biol.* *16*, 551–559.

Clague, M.J., Urbé, S., and Komander, D. (2019). Breaking the chains: deubiquitylating enzyme specificity begets function. *Nat. Rev. Mol. Cell Biol.* *20*, 338–352.

Clarke, I.J. (2015). Hypothalamus as an endocrine organ. *Compr. Physiol.* *5*, 217–253.

Cohen, M., Persky, R., Stegemann, R., Hernández-Ramírez, L.C., Zeltser, D., Lodish, M.B., Chen, A., Keil, M.F., Tatsi, C., Faucz, F.R., et al. (2019). Germline USP8 Mutation

Associated With Pediatric Cushing Disease and Other Clinical Features: A New Syndrome. *J. Clin. Endocrinol. Metab.* *104*, 4676–4682.

Colland, F., Formstecher, E., Jacq, X., Reverdy, C., Planquette, C., Conrath, S., Trouplin, V., Bianchi, J., Aushev, V.N., Camonis, J., et al. (2009). Small-molecule inhibitor of USP7/HAUSP ubiquitin protease stabilizes and activates p53 in cells. *Mol. Cancer Ther.* *8*, 2286–2295.

Colombo, M., Vallese, S., Peretto, I., Jacq, X., Rain, J.-C., Colland, F., and Guedat, P. (2010). Synthesis and biological evaluation of 9-oxo-9H-indeno[1,2-b]pyrazine-2,3-dicarbonitrile analogues as potential inhibitors of deubiquitinating enzymes. *ChemMedChem* *5*, 552–558.

Cornelissen, T., Haddad, D., Wauters, F., Van Humbeeck, C., Mandemakers, W., Koentjoro, B., Sue, C., Gevaert, K., De Strooper, B., Verstreken, P., et al. (20141001). The deubiquitinase USP15 antagonizes Parkin-mediated mitochondrial ubiquitination and mitophagy. *Hum. Mol. Genet.* *23*, 5227–5242.

Costanzo, L.S. (2019). *Physiology*.

Cotto-Rios, X.M., Békés, M., Chapman, J., Ueberheide, B., and Huang, T.T. (2012). Deubiquitinases as a signaling target of oxidative stress. *Cell Rep.* *2*, 1475–1484.

Courtois, G., and Fauvarque, M.-O. (2018). The Many Roles of Ubiquitin in NF- $\kappa$ B Signaling. *Biomedicines* *6*.

Crespo-Yañez, X., Aguilar-Gurrieri, C., Jacomin, A.-C., Journet, A., Mortier, M., Taillebourg, E., Soleilhac, E., Weissenhorn, W., and Fauvarque, M.-O. (2018). CHMP1B is a target of USP8/UBPY regulated by ubiquitin during endocytosis. *PLOS Genet.* *14*, e1007456.

Cristante, J., Lefournier, V., Sturm, N., Passagia, J.G., Gauchez, A.S., Tahon, F., Cantin, S., Chabre, O., and Gay, E. (2019). Why We Should Still Treat by Neurosurgery Patients With Cushing Disease and a Normal or Inconclusive Pituitary MRI. *J. Clin. Endocrinol. Metab.* *104*, 4101–4113.

Curtiss, M., Jones, C., and Babst, M. (2006). Efficient Cargo Sorting by ESCRT-I and the Subsequent Release of ESCRT-I from Multivesicular Bodies Requires the Subunit Mvb12. *Mol. Biol. Cell* *18*, 636–645.

Cvetkovic, I., Al-Abed, Y., Miljkovic, D., Maksimovic-Ivanic, D., Roth, J., Bacher, M., Lan, H.Y., Nicoletti, F., and Stosic-Grujicic, S. (2005). Critical role of macrophage migration inhibitory factor activity in experimental autoimmune diabetes. *Endocrinology* *146*, 2942–2951.

Damgaard, R.B. (2021). The ubiquitin system: from cell signalling to disease biology and new therapeutic opportunities. *Cell Death Differ.*

Dammer, E.B., Na, C.H., Xu, P., Seyfried, N.T., Duong, D.M., Cheng, D., Gearing, M., Rees, H., Lah, J.J., Levey, A.I., et al. (2011). Polyubiquitin linkage profiles in three models of proteolytic stress suggest the etiology of Alzheimer disease. *J. Biol. Chem.* *286*, 10457–10465.

David H. Ilson, M.D. (2019). EGFR-Inhibitor Therapy for non-V600E. *NEJM J. Watch* *2019*.

De Ceuninck, L., Wauman, J., Masschaele, D., Peelman, F., and Tavernier, J. (2013). Reciprocal cross-regulation between RNF41 and USP8 controls cytokine receptor sorting and processing. *J. Cell Sci.* *126*, 3770–3781.

Debono, M., Ghobadi, C., Rostami-Hodjegan, A., Huatan, H., Campbell, M.J., Newell-Price, J., Darzy, K., Merke, D.P., Arlt, W., and Ross, R.J. (2009). Modified-Release Hydrocortisone to Provide Circadian Cortisol Profiles. *J. Clin. Endocrinol. Metab.* *94*, 1548–1554.

Deng, Z., Purtell, K., Lachance, V., Wold, M.S., Chen, S., and Yue, Z. (2017). Autophagy Receptors and Neurodegenerative Diseases. *Trends Cell Biol.* *27*, 491–504.

- Dey, S., Li, X., Teng, R., Alnaeeli, M., Chen, Z., Rogers, H., and Noguchi, C.T. (2016). Erythropoietin regulates POMC expression via STAT3 and potentiates leptin response. *J. Mol. Endocrinol.* *56*, 55–67.
- Dikic, I., and Bremm, A. (2014). DUBs counteract parkin for efficient mitophagy. *EMBO J.* *33*, 2442–2443.
- Dimaano, C., Jones, C.B., Hanono, A., Curtiss, M., and Babst, M. (2007). Ist1 Regulates Vps4 Localization and Assembly. *Mol. Biol. Cell* *19*, 465–474.
- Doherty, G.J., and McMahon, H.T. (2009). Mechanisms of endocytosis. *Annu. Rev. Biochem.* *78*, 857–902.
- Dong, X., and Levine, B. (2013). Autophagy and viruses: adversaries or allies? *J. Innate Immun.* *5*, 480–493.
- Dubiel, W., Dubiel, D., Wolf, D.A., and Naumann, M. (2018). Cullin 3-Based Ubiquitin Ligases as Master Regulators of Mammalian Cell Differentiation. *Trends Biochem. Sci.* *43*, 95–107.
- Dubinon John H., do Carmo Jussara M., Adi Ahmad, Hamza Shereen, da Silva Alexandre A., and Hall John E. (2013). Role of Proopiomelanocortin Neuron Stat3 in Regulating Arterial Pressure and Mediating the Chronic Effects of Leptin. *Hypertension* *61*, 1066–1074.
- Dufner, A., and Knobeloch, K.-P. (2019). Ubiquitin-specific protease 8 (USP8/UBPy): a prototypic multidomain deubiquitinating enzyme with pleiotropic functions. *Biochem. Soc. Trans.* *47*, 1867–1879.
- Eiyama, A., and Okamoto, K. (2015). PINK1/Parkin-mediated mitophagy in mammalian cells. *Curr. Opin. Cell Biol.* *33*, 95–101.
- Enchev, R.I., Schulman, B.A., and Peter, M. (2015). Protein Neddylation: Beyond Cullin-RING Ligases. *Nat. Rev. Mol. Cell Biol.* *16*, 30–44.
- Engelman, J.A., Zejnullahu, K., Mitsudomi, T., Song, Y., Hyland, C., Park, J.O., Lindeman, N., Gale, C.-M., Zhao, X., Christensen, J., et al. (2007). MET amplification leads to gefitinib resistance in lung cancer by activating ERBB3 signaling. *Science* *316*, 1039–1043.
- Ernst, M.B., Wunderlich, C.M., Hess, S., Paehler, M., Mesaros, A., Koralov, S.B., Kleinriders, A., Husch, A., Münzberg, H., Hampel, B., et al. (2009). Enhanced Stat3 Activation in POMC Neurons Provokes Negative Feedback Inhibition of Leptin and Insulin Signaling in Obesity. *J. Neurosci.* *29*, 11582–11593.
- Essabar, L., Meskini, T., Ettair, S., Erreimi, N., and Mouane, N. (2014). Harmful Use of Veterinary Drugs: Blindness Following Closantel Poisoning in a 5-Year-Old Girl. *Asia Pac. J. Med. Toxicol.* *3*, 173–175.
- Etxabe, J., and Vazquez, J.A. (1994). Morbidity and mortality in Cushing's disease: an epidemiological approach. *Clin. Endocrinol. (Oxf.)* *40*, 479–484.
- Fabrikant, G., Lata, S., Riches, J.D., Briggs, J.A.G., Weissenhorn, W., and Kozlov, M.M. (2009). Computational Model of Membrane Fission Catalyzed by ESCRT-III. *PLOS Comput. Biol.* *5*, e1000575.
- Fakheri, R.J., and Volpicelli, F.M. (2019). Things We Do for No Reason: Prescribing Docusate for Constipation in Hospitalized Adults. *J. Hosp. Med.* *14*, 110–113.
- Fang, S., and Wang, Z. (2014). EGFR mutations as a prognostic and predictive marker in non-small-cell lung cancer. *Drug Des. Devel. Ther.* *8*, 1595–1611.
- Faucz, F.R., Tirosh, A., Tatsi, C., Berthon, A., Hernández-Ramírez, L.C., Settas, N., Angelousi, A., Correa, R., Papadakis, G.Z., Chittiboina, P., et al. (2017). Somatic USP8 Gene Mutations Are a Common Cause of Pediatric Cushing Disease. *J. Clin. Endocrinol. Metab.* *102*, 2836–2843.
- Fauvarque, M.-O., Mortier, M., Pillet, C., Aguilar, C., Soleilhac, E., Barette, C., Remusat, V., Terme, T., and Vanelle, P. (2016). Heterocyclic Naphthoquinones Derivatives

for Use in the Treatment of Cancers Including Cushing Disease. European Patent 3281940 A1. International application no. WO/2018/029137.

Franquelim, H.G., and Schwille, P. (2017). Revolving around constriction by ESCRT-III. *Nat. Cell Biol.* *19*, 754–756.

Fritsch, L.E., Moore, M.E., Sarraf, S.A., and Pickrell, A.M. (2019). Ubiquitin and Receptor-Dependent Mitophagy Pathways and Their Implication in Neurodegeneration. *J. Mol. Biol.*

Fukuda, S., and Morimoto, K. (2001). Lifestyle, stress and cortisol response: Review II. *Environ. Health Prev. Med.* *6*, 15–21.

Fukuoka, H., Cooper, O., Ben-Shlomo, A., Mamelak, A., Ren, S.-G., Bruyette, D., and Melmed, S. (2011). EGFR as a therapeutic target for human, canine, and mouse ACTH-secreting pituitary adenomas. *J. Clin. Invest.* *121*, 4712.

Gao, J., Wang, Y., Yang, J., Zhang, W., Meng, K., Sun, Y., Li, Y., and He, Q.-Y. (2019). RNF128 Promotes Invasion and Metastasis Via the EGFR/MAPK/MMP-2 Pathway in Esophageal Squamous Cell Carcinoma. *Cancers* *11*.

Gassen, N.C., Niemeyer, D., Muth, D., Corman, V.M., Martinelli, S., Gassen, A., Hafner, K., Papies, J., Mösbauer, K., Zellner, A., et al. (2019). SKP2 attenuates autophagy through Beclin1-ubiquitination and its inhibition reduces MERS-Coronavirus infection. *Nat. Commun.* *10*.

Gassen, N.C., Papies, J., Bajaj, T., Dethloff, F., Emanuel, J., Weckmann, K., Heinz, D.E., Heinemann, N., Lennarz, M., Richter, A., et al. (2020). Analysis of SARS-CoV-2-controlled autophagy reveals spermidine, MK-2206, and niclosamide as putative antiviral therapeutics. *BioRxiv* 2020.04.15.997254.

Gaullier, J.M., Simonsen, A., D'Arrigo, A., Bremnes, B., Stenmark, H., and Aasland, R. (1998). FYVE fingers bind PtdIns(3)P. *Nature* *394*, 432–433.

Gill, D.J., Teo, H., Sun, J., Perisic, O., Veprintsev, D.B., Emr, S.D., and Williams, R.L. (2007). Structural insight into the ESCRT-I/-II link and its role in MVB trafficking. *EMBO J.* *26*, 600–612.

Goldstein, J.L., Anderson, R.G.W., and Brown, M.S. (1979). Coated pits, coated vesicles, and receptor-mediated endocytosis. *Nature* *279*, 679–685.

Gore, D.C., Jahoor, F., Wolfe, R.R., and Herndon, D.N. (1993). Acute response of human muscle protein to catabolic hormones. *Ann. Surg.* *218*, 679–684.

Graversen, D., Vestergaard, P., Stochholm, K., Gravholt, C.H., and Jørgensen, J.O.L. (2012). Mortality in Cushing's syndrome: a systematic review and meta-analysis. *Eur. J. Intern. Med.* *23*, 278–282.

Grou, C.P., Pinto, M.P., Mendes, A.V., Domingues, P., and Azevedo, J.E. (2015). The de novo synthesis of ubiquitin: identification of deubiquitinases acting on ubiquitin precursors. *Sci. Rep.* *5*, 1–16.

Gruenberg, J. (2001). The endocytic pathway: a mosaic of domains. *Nat. Rev. Mol. Cell Biol.* *2*, 721–730.

Guerrero, J. (2017). [Understanding cortisol action in acute inflammation: A view from the adrenal gland to the target cell]. *Rev. Med. Chil.* *145*, 230–239.

Guizetti, J., Schermelleh, L., Mäntler, J., Maar, S., Poser, I., Leonhardt, H., Müller-Reichert, T., and Gerlich, D.W. (2011). Cortical Constriction During Abscission Involves Helices of ESCRT-III-Dependent Filaments. *Science* *331*, 1616–1620.

Guo, J., Tao, H., Alasadi, A., Huang, Q., and Jin, S. (2019). Niclosamide piperazine prevents high-fat diet-induced obesity and diabetic symptoms in mice. *Eat. Weight Disord.* *EWD* *24*, 91–96.

Gyamfi, J., Lee, Y.-H., Min, B.S., and Choi, J. (2019). Niclosamide reverses adipocyte induced epithelial-mesenchymal transition in breast cancer cells via suppression of the interleukin-6/STAT3 signalling axis. *Sci. Rep.* *9*, 11336.

Haakonsen, D.L., and Rape, M. (2019). Branching Out: Improved Signaling by Heterotypic Ubiquitin Chains. *Trends Cell Biol.* *29*, 704–716.

Haglund, K., and Dikic, I. (2012). The role of ubiquitylation in receptor endocytosis and endosomal sorting. *J Cell Sci* *125*, 265–275.

Hammond-Martel, I., Yu, H., and Affar, E.B. (2012). Roles of ubiquitin signaling in transcription regulation. *Cell. Signal.* *24*, 410–421.

Han, J., Tian, Y., Yu, L., Zhang, Q., Xu, X., Zhang, Y., Wang, J., Ma, Z., Bian, J., Luo, C., et al. (2020). Discovery of novel USP8 inhibitors via Ubiquitin-Rho-110 fluorometric assay based high throughput screening. *Bioorganic Chem.* *101*, 103962.

Han, P., Shao, M., Guo, L., Wang, W., Song, G., Yu, X., Zhang, C., Ge, N., Yi, T., Li, S., et al. (2018). Niclosamide ethanolamine improves diabetes and diabetic kidney disease in mice. *Am. J. Transl. Res.* *10*, 1071–1084.

Hannibal, K.E., and Bishop, M.D. (2014). Chronic Stress, Cortisol Dysfunction, and Pain: A Psychoneuroendocrine Rationale for Stress Management in Pain Rehabilitation. *Phys. Ther.* *94*, 1816–1825.

Hansen, M., Rubinsztein, D.C., and Walker, D.W. (2018). Autophagy as a promoter of longevity: insights from model organisms. *Nat. Rev. Mol. Cell Biol.* *19*, 579–593.

Hanson, P.I., Roth, R., Lin, Y., and Heuser, J.E. (2008). Plasma membrane deformation by circular arrays of ESCRT-III protein filaments. *J. Cell Biol.* *180*, 389–402.

Harhaj, E.W., and Dixit, V.M. (2012). Regulation of NF- $\kappa$ B by deubiquitinases. *Immunol. Rev.* *246*, 107–124.

He, K.-L., and Ting, A.T. (2002). A20 Inhibits Tumor Necrosis Factor (TNF) Alpha-Induced Apoptosis by Disrupting Recruitment of TRADD and RIP to the TNF Receptor 1 Complex in Jurkat T Cells. *Mol. Cell. Biol.* *22*, 6034.

Henne, W.M., Buchkovich, N.J., and Emr, S.D. (2011). The ESCRT Pathway. *Dev. Cell* *21*, 77–91.

Henne, W.M., Stenmark, H., and Emr, S.D. (2013). Molecular Mechanisms of the Membrane Sculpting ESCRT Pathway. *Cold Spring Harb. Perspect. Biol.* *5*, a016766.

Hernández-Ramírez, L.C., and Stratakis, C.A. (2018). Genetics of Cushing's syndrome. *Endocrinol. Metab. Clin. North Am.* *47*, 275–297.

Hershko, A., Ciechanover, A., Heller, H., Haas, A.L., and Rose, I.A. (1980). Proposed role of ATP in protein breakdown: conjugation of protein with multiple chains of the polypeptide of ATP-dependent proteolysis. *Proc. Natl. Acad. Sci.* *77*, 1783–1786.

Hierro, A., Sun, J., Rusnak, A.S., Kim, J., Prag, G., Emr, S.D., and Hurley, J.H. (2004). Structure of the ESCRT-II endosomal trafficking complex. *Nature* *431*, 221–225.

Holderfield, M., Deuker, M.M., McCormick, F., and McMahon, M. (2014). Targeting RAF kinases for cancer therapy: BRAF mutated melanoma and beyond. *Nat. Rev. Cancer* *14*, 455–467.

Holding, A.N. (2015). XL-MS: Protein cross-linking coupled with mass spectrometry. *Methods* *89*, 54–63.

Huang, F., Kirkpatrick, D., Jiang, X., Gygi, S., and Sorkin, A. (2006). Differential regulation of EGF receptor internalization and degradation by multiubiquitination within the kinase domain. *Mol. Cell* *21*, 737–748.

Hutti, J.E., Turk, B.E., Asara, J.M., Ma, A., Cantley, L.C., and Abbott, D.W. (2007). I $\kappa$ B Kinase  $\beta$  Phosphorylates the K63 Deubiquitinase A20 To Cause Feedback Inhibition of the NF- $\kappa$ B Pathway. *Mol. Cell. Biol.* *27*, 7451–7461.

- Imperi, F., Massai, F., Ramachandran Pillai, C., Longo, F., Zennaro, E., Rampioni, G., Visca, P., and Leoni, L. (2013). New Life for an Old Drug: the Anthelmintic Drug Niclosamide Inhibits *Pseudomonas aeruginosa* Quorum Sensing. *Antimicrob. Agents Chemother.* *57*, 996–1005.
- Ioachimescu, A.G. (2018). Cushing's Syndrome 2018: Best Practices and Looking Ahead. *Endocrinol. Metab. Clin. North Am.* *47*, xiii–xiv.
- Jacomin, A.-C., Taillebourg, E., and Fauvarque, M.-O. (2018). Deubiquitinating Enzymes Related to Autophagy: New Therapeutic Opportunities? *Cells* *7*.
- Jacq, X., Kemp, M., Martin, N.M.B., and Jackson, S.P. (2013). Deubiquitylating Enzymes and DNA Damage Response Pathways. *Cell Biochem. Biophys.* *67*, 25–43.
- Jeon, S., Ko, M., Lee, J., Choi, I., Byun, S.Y., Park, S., Shum, D., and Kim, S. (2020). Identification of Antiviral Drug Candidates against SARS-CoV-2 from FDA-Approved Drugs. *Antimicrob. Agents Chemother.* *64*.
- Jeong, M., Lee, E.-W., Seong, D., Seo, J., Kim, J.-H., Grootjans, S., Kim, S.-Y., Vandenabeele, P., and Song, J. (2017). USP8 suppresses death receptor-mediated apoptosis by enhancing FLIPL stability. *Oncogene* *36*, 458–470.
- Ji, C.H., and Kwon, Y.T. (2017). Crosstalk and Interplay between the Ubiquitin-Proteasome System and Autophagy. *Mol. Cells* *40*, 441–449.
- Jian, F., Cao, Y., Bian, L., and Sun, Q. (2015). USP8: a novel therapeutic target for Cushing's disease. *Endocrine* *50*, 292–296.
- Jian, F.-F., Li, Y.-F., Chen, Y.-F., Jiang, H., Chen, X., Zheng, L.-L., Zhao, Y., Wang, W.-Q., Ning, G., Bian, L.-G., et al. (2016). Inhibition of Ubiquitin-specific Peptidase 8 Suppresses Adrenocorticotrophic Hormone Production and Tumorous Corticotroph Cell Growth in AtT20 Cells. *Chin. Med. J. (Engl.)* *129*, 2102–2108.
- Johansen, T., and Lamark, T. (2020). Selective Autophagy: ATG8 Family Proteins, LIR Motifs and Cargo Receptors. *J. Mol. Biol.* *432*, 80–103.
- Jurgeit, A., McDowell, R., Moese, S., Meldrum, E., Schwendener, R., and Greber, U.F. (2012). Niclosamide Is a Proton Carrier and Targets Acidic Endosomes with Broad Antiviral Effects. *PLoS Pathog.* *8*.
- Kadri, H., Lambourne, O.A., and Mehellou, Y. (2018). Niclosamide, a Drug with Many (Re)purposes. *ChemMedChem* *13*, 1088–1091.
- Kageyama, K., Asari, Y., Sugimoto, Y., Niioka, K., and Daimon, M. (2020). Ubiquitin-specific protease 8 inhibitor suppresses adrenocorticotrophic hormone production and corticotroph tumor cell proliferation. *Endocr. J.* *67*, 177–184.
- Kaksonen, M., and Roux, A. (2018). Mechanisms of clathrin-mediated endocytosis. *Nat. Rev. Mol. Cell Biol.* *19*, 313–326.
- Kapadia, B.B., and Gartenhaus, R.B. (2019). DUBbing Down Translation: The Functional Interaction of Deubiquitinases with the Translational Machinery. *Mol. Cancer Ther.* *18*, 1475–1483.
- Kasahara, K., Aoki, H., Kiyono, T., Wang, S., Kagiwada, H., Yuge, M., Tanaka, T., Nishimura, Y., Mizoguchi, A., Goshima, N., et al. (2018). EGF receptor kinase suppresses ciliogenesis through activation of USP8 deubiquitinase. *Nat. Commun.* *9*, 758.
- Kasper, D.L., Fauci, A.S., Hauser, S.L., Longo, D.L., Jameson, J.L., and Loscalzo, J. (2018). *Harrison's Principles of Internal Medicine 20/E* (McGraw-Hill Education / Medical).
- Kato, M., Miyazawa, K., and Kitamura, N. (2000). A Deubiquitinating Enzyme UBPY Interacts with the Src Homology 3 Domain of Hrs-binding Protein via a Novel Binding Motif PX(V/I)(D/N)RXXKP. *J. Biol. Chem.* *275*, 37481–37487.
- Katzmann, D.J., Babst, M., and Emr, S.D. (2001). Ubiquitin-Dependent Sorting into the Multivesicular Body Pathway Requires the Function of a Conserved Endosomal Protein Sorting Complex, ESCRT-I. *Cell* *106*, 145–155.



Kelloway, J.S. (1997). Zafirlukast: the first leukotriene-receptor antagonist approved for the treatment of asthma. *Ann. Pharmacother.* *31*, 1012–1021.

Khani, S., and Tayek, J.A. (2001). Cortisol increases gluconeogenesis in humans: its role in the metabolic syndrome. *Clin. Sci. Lond. Engl.* *1979 101*, 739–747.

Kiss, A.K., and Piwowarski, J.P. (2018). Ellagitannins, Gallotannins and their Metabolites- The Contribution to the Anti-Inflammatory Effect of Food Products and Medicinal Plants. *Curr. Med. Chem.* *25*, 4946–4967.

Kniss, A., Schuetz, D., Kazemi, S., Pluska, L., Spindler, P.E., Rogov, V.V., Husnjak, K., Dikic, I., Güntert, P., Sommer, T., et al. (2018). Chain Assembly and Disassembly Processes Differently Affect the Conformational Space of Ubiquitin Chains. *Structure* *26*, 249–258.e4.

Kobayashi, S., Boggon, T.J., Dayaram, T., Jänne, P.A., Kocher, O., Meyerson, M., Johnson, B.E., Eck, M.J., Tenen, D.G., and Halmos, B. (2005). EGFR mutation and resistance of non-small-cell lung cancer to gefitinib. *N. Engl. J. Med.* *352*, 786–792.

Komada, M. (2008). Controlling Receptor Downregulation by Ubiquitination and Deubiquitination.

Komander, D., and Rape, M. (2012). The Ubiquitin Code. *Annu. Rev. Biochem.* *81*, 203–229.

Kosaka, T., Yatabe, Y., Endoh, H., Yoshida, K., Hida, T., Tsuboi, M., Tada, H., Kuwano, H., and Mitsudomi, T. (2006). Analysis of epidermal growth factor receptor gene mutation in patients with non-small cell lung cancer and acquired resistance to gefitinib. *Clin. Cancer Res. Off. J. Am. Assoc. Cancer Res.* *12*, 5764–5769.

Kostelansky, M.S., Sun, J., Lee, S., Kim, J., Ghirlando, R., Hierro, A., Emr, S.D., and Hurley, J.H. (2006). Structural and Functional Organization of the ESCRT-I Trafficking Complex. *Cell* *125*, 113–126.

Koziolok, M.J., Patschan, D., Desel, H., Wallbach, M., and Callizo, J. (2015). Closantel Poisoning Treated With Plasma Exchange. *JAMA Ophthalmol.* *133*, 718–720.

Kräutler, B. (2012). Biochemistry of B12-cofactors in human metabolism. *Subcell. Biochem.* *56*, 323–346.

Kumar, K., Mishra, C., Anjanamurthy, R., Kannan, N.B., and Ramasamy, K. (2019). Reversible blindness in a patient with closantel toxicity. *Indian J. Ophthalmol.* *67*, 1768–1771.

Kwon, Y.T., and Ciechanover, A. (2017). The Ubiquitin Code in the Ubiquitin-Proteasome System and Autophagy. *Trends Biochem. Sci.* *42*, 873–886.

Landré, V., Revi, B., Mir, M.G., Verma, C., Hupp, T.R., Gilbert, N., and Ball, K.L. (2017). Regulation of transcriptional activators by DNA-binding domain ubiquitination. *Cell Death Differ.* *24*, 903–916.

Langelier, C., Schwedler, U.K. von, Fisher, R.D., Domenico, I.D., White, P.L., Hill, C.P., Kaplan, J., Ward, D., and Sundquist, W.I. (2006). Human ESCRT-II Complex and Its Role in Human Immunodeficiency Virus Type 1 Release. *J. Virol.* *80*, 9465–9480.

Lata, S., Schoehn, G., Jain, A., Pires, R., Piehler, J., Göttinger, H.G., and Weissenhorn, W. (2008). Helical Structures of ESCRT-III Are Disassembled by VPS4. *Science* *321*, 1354–1357.

Le Tissier, P., Fiordelisio Coll, T., and Mollard, P. (2018). The Processes of Anterior Pituitary Hormone Pulse Generation. *Endocrinology* *159*, 3524–3535.

Lecker, S.H., Goldberg, A.L., and Mitch, W.E. (2006). Protein Degradation by the Ubiquitin-Proteasome Pathway in Normal and Disease States. *J. Am. Soc. Nephrol.* *17*, 1807–1819.

Lee, D.Y., Kim, E., and Choi, M.H. (2015). Technical and clinical aspects of cortisol as a biochemical marker of chronic stress. *BMB Rep.* *48*, 209–216.

Lee, J.-G., Baek, K., Soetandyo, N., and Ye, Y. (2013). Reversible inactivation of deubiquitinases by reactive oxygen species in vitro and in cells. *Nat. Commun.* 4, 1568.

Lee, M.-C., Chen, Y.-K., Hsu, Y.-J., and Lin, B.-R. (2020). Niclosamide inhibits the cell proliferation and enhances the responsiveness of esophageal cancer cells to chemotherapeutic agents. *Oncol. Rep.* 43, 549–561.

Lefournier, V., Martinie, M., Vasdev, A., Bessou, P., Passagia, J.-G., Labat-Moleur, F., Sturm, N., Bosson, J.-L., Bachelot, I., and Chabre, O. (2003). Accuracy of Bilateral Inferior Petrosal or Cavernous Sinuses Sampling in Predicting the Lateralization of Cushing's Disease Pituitary Microadenoma: Influence of Catheter Position and Anatomy of Venous Drainage. *J. Clin. Endocrinol. Metab.* 88, 196–203.

Li, R., Hu, Z., Sun, S.-Y., Chen, Z.G., Owonikoko, T.K., Sica, G.L., Ramalingam, S.S., Curran, W.J., Khuri, F.R., and Deng, X. (2013). Niclosamide overcomes acquired resistance to erlotinib through suppression of STAT3 in non-small cell lung cancer. *Mol. Cancer Ther.* 12, 2200–2212.

Li, W., Bengtson, M.H., Ulbrich, A., Matsuda, A., Reddy, V.A., Orth, A., Chanda, S.K., Batalov, S., and Joazeiro, C.A.P. (2008). Genome-Wide and Functional Annotation of Human E3 Ubiquitin Ligases Identifies MULAN, a Mitochondrial E3 that Regulates the Organelle's Dynamics and Signaling. *PLOS ONE* 3, e1487.

Li, Y., Macdonald-Obermann, J., Westfall, C., Piwnica-Worms, D., and Pike, L.J. (2012). Quantitation of the effect of ErbB2 on epidermal growth factor receptor binding and dimerization. *J. Biol. Chem.* 287, 31116–31125.

Li, Y., Guo, B., Xu, Z., Li, B., Cai, T., Zhang, X., Yu, Y., Wang, H., Shi, J., and Zhu, W. (2016). Repositioning organohalogen drugs: a case study for identification of potent B-Raf V600E inhibitors via docking and bioassay. *Sci. Rep.* 6.

Liddle, G.W. (1977). Cushing's syndrome\*. *Ann. N. Y. Acad. Sci.* 297, 594–601.

Lindholm, J., Juul, S., Jørgensen, J.O., Astrup, J., Bjerre, P., Feldt-Rasmussen, U., Hagen, C., Jørgensen, J., Kosteljanetz, M., Kristensen, L., et al. (2001). Incidence and late prognosis of cushing's syndrome: a population-based study. *J. Clin. Endocrinol. Metab.* 86, 117–123.

Liu, Q., Wu, Y., Qin, Y., Hu, J., Xie, W., Qin, F.X.-F., and Cui, J. (2018). Broad and diverse mechanisms used by deubiquitinase family members in regulating the type I interferon signaling pathway during antiviral responses. *Sci. Adv.* 4, eaar2824.

Liu, X., Feng, M., Dai, C., Bao, X., Deng, K., Yao, Y., and Wang, R. (2019a). Expression of EGFR in Pituitary Corticotroph Adenomas and Its Relationship With Tumor Behavior. *Front. Endocrinol.* 10.

Liu, Z., Zanata, S.M., Kim, J., Peterson, M.A., Di Vizio, D., Chirieac, L.R., Pyne, S., Agostini, M., Freeman, M.R., and Loda, M. (2013). The ubiquitin-specific protease USP2a prevents endocytosis-mediated EGFR degradation. *Oncogene* 32, 1660–1669.

Liu, Z., Dong, X., Yi, H.-W., Yang, J., Gong, Z., Wang, Y., Liu, K., Zhang, W.-P., and Tang, C. (2019b). Structural basis for the recognition of K48-linked Ub chain by proteasomal receptor Rpn13. *Cell Discov.* 5, 1–15.

Lonser, R.R., Nieman, L., and Oldfield, E.H. (2017). Cushing's disease: pathobiology, diagnosis, and management. *J. Neurosurg.* 126, 404–417.

Lopez-Castejon, G., and Edelmann, M.J. (2016). Deubiquitinases: Novel Therapeutic Targets in Immune Surveillance? *Mediators Inflamm.* 2016.

Lork, M., Verhelst, K., and Beyaert, R. (2017). CYLD, A20 and OTULIN deubiquitinases in NF- $\kappa$ B signaling and cell death: so similar, yet so different. *Cell Death Differ.* 24, 1172–1183.

Lottridge, J.M., Flannery, A.R., Vincelli, J.L., and Stevens, T.H. (2006). Vta1p and Vps46p regulate the membrane association and ATPase activity of Vps4p at the yeast multivesicular body. *Proc. Natl. Acad. Sci. U. S. A.* *103*, 6202–6207.

Lubetsky, J.B., Dios, A., Han, J., Aljabari, B., Ruzsicska, B., Mitchell, R., Lolis, E., and Al-Abed, Y. (2002). The tautomerase active site of macrophage migration inhibitory factor is a potential target for discovery of novel anti-inflammatory agents. *J. Biol. Chem.* *277*, 24976–24982.

Lynch, T.J., Bell, D.W., Sordella, R., Gurubhagavatula, S., Okimoto, R.A., Brannigan, B.W., Harris, P.L., Haserlat, S.M., Supko, J.G., Haluska, F.G., et al. (2004). Activating mutations in the epidermal growth factor receptor underlying responsiveness of non-small-cell lung cancer to gefitinib. *N. Engl. J. Med.* *350*, 2129–2139.

M, G., C, G., Af, S., Ma, M., S, M., and D, K. (2017). Mechanism and regulation of the Lys6-selective deubiquitinase USP30. *Nat. Struct. Mol. Biol.* *24*, 920–930.

Ma, Z.-Y., Song, Z.-J., Chen, J.-H., Wang, Y.-F., Li, S.-Q., Zhou, L.-F., Mao, Y., Li, Y.-M., Hu, R.-G., Zhang, Z.-Y., et al. (2015). Recurrent gain-of-function *USP8* mutations in Cushing's disease. *Cell Res.* *25*, 306–317.

Mashtalir, N., Daou, S., Barbour, H., Sen, N.N., Gagnon, J., Hammond-Martel, I., Dar, H.H., Therrien, M., and Affar, E.B. (2014). Autodeubiquitination protects the tumor suppressor BAP1 from cytoplasmic sequestration mediated by the atypical ubiquitin ligase UBE2O. *Mol. Cell* *54*, 392–406.

McClellan, A.J., Laugesen, S.H., and Ellgaard, L. (2019). Cellular functions and molecular mechanisms of non-lysine ubiquitination. *Open Biol.* *9*.

McCullough, J., Clague, M.J., and Urbé, S. (2004). AMSH is an endosome-associated ubiquitin isopeptidase. *J. Cell Biol.* *166*, 487–492.

McCullough, J., Row, P.E., Lorenzo, Ó., Doherty, M., Beynon, R., Clague, M.J., and Urbé, S. (2006). Activation of the Endosome-Associated Ubiquitin Isopeptidase AMSH by STAM, a Component of the Multivesicular Body-Sorting Machinery. *Curr. Biol.* *16*, 160–165.

McCullough, J., Colf, L.A., and Sundquist, W.I. (2013). Membrane Fission Reactions of the Mammalian ESCRT Pathway. *Annu. Rev. Biochem.* *82*, 663–692.

McCullough, J., Clippinger, A.K., Talledge, N., Skowyra, M.L., Saunders, M.G., Naismith, T.V., Colf, L.A., Afonine, P., Arthur, C., Sundquist, W.I., et al. (2015). Structure and membrane remodeling activity of ESCRT-III helical polymers. *Science* *350*, 1548–1551.

McDowell, G.S., and Philpott, A. (2013). Non-canonical ubiquitylation: Mechanisms and consequences. *Int. J. Biochem. Cell Biol.* *45*, 1833–1842.

Melker, A.A. de, Horst, G. van der, Calafat, J., Jansen, H., and Borst, J. (2001). c-Cbl ubiquitinates the EGF receptor at the plasma membrane and remains receptor associated throughout the endocytic route. *J. Cell Sci.* *114*, 2167–2178.

Mevissen, T.E.T., and Komander, D. (2017). Mechanisms of Deubiquitinase Specificity and Regulation. *Annu. Rev. Biochem.* *86*, 159–192.

Miaczynska, M., and Bar-Sagi, D. (2010). Signaling endosomes: seeing is believing. *Curr. Opin. Cell Biol.* *22*, 535–540.

Mizuno, E., Iura, T., Mukai, A., Yoshimori, T., Kitamura, N., and Komada, M. (2005). Regulation of epidermal growth factor receptor down-regulation by UBPY-mediated deubiquitination at endosomes. *Mol. Biol. Cell* *16*, 5163–5174.

Mizuno, E., Kobayashi, K., Yamamoto, A., Kitamura, N., and Komada, M. (2006). A Deubiquitinating Enzyme UBPY Regulates the Level of Protein Ubiquitination on Endosomes. *Traffic* *7*, 1017–1031.

Molina, P. (2013). *Endocrine Physiology, Fourth Edition* (New York, N.Y.: McGraw-Hill Education / Medical).

- Mulas, F., Wang, X., Song, S., Nishanth, G., Yi, W., Brunn, A., Larsen, P.-K., Isermann, B., Kalinke, U., Barragan, A., et al. (2020). The deubiquitinase OTUB1 augments NF- $\kappa$ B-dependent immune responses in dendritic cells in infection and inflammation by stabilizing UBC13. *Cell. Mol. Immunol.* 1–16.
- Münzberg, H., Huo, L., Nillni, E.A., Hollenberg, A.N., and Bjørnbæk, C. (2003). Role of Signal Transducer and Activator of Transcription 3 in Regulation of Hypothalamic Proopiomelanocortin Gene Expression by Leptin. *Endocrinology* 144, 2121–2131.
- Muzioł, T., Pineda-Molina, E., Ravelli, R.B., Zamborlini, A., Usami, Y., Göttlinger, H., and Weissenhorn, W. (2006). Structural Basis for Budding by the ESCRT-III Factor CHMP3. *Dev. Cell* 10, 821–830.
- Naba, A., Reverdy, C., Louvard, D., and Arpin, M. (2008). Spatial recruitment and activation of the Fes kinase by ezrin promotes HGF-induced cell scattering. *EMBO J.* 27, 38–50.
- Nam, T., Han, J.H., Devkota, S., and Lee, H.-W. (2017). Emerging Paradigm of Crosstalk between Autophagy and the Ubiquitin-Proteasome System. *Mol. Cells* 40, 897–905.
- Naslavsky, N., and Caplan, S. (2018). The enigmatic endosome – sorting the ins and outs of endocytic trafficking. *J. Cell Sci.* 131.
- Naviglio, S., Mattecucci, C., Matoskova, B., Nagase, T., Nomura, N., Di Fiore, P.P., and Draetta, G.F. (1998). UBPY: a growth-regulated human ubiquitin isopeptidase. *EMBO J.* 17, 3241–3250.
- Newton, P.T. (2019). New insights into niclosamide action: autophagy activation in colorectal cancer. *Biochem. J.* 476, 779–781.
- Nguyen, H.C., Wang, W., and Xiong, Y. (2017). Cullin-RING E3 Ubiquitin Ligases: Bridges to Destruction. *Subcell. Biochem.* 83, 323–347.
- Nickerson, D.P., West, M., and Odorizzi, G. (2006). Did2 coordinates Vps4-mediated dissociation of ESCRT-III from endosomes. *J. Cell Biol.* 175, 715–720.
- Niendorf, S., Oksche, A., Kisser, A., Löhler, J., Prinz, M., Schorle, H., Feller, S., Lewitzky, M., Horak, I., and Knobeloch, K.-P. (2007). Essential Role of Ubiquitin-Specific Protease 8 for Receptor Tyrosine Kinase Stability and Endocytic Trafficking In Vivo. *Mol. Cell. Biol.* 27, 5029–5039.
- Oakley, R.H., and Cidlowski, J.A. (2013). The Biology of the Glucocorticoid Receptor: New Signaling Mechanisms in Health and Disease. *J. Allergy Clin. Immunol.* 132, 1033.
- Obita, T., Saksena, S., Ghazi-Tabatabai, S., Gill, D.J., Perisic, O., Emr, S.D., and Williams, R.L. (2007). Structural basis for selective recognition of ESCRT-III by the AAA ATPase Vps4. *Nature* 449, 735–739.
- Oh, C.-K., Sultan, A., Platzer, J., Dolatabadi, N., Soldner, F., McClatchy, D.B., Diedrich, J.K., Yates, J.R., Ambasadhan, R., Nakamura, T., et al. (2017). S-Nitrosylation of PINK1 Attenuates PINK1/Parkin-Dependent Mitophagy in hiPSC-Based Parkinson’s Disease Models. *Cell Rep.* 21, 2171–2182.
- Olmos, Y., Hodgson, L., Mantell, J., Verkade, P., and Carlton, J.G. (2015). ESCRT-III controls nuclear envelope reformation. *Nature* 522, 236–239.
- Orvedahl, A., MacPherson, S., Sumpter, R., Tallóczy, Z., Zou, Z., and Levine, B. (2010). Autophagy Protects against Sindbis Virus Infection of the Central Nervous System. *Cell Host Microbe* 7, 115–127.
- Paez, J.G., Jänne, P.A., Lee, J.C., Tracy, S., Greulich, H., Gabriel, S., Herman, P., Kaye, F.J., Lindeman, N., Boggon, T.J., et al. (2004). EGFR mutations in lung cancer: correlation with clinical response to gefitinib therapy. *Science* 304, 1497–1500.
- Pao, W., Miller, V., Zakowski, M., Doherty, J., Politi, K., Sarkaria, I., Singh, B., Heelan, R., Rusch, V., Fulton, L., et al. (2004). EGF receptor gene mutations are common in

lung cancers from “never smokers” and are associated with sensitivity of tumors to gefitinib and erlotinib. *Proc. Natl. Acad. Sci. U. S. A.* *101*, 13306–13311.

Pao, W., Miller, V.A., Politi, K.A., Riely, G.J., Somwar, R., Zakowski, M.F., Kris, M.G., and Varmus, H. (2005). Acquired resistance of lung adenocarcinomas to gefitinib or erlotinib is associated with a second mutation in the EGFR kinase domain. *PLoS Med.* *2*, e73.

Pareja, F., Ferraro, D.A., Rubin, C., Cohen-Dvashi, H., Zhang, F., Aulmann, S., Ben-Chetrit, N., Pines, G., Navon, R., Crosetto, N., et al. (2012). Deubiquitination of EGFR by Cezanne-1 contributes to cancer progression. *Oncogene* *31*, 4599–4608.

Pearson, G., Chai, B., Vozheiko, T., Liu, X., Kandarpa, M., Piper, R.C., and Soleimanpour, S.A. (2018). Clec16a, Nrdp1, and USP8 Form a Ubiquitin-Dependent Tripartite Complex That Regulates  $\beta$ -Cell Mitophagy. *Diabetes* *67*, 265–277.

Perez-Rivas, L.G., and Reincke, M. (2016). Genetics of Cushing’s disease: an update. *J. Endocrinol. Invest.* *39*, 29–35.

Petroski, M.D., and Deshaies, R.J. (2005). Function and regulation of cullin–RING ubiquitin ligases. *Nat. Rev. Mol. Cell Biol.* *6*, 9–20.

Ph.D, J.E.H. (2015). *Guyton and Hall Textbook of Medical Physiology* (Philadelphia, PA: W B Saunders Co Ltd).

Piper, R.C., Dikic, I., and Lukacs, G.L. (2014). Ubiquitin-Dependent Sorting in Endocytosis. *Cold Spring Harb. Perspect. Biol.* *6*.

Pivonello, R., De Leo, M., Cozzolino, A., and Colao, A. (2015). The Treatment of Cushing’s Disease. *Endocr. Rev.* *36*, 385–486.

Pivonello, R., De Martino, M.C., De Leo, M., Simeoli, C., and Colao, A. (2017). Cushing’s disease: the burden of illness. *Endocrine* *56*, 10–18.

Prabhakara, C., Godbole, R., Sil, P., Jahnavi, S., Zanten, T.S. van, Sheth, D., Subhash, N., Chandra, A., Nuthakki, V.K., Puthiyapurayil, T.P., et al. (2020). Niclosamide inhibits SARS-CoV2 entry by blocking internalization through pH-dependent CLIC/GEEC endocytic pathway. *BioRxiv* 2020.12.16.422529.

Prag, G., Watson, H., Kim, Y.C., Beach, B.M., Ghirlando, R., Hummer, G., Bonifacino, J.S., and Hurley, J.H. (2007). The Vps27/Hse1 Complex Is a GAT Domain-Based Scaffold for Ubiquitin-Dependent Sorting. *Dev. Cell* *12*, 973–986.

Rajamuthiah, R., Fuchs, B.B., Conery, A.L., Kim, W., Jayamani, E., Kwon, B., Ausubel, F.M., and Mylonakis, E. (2015). Repurposing salicylanilide anthelmintic drugs to combat drug resistant *Staphylococcus aureus*. *PLoS One* *10*, e0124595.

Reincke, M., Sbiera, S., Hayakawa, A., Theodoropoulou, M., Osswald, A., Beuschlein, F., Meitinger, T., Mizuno-Yamasaki, E., Kawaguchi, K., Saeki, Y., et al. (2015). Mutations in the deubiquitinase gene USP8 cause Cushing’s disease. *Nat. Genet.* *47*, 31–38.

in the deubiquitinase gene USP8 cause Cushing’s disease. *Nat. Genet.* *47*, 31–38.

Ren, X., Duan, L., He, Q., Zhang, Z., Zhou, Y., Wu, D., Pan, J., Pei, D., and Ding, K. (2010). Identification of Niclosamide as a New Small-Molecule Inhibitor of the STAT3 Signaling Pathway. *ACS Med. Chem. Lett.* *1*, 454–459.

Ritorto, M.S., Ewan, R., Perez-Oliva, A.B., Knebel, A., Buhrlage, S.J., Wightman, M., Kelly, S.M., Wood, N.T., Virdee, S., Gray, N.S., et al. (2014). Screening of DUB activity and specificity by MALDI-TOF mass spectrometry. *Nat. Commun.* *5*, 4763.

Rovit, R.L., and Duane, T.D. (1968). Eye Signs in Patients With Cushing’s Syndrome and Pituitary Tumors. *Arch. Ophthalmol.* *79*, 512–522.

Row, P.E., Prior, I.A., McCullough, J., Clague, M.J., and Urbé, S. (2006). The Ubiquitin Isopeptidase UBPY Regulates Endosomal Ubiquitin Dynamics and Is Essential for Receptor Down-regulation\*. *J. Biol. Chem.* *281*, 12618–12624.

Row, P.E., Liu, H., Hayes, S., Welchman, R., Charalabous, P., Hofmann, K., Clague, M.J., Sanderson, C.M., and Urbé, S. (2007). The MIT Domain of UBPY Constitutes a CHMP

Binding and Endosomal Localization Signal Required for Efficient Epidermal Growth Factor Receptor Degradation. *J. Biol. Chem.* 282, 30929–30937.

Rue, S.M., Mattei, S., Saksena, S., and Emr, S.D. (2008). Novel Ist1-Did2 complex functions at a late step in multivesicular body sorting. *Mol. Biol. Cell* 19, 475–484.

Sadowski, M., Suryadinata, R., Tan, A.R., Roesley, S.N.A., and Sarcevic, B. (2012). Protein monoubiquitination and polyubiquitination generate structural diversity to control distinct biological processes. *IUBMB Life* 64, 136–142.

Sarkis, P., Rabilloud, M., Lifante, J.-C., Siamand, A., Jouanneau, E., Gay, E., Chaffanjon, P., Chabre, O., and Raverot, G. (2019). Bilateral adrenalectomy in Cushing's disease: Altered long-term quality of life compared to other treatment options. *Ann. Endocrinol.* 80, 32–37.

Satir, P., Pedersen, L.B., and Christensen, S.T. (2010). The primary cilium at a glance. *J. Cell Sci.* 123, 499–503.

Sbiera, S., Perez-Rivas, L.G., Taranets, L., Weigand, I., Flitsch, J., Graf, E., Monoranu, C.-M., Saeger, W., Hagel, C., Honegger, J., et al. (2019). Driver mutations in USP8 wild-type Cushing's disease. *Neuro-Oncol.* 21, 1273–1283.

Schauer, N.J., Liu, X., Magin, R.S., Doherty, L.M., Chan, W.C., Ficarro, S.B., Hu, W., Roberts, R.M., Iacob, R.E., Stolte, B., et al. (2020). Selective USP7 inhibition elicits cancer cell killing through a p53-dependent mechanism. *Sci. Rep.* 10.

Scheffner, M., and Kumar, S. (2014). Mammalian HECT ubiquitin-protein ligases: Biological and pathophysiological aspects. *Biochim. Biophys. Acta BBA - Mol. Cell Res.* 1843, 61–74.

Schmidt, O., and Teis, D. (2012). The ESCRT machinery. *Curr. Biol.* 22, R116–R120.

Schweizer, M.T., Haugk, K., McKiernan, J.S., Gulati, R., Cheng, H.H., Maes, J.L., Dumpit, R.F., Nelson, P.S., Montgomery, B., McCune, J.S., et al. (2018). A phase I study of niclosamide in combination with enzalutamide in men with castration-resistant prostate cancer. *PLoS One* 13, e0198389.

Scott, A., Gaspar, J., Stuchell-Breteron, M.D., Alam, S.L., Skalicky, J.J., and Sundquist, W.I. (2005). Structure and ESCRT-III protein interactions of the MIT domain of human VPS4A. *Proc. Natl. Acad. Sci.* 102, 13813–13818.

Sharma, P., and Nag, A. (2014). CUL4A ubiquitin ligase: A promising drug target for cancer and other human diseases. *Open Biol.* 4, 130217.

Shibli-Rahhal, A., Van Beek, M., and Schlechte, J.A. (2006). Cushing's syndrome. *Clin. Dermatol.* 24, 260–265.

Sierra, M.I., Wright, M.H., and Nash, P.D. (2010). AMSH Interacts with ESCRT-0 to Regulate the Stability and Trafficking of CXCR4. *J. Biol. Chem.* 285, 13990–14004.

Singer, N., Sommer, M., Döhnel, K., Zänkert, S., Wüst, S., and Kudielka, B.M. (2017). Acute psychosocial stress and everyday moral decision-making in young healthy men: The impact of cortisol. *Horm. Behav.* 93, 72–81.

Singh, N., and Singh, A.B. (2016). Deubiquitinases and cancer: A snapshot. *Crit. Rev. Oncol. Hematol.* 103, 22–26.

Slagsvold, T., Aasland, R., Hirano, S., Bache, K.G., Raiborg, C., Trambaiolo, D., Wakatsuki, S., and Stenmark, H. (2005). Eap45 in Mammalian ESCRT-II Binds Ubiquitin via a Phosphoinositide-interacting GLUE Domain\*♦. *J. Biol. Chem.* 280, 19600–19606.

Smeriglio, A., Barreca, D., Bellocco, E., and Trombetta, D. (2017). Proanthocyanidins and hydrolysable tannins: occurrence, dietary intake and pharmacological effects. *Br. J. Pharmacol.* 174, 1244–1262.

Smit, J.J., and Sixma, T.K. (2014). RBR E3-ligases at work. *EMBO Rep.* 15, 142–154.

- Soares, L., Seroogy, C., Skrenta, H., Anandasabapathy, N., Lovelace, P., Chung, C.D., Engleman, E., and Fathman, C.G. (2004). Two isoforms of otubain 1 regulate T cell anergy via GRAIL. *Nat. Immunol.* 5, 45–54.
- Soedarso, M.A., Nugroho, K.H., and Meira Dewi, K.A. (2018). A case report: Addison disease caused by adrenal tuberculosis. *Urol. Case Rep.* 20, 12–14.
- Song, X.Q., Fukao, T., Yamaguchi, S., Miyazawa, S., Hashimoto, T., and Orii, T. (1994). Molecular cloning and nucleotide sequence of complementary DNA for human hepatic cytosolic acetoacetyl-coenzyme A thiolase. *Biochem. Biophys. Res. Commun.* 201, 478–485.
- Sorkin, A., and Goh, L.K. (2008). Endocytosis and intracellular trafficking of ErbBs. *Exp. Cell Res.* 314, 3093–3106.
- Sowa, M.E., Bennett, E.J., Gygi, S.P., and Harper, J.W. (2009). Defining the human deubiquitinating enzyme interaction landscape. *Cell* 138, 389–403.
- Srinivasa, S., Ding, X., and Kast, J. (2015). Formaldehyde cross-linking and structural proteomics: Bridging the gap. *Methods* 89, 91–98.
- Stockum, S. von, Sanchez-Martinez, A., Corrà, S., Chakraborty, J., Marchesan, E., Locatello, L., Rè, C.D., Cusumano, P., Caicci, F., Ferrari, V., et al. (2019). Inhibition of the deubiquitinase USP8 corrects a Drosophila PINK1 model of mitochondria dysfunction. *Life Sci. Alliance* 2.
- Straub, R.H., and Cutolo, M. (2016). Glucocorticoids and chronic inflammation. *Rheumatol. Oxf. Engl.* 55, ii6–ii14.
- Stuchell-Breerton, M.D., Skalicky, J.J., Kieffer, C., Karren, M.A., Ghaffarian, S., and Sundquist, W.I. (2007). ESCRT-III recognition by VPS4 ATPases. *Nature* 449, 740–744.
- Sun, Y. (2020). Cullin-RING Ligases and Protein Neddylation: Biology and Therapeutics (Springer Nature).
- Sun, Z., and Zhang, Y. (1999). Antituberculosis activity of certain antifungal and antihelminthic drugs. *Tuber. Lung Dis. Off. J. Int. Union Tuberc. Lung Dis.* 79, 319–320.
- Sung, H., Ferlay, J., Siegel, R.L., Laversanne, M., Soerjomataram, I., Jemal, A., and Bray, F. (2021). Global cancer statistics 2020: GLOBOCAN estimates of incidence and mortality worldwide for 36 cancers in 185 countries. *CA. Cancer J. Clin.* *n/a*.
- Suryadinata, R., Roesley, S.N.A., Yang, G., and Šarčević, B. (2014). Mechanisms of Generating Polyubiquitin Chains of Different Topology. *Cells* 3, 674–689.
- Swan, G.E. (1999). The pharmacology of halogenated salicylanilides and their anthelmintic use in animals. *J. S. Afr. Vet. Assoc.* 70, 61–70.
- Swatek, K.N., and Komander, D. (2016). Ubiquitin modifications. *Cell Res.* 26, 399–422.
- Sykes, N.P. (1994). Current approaches to the management of constipation. *Cancer Surv.* 21, 137–146.
- Szklarczyk, D., Gable, A.L., Lyon, D., Junge, A., Wyder, S., Huerta-Cepas, J., Simonovic, M., Doncheva, N.T., Morris, J.H., Bork, P., et al. (2019). STRING v11: protein-protein association networks with increased coverage, supporting functional discovery in genome-wide experimental datasets. *Nucleic Acids Res.* 47, D607–D613.
- Tabatabaei, S.A., Soleimani, M., Mansouri, M.R., Mirshahi, A., Inanlou, B., Abrishami, M., Pakrah, A.R., and Masarat, H. (2016). Closantel; a veterinary drug with potential severe morbidity in humans. *BMC Ophthalmol.* 16, 207.
- Tao, H., Zhang, Y., Zeng, X., Shulman, G.I., and Jin, S. (2014). Niclosamide ethanolamine-induced mild mitochondrial uncoupling improves diabetic symptoms in mice. *Nat. Med.* 20, 1263–1269.
- Tayri-Wilk, T., Slavina, M., Zamel, J., Blass, A., Cohen, S., Motzik, A., Sun, X., Shalev, D.E., Ram, O., and Kalisman, N. (2020). Mass spectrometry reveals the chemistry of formaldehyde cross-linking in structured proteins. *Nat. Commun.* 11, 3128.

- Teixeira, L.K., and Reed, S.I. (2013). Ubiquitin ligases and cell cycle control. *Annu. Rev. Biochem.* 82, 387–414.
- Teo, H., Perisic, O., González, B., and Williams, R.L. (2004). ESCRT-II, an Endosome-Associated Complex Required for Protein Sorting: Crystal Structure and Interactions with ESCRT-III and Membranes. *Dev. Cell* 7, 559–569.
- Teo, H., Gill, D.J., Sun, J., Perisic, O., Veprintsev, D.B., Vallis, Y., Emr, S.D., and Williams, R.L. (2006). ESCRT-I Core and ESCRT-II GLUE Domain Structures Reveal Role for GLUE in Linking to ESCRT-I and Membranes. *Cell* 125, 99–111.
- Thau, L., and Sharma, S. (2020). Physiology, Cortisol. In *StatPearls*, (Treasure Island (FL): StatPearls Publishing), p.
- Tomas, A., Futter, C.E., and Eden, E.R. (2014). EGF receptor trafficking: consequences for signaling and cancer. *Trends Cell Biol.* 24, 26–34.
- Tran, T.B., Cheah, S.-E., Yu, H.H., Bergen, P.J., Nation, R.L., Creek, D.J., Purcell, A., Forrest, A., Doi, Y., Song, J., et al. (2016). Anthelmintic closantel enhances bacterial killing of polymyxin B against multidrug-resistant *Acinetobacter baumannii*. *J. Antibiot. (Tokyo)* 69, 415–421.
- Trinh, H.K.T., Lee, S.-H., Cao, T.B.T., and Park, H.-S. (2019). Asthma pharmacotherapy: an update on leukotriene treatments. *Expert Rev. Respir. Med.* 13, 1169–1178.
- Turakhiya, A. (2018). Functional Characterization of the Role of ZFAND1 in Stress Granule Turnover (Julius-Maximilians-Universität Würzburg).
- Uhlen, M., Zhang, C., Lee, S., Sjöstedt, E., Fagerberg, L., Bidkhori, G., Benfante, R., Arif, M., Liu, Z., Edfors, F., et al. (2017). A pathology atlas of the human cancer transcriptome. *Science* 357.
- Umebayashi, K., Stenmark, H., and Yoshimori, T. (2008). Ubc4/5 and c-Cbl Continue to Ubiquitinate EGF Receptor after Internalization to Facilitate Polyubiquitination and Degradation. *Mol. Biol. Cell* 19, 3454–3462.
- Urbé, S., Liu, H., Hayes, S.D., Heride, C., Rigden, D.J., and Clague, M.J. (2012). Systematic survey of deubiquitinase localization identifies USP21 as a regulator of centrosome- and microtubule-associated functions. *Mol. Biol. Cell* 23, 1095–1103.
- Valenzuela, S.M., Martin, D.K., Por, S.B., Robbins, J.M., Warton, K., Bootcov, M.R., Schofield, P.R., Campbell, T.J., and Breit, S.N. (1997). Molecular cloning and expression of a chloride ion channel of cell nuclei. *J. Biol. Chem.* 272, 12575–12582.
- Venanzi, A.D., Alencar, G., Bourdeau, I., Fragoso, M.C.B., and Lacroix, A. (2014). Primary bilateral macronodular adrenal hyperplasia. *Curr. Opin. Endocrinol. Diabetes Obes.* 21, 177–184.
- Vietri, M., Radulovic, M., and Stenmark, H. (2020). The many functions of ESCRTs. *Nat. Rev. Mol. Cell Biol.* 21, 25–42.
- Visser Smit, G.D., Place, T.L., Cole, S.L., Clausen, K.A., Vemuganti, S., Zhang, G., Koland, J.G., and Lill, N.L. (2009). Cbl controls EGFR fate by regulating early endosome fusion. *Sci. Signal.* 2, ra86.
- Votteler, J., and Sundquist, W.I. (2013). Virus Budding and the ESCRT Pathway. *Cell Host Microbe* 14.
- Wang, Y., Argiles-Castillo, D., Kane, E.I., Zhou, A., and Spratt, D.E. (2020). HECT E3 ubiquitin ligases – emerging insights into their biological roles and disease relevance. *J. Cell Sci.* 133.
- Weber, J., Polo, S., and Maspero, E. (2019). HECT E3 Ligases: A Tale With Multiple Facets. *Front. Physiol.* 10.
- Wei, R., Liu, X., Yu, W., Yang, T., Cai, W., Liu, J., Huang, X., Xu, G., Zhao, S., Yang, J., et al. (2015). Deubiquitinases in cancer. *Oncotarget* 6, 12872–12889.



Weitzman, E.D., Fukushima, D., Nogueira, C., Roffwarg, H., Gallagher, T.F., and Hellman, L. (1971). Twenty-four hour pattern of the episodic secretion of cortisol in normal subjects. *J. Clin. Endocrinol. Metab.* *33*, 14–22.

Whiting, C.C., Su, L.L., Lin, J.T., and Fathman, C.G. (2011). GRAIL: A unique mediator of CD4 T lymphocyte unresponsiveness. *FEBS J.* *278*, 47–58.

Willems, A.R., Schwab, M., and Tyers, M. (2004). A hitchhiker's guide to the cullin ubiquitin ligases: SCF and its kin. *Biochim. Biophys. Acta BBA - Mol. Cell Res.* *1695*, 133–170.

Wong, B.R., Parlati, F., Qu, K., Demo, S., Pray, T., Huang, J., Payan, D.G., and Bennett, M.K. (2003). Drug discovery in the ubiquitin regulatory pathway. *Drug Discov. Today* *8*, 746–754.

Wu, C.-J., Jan, J.-T., Chen, C.-M., Hsieh, H.-P., Hwang, D.-R., Liu, H.-W., Liu, C.-Y., Huang, H.-W., Chen, S.-C., Hong, C.-F., et al. (2004a). Inhibition of severe acute respiratory syndrome coronavirus replication by niclosamide. *Antimicrob. Agents Chemother.* *48*, 2693–2696.

Wu, X., Yen, L., Irwin, L., Sweeney, C., and Carraway, K.L. (2004b). Stabilization of the E3 ubiquitin ligase Nrdp1 by the deubiquitinating enzyme USP8. *Mol. Cell. Biol.* *24*, 7748–7757.

Xiao, J., Chen, X.-W., Davies, B.A., Saltiel, A.R., Katzmann, D.J., and Xu, Z. (2009). Structural Basis of Ist1 Function and Ist1–Did2 Interaction in the Multivesicular Body Pathway and Cytokinesis. *Mol. Biol. Cell* *20*, 3514–3524.

Xu, J., Shi, P.-Y., Li, H., and Zhou, J. (2020). Broad Spectrum Antiviral Agent Niclosamide and Its Therapeutic Potential. *ACS Infect. Dis.* *6*, 909–915.

Yang, D., and Hurley, J.H. (2010). Structural role of the Vps4-Vta1 interface in ESCRT-III recycling. *Struct. Lond. Engl.* *1993* *18*, 976–984.

Yang, X.-D., and Sun, S.-C. (2018). Deubiquitinases as pivotal regulators of T cell functions. *Front. Med.* *12*, 451–462.

Yang, Y., He, Y., Wang, X., Liang, Z., He, G., Zhang, P., Zhu, H., Xu, N., and Liang, S. (2017). Protein SUMOylation modification and its associations with disease. *Open Biol.* *7*.

Yao, L., Xue, X., Yu, P., Ni, Y., and Chen, F. (2018). Evans Blue Dye: A Revisit of Its Applications in Biomedicine. *Contrast Media Mol. Imaging* *2018*, 7628037.

Yu, C., and Huang, L. (2018). Cross-Linking Mass Spectrometry (XL-MS): an Emerging Technology for Interactomics and Structural Biology. *Anal. Chem.* *90*, 144–165.

Yu, Z., Gonciarz, M.D., Sundquist, W.I., Hill, C.P., and Jensen, G.J. (2008). Cryo-EM Structure of Dodecameric Vps4p and Its 2:1 Complex with Vta1p. *J. Mol. Biol.* *377*, 364–377.

Zeng, X., Li, Y., Ling, H., Liu, S., Liu, M., Chen, J., and Guo, S. (2017). Transcriptomic analyses reveal clathrin-mediated endocytosis involved in symbiotic seed germination of *Gastrodia elata*. *Bot. Stud.* *58*, 1–11.

Zhang, L., Zhou, F., Drabsch, Y., Gao, R., Snaar-Jagalska, B.E., Mickanin, C., Huang, H., Sheppard, K.-A., Porter, J.A., Lu, C.X., et al. (2012). USP4 is regulated by AKT phosphorylation and directly deubiquitylates TGF- $\beta$  type I receptor. *Nat. Cell Biol.* *14*, 717–726.

Zheng, N., and Shabek, N. (2017). Ubiquitin Ligases: Structure, Function, and Regulation. *Annu. Rev. Biochem.* *86*, 129–157.

Zhou, H., Su, X., Lin, L., Zhang, J., Qi, Q., Guo, F., Xu, F., and Yang, B. (2019). Inhibitory Effects of Antiviral Drug Candidates on Canine Parvovirus in F81 cells. *Viruses* *11*.

Zhou, W., Wei, W., and Sun, Y. (2013). Genetically engineered mouse models for functional studies of SKP1-CUL1-F-box-protein (SCF) E3 ubiquitin ligases. *Cell Res.* *23*, 599–619.

Zhu, H.-Q., and Gao, F.-H. (2017). The Molecular Mechanisms of Regulation on USP2's Alternative Splicing and the Significance of Its Products. *Int. J. Biol. Sci.* *13*, 1489–1496.

Zhu, P.J., Hobson, J.P., Southall, N., Qiu, C., Thomas, C.J., Lu, J., Inglese, J., Zheng, W., Leppla, S.H., Bugge, T.H., et al. (2009). Quantitative high-throughput screening identifies inhibitors of anthrax-induced cell death. *Bioorg. Med. Chem.* *17*, 5139–5145.

Zhu, X.-Y., Xia, B., Liu, H.-C., Xu, Y.-Q., Huang, C.-J., Gao, J.-M., Dong, Q.-X., and Li, C.-Q. (2016). Closantel Suppresses Angiogenesis and Cancer Growth in Zebrafish Models. *Assay Drug Dev. Technol.* *14*, 282–290.

Ziv, I., Matiuhin, Y., Kirkpatrick, D.S., Erpapazoglou, Z., Leon, S., Pantazopoulou, M., Kim, W., Gygi, S.P., Haguenaer-Tsapis, R., Reis, N., et al. (2011). A perturbed ubiquitin landscape distinguishes between ubiquitin in trafficking and in proteolysis. *Mol. Cell. Proteomics MCP* *10*, M111.009753.





## **Résumé**

Ma thèse porte sur la régulation de la voie endocytaire et le trafic des récepteurs de la membrane plasmique. Une attention particulière a été accordée à l'étude du rôle de la protéase spécifique d'ubiquitine USP8 dans la régulation du récepteur au facteur de croissance épithéliale EGF et dans la maladie de Cushing, une maladie rare causée par un micro-adénome hypophysaire conduisant à une augmentation de la libération de l'hormone adrénocorticotrope (ACTH) et à des troubles métaboliques majeurs. Je présente ici une campagne de criblage à haut débit d'une collection de petites molécules ayant fait l'objet d'études cliniques ou pré-cliniques, qui a conduit à la sélection d'un inhibiteur chimique de l'activité catalytique USP8. Je montre également que cet inhibiteur diminue la libération d'ACTH dans des cellules corticotropes murines. En outre, j'ai étudié la régulation de CHMP1B, un substrat connu d'USP8, jouant un rôle majeur dans le trafic intracellulaire et la stabilité du récepteur à l'EGF. J'ai mis en évidence, par une approche par spectrométrie de masse, que l'ubiquitine protéase OTUB1 est un autre partenaire de CHMP1B et mis en évidence une régulation de l'ubiquitination et la stabilité de CHMP1B par OTUB1. Mon travail de thèse apporte de nouvelles connaissances fondamentales pour mieux comprendre le rôle des cibles et des partenaires d'USP8 dans l'endocytose, et un nouvel inhibiteur qui pourra accélérer la découverte de composés thérapeutiques pour le traitement de la maladie de Cushing et des cancers présentant une sur-expression d'USP8.

## **Abstract**

My thesis focuses on the regulation of the endocytic pathway and the trafficking of plasma membrane receptors. Particular attention was paid to the study of the role of the ubiquitin-specific protease USP8 in the regulation of the receptor for the epithelial growth factor (EGF) and in Cushing's disease, a rare disease caused by a pituitary microadenoma leading to increased release of adrenocorticotrophic hormone (ACTH) and major metabolic disturbances. I present here a high throughput screening campaign of a collection of 2,140 small molecules having been the subject of clinical or pre-clinical studies, which led to the selection of a chemical inhibitor of the catalytic activity USP8. I further showed that this inhibitor decreases the release of ACTH in murine corticotroph cells. In addition to this, I investigated the regulation of CHMP1B, a known USP8 substrate playing a major role in EGF receptor trafficking and sorting. I identified, by a mass spectrometry approach, that the ubiquitin protease OTUB1 is another partner of CHMP1B and demonstrated the regulation of the ubiquitination and stability of CHMP1B by OTUB1. My thesis work brings both new fundamental knowledge to understand better the role of USP8 targets and partners in endocytosis, and a new inhibitor that may accelerate the discovery of therapeutic compounds for the treatment of Cushing's disease and cancers with increased USP8 activity.